Tuning the biological performance of calcium phosphates through microstructural and chemical modifications

PhD Thesis

Candidate: Anna Díez Escudero

Supervisors: Prof. Maria Pau Ginebra Molins
Dr. Montserrat Español Pons

UNIVERSITAT POLITÈCNICA DE CATALUNYA BARCELONATECH

BBT

Tuning the biological performance of calcium phosphates through microstructural and chemical modifications

Anna Díez Escudero

Front cover: *TRAP-Hoechst staining of osteoclasts on heparinized CDHA*

Back cover: *Osteoclast filopodia detail on carbonated CDHA*

TUNING THE BIOLOGICAL PERFORMANCE OF CALCIUM PHOSPHATES THROUGH MICROSTRUCTURAL AND CHEMICAL MODIFICATIONS

Doctoral Program of Material Science and Engineering

Anna Díez-Escudero

Supervisors:

Dr. Montserrat Español Pons

Prof. Maria-Pau Ginebra Molins

Biomaterials, Biomechanics and Tissue engineering Group

Department of Material Science and Metallurgical Engineering

Universitat Politècnica de Catalunya

Barcelona, 2017

A Blanca y Víctor

Mucha gente pequeña,
en lugares pequeños,
haciendo cosas pequeñas,
pueden cambiar el mundo.
Eduardo Galeano

Table of Contents

CHAPTER 3
CARBONATION OF LOW TEMPERATURE MACROPOROUS CALCIUM PHOSPHATES 61

CHAPTER 4
HEPARINIZATION OF BETA TRICALCIUM PHOSPHATE: IMMUNOMODULATORY EFFECTS AND OSTEOGENIC POTENTIAL 77

x

Abstract

Bone is the most transplanted tissue after blood. As pointed out by the World Health Organization, musculoskeletal diseases can potentially rise as the fourth largest cause of disability within the next years. Unfortunately, despite the natural ability of bone to self-heal it cannot bridge large bone defects without the help of a material. Still today the gold standard to restore bone function remains the use of natural bone grafts. However, they have several limitations that need to be overcome to accommodate the high demands of a global ageing population.

Calcium phosphate (CaP) bone grafts have been known since the 1970s and stand as excellent synthetic candidates due to their composition, similar to the mineral phase of bone which consists of approximately 70% of hydroxyapatite (HA). CaPs, and in particular HA, possess outstanding intrinsic properties such as biocompatibility, bioactivity and the ability to support bone growth. However, HA is chemically stable and once implanted it hardly degrades. Ideal synthetic bone grafts should integrate in the bone remodeling cycle, balancing implant resorption with its progressive replacement by new bone. This can be achieved either by modulating the material's physicochemical properties, or by combining the substrate with biological molecules capable of adequately orchestrating the various cells involved in the bone healing process.

The present thesis seeks to explore, on the one hand, the feasibility of modulating the physicochemical properties of CaPs towards improving its degradation behavior, and, on the other hand, to investigate the potential CaP functionalization with heparin as a strategy to improve their biological performance at the various stages of bone healing: during the initial phase of inflammation, and during the stages of bone resorption and bone growth.

Chapter 1 offers an overview on bone composition and biology, as well as on bone grafting strategies and their potential to heal bone. *Chapter 2* deals with the *in vitro* degradation of CaPs in a solution mimicking the osteoclastic environment, focusing specifically on the effect of some properties like porosity, specific surface area, microstructure and composition. The interrelation of all these parameters sometimes masks the relative importance of textural over compositional features, making difficult the prediction of their degradation behavior. *Chapter 3* explores different strategies to incorporate carbonate ions in the crystal structure of HA as a route to obtain materials that more closely mimic natural bone.

To further mimic the biological environment of bone, the second part of the thesis is focused on grafting heparin, a highly sulfated glycosaminoglycan present in the bone

extracellular matrix, to CaPs. The affinity of heparin for growth factors (GF) makes this molecule an excellent candidate to capture endogenous GF bringing many benefits in the regulation of cell behavior. It is hypothesized that heparin, given its anti-inflammatory role, together with the known involvement in osteoblasts differentiation (bone forming cells) and osteoclastogenesis (bone resorbing cells formation) could enhance the biological performance of synthetic bone grafts. To this aim, CaPs were heparinized and their biological performance was assessed using human immune system cells, bone forming cells and bone resorbing cells, in an attempt to elucidate the synergies of both immune cells and cells of the skeletal system (***Chapter 4*** and ***Chapter 5***). The presence of heparin on the CaPs surface was shown to modulate inflammation by down-regulating the expression of pro-inflammatory cytokines, which actively provoke acute inflammation resulting in fibrous encapsulation of the implant. The immobilization of heparin also contributed to modulate the inflammatory response towards a pro-healing stimulation. Additionally, heparin fostered the differentiation of mesenchymal stem cells to the osteoblastic lineage, without the addition of any exogenous agent.

Osteoclasts, the bone resorbing cells, are closely related to the immune system since monocytes are their precursor cells. The interaction of CaPs, and their heparin-grafted analogues were studied in contact with immune cells to determine the capacity of the material to foster osteoclast formation, maturation and activity (***Chapter 5***). The last chapter of the thesis, ***Chapter 6***, was devoted to the characterization of the activity of osteoclasts on complex materials by cross-sectioning cells on the CaP biomaterials using focus ion beam (FIB). This technique allowed investigation of the early stages of resorption on materials with complex microstructures, such as CaP cements, which are often difficult to evaluate by other techniques.

Resum

L'os és un dels teixits més trasplantats arreu del món desprès de la sang. L'organització Mundial de la Salut ha posat de relleu l'increment de les malalties musculoesquelètiques, les quals esdevindran la quarta causa mundial de discapacitat en el següents anys. Malgrat la capacitat natural de l'ós per autoreparar-se, els defectes ossis de grans dimensions necessiten l'ajuda de materials per restaurar-se completament. Actualment, l'ús d'empelts naturals és l'alternativa més emprada clínicament. Tot i això, els autoempelts comporten certes limitacions que requereixen ser adreçades per tal de fer front a les elevades demandes d'una població mundial amb un grau d'envelliment creixent.

Els empelts basats en fosfats càlcics (CaPs) són coneguts des de la dècada del 1970 i són uns excel·lents candidats per a la regeneració òssia donada la seva composició, similar a la fase mineral de l'os, que consisteix en aproximadament un 70% d'hidroxiapatita (HA). Els CaPs, en particular l'HA, posseeixen unes propietats intrínseques excepcionals com ara biocompatibilitat, bioactivitat o la capacitat de suportar el creixement de nou os. Malgrat la seva semblança amb l'os, l'HA és massa estable químicament, i un cop implantada es degrada molt lentament. L'empelt ossi sintètic idealment s'hauria d'integrar en el cicle de remodelació òssia, el que requereix d'un balanç entre la seva reabsorció i la progressiva substitució per os nou. Aquesta capacitat es pot modular mitjançant propietats inherents del material o per mitjà de la combinació de substrats amb molècules capaces d'orquestrar adequadament les respostes de les diverses cèl·lules implicades en la restauració o curació òssia.

La present tesis cerca explorar, per una banda, la possibilitat de modular les propietats físico-químiques dels CaPs per tal de millorar la seva degradació, i per una altra, el potencial per funcionalitzar els CaPs amb heparina, amb la finalitat de millorar les interaccions biològiques a les diferents etapes de la restauració òssia, tant durant la primera etapa inflamatòria, com durant la resorció i el creixement d'os nou.

El *Capítol 1* descriu l'estat de l'art respecte a les principals característiques de l'os, els empelts disponibles i el seu potencial per curar o regenerar el teixit ossi. El *Capítol 2* de la present tesi explora la manera en què la modificació de propietats com la porositat, la superfície específica, la microestructura o la composició dels CaPs pot ser emprada per regular la degradació d'aquests materials en una solució acídica similar a l'emprada pels osteoclasts durant la resorció òssia. La interrelació de totes aquestes propietats emmascara de vegades la importància relativa de les propietats texturals, molt lligades a les composicionals, dificultant la predicció dels nivells de degradació dels materials depenent de cada propietat. El *Capítol 3* es centra en les diferents estratègies per incorporar ions carbonat en l'estructura cristal·lina de l'HA per tal de mimetitzar encara més la composició natural de l'os.

Per tal de mimetitzar més l'entorn biològic de l'os, la segona part d'aquesta tesi ha estat focalitzada en immobilitzar heparina, un tipus de glicosaminoglicà altament sulfonat present en la matriu extracel·lular de l'os, sobre els CaPs. L'afinitat de l'heparina per captar factors de creixement fan d'aquesta molècula un candidat excel·lent per capturar factors de creixement endògens capaços de regular la resposta cel·lular. Així doncs, partint de les propietats anti-inflamatòries de l'heparina, i de la seva implicació en els processos d'osteogènesi i osteoclastogènesi, s'ha formulat la hipòtesi de que aquesta biomolècula podria contribuir a millorar les prestacions dels empelts ossis sintètics. Amb aquest objectiu, s'ha posat a punt un procés d'heparinització de CaPs i s`ha avaluat el seu efecte sobre la resposta de cèl·lules humanes del sistema immune, cèl·lules osteogèniques i osteoclàstiques, per tal d'escatir les possibles sinèrgies de tots dos sistemes, l'immune i l'ossi en la regeneració (*Capítol 4* i *Capítol 5*). S'ha demostrat que la presència d'heparina a la superfície dels CaPs regula la inflamació per mitjà de la supressió parcial de citocines que provoquen processos d'inflamació aguda, conduents a una encapsulació fibrosa de l'empelt. Per altra banda, l'heparinització modula la inflamació cap a l'estimulació de la restauració natural de l'os. Addicionalment, s'ha observat que l'heparina estimula la diferenciació de cèl·lules mesenquimals sense l'addició de cap agent exogen.

Els osteoclasts, les cèl·lules responsables de reabsorbir os, estan íntimament lligades al sistema immune donat que els monòcits en són els seus precursors. En el *Capítol 5* s'ha analitzat l'efecte de l'heparinització en la interacció dels CaPs amb cèl·lules del sistema inmune, per determinar la capacitat de fomentar la formació de cèl·lules osteoclàstiques, així com la seva maduració i activitat. S'ha observat que la presència d'heparina accelera la fusió de precursors per formar osteoclasts madurs. L'últim capítol de la tesi, *Capítol 6*, s'ha dedicat a la caracterització de l'activitat osteoclàstica en materials complexos per mitjà del seccionament de les cèl·lules fent ús de la litografia per feix de ions. Aquesta innovadora tècnica ha permès l'avaluació d'etapes primàries de reabsorció en materials amb microestructures complexes com són els CaPs, els quals representen un repte per ser avaluats amb altres tècniques.

Acknowledgements

A la gent multi-escala, Carla, Lluís, Montse, Trifon, gràcies per la vostra disposició a ajudar-me sempre. Especialment al Trifon, por enseñarme tanto SEM con inmensa paciencia e infinitas conversaciones y alegría; i a la Montse, per tantes altres xerrades, riures i memes per afrontar el doctorat.

Al equipo Mimetis, gracias, en especial a David y Yassine, por confiar en mí para esta pequeña aventura y porque me habéis ayudado a seguir al pie del cañón en las arduas horas de escritura pudiendo compaginar horas en el lab que me han dado mucha vida.

I would like to thank Prof. Cecilia Persson for the opportunity of a very enriching experience at Uppsala University. Thanks for allowing my stay in Sweden, for giving me the opportunity to work in your group and very specially for teaching me how to do science significantly interesting ($p<0.01$). Thanks to all MiM group for immersing me in such broad intercultural experience. I would like to specially thank Viviana Lopes for her altruistic guidance with the biological testing. This Swedish experience has been really enriching in several facets. I have met old colleagues and made new ones. Thanks to Gemma and Sara, for helping me to feel a bit closer to home. Especialmente a Sara, mi cara, por cuidarme tanto y, con la ayuda de nuestras salidas por Vit D, mantener una vida social increíble. Gracias por mostrarme Uppsala, pero sobretodo, por darme luz durante el oscuro invierno sueco. Caroline and Daniel, you have been part of this Swedish family, a great part, with our dinners, cheering and philosophical talks, you have made my stay so easy, grateful and enlightening. Thanks for showing me the 'hidden' Swedish warmth. Natalie, Shirin, Sotiris, part of this family, thanks for keeping up my level of laughter at any time.

Vorrei ringraziare in modo particolare la Dr.ssa Gabriela Ciapetti, ti sarò sempre grata per l'opportunità che mi hai dato. Sei un grande esempio, sia a livello professionale che umano, grazie a te ho imparato cosa sia la passione per la biologia. Sei stata tanto generosa con me, e mi hai sempre fatto sentire a casa. Ringrazio il Prof. Baldini e tutto il gruppo di Patofisiologia per avermi dato l'opportunità di imparare cosa significhi fare del bene all'umanità grazie alla ricerca sull' osso e le sue malattie. Gemma, Elena, è stata una vera goia lavorare con voi, vi ringrazio per aver avuto pazienza con la mia incapacità di capire tanti concetti di biologia e per essere sempre state pronte a darmi una mano. Alle ragazze de Patofisiologia: Francesca, Fra, AnnaMaria, Silvia, Marghe, Sofia, tutte voi avete fatto del mio soggiorno un'esperienza indimenticabile. A tutto il personale del Rizzoli: purtroppo sapete che parlo troppo e, nonostante ciò, mi avete sempre ascoltato e avete riso con me, facendomi così sentire a casa. Vorrei aggiungere a questa esperienza bolognese Luna e Gianni, per essere stati il primo contatto con questa incredibile città e per aver condiviso con me l'amore per la bella Bologna e la bella vita. Bianca, per essere un vero cuore con gambe, per essere stata la mia famiglia assieme a Dana e Dario e per avermi insegnato ad essere una persona migliore. A tutti

un grazie anche per avermi aiutato con l'italiano, e per condividere con me la passione per questa bella lingua.

Mi familia, que me acompaña siempre, que me ayuda a sacar el velo del que a veces se cubre la vida, y mostrarme lo que verdaderamente importa con vuestras sonrisas. Porque hay dos palabras que conozco gracias a vosotros, especialmente a mis hermanos, amor incondicional.

Parte de mi familia: a mis amigos. No os nombro que seguro olvido a alguien, ya me conocéis. Gracias por estar ahí pese a las intermitencias y por estar siempre dispuestos a pasar buenos momentos.

Finally, you know I like to leave the best for the end. Victoria, thanks infinitely for being such a bright light. You have inspired and encouraged me to shape this thesis in my head even when I couldn't see how. Thanks for making futile things to be noise, for stopping time when I needed, for being always there.

A todos, habéis sido fuegos ardiendo con pasión durante este viaje. GRACIAS. MERCI. THANKS. GRAZIE. TACK

"Un hombre del pueblo de Neguá, en la costa de Colombia, pudo subir al alto cielo.
A la vuelta contó. Dijo que había contemplado desde arriba, la vida humana. Y dijo que somos un mar de fueguitos.
-El mundo es eso -reveló- un montón de gente, un mar de fueguitos.
Cada persona brilla con luz propia entre todas las demás.
No hay dos fuegos iguales. Hay fuegos grandes y fuegos chicos y fuegos de todos los colores. Hay gente de fuego sereno, que ni se entera del viento, y gente de fuego loco que llena el aire de chispas. Algunos fuegos, fuegos bobos, no alumbran ni queman; pero otros arden la vida con tanta pasión que no se puede mirarlos sin parpadear, y quien se acerca se enciende".
Eduardo Galeano

Scope and aim of the thesis

Despite the excellent osseointegration potential of CaP bone grafts, the major drawback for most apatitic formulations is their limited resorption rates. Consequently, CaPs remain at the bony site instead of being gradually replaced by new bone. It is fundamental to develop more interactive biomaterials, capable not only of replacing bone, but also of stimulating its regeneration. The process of bone regeneration is complex and involves many cell types operating simultaneously. Among them, there are cells of the immune and skeletal system. Inflammation, which is the first barrier faced by the implant, is often overlooked. Recently, the emerging field of osteoimmunology has shed light on the importance of the cross-talk between the immune and skeletal system in bone regeneration.

The present thesis focuses on boosting the limited regenerative potential of specific CaP formulations through different strategies: i) by modifying its physicochemical properties (by changing composition, microstructure, porosity, specific surface area, etc.); and ii) through grafting on the CaP surface extracellular matrix molecules, such as heparin, known for its anti-inflammatory, osteogenic, and osteoclastogenic effects. The materials are analyzed in terms of cell response, using cells of the immune and skeletal systems, to understand the contribution of these cell types in bone regeneration.

The specific objectives to achieve the aforementioned goals are:

<u>Objective 1:</u> Development of calcium phosphate bone grafts with different physicochemical properties to control the materials' degradation behavior and improve the biomimicry of bone.

- Development and characterization of calcium phosphates with different physicochemical properties in terms of microstructure, porosity, specific surface area, and composition. Assessment of the relative effect of each parameter on degradation under conditions similar to the osteoclastic resorption.

- Assessment of different routes for the incorporation of carbonate ions into calcium deficient hydroxyapatite through biomimetic and hydrothermal synthesis.

<u>Objective 2:</u> Functionalization of CaPs with heparin, present in the natural extracellular bone matrix to mimic cell microenvironment and the evaluation of the *in vitro* cell response to the modified CaPs, focusing on those cell types involved in the bone regeneration process:

- Immobilization of heparin on the surface of CaPs by different grafting procedures (physisorption and chemisorption) and characterization of the heparinized surfaces.

- Study of the immunomodulatory effects of heparin grafted surfaces in contact with inflammatory primary human cells.

- Study of the adhesion, proliferation and differentiation of rat mesenchymal stem cells on heparin functionalized CaPs.

- Study the effects of heparin on the osteoclastogenesis process, and on human osteoclast adhesion, proliferation and activity.

- Evaluation of the resorptive activity of osteoclasts on rough biomimetic CaP surfaces by focus ion beam–scanning electron microscopy.

Abbreviations

ACP	Amorphous calcium phosphate		**Mφ**	Macrophage
ATPase	Adenosintriphosphatase		**MCPA**	Monocalcium phosphate anhydrous
ALP	Alkaline phosphatase		**MCPM**	Monocalcium phosphate monohydrate
α-TCP	Alpha-tricalcium phosphate		**M-CSF**	Macrophage colony stimulating factor
APTES	(3-aminopropyl)triethoxysilane		**MIP**	Mercury intrusion porosimetry
ATR	Attenuated total reflectance		**MNC**	Mononuclear cells
BCP	Biphasic calcium phosphate		**MMP**	Matrix metalloproteinase
BET	Brunauer-Emmett-Teller		**MSC**	Mesenchymal stem cell
BMP	Bone morphogenetic protein		**NOS**	Nitric oxide synthase
BMU	Basic multicellular unit		**OB**	Osteoblast
BSP	Bone sialoprotein		**OC**	Osteoclast
β-TCP	Beta-tricalcium phosphate		**OCN**	Osteocalcin
CDHA	Calcium deficient hydroxyapatite		**OCP**	Octacalcium phosphate
CaP	Calcium phosphate		**ON**	Osteonectin
CathK	Cathepsin K		**OPG**	Osteoprotegerin
COLL	Collagen		**OPN**	Osteopontin
CPC	Calcium phosphate cement		**PBS**	Phosphate buffered saline
CPF	Calcium phosphate foam		**PG**	Proteoglycan
CSF	Colony stimulating factor		**PGE$_2$**	Prostaglandin E2
DBM	Demineralized bone matrix		**PMA**	Phorbol-12-myristate-13-acetate
DCPA	Dicalcium phosphate anhydrous		**PMNC**	Polymorphonuclear cells
DCPD	Dicalcium phosphate dihydrate		**PTFE**	Polytetrafluoroethylene
DNA	Deoxyribonucleic acid		**PTH**	Parathyroid hormone
ECM	Extracellular matrix		**RANK**	Receptor activator of nuclear factor κ B
FBGC	Foreign body giant cell		**RANKL**	RANK ligand
FBS	Fetal bovine serum		**RGD**	Arginylglycylaspartic acid
FGF	Fibroblast growth factor		**RNA**	Ribonucleic acid
FIB	Focus ion beam		**ROS**	Reactive oxygen species
FTIR	Fourier transform infrared spectroscopy		**RUNX2**	Runt-related transcription factor 2
GAG	Glycosaminoglycan		**TCPS**	Tissue culture polystyrene
GF	Growth factor		**TGF**	Transforming growth factor
HA	Hydroxyapatite		**TNF**	Tumor necrosis factor
IGF	Insulin-like growth factor		**SEM**	Scanning electron microscope
IL	Interleukin		**SSA**	Specific surface area
IL-1ra	Interleukin-1 receptor antagonist		**VEGF**	Vascular endothelial growth factor
LPS	Lipopolysaccharide		**XPS**	X-ray photoelectron spectroscopy
TRAP	Tartrate-resistant acid phosphatase		**XRD**	X-ray diffraction

Chapter 1

INTRODUCTION

Bone tissue is a complex organ which exerts different functions, such as mechanical support, protection of soft tissue, calcium and phosphate storage, and hematopoiesis among others.[1,2] Bone is one of the most transplanted tissues, and according to the World Health Organization (WHO), it is expected that musculoskeletal diseases arise as the fourth main cause of disability by the year 2020.[3] These data make relevant the importance of designing adequate bone substitutes capable of replacing or stimulating the regeneration potential of bone in the coming years.

The following sections will provide an overview of the basic concepts of bone, its hierarchy, features and remodeling processes in order to help understanding the necessity and the characteristics of biomaterials for bone regeneration.

1.1.   Bone composition

Bone is a composite material formed by a main inorganic component and an organic matrix. The inorganic part of bone consists of poorly crystalline hydroxyapatite, with a structure close to that of hydroxyapatite (HA, $Ca_{10}(PO_4)_6(OH)_2$), and accounts for approximately 70% in weight of its structure; the remaining 30% is constituted by collagen (90%) and non-collagenous structural proteins such as proteoglycans, sialoproteins, in addition to growth factors and cytokines. Bone also contains cells, such as osteoblasts, osteoclasts and osteocytes. Bone hydroxyapatite consists of nano-sized, plate-like crystals discrete and discontinuously located throughout the organic matrix. Hydroxyapatite has an open crystal structure which allows several ionic substitutions such as sodium, magnesium, fluoride or citrate, the most common being carbonate, which accounts for 4-8wt%.[4] Biological apatites are poorly crystalline since they contain several foreign ions, and non-stoichiometric, due to the presence of these ionic substitutions.[5] Depending on the type and amount of substitutions, the apatite reactivity and chemical behavior becomes altered. The HA crystal structure in bone is hexagonal since it allows the habit of foreign ions, whilst monoclinic, which is easily destabilized by ions, is more typical of high temperature apatites.

1.2.   Bone structure

The human skeleton has a total of 213 bones, which are classified in four main categories: long bones, short bones, flat bones and irregular bones. In an adult human skeleton, 80% of bone consists of cortical bone and 20% of trabecular. Cortical bone is dense and surrounds the marrow space, whereas trabecular bone has a honeycomb network interposed in the bone marrow compartment.[6] Bone is a highly hierarchical connective tissue. The sophisticated architecture of bone and the high organization level of the bone matrix not only account for its optimized mechanical performance,

but also provide the adequate niche for bone cells and bone marrow, and play a significant role in several biological pathways.

Weiner and Wagner[7] described extensively the hierarchy of bone and established seven levels from the nano to the macroscale (Figure 1-1). The hierarchical structure of bone is irregular yet highly oriented, making bone a heterogeneous and anisotropic composite material.[8] The smallest scale level corresponds to tropocollagen molecules, which form fibrils that are later mineralized and self-arrayed, contributing to bone's intrinsic toughness.[9,10] These collagen arrangements are called lamellae, which eventually wrap into concentric layers around a central canal called osteon or Harversian system. Osteons are around 200 to 250 µm in diameter and run parallel to the long axis of bone.[8] Bone hierarchy is responsible for its high mechanical performance, and specifically for its inherent capacity to arrest crack propagation.
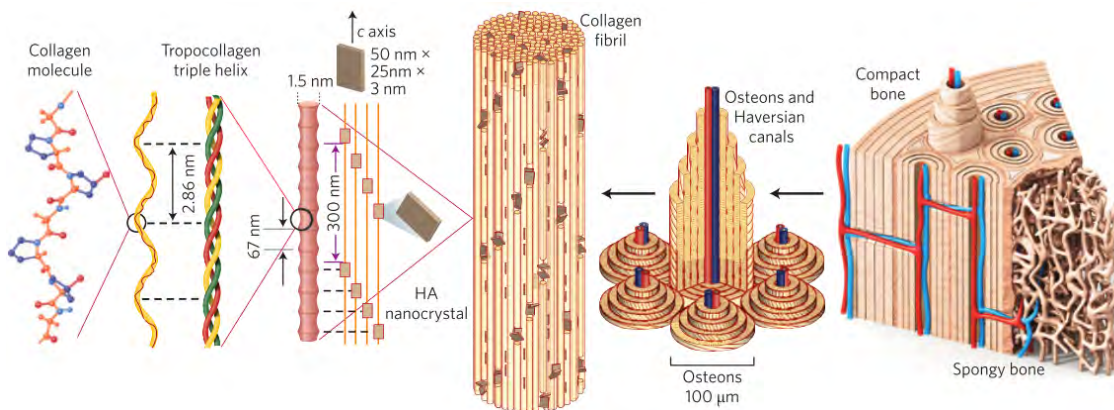
Figure 1-1. Hierarchical structure of bone.[11]

1.3. Bone biology

Bone is an active tissue and hosts several types of bone cells, mainly four subsets: osteoblasts (OB), osteoclasts (OC), osteocytes and bone lining cells. Osteoblasts, osteocytes and bone lining cells are originated from local osteoprogenitor cells, whilst osteoclasts are derived from the fusion of mononuclear precursors, from the monocyte-macrophage lineage.[12]

Bone lining cells are present at the bone surface and are usually inactive; they have often been named as osteoblasts precursors.[12] Oppositely, osteocytes are active cells which are located in the interior of the mineralized matrix. Osteocytes trapped in the bone matrix are the most abundant cells in bone and are active mechanosensors guiding both osteoblasts and osteoclasts activity during bone remodeling[13] due to an extended network of filopodia, connected through bone matrix canaliculi. Osteoblasts are derived from stromal cells and their main function is the deposition of collagen matrix and its mineralization. Oppositely, osteoclasts are bone-resorbing cells. They are able to resorb the extracellular bone matrix by generating an acidic environment to

dissolve the mineral phase of bone, and by secreting enzymes (matrix metalloproteinases, MMP) to degrade the organic matrix.

Each type of cell exerts different functions during bone remodeling by a tight cross-talk among them, based on a complex protein-protein receptor network. These biological mechanisms will be described in the following sections.

1.3.1. Bone remodeling

The remodeling of bone occurs lifelong by removing old bone from the skeleton and forming new bone, firstly described by Frost in 1990.[14] It is a key process during which the newly formed bone grows adjusting to the mechanical demands and the activity of the person while maintaining its structural integrity and metabolic functions.[14] The degree of remodeling of cortical bone ranges from 2 to 5% per year whilst trabecular bone is even more actively remodeled, up to 10%, due to the much larger surface to volume ratio.[13]

The bone remodeling process is complex and requires the interaction of many cells regulated by a wide range of biochemical and mechanical factors. Proteins and receptors in cells orchestrate the biochemical activities according to the microenvironmental stimuli. Remodeling can be divided in five phases: activation, resorption, reversal, formation, and mineralization; although, some authors described it as a four step process regarding fracture repair.[15] The remodeling process starts in small packets of cells called basic multicellular unit (BMU) in which activation is controlled by paracrine factors (parathyroid hormone, PTH) present in the bone microenvironment. Both osteoclasts and osteoblasts have a synergistic activity within the BMU. The first event occurring is the activation and consequent resorption by transduction pathways established in the cross-talk of the cells in the BMU,[16] as depicted in Figure 1-2.

Paracrine signals such as PTH are responsible for activating the crosstalk by binding to receptors in pre-osteoblasts that secrete other proteins signaling for instance osteoclasts differentiation and hence starting resorption. Transition signals are generated halting bone resorption and stimulating the bone formation process.[17] At the termination step, expression of molecules such as sclerostin bind to osteoblasts and bone formation ceases. The balance between resorption and formation is influenced by several factors as genetic, mechanical, vascular, nutritional, hormonal and local.[18] Other mediator proteins participate in bone remodeling, such as bone morphogenetic proteins (BMP), endothelial growth factor (VEGF), transforming growth factor (TGF), fibroblast growth factor (FGF), and insulin-like growth factors (IGF)[18–20] driving the remodeling response.
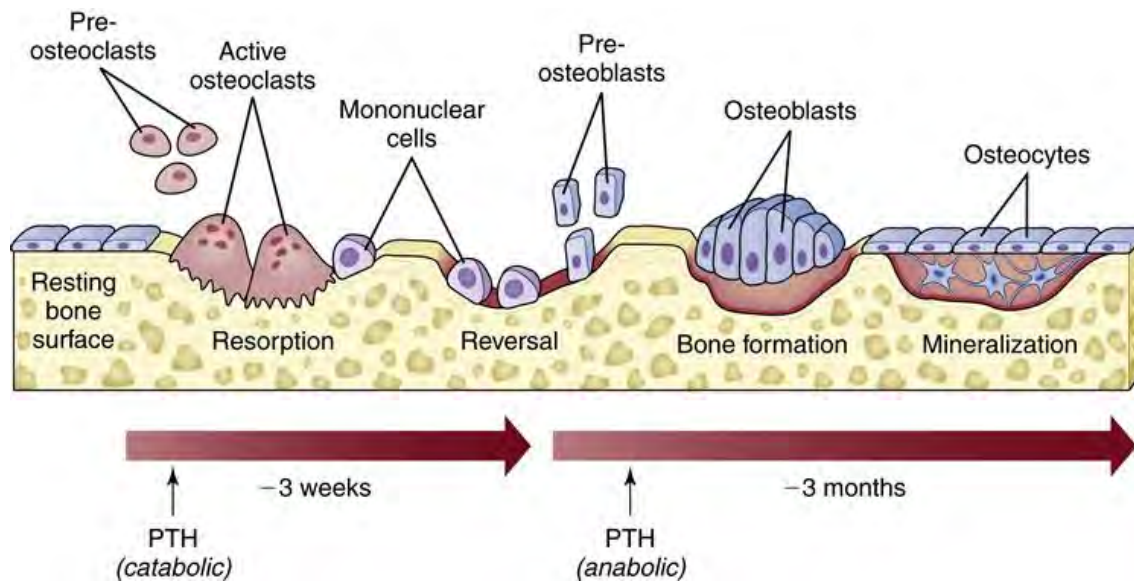
Figure 1-2. Schematic representation of a BMU and the associated bone remodeling process.[21]

Bone remodeling is of major importance during healing. Any injury starts with the formation of a clot of platelets and blood cells which recruit inflammatory cells from the immune system to resolve a wound. Eventually, this clot transforms into a ECM-hematoma,[22] which signals the following revascularization at the injured site by means of several interleukins, specific cytokine-proteins influencing immune pathways, and further recruits stem cells to promote the formation of soft callus, which finally is mineralized.[23]

As depicted, several orchestrators play a role during the complex bone remodeling process. Hence, it is crucial to understand each stage of the process to overcome the different necessities during, for instance, a biomaterial implantation. Bone grafting is leading to an injury which triggers different biological cascades. Implants interact with host tissue, for instance bone, and can integrate in it. The extent of this integration is tightly linked to the characteristics of the implant material. In order to understand the potential interactions triggered upon an exogenous material implantation, the following sections describe the main actors orchestrating the bone remodeling process.

1.3.1.1. Bone microenvironment: The role of the extracellular matrix in bone remodeling

As described in Section 1.1, the extracellular matrix (ECM) of bone consists mainly of secreted products of many cell types that form an organized scaffold for cell support. The main structural component is mineralized collagen. However, it contains also other molecules like laminins or proteoglycans (PGs) among others, with a 3D insoluble ultrastructure. Many of the proteins contained in the ECM are glycosylated, partially due to the presence of glycosaminoglycans (GAG). GAGs which are present in the ECM assembled into PGs through a core protein, are long negatively charged

heteropolysaccharides that occupy large areas providing many sites for interaction with various molecules such as growth factors or cytokines.[24,25] Since all cell types are in close contact with the ECM, they benefit from the high affinity of GAGs for GFs. It is widely accepted that the ECM can integrate and deliver multiple signals to cells through the release of GFs upon ECM degradation or by the degradation of GAGs.[25–27] Additionally, GFs can also bind to ECM by GAG-mediated interactions through specific protein domains and membrane proteins acting on cells.[23,28] In fact, the microenvironment that the ECM creates is fundamental for cells as most interactions of cells and proteins are mediated by the ECM components. All the functions associated to the ECM have been summarized in Figure 1-3.
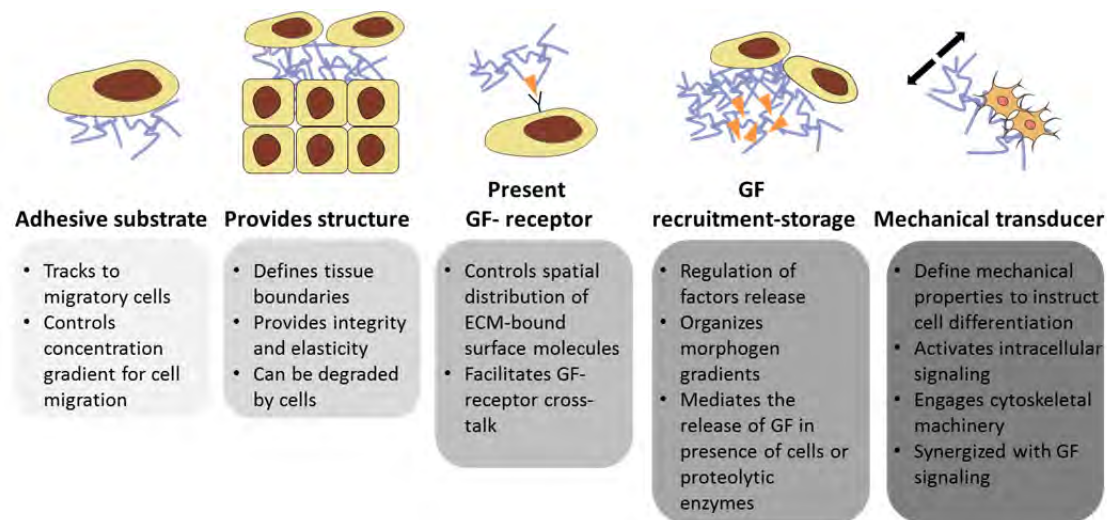
Figure 1-3. Main functions of the ECM and its influence in biochemical and mechanical processes, adapted.[26]

1.3.1.2.   Inflammation

Inflammation is necessary to different extents during bone remodeling. Any injured site in bone and in any other tissue undergoes inflammation. Thus, a fracture or a bone replacement will both be raising an injury. Upon injury, exudation of proteins, fluids and blood cells occur at the injured site[29,30] leading to inflammation. Immune cells arriving at the injured site are responsible for degrading and phagocytizing any pathogen or injured tissue, as well as signaling the pathways for cells to resolve inflammation and restore tissue. Leukocytes, connective tissue cells and extracellular matrix components are the main factors regulating the chemical signaling to resolve inflammation. Initially, a provisional matrix is formed consisting mainly of fibrin which furnishes structural and biochemical components to the process of wound healing.[29] Neutrophils and monocytes, intravascular cells, arrive at this provisional network and release chemotactic factors over different time periods activating in turn, different cell functions. The first released chemical factors are reactive oxygen and nitrogen species (ROS and NOS, respectively)[31] which generate oxidative stresses

into the microenvironment. ROS levels dictate the effect on cellular mechanisms; high concentrations are deleterious to cells due to their oxidizing effect on cell proteins, lipids and DNA. Low ROS concentrations instead, function as signaling molecules for cell growth, adhesion, differentiation and apoptosis.

Neutrophils are short-life cells and undergo apoptosis within hours or few days. On the contrary, when monocytes adhere to tissue, they transform into different types of macrophages depending of the microenvironment stimuli. According to these stimuli, macrophages release cytokines[32–35] to help address healing by signaling other cell types such as fibroblast, endothelial, and mesenchymal cells. Even though inflammation is necessary to start healing, an overexposure to inflammatory signals can lead to fibrotic tissue encapsulation by chronic inflammation and tissue granulation. Thus, a balance between pro-inflammatory and pro-healing cytokines is fundamental as depicted from Figure 1-4.
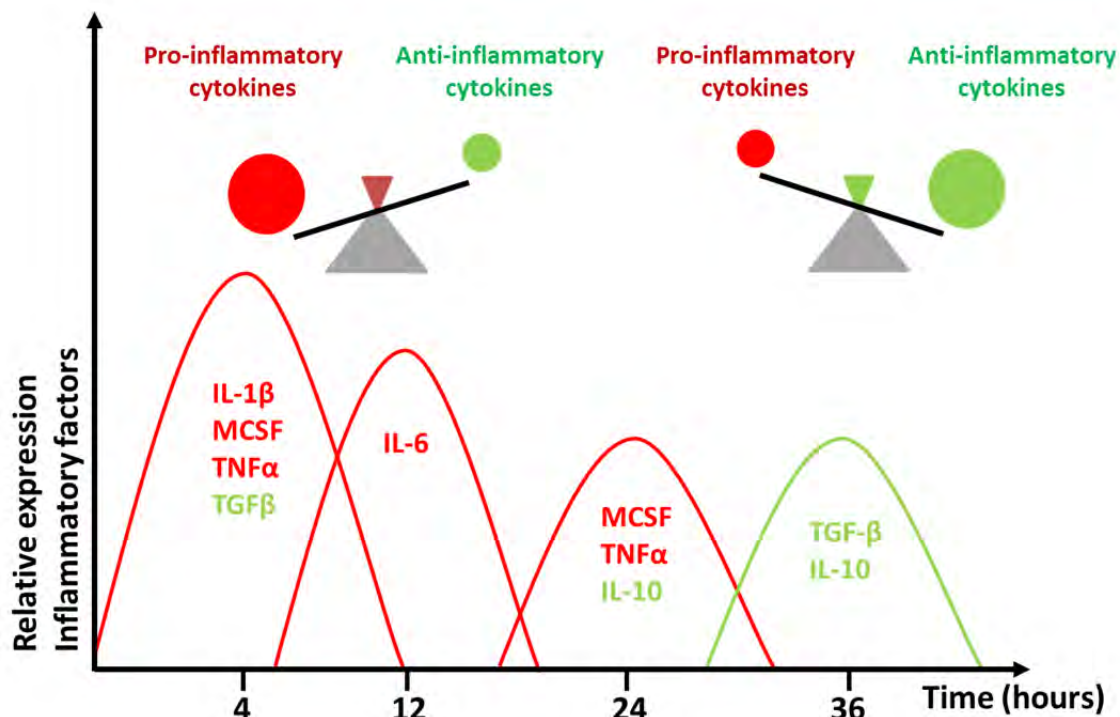
Figure 1-4. Peak expression of cytokines over time during inflammation, adapted.[36]

Macrophages assume diverse and context dependent phenotypes (known as macrophage polarization) between pro-inflammatory and anti-inflammatory phenotypes, as summarized in Figure 1-5. They are classified as M1 and M2, according to their pro- or anti-inflammatory phenotypes, respectively.[37] The early stage of the healing process is dominated by the pro-inflammatory M1 phenotype where cytokines such as tumor necrosis factor alpha (TNF-α) or interleukin 1 beta (IL-1β) are released.[38] In an ideal scenario after the first hours, M1 cytokines would be down-regulated by the release of anti-inflammatory cytokines such as IL-10, IL-4, IL-

13 or TGF-β restraining inflammation and initiating tissue repair.[39] This tight interrelation between the immune and the skeletal system has led to a new emerging field called osteoimmunology that seeks to understand and benefit from the tight crosstalk between both systems.

As depicted, both the immune and skeletal system share several regulatory, signaling molecules and transcription factors which modulate their crosstalk. Leukocytes and macrophages release proteins which can activate for instance osteoclast maturation, such as IL-1, IL-6 and TNF (osteolytic cytokines) or RANKL[40] or promote osteogenesis by the regulation of BMP.[41] Understanding the different pathways established between both cell lineage is crucial to develop more integrating materials. An adequate inflammatory response is a requisite of successful bone repair since it is also coupled with coagulation and angiogenesis, which are also requisite for cells survival.
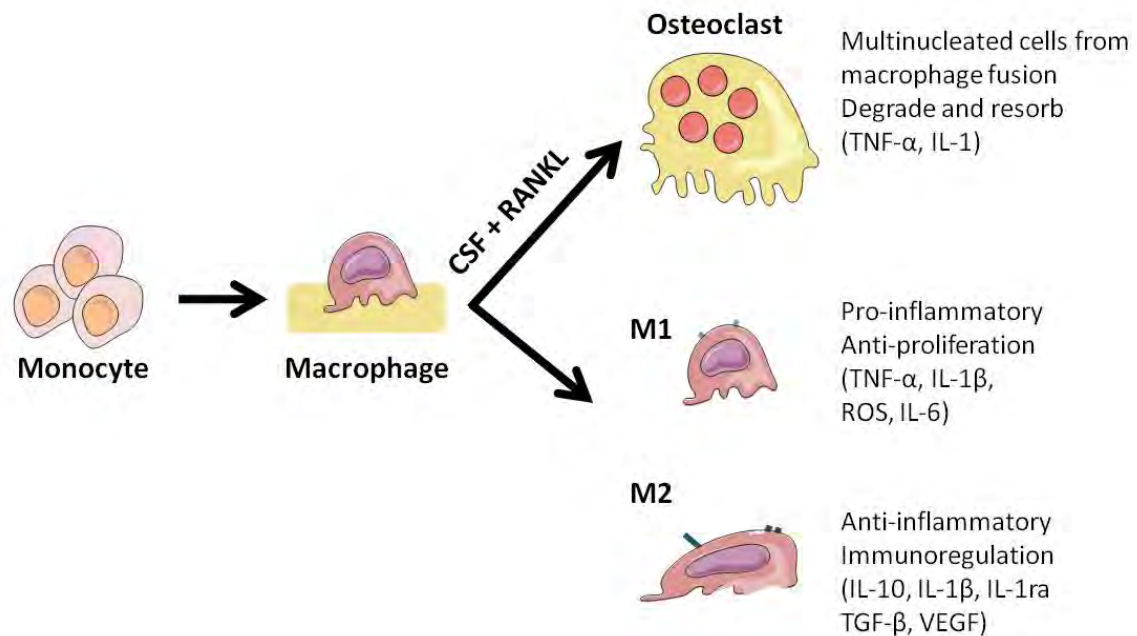
Figure 1-5. Macrophage polarization and their function and cytokines released, adapted.[32,42]

1.3.1.3. Osteoclastogenesis

Osteoclasts are responsible for bone resorption. They can degrade both the inorganic phase of bone by releasing acidic species, i.e. protons, and the organic phase through specific enzymes that degrade the organic components.

Osteoclasts are multinucleated cells formed by fusion of cells of the monocyte-macrophage lineage upon stimulation with proteins. These proteins are often secreted by bone marrow stromal cells or cells of the osteoblastic lineage.[43] Macrophage colony-stimulating factor (M-CSF), receptor activator of nuclear factor kappa B (RANK), RANK ligand (RANKL), and osteoprotegerin (OPG) are secreted by

osteoblasts or stromal cells and regulate osteoclast activity in what is known as the RANK/RANKL/OPG pathway. Specifically, RANK-RANKL interactions lead to osteoclast maturation, while OPG is a decoy receptor inhibiting RANK-RANKL interactions, as shown in Figure 1-6. Other environmental stimuli can foster osteoclast formation such as PTH, prostaglandin E (PGE_2), vitamin D, or cytokines such as interleukin 11 (IL-11) or tumor necrosis factor alpha (TNF-α).[43–45]
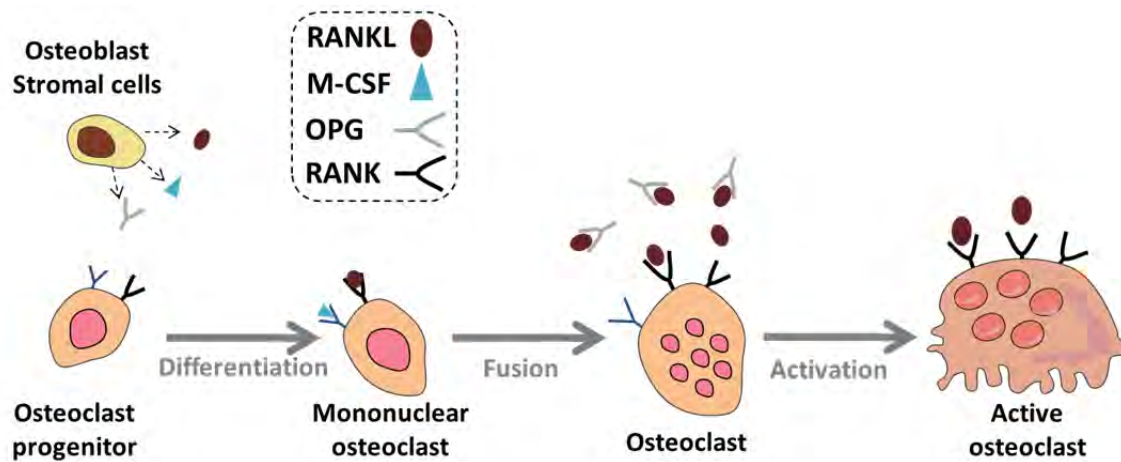
Figure 1-6. Osteoclast differentiation and activation, adapted.[12]

As previously mentioned, osteoclasts are derived from the monocyte-macrophage lineage. Monocytes belong to the immune system and can arrive to bone after an injury, where they become macrophages which have the potential to actively phagocytize pathogens. Fusion of macrophages under the stimulation with CSF and RANKL, among others, generates mature osteoclasts. In fact, during maturation, osteoclasts resemble foreign body giant cells (FBGC). Prior to bone resorption, osteoclasts attach to bone by polarizing their membrane forming a 'ruffled membrane' typical from this type of cells. Once attached and sealed by the ruffled membrane, osteoclasts transport acidifying vesicles to degrade bone. Thus, bone resorption by osteoclasts takes places under acidic conditions, normally at pH around 4.5. Adenosintriphosphatase (ATPase) and carbonic anhydrase are some of the proteases mediating this acidification which degrades bone mineral, whereas cathepsin K (CathK) and MMPs degrade the organic components of bone.[46,47]

1.3.1.4. Osteogenesis

There are two paths for bone formation both involving the transformation of a pre-existing connective tissue (mesenchyme) into bone tissue; intramembranous ossification occurs by direct conversion from mesenchyme to bone and takes place specifically in flat bones; endochondral ossification occurs by a cartilage intermediate which is later replaced by bone.[13]

The main actors during osteogenesis are osteoblasts, which are in charge of the secretion of the organic component of bone ECM and its subsequent mineralization. Osteoblasts differentiate from the mesenchyme; i.e. from mesenchymal stem cells (MSC). The microenvironment of MSC will dictate the differentiation into the bone lineage cells. Osteoblasts differentiation can be activated by different pathways, being the main regulators bone morphogenetic proteins (BMP), firstly identified by Urist in 1967. BMPs are members of the TGF-β superfamily and are known to be able to recruit immature cells and trigger their subsequent differentiation into the bone lineage.[19]

Fully differentiated osteoblasts are typically protein producing cells, both collagenous and non-collagenous proteins, and are responsible also for regulating the bone matrix mineralization. During OB maturation, typical genes are expressed which are associated to different events; proliferation, ECM development and maturation, and finally, mineralization. The first stage is related to the secretion of collagen type I (COLL1), alkaline phosphatase (ALP), osteopontin (OPN), bone sialoprotein (BSP), and RUNX2 that regulates osteocalcin (OCN), which is a later marker during the mineralization stage. The osteoblasts trapped in the ECM during mineralization will later become osteocytes, as shown in Figure 1-7, by down-regulation of ALP and COLL expression.
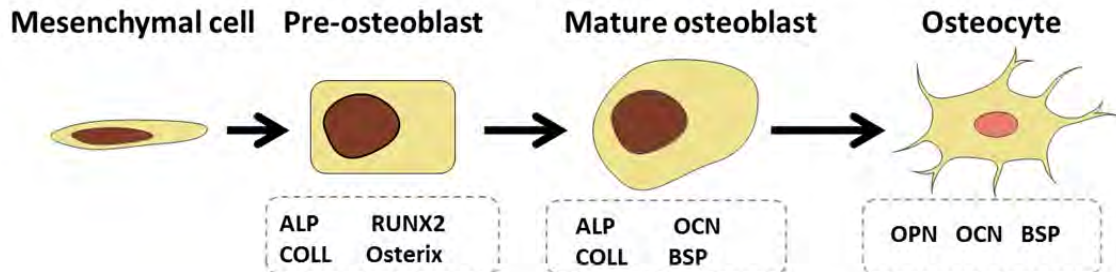
Figure 1-7. Differentiation of MSC into osteoblasts and osteocytes and the markers at each stage, adapted.[48]

1.4.   Synthetic bone grafts

Bone is the most commonly replaced tissue except for blood. Despite its natural self-healing ability, large bone defects or critically sized defects cannot heal by themselves and the need of bone grafts, either natural or synthetic, to replace or regenerate the damaged tissue is fundamental. Autografts harvested from the patient are known to be the gold standard; however, their low volume availability and associated morbidity limit their application.[49,50] Cadaveric allografts, demineralized bone matrix (DBM) or interspecies xenografts are also alternatives but they have also some limitations, such as the associated immunogenic response, risk of disease transmission, as well as cultural and ethical considerations.[51] For all these reasons, the use of synthetic bone

grafts represents a good alternative, although it is necessary to enhance their performance in order for them to be truly competitive with the autografts.

Synthetic bone graft must be biocompatible, and ideally, they should undergo remodeling and support new bone formation. However, it is difficult to have synthetic bone grafts combining all this features. Calcium phosphates (CaPs), owing to their close similarity to the mineral phase are good candidates for this application. However, the *in vivo* performance is uneven, depending not only on the composition but also on the processing route used for the synthesis, as described in the following sections.

1.4.1.   Calcium Phosphates

CaPs as already mentioned, have a composition similar to that of natural bone and possesses several of the required properties for optimal bone regeneration since they can be bioactive, resorbable, osteoconductive and osteoinductive[*].[52–56] However, the combination of all these properties into one material requires a tight control and a thorough understanding of the material and the biological site. Still now, this control is not easy and efficient enough.

CaPs can be considered as salts of orthophosphoric acid which can be obtained through several synthesis methods. The synthesis path usually dictates the final physicochemical properties of the compound. There exist eleven known CaPs with Ca/P molar ratio within 0.5 and 2.0. Four of them are obtained by solid state reactions at high temperature, and the rest through precipitation in aqueous environment by low temperature synthesis routes. Additionally to the Ca/P molar ratio, acidity/basicity and solubility are the parameters influencing mostly their physicochemical properties,[57] as depicted from Table 1-1. In general, the lower the Ca/P molar ratio is, the more acidic and water-soluble the calcium orthophosphate becomes.

---

[*]

Bioactive: the ability to form a bone-like apatite layer on implant surface in the living body.
Resorbable: the ability to degrade or be resorbed by surrounding tissues.
Osteoconductive: the provision of a scaffold for the growth of new bone cells on implant surface
Osteoinductive: the capacity of the implant to stimulate primitive, undifferentiated and pluripotent cells to develop into bone-forming lineage.

Table 1-1. Existing Calcium phosphates (CaP).[57]

Ca/P ratio	Compound	Chemical formula	Solubility[a]
0.5	Monocalcium phosphate monohydrate (MCPM)	$Ca(H_2PO_4)_2 \cdot 2H_2O$	~18
0.5	Monocalcium phosphate anhydrous (MCPA)	$Ca(H_2PO_4)_2$	~17
1.0	Dicalcium phosphate dihydrate (DCPD)	$CaHPO_4 \cdot 2H_2O$	~0.088
1.0	Dicalcium phosphate anhydrous (DCPA)	$CaHPO_4$	~0.048
1.33	Octacalcium phosphate (OCP)	$Ca_8(HPO_4)_2 (PO_4)_4 \cdot 5H_2O$	~0.0081
1.5	α-Tricalcium phosphate (α-TCP)	$\alpha\text{-}Ca_3(PO4)_2$	~0.0025
1.5	β-Tricalcium phosphate (β-TCP)	$\beta\text{-}Ca_3(PO4)_2$	~0.0005
1.2-2.2	Amorphous calcium phosphate (ACP)	$Ca_XH_Y(PO_4)_Z \cdot nH_2O$	N.A.
1.5-1.67	Calcium-deficient hydroxyapatite (CDHA)	$Ca_{10-X}(HPO_4)_X(PO_4)_{6-X}(OH)_{2-X}$	~0.0094
1.67	Hydroxyapatite (HA)	$Ca_{10}(PO_4)_6(OH)_2$	~0.0003
2.0	Tetracalcium phosphate (TTCP)	$Ca_4(PO_4)_2O$	~0.0007

[a]Solubility in g/L in water at 25°C

1.4.2. High temperature CaPs

There are four of the eleven CaP salts which are obtained by solid state reaction at high temperatures. One of the most used as synthetic bone graft is tricalcium phosphate ($Ca_3(PO_4)_2$), which exhibits two allotropic forms (α-TCP and β-TCP, respectively). β-TCP is obtained by solid-state reaction of calcium and phosphate precursors, for instance through the following reaction (Equation 1)[58]:

$$2CaHPO_4 + CaCO_3 + heat \rightarrow Ca_3(PO_4)_2 + CO_2 \qquad \text{(Equation 1)}$$
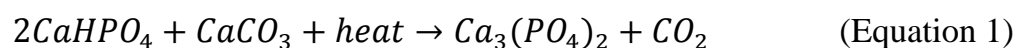
At temperature above 1125°C, β-TCP transforms to α-TCP, which is a metastable phase that in contact with water hydrolyses rapidly to calcium deficient hydroxyapatite (CDHA). Tetracalcium phosphate (TTCP) is the most basic salt, which possesses a higher solubility than HA. It can be obtained at temperatures above 1300°C by reaction of DCPA with calcium carbonate ($CaCO_3$). TTCP is not stable in water and hydrolyses rapidly to HA and calcium hydroxide ($Ca(OH)_2$).[59]

HA can be obtained both by solid state reaction at high temperature, and by precipitation in aqueous solutions at low temperature. The high temperature HA is obtained by solid-state reaction of other calcium phosphates (e.g., MCPM, DCPA, DCPD, OCP) with CaO, $Ca(OH)_2$, or $CaCO_3$ at temperatures above 1200 ºC.[57,60] The solubility of HA is the lowest among the listed CaPs in Table 1-1. Biphasic CaPs (BCP), traditionally mixtures of HA and β-TCP, combine a stable and poorly soluble phase like HA with the more soluble β-TCP, and can also be prepared by solid state

reaction. The properties of the resulting material lie in between each of the components. Due to the higher degradability of TCP, the reactivity of BCP increases with the increase in the TCP/HA ratio. Thus, *in vivo* bioresorbability of BCP can be controlled through phase composition.[61,62]

The microstructure of the high temperature CaPs is dependent on the sintering temperature and time. For instance, higher sintering temperatures result in lower specific surface area and lower porosity, but improved compression resistance.[61] Figure 1-8 shows the typical sintered microstructure of a BCP scaffold. Upon sintering, atoms diffuse across the boundaries of the particles fusing them together and forming sintering necks which lead to denser and smoother pieces.[63]

Biological apatites contain several ionic substitutions within the hydroxyapatite structure. Chemical modifications can be inserted in high temperature CaPs, generating different chemical behaviors, such as higher solubility or reactivity. Pietak *et al.* successfully incorporated silicon ions and proved its effect as an inhibitor of grain growth.[64] Several authors have focused their efforts in the production and characterization of high temperature doped CaPs with silicon, magnesium or carbonate.[65–70]
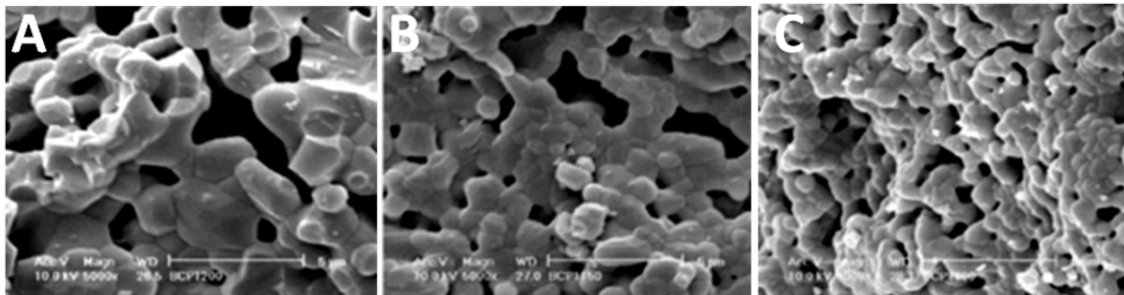
Figure 1-8. SEM images of a BCP scaffold obtained at different sintering temperatures: A: 1200; B: 1150, and C: 1100ºC. Lower sintering temperature results in an increase of micropores and a decrease in the crystal size.[71]

Macroporosity can also be incorporated in high temperature CaPs. Macropores are usually formed due to the release of volatile materials, i.e. the incorporation of pore-creating additives, so-called porogens. The ideal porogen should be non-toxic and, in the case of sintered ceramics, should be finally volatilized upon sintering.[60] Porosity has been demonstrated to have a great effect on the resorbability of the material.[52,72]

1.4.3.   Low temperature CaPs

Monocalcium phosphate monohydrate (MCPM), monocalcium phosphate anhydrous (MCPA), octacalcium phosphate (OCP), dicalcium phosphate dihydrate (DCPD), dicalcium phosphate anhydrous (DCPA), amorphous calcium phosphate (ACP), and calcium deficient hydroxyapatite (CDHA) can all be produced by a precipitation

reaction in aqueous solutions at low temperature. However, some of them can also be obtained through high temperature methods.

The most relevant low temperature CaP for bone regeneration applications are those compounds found in the body (HA, OCP, ACP, and occasionally DCPD). MCPM and its anhydrous form MCPA (formed upon heating MCPM above 100°C), for instance, are the most acidic CaP and are not naturally found in the body. They are rarely employed as substitutes for bone replacement. Similarly, DCPD can be crystallized at low pH, pH <6.5, and transformed to the anhydrous counterpart (DCPA) at temperature above 80°C. Their minerals are called brushite and monetite, respectively. Oppositely to MCPM, DCPD is found biologically in pathological calcifications and is proposed as one of the intermediates in bone mineralization.[73] OCP is thought to be an unstable transient intermediate during precipitation of hydroxyapatite, and it is found as component in human dental and urinary calculi and plays a crucial role in *in vivo* formation of apatitic biominerals.[74,75] Analogously, ACP can be encountered as a transient phase during precipitation of CaPs in aqueous systems. Usually, it is described as the first phase appearing when precipitation occurs from high supersaturated solutions.[74] HA can also be synthesized at low temperature, mainly by precipitation, hydrothermal treatments or hydrolysis.

By far, the most interesting low temperature CaP is HA or its analogous CDHA due to their similarity both in structure and composition to the mineral phase of bone. Low temperature CDHA is not a stoichiometric compound, but a solid solution with the following formula: $Ca_{10-x}(PO_4)_{6-x}(HPO_4)_x(OH)_{2-x}$, (where x is between 0 and 1). Therefore, it has a Ca/P ratio between 1.67 and 1.5. CDHA is crystal structured like hydroxyapatite, but possesses cation vacancies (Ca^{2+}) and anion (OH^-) vacancies. Some of the sites occupied solely by phosphate anions in stoichiometric hydroxyapatite are substituted by hydrogen phosphate (HPO_4^{2-}) anions. It can be obtained by precipitation, with poor crystallinity and high specific surface area, which enhance their solubility compared to stoichiometric HA. Thermal decomposition of CDHA results in its transformation to β-TCP when the Ca/P ratio is 1.5, or to biphasic β-TCP/HA if the Ca/P lies between 1.5 and 1.67.

1.4.3.1. Calcium phosphate cements

Among the low temperature CaPs, calcium phosphate cements (CPC) stand as a very particular type of material that has generated great interest as bone grafts. CPC were discovered by Brown and Chow in the 1980s and LeGeros *et al.*[77,78] CPC are formed through a mixture of a calcium orthophosphate salts with a liquid phase, normally water or an aqueous solution, and forms a paste able to harden and set through a dissolution and precipitation process in physiological conditions. The most commonly

used CPCs are based on final products of hydroxyapatite or brushite, as shown in Figure 1-9.

One of the most exciting properties of CPCs consists of their ability to form an injectable paste that is able to self-set in physiological conditions. This enables them to be handled directly by clinicians and to be injected into bone cavities with minimal invasive surgery.[5] One of the first kinds of CPCs to be commercialized was the Constanz cement,[79] which consisted of a poorly crystalline carbonated apatite (dahllite). Upon implantation, cements have shown to resorb slowly, which causes the problematic of mismatch of the resorption rates accomplished naturally in bone. Great efforts have been put towards the development of these materials in an attempt to achieve better resorption rates, similar to those of bone, coupling bone formation with implant resorption.

Figure 1-9. Calcium phosphate cement formulations.[80]

Since cementitious reactions involve mixing a powder with a liquid phase, this simple reaction offers a wide range of tunable properties depending on the particle size of the reactants, liquid phase composition, liquid to powder ratio (L/P), setting environment, and setting time. CPCs are intrinsically porous due to the formation of an entangled network of crystals during precipitation, resulting in high specific surface areas that enhance bioactivity.[81] The use of starting powders with small particle sizes makes them more reactive and this favors the formation of many nuclei leading to the precipitation of a higher number of smaller crystals.[82] Cements also possess nanoporosity due to the voids in between crystals. Moreover, increasing the high liquid to powder ratio of the cement formulation leads to microstructures with a higher content of micropores caused by the higher distance between particles.[83]

Despite the intrinsic porous nature of CPCs –with pores in the nano- and micrometric ranges, they lack macroporosity, which is crucial for bone ingrowth and to spur resorbability. Similarly to the sintered materials, macroporosity can be easily obtained through the addition of non-toxic porogens[84] or by surfactants that allow creating and stabilizing foamed pastes.[82,85] All porosity levels achievable with CPCs are depicted in Figure 1-10.
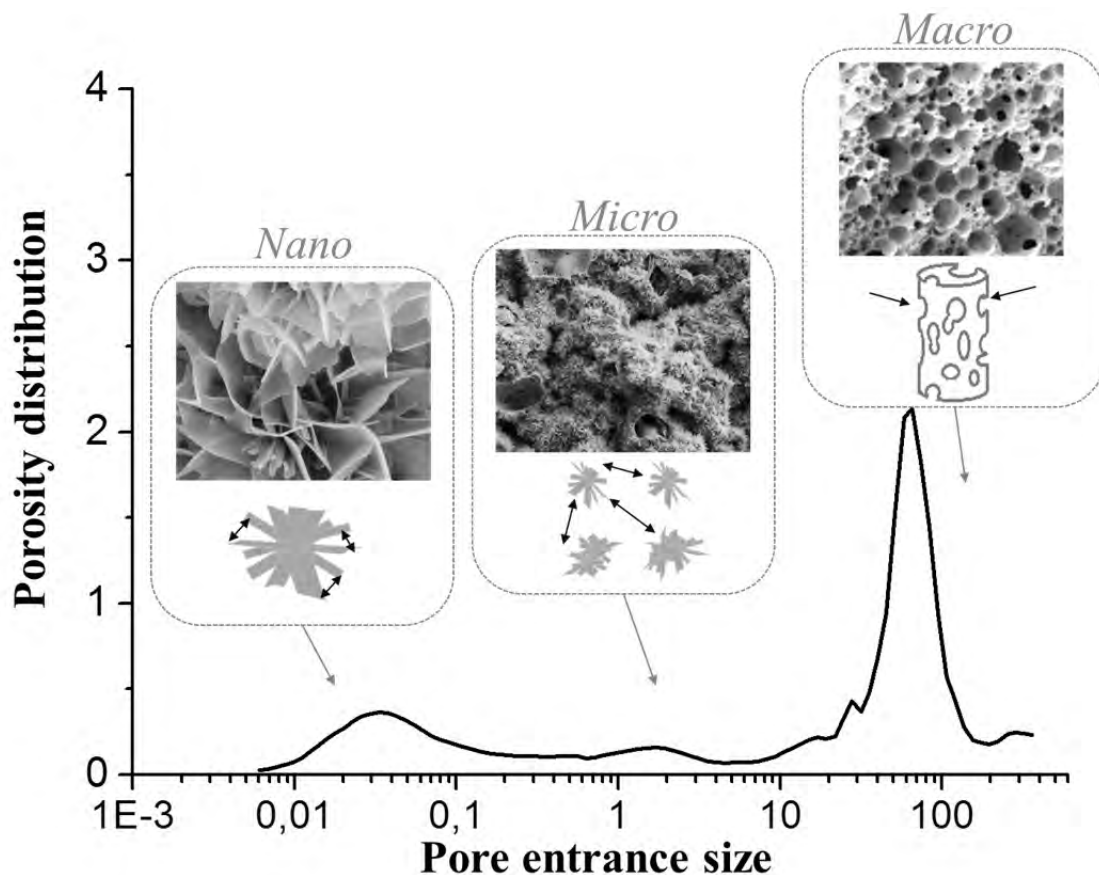
Figure 1-10. Pore entrance size distribution associated to the microstructure in macroporous CDHA CPC; a) crystal entanglement due to setting reaction, b) crystal agglomerated due to L/P ratio and c) macropores due to foaming process, adapted.[83]

17

As earlier mentioned, CDHA crystal structure allows many ionic substitutions. In order to further mimic biological apatite, CDHA can be synthesized incorporating the ion substitutions present in bone, such as carbonate, magnesium, strontium, etc. Carbonate represents the major natural ionic substitution, and carbonate ions can be placed both at phosphate and hydroxyl positions in the apatite lattice, named as B-type or A-type respectively. The B-type substitution is the most frequently found in biological apatites, together with charge compensation by a calcium vacancy, and with a hydrogen atom which bonds to a neighboring phosphate.[86]

Ionic substitutions have been shown not only to affect the physicochemical properties of CaP bone grafts materials, but also their biological performance which will be addressed in the following sections.

1.5. Biological performance of synthetic bone grafts

As previously mentioned, bone grafts, and particularly CaPs, have the great advantage of being recognized by the body since they have similar composition to that of natural mineral bone phase. When properly designed, CaPs can actively participate in the bone remodeling process. CaPs can foster new bone formation and are also susceptible to osteoclastic degradation, which makes them excellent candidates for bone regeneration. During bone remodeling, there is a tight synchronization between bone resorption and new bone formation that needs to be taken into account in the design of CaP materials. The balance between formation and resorption is complex, and as described earlier, there are several different actors guiding the process. The modulation of CaPs biological performance has been investigated by different authors who have described different routes to enhance the biomaterials output.[87,88]

It is of paramount importance to approach bone regeneration from a multidisciplinary view. It is necessary to understand the interaction of the different material properties (chemical, textural, mechanical, etc) with the surrounding cells, in order to identify the possible directions to enhance biomaterial's performance. In addition to chemical composition, microstructural properties, grain and crystal size, microporosity, surface roughness and specific surface area have also been proposed as crucial parameters controlling the biological response of biomaterials. An important property required in bone regeneration is osteoinduction. The ability of a material to induce osteogenic cell differentiation represents a clear advantage to integrate grafts into tissue.[89] Several authors have investigated chemical and textural properties of biomaterials, both *in vitro* and *in vivo*, in order to understand the biological reactions triggered by each feature.[90-92]

The following sections summarize the main strategies that researchers have adopted to modulate materials properties in views of improving their integration and facilitating bone remodeling.

1.5.1. Physical properties

Physical properties mainly concern textural properties such as roughness, topography, specific surface area and porosity. Biomaterial geometry and topography are crucial for cell attachment for instance. It has been shown that nanosized surface features can act as a direct physical trigger on MSC osteogenic differentiation, even without additional osteogenic supplements.[93,94] Importantly, high specific surface areas have been demonstrated to play a key role. High surface areas of low temperature CaP allows high adsorption and retention of important proteins for the chemical signaling, as depicted from the work of Espanol *et al.*[95]

Porosity also has a great influence on the success of biomaterials. Generally, the importance of pores is related to the invasion of the materials by blood vessels, therefore sustaining the metabolism of cells inside the scaffold.[96] Pore geometry has been pointed as crucial by Habibovic *et al.* demonstrating that bone formation was exclusively limited to the inside of concavities of pores which helped to entrap and concentrate proteins.[71] Parameters such as pore interconnectivity, pore geometry, strut topography and porosity, contribute to modulate the process of osteogenesis. Cell survival depends on nutrients and oxygen supply, hence the need of an interconnected pore network that allows for vasculogenesis.

Pore sizes are dictating the extent of bone formation (Table 1-2). It is known that pore sizes above 100µm in solid ceramics boost their potential to allow angiogenesis and bone growth *in vivo*.[97] Additionally, smaller pore sizes allow interactions with proteins and cells, as well as hosting secretory matrix which provide promoting factors such as BMPs. In sintered CaP ceramics, a decrease in sintering temperature while keeping composition constant, leads to an increase in the number of micropores, which enhanced biological response, and specifically the osteoinductive potential.[98] Similarly, Fellah *et al.* demonstrated that an increased microporosity and specific surface area were beneficial for the amount of bone formed in a study in critical-sized femoral defects in goats.[99] However, higher porosities lead to decreased mechanical strength restricting their application to light load bearing sites.

Table 1-2.Biological implications of the different pore sizes in 3D scaffolds.[100]

Pore size of a 3D scaffold	Biochemical effect or function
<1 μm	Interaction with proteins Responsible for bioactivity
1-20 μm	Type of cells attracted Cellular development Orientation and directionality of cellular ingrowth
100-1000 μm	Cellular growth Bone ingrowth Predominant function in the mechanical strength
>1000 μm	Implant functionality Implant shape

1.5.2. Chemical properties

Besides the effect that the physical properties of CaPs have on cell behavior, changes in the materials' composition can also be used to guide the biological behavior. The most common strategies to modify CaP composition is to combine soluble CaPs phases to improve the remodeling capacity of the material, to dope the CaPs with key ions to regulate specific biological cascades,[104] and to alter the surface charge of the material to selectively adsorb certain proteins and modulate cell response.

Biphasic CaP mixtures combining phases with different chemical reactivity or solubility is a common strategy to improve the biological performance of scaffolds. Several authors have investigated the effect of more soluble phases such as brushite or monetite[103–105] and the combination of HA with β-TCP.[62,106] Gisep *et al.* showed that biphasic cements resorb faster than monophasic ones.[107] However, resorbability often restricts the structural integrity of scaffolds, so a balanced compromise between biological and mechanical properties is mandatory for successful bone grafts. In addition to improve resorption, the liberation of calcium and phosphate ions from the material into the surroundings may increase the local supersaturation of the biological fluid, causing precipitation of carbonated apatite while also entrapping important proteins such as BMPs.[71]

Doping CaPs with specific ions can also be used to influence cellular signaling and improve bone remodeling. The release of ions upon dissolution of the scaffold can trigger different cell behavior. Boanini *et al.* reviewed the effect of ionic substitutions in low temperature CaPs with respect to their cellular response.[102] Carbonate doping of apatites was shown to distort the crystal lattice increasing resorbability compared to stoichiometric HA and also to promote osteoclastic activity. Landi *et al.* achieved higher osteoconductive properties and increased the quantity of newly formed bone on carbonated HA compared to HA.[108] Spence *et al.* found enhanced osteoclastic

mediated resorption for carbonated HA, which was further triggered by the amount of carbonate in the HA structure,[109] and used it as a tool to boost the poor resorption of synthetic HA.

Silicon doped HA have also shown improved bioactivity by stabilizing amorphous CaPs and fostering dissolution.[68] Cardenas *et al.* studied the *in vitro* cell response to α-TCP-based cement containing calcium silicates and showed improved osteogenic response.[110] Strontium substituted CaPs have been shown to stimulate bone formation and hamper osteoclastic proliferation.[111] Landi *et al.* demonstrated an enhancement of osteoconduction and resorption rate of magnesium-doped HA compared to control stoichiometric HA.[112] Webster *et al.* also studied the osteoblast response to trivalent and divalent doped HA such as bismuth or zinc and magnesium.[113] Interestingly, they found that bismuth doped HA could enhance osteoblast mineral deposition for longer time than divalent cations. Zinc has also been successfully incorporated to CaP structures. This element is an essential trace element acting as cofactor for numerous enzymes, including DNA and RNA replication and protein synthesis.[114]

A different way of guiding cell behavior through compositional modification is by modifying the surface charge of the materials. The works of Yamashita and Nakamura *et al.* proved an accelerated bone growth on negatively charged surfaces compared to positively charged HA.[115,116] In general, the surface charge of CaP varies depending on the synthesis method and this causes differences in the electrostatic interactions with the surrounding environment influencing cell behavior. According to their charge, biomaterials interact differently with proteins driving different cell responses.[117–119]

To further engineer the biomaterials surface, a rather widely spread strategy is through grafting of organic motifs present in ECM or in cell microenvironment on the biomaterials surface. This strategy has been shown to greatly modulate biological responses as will be shown in the following section.

1.5.3.   Functionalization with biomolecules

The functionalization of materials with specific biomolecules has attracted great scientific interest as an alternative way to tune the biological response to biomaterials. During the last decades, this strategy has been exploited in different applications, such as engineered platforms for cell proliferation and differentiation or drug delivery systems for controlled release of molecules, such as antibiotics, proving effective in enhancing the bone regeneration process.[23,80,120–123]

A vast range of molecules have been explored for immobilization on materials surface. Special attention has been paid to GF, and specifically to BMPs, as they are known to foster the osteogenic response,[20,124,125] and VEGF, which improves blood vessels generation or angiogenesis. Also short peptide sequences with specific functions have

been explored, such as RGD, which is a cell adhesion motif able to interact with integrins. However, both peptides and proteins have several drawbacks still to overcome. Proteins can easily be denaturalized, hence losing their conformation and biological activity. On the contrary, peptides possess higher stability to pH and temperature changes than proteins, but they are less efficient than proteins and their enzymatic stability *in vivo* is often too low.

However, since growth factors are naturally occurring in the body, an alternative strategy is also possible based on the recruitment of these naturally occurring proteins without the need of grafting them on the surface of the biomaterial.[123–130] The functionalization of CaP with molecules able to attract GF represents a smart strategy to overcome the drawbacks of proteins and peptides.

An interesting molecule ubiquitous in the body and present in several transduction pathways is the family of glycosaminoglycans (GAGs). As previously mentioned, GAGs are present in the stem cells niche and in the extracellular matrix and have great affinity for proteins and GFs.[131–133] They can bind to core proteins to form proteoglycans (PG) or to other proteins and cell receptors.[131]

Salbach *et al.* pointed at the potential of GAGs to enhance the regenerative properties of biomaterials,[134] due to the wide range of interactions they can exert with different cell lineages such as endothelial and fibroblast cells, skeletal, and immune system cells.[131,135,136] The GAGs family includes hyaluronic acid, chondroitin, heparan and keratin sulphates, and heparin, which is the most sulfated GAG. The sulfonation degree of GAGs has been demonstrated to affect their binding affinity with proteins.[137–141] Unlike peptides that often bind GFs via specific molecular recognition, heparin can bind numerous GF target via less specific electrostatic interactions by virtue of the negatively charged sulfate and carboxylate groups on their constituent GAG chains. Although heparin has been used for decades as anticoagulant due to its capacity to bind antithrombin, its regenerative potential is nowadays attracting much attention.

Indeed, GAGs are able to interact directly with BMP and interleukins, influencing osteogenesis, osteoclastogenesis and the immune system, as shown in recent works.[142–145] Despite the potential of GAGs, their biological activity has been mainly studied on organic materials such as the collagen matrix and polymers, or by direct supplementation on the cell culture media.[137,146] Salbach, Hempel and Hintze *et al.* focused their works on unraveling the mechanisms of the interactions between GAGs and proteins involved in osteogenesis, mainly BMP-2, BMP-4, sclerostin-Wnt, and TGF-β.[137,139,140,147–149] Edlund *et al.* covalently functionalized heparin and BMP-2 on resorbable polymers, showing enhanced bioactivity, growth and proliferation of MSC.[122] Among the limited works performed on CaPs, pro-angiogenic GF combined

with heparin was used by Lode *et al.* for the sustained release of VEGF from CaP cements.[150] Gittens *et al.* instead, investigated the feasibility of anchoring heparin on HA for drug delivery purposes and proved an increased affinity of b-FGF and BMP-2 on the heparin modified HA.[128] In the study by Goonasekera *et al.*, it was proved that the mechanisms of heparin anchoring to HA affected its interaction with BMP-2 and therefore its release profile.[151]

In the above-mentioned studies, the purpose of combining GAGs with CaP substrates were clearly focused towards addressing the release of pre-loaded GF in views of improving the bone regenerative potential of CaPs. However, the strategy of using GAGs to sequester endogenous GF had so far not been reported for CaPs.
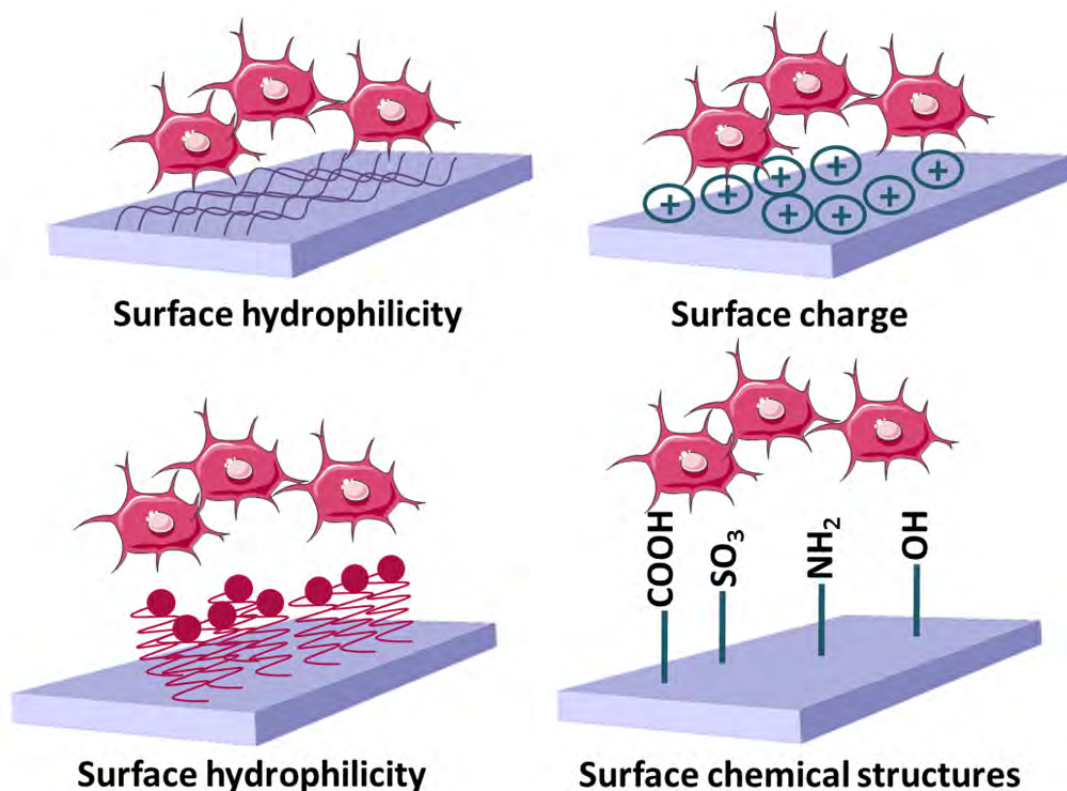
Figure 1-11. Surface interactions between biomaterials and cells; adapted.[152]

The present thesis seeks to exploit different strategies to improve the regenerative potential of CaPs bone grafts either through chemical or physical modification of the CaPs, as depicted in Figure 1-11. Particular attention will be paid to characterize the material's response at different stages of the bone healing process using cells of the immune and skeletal systems to better understand and predict the in vivo behavior.

1.6.   REFERENCES

[1]   R. Florencio-Silva, G.R. da S. Sasso, E. Sasso-Cerri, M.J. Simões, P.S.S. Cerri, P.S.S. Cerri, rgio, Biology of Bone Tissue: Structure, Function, and Factors That Influence Bone Cells., Biomed Res. Int. **2015** (2015) 421746.

[2]   A.G. Robling, A.B. Castillo, C.H. Turner, Biomechanical and molecular regulation of bone remodeling, Annu. Rev. Biomed. Eng. **8** (2006) 455–498.

[3]   World Health Organization, Scientific group on the assessment of osteoporosis at primary health, **2004**.

[4]   A. Bigi, G. Cojazzi, S. Panzavolta, A. Ripamonti, N. Roveri, M. Romanello, K. Noris Suarez, L. Moro, Chemical and structural characterization of the mineral phase from cortical and trabecular bone, J. Inorg. Biochem. **68** (1997) 45–51.

[5]   M. Vallet-Regi, Calcium phosphates as substitution of bone tissues, Prog. Solid State Chem. **32** (2004) 1–31.

[6]   B. Clarke, Normal bone anatomy and physiology., Clin. J. Am. Soc. Nephrol. **3** Suppl 3 (2008) S131–9.

[7]   S. Weiner, H.D. Wagner, THE MATERIAL BONE: Structure-Mechanical Function Relations, Annu. Rev. Mater. Sci. **28** (1998) 271–298.

[8]   J.-Y. Rho, L. Kuhn-Spearing, P. Zioupos, Mechanical properties and the hierarchical structure of bone, Med. Eng. Phys. **20** (1998) 92–102.

[9]   R.O. Ritchie, The conflicts between strength and toughness., Nat. Mater. **10** (2011) 817–22.

[10]   M.E. Launey, M.J. Buehler, R.O. Ritchie, On the Mechanistic Origins of Toughness in Bone, Annu. Rev. Mater. Res. **40** (2010) 25–53.

[11]   U.G.K. Wegst, H. Bai, E. Saiz, A.P. Tomsia, R.O. Ritchie, C. Ortiz, M. Boyce, U.G.K. Wegst, H. Bai, E. Saiz, A.P. Tomsia, R.O. Ritchie, Bioinspired structural materials, Nat. Mater. **14** (2014) 23–36.

[12]   R.C.& R.G. Bilezikian JP, Principles of Bone Biology, Second, Academic Press, **2001**.

[13]   U. Kini, B.N. Nandeesh, Radionuclide and Hybrid Bone Imaging, Springer Berlin Heidelberg, Berlin, Heidelberg, **2012**.

[14]   H.M. Frost, Skeletal structural adaptations to mechanical usage (SATMU): 1. Redefining Wolff's law: the bone modeling problem., Anat. Rec. **226** (1990) 403–13.

[15]   A. Schindeler, M.M. McDonald, P. Bokko, D.G. Little, Bone remodeling during fracture repair: The cellular picture., Semin. Cell Dev. Biol. **19** (2008) 459–66.

[16]   L.J. Raggatt, N.C. Partridge, Cellular and molecular mechanisms of bone remodeling., J. Biol. Chem. **285** (2010) 25103–8.

[17]   P.A. Hill, M. Orth, Bone Remodelling, Br. J. Orthod. **25** (1998) 101–107.

[18]   D.J. Hadjidakis, I.I. Androulakis, Bone remodeling., Ann. N. Y. Acad. Sci. **1092** (2006) 385–96.

[19]   J.M. Wozney, V. Rosen, A.J. Celeste, L.M. Mitsock, M.J. Whitters, R.W. Kriz, R.M. Hewick, E.A. Wang, Novel regulators of bone formation: molecular clones and activities., Science. **242** (1988) 1528–34.

[20]   E. Verron, J.M. Bouler, J. Guicheux, Controlling the biological function of calcium phosphate bone substitutes with drugs., Acta Biomater. **8** (2012) 3541–51.

[21]   A.K. Garg, Implant dentistry : a practical approach, Mosby/Elsevier, **2010**.

[22]   J. Street, D. Winter, J.H. Wang, A. Wakai, A. McGuinness, H.P. Redmond, Is human fracture hematoma inherently angiogenic?, Clin. Orthop. Relat. Res. Sep (**2000**) 224–37.

[23]   M. Mehta, K. Schmidt-Bleek, G.N. Duda, D.J. Mooney, Biomaterial delivery of morphogens to mimic the natural healing cascade in bone ☆, Adv. Drug Deliv. Rev. **64** (2012) 1257–1276.

[24]   E. Hohenester, J. Engel, Domain structure and organisation in extracellular matrix proteins, Matrix Biol. **21** (2002) 115–128.

[25]   A.D. Theocharis, S.S. Skandalis, C. Gialeli, N.K. Karamanos, Extracellular matrix structure, Adv. Drug Deliv. Rev. **97** (2016) 4–27.

[26]   T. Rozario, D.W. DeSimone, The extracellular matrix in development and morphogenesis: A dynamic view, Dev. Biol. **341** (2010) 126–140.

[27]   R.O. Hynes, The extracellular matrix: not just pretty fibrils., Science. **326** (2009) 1216–9.

[28] L. Sorokin, The impact of the extracellular matrix on inflammation, Nat. Rev. Immunol. **10** (2010) 712–723.

[29] J.M. Anderson, Biological responses to biomaterials, Annu. Rev. Mater. Res. **31** (2001) 81–110.

[30] J.M. Anderson, A. Rodriguez, D.T. Chang, Foreign body reaction to biomaterials., Semin. Immunol. **20** (2008) 86–100.

[31] M. Mittal, M.R. Siddiqui, K. Tran, S.P. Reddy, A.B. Malik, Reactive Oxygen Species in Inflammation and Tissue Injury, Antioxid. Redox Signal. **20** (2014) 1126–1167.

[32] A. Mantovani, A. Sica, S. Sozzani, P. Allavena, A. Vecchi, M. Locati, The chemokine system in diverse forms of macrophage activation and polarization, Trends Immunol. **25** (2004) 677–86.

[33] A. Mantovani, S.K. Biswas, M.R. Galdiero, A. Sica, M. Locati, Macrophage plasticity and polarization in tissue repair and remodelling, J. Pathol. **229** (2013) 176–185.

[34] S. Gordon, Alternative activation of macrophages., Nat. Rev. Immunol. **3** (2003) 23–35.

[35] S. Gordon, F.O. Martinez, Alternative activation of macrophages: mechanism and functions., Immunity. **32** (2010) 593–604.

[36] K. Schmidt-Bleek, H. Schell, J. Lienau, N. Schulz, P. Hoff, M. Pfaff, G. Schmidt, C. Martin, C. Perka, F. Buttgereit, H.-D. Volk, G. Duda, Initial immune reaction and angiogenesis in bone healing, J. Tissue Eng. Regen. Med. **8** (2014) 120–130.

[37] D.M. Mosser, J.P. Edwards, Exploring the full spectrum of macrophage activation., Nat. Rev. Immunol. **8** (2008) 958–69. doi:10.1038/nri2448.

[38] N. Parameswaran, S. Patial, Tumor necrosis factor-α signaling in macrophages., Crit. Rev. Eukaryot. Gene Expr. **20** (2010) 87–103.

[39] Z. Chen, T. Klein, R.Z. Murray, R. Crawford, J. Chang, C. Wu, Y. Xiao, Osteoimmunomodulation for the development of advanced bone biomaterials, Mater. Today. **19** (2016) 304–321.

[40] H. Takayanagi, Osteoimmunology: shared mechanisms and crosstalk between the immune and bone systems, Nat. Rev. Immunol. **7** (2007) 292–304.

[41] Z. Chen, C. Wu, W. Gu, T. Klein, R. Crawford, Y. Xiao, Osteogenic differentiation of bone marrow MSCs by β-tricalcium phosphate stimulating macrophages via BMP2 signalling pathway, Biomaterials. **35** (2014) 1507–1518.

[42] R.J. Miron, D.D. Bosshardt, OsteoMacs: key players around bone biomaterials, Biomaterials. **82** (2015) 1–19.

[43] N. Udagawa, N. Takahashi, T. Akatsu, H. Tanaka, T. Sasaki, T. Nishiharat, T. Kogat, T.J. Martins, T. Suda, Origin of osteoclasts: Mature monocytes and macrophages are capable of differentiating into osteoclasts under a suitable microenvironment prepared by bone marrow-derived stromal cells, Cell Biol. **87** (1990) 7260–7264.

[44] S.L. Teitelbaum, Bone Resorption by Osteoclasts, Science (80-.). **289** (2000) 1504–1508.

[45] H.K. Väänänen, H. Zhao, M. Mulari, J.M. Halleen, The cell biology of osteoclast function, J Cell Sci. **113** (Pt 3 (2000) 377–381.

[46] Y.-P. Li, W. Chen, Y. Liang, E. Li, P. Stashenko, Atp6i-deficient mice exhibit severe osteopetrosis due to loss of osteoclast-mediated extracellular acidification, Nat. Genet. **23** (1999) 447–451.

[47] M. Gowen, F. Lazner, R. Dodds, R. Kapadia, J. Feild, M. Tavaria, I. Bertoncello, F. Drake, S. Zavarselk, I. Tellis, P. Hertzog, C. Debouck, I. Kola, Cathepsin K Knockout Mice Develop Osteopetrosis Due to a Deficit in Matrix Degradation but Not Demineralization, J. Bone Miner. Res. **14** (1999) 1654–1663.

[48] R.J. Miron, Y.F. Zhang, Osteoinduction: a review of old concepts with new standards., J. Dent. Res. **91** (2012) 736–44.

[49] A.L. Ladd, N.B. Pliam, Use of bone-graft substitutes in distal radius fractures., J. Am. Acad. Orthop. Surg. **7** (1999) 279–90.

[50] E.M. Younger, M.W. Chapman, Morbidity at bone graft donor sites., J. Orthop. Trauma. **3** (1989) 192–5.

[51] R.A. Bhatt, T.D. Rozental, Bone graft substitutes., Hand Clin. **28** (2012) 457–68.

[52] N. Miño-Fariña, F. Muñoz-Guzón, M. López-Peña, M.-P. Ginebra, S. Del Valle-Fresno, D.

Ayala, A. González-Cantalapiedra, Quantitative analysis of the resorption and osteoconduction of a macroporous calcium phosphate bone cement for the repair of a critical size defect in the femoral condyle., Vet. J. **179** (2009) 264–72.

[53] A. Ogose, T. Hotta, H. Kawashima, N. Kondo, W. Gu, T. Kamura, N. Endo, Comparison of hydroxyapatite and beta tricalcium phosphate as bone substitutes after excision of bone tumors, J. Biomed. Mater. Res. **72B** (2005) 94–101.

[54] C. Rey, C. Combes, C. Drouet, D. Grossin, Bioactive Ceramics: Physical Chemistry, Elsevier Ltd., **2011**.

[55] P. Ducheyne, Bioactive ceramics: the effect of surface reactivity on bone formation and bone cell function, Biomaterials. **20** (1999) 2287–2303..

[56] H. Yuan, H. Fernandes, P. Habibovic, J. de Boer, A.M.C. Barradas, A. de Ruiter, W.R. Walsh, C.A. van Blitterswijk, J.D. de Bruijn, Osteoinductive ceramics as a synthetic alternative to autologous bone grafting., Proc. Natl. Acad. Sci. U. S. A. **107** (2010) 13614–9..

[57] S. V. Dorozhkin, Calcium Orthophosphates in Nature, Biology and Medicine, Materials (Basel). **2** (2009) 399–498.

[58] R.C. Ropp, Encyclopedia of the Alkaline Earth Compounds.(1st Ed.) Elsevier, **2012**.

[59] J.C. Elliott, R.M. Wilson, S.E.P. Dowker, APATITE STRUCTURES **v45_28**, (2002) 172-181.

[60] S. V Dorozhkin, Bioceramics of calcium orthophosphates., Biomaterials. **31** (2010) 1465–85..

[61] P. Habibovic, T.M. Sees, M.A. Van Den Doel, C.A. Van Blitterswijk, K. De Groot, Osteoinduction by biomaterials — Physicochemical and structural influences, J. Biomed. Mater. Res. **77A** (2006) 747–762.

[62] H. Yuan, C. Van Blitterswijk, A comparison of bone formation in biphasic calcium phosphate (BCP) and hydroxyapatite (HA) implanted in muscle and bone of dogs at different time periods, J. Biomed. Mater. Res. Part A. **78**(2006) 139-147.

[63] I.R. Gibson, W. Bonfield, Novel synthesis and characterization of an AB-type carbonate-substituted hydroxyapatite, J. Biomed. Mater. Res. **59** (2002) 697–708.

[64] A.M. Pietak, J.W. Reid, M.J. Stott, M. Sayer, Silicon substitution in the calcium phosphate bioceramics., Biomaterials. **28** (2007) 4023–32.

[65] I.R. Gibson, S.M. Best, W. Bonfield, Effect of Silicon Substitution on the Sintering and Microstructure of Hydroxyapatite, J. Am. Ceram. Soc. **85** (2004) 2771–2777.

[66] I.R. Gibson, S.M. Best, W. Bonfield, Chemical characterization of silicon-substituted hydroxyapatite., J. Biomed. Mater. Res. **44** (1999) 422–8.

[67] M. Bohner, Silicon-substituted calcium phosphates – A critical view, Biomaterials. **30** (2009) 6403–6406. doi:10.1016/j.biomaterials.2009.08.007.

[68] M. Vallet-Regi, D. Arcos, Silicon substituted hydroxyapatites. A method to upgrade calcium phosphate based implants, J. Mater. Chem. **15** (2005) 1509.

[69] S.R. Kim, J.H. Lee, Y.T. Kim, D.H. Riu, S.J. Jung, Y.J. Lee, S.C. Chung, Y.H. Kim, Synthesis of Si, Mg substituted hydroxyapatites and their sintering behaviors., Biomaterials. **24** (2003) 1389–98.

[70] J.E. Barralet, S.M. Best, W. Bonfield, Effect of sintering parameters on the density and microstructure of carbonate hydroxyapatite, J. Mater. Sci. Mater. Med. **11** (2000) 719–724.

[71] P. Habibovic, H. Yuan, C.M. van der Valk, G. Meijer, C. a van Blitterswijk, K. de Groot, 3D microenvironment as essential element for osteoinduction by biomaterials., Biomaterials. **26** (2005) 3565–75.

[72] T. Guda, M. Appleford, S. Oh, J.L. Ong, A cellular perspective to bioceramic scaffolds for bone tissue engineering: the state of art, Curr. Top. Med. Chem. **8** (2008) 290–299.

[73] W.C. O'Neill, The fallacy of the calcium-phosphorus product., Kidney Int. **72** (2007) 792–6.

[74] W.E. Brown, Clinical Orthopaedics and Related Research, Clin. Orthop. Relat. Res. **44** (1966) 205–220.

[75] S. Kamakura, Y. Sasano, H. Homma, O. Suzuki, M. Kagayama, K. Motegi, Implantation of Octacalcium Phosphate (OCP) in Rat Skull Defects Enhances Bone Repair, J. Dent. Res. **78** (1999) 1682–1687.

[76] J.M. Hughes, Structure and Chemistry of the Apatites and Other Calcium Orthophosphates, J. Am. Chem. Soc. **118** (1996) 3072–3072.

[77] W.E.. Brown, L.C. Chow, Combinations of sparingly soluble calcium phosphates in slurries

and pastes as mineralizers and cements, USRE33161 E, **1986**.

[78]   R.Z. Legeros, Calcium Phosphate Materials in Restorative Dentistry: a Review, Adv. Dent. Res. **2** (1988) 164–180.

[79]   B.R. Constantz, I.C. Ison, M.T. Fulmer, R.D. Poser, S.T. Smith, M. VanWagoner, J. Ross, S.A. Goldstein, J.B. Jupiter, D.I. Rosenthal, Skeletal repair by in situ formation of the mineral phase of bone., Science. **267** (1995) 1796–9.

[80]   M.-P. Ginebra, C. Canal, M. Espanol, D. Pastorino, E.B. Montufar, Calcium phosphate cements as drug delivery materials., Adv. Drug Deliv. Rev. **64** (2012) 1090–110.

[81]   M. Espanol, R.A. Perez, E.B. Montufar, C. Marichal, A. Sacco, M.P. Ginebra, Intrinsic porosity of calcium phosphate cements and its significance for drug delivery and tissue engineering applications, Acta Biomater. **5** (2009) 2752–2762.

[82]   M.-P. Ginebra, J.-A. Delgado, I. Harr, A. Almirall, S. Del Valle, J.A. Planell, Factors affecting the structure and properties of an injectable self-setting calcium phosphate foam, J. Biomed. Mater. Res. Part A. **80A** (2007) 351–361.

[83]   E.B. Montufar Jiménez, Espumas inyectables de hidroxiapatita obtenidas por el método de espumado de la fase líquida de un cemento de fostato tricálcico alfa, Universitat Politècnica de Catalunya. Departament d'Enginyeria de Sistemes, Automàtica i Informàtica Industrial, **2010**.

[84]   B. Feng, M. Guolin, Y. Yuan, L. Changshen, W. Zhen, L. Jian, Role of macropore size in the mechanical properties and in vitro degradation of porous calcium phosphate cements, Mater. Lett. **64** (2010) 2028–2031.

[85]   E.B.B. Montufar, T. Traykova, C. Gil, I. Harr, A. Almirall, A. Aguirre, E. Engel, J.A.A. Planell, M.P.P. Ginebra, Foamed surfactant solution as a template for self-setting injectable hydroxyapatite scaffolds for bone regeneration, Acta Biomater. **6** (2010) 876–885..

[86]   R. Astala, M.J. Stott, First Principles Investigation of Mineral Component of Bone: CO 3 Substitutions in Hydroxyapatite, Chem. Mater. **17** (2005) 4125–4133.

[87]   D.W. Hutmacher, J.T. Schantz, C.X.F. Lam, K.C. Tan, T.C. Lim, State of the art and future directions of scaffold-based bone engineering from a biomaterials perspective, J. Tissue Eng. Regen. Med. **1** (2007) 245–260.

[88]   D.W. Hutmacher, Dietmar W. Hutmacher, Scaffolds in tissue engineering bone and cartilage, Biomaterials. **21** (2000) 2529–2543.

[89]   T.J. Blokhuis, J.J.C. Arts, Bioactive and osteoinductive bone graft substitutes: definitions, facts and myths., Injury. **42** Suppl 2 (2011) S26–9.

[90]   R.Z. LeGeros, Calcium phosphate-based osteoinductive materials., Chem. Rev. **108** (2008) 4742–53.

[91]   O. Chan, M.J. Coathup, a Nesbitt, C.-Y. Ho, K. a Hing, T. Buckland, C. Campion, G.W. Blunn, The effects of microporosity on osteoinduction of calcium phosphate bone graft substitute biomaterials., Acta Biomater. **8** (2012) 2788–94.

[92]   B. Li, X. Liao, L. Zheng, X. Zhu, Z. Wang, H. Fan, X. Zhang, Effect of nanostructure on osteoinduction of porous biphasic calcium phosphate ceramics, Acta Biomater. **8** (2012) 3794–3804.

[93]   M.J. Dalby, N. Gadegaard, R. Tare, A. Andar, M.O. Riehle, P. Herzyk, C.D.W. Wilkinson, R.O.C. Oreffo, The control of human mesenchymal cell differentiation using nanoscale symmetry and disorder., Nat. Mater. **6** (2007) 997–1003.

[94]   J.M. Sadowska, J. Guillem-Marti, E.B. Montufar, M. Espanol, M.-P. Ginebra, Biomimetic versus Sintered Calcium Phosphates: The in vitro Behavior of Osteoblasts and Mesenchymal Stem Cells, Tissue Eng. Part A. (**2017**) ten.TEA.2016.0406.

[95]   M. Espanol, I. Casals, S. Lamtahri, M.-T. Valderas, M.-P. Ginebra, Assessment of protein entrapment in hydroxyapatite scaffolds by size exclusion chromatography., Biointerphases. **7** (2012) 37.

[96]   G.F. Muschler, C. Nakamoto, L.G. Griffith, Engineering principles of clinical cell-based tissue engineering., J. Bone Joint Surg. Am. **86-A** (2004) 1541–58.

[97]   O. Gauthier, J.M. Bouler, P. Weiss, J. Bosco, G. Daculsi, E. Aguado, Kinetic study of bone ingrowth and ceramic resorption associated with the implantation of different injectable calcium-phosphate bone substitutes., J. Biomed. Mater. Res. **47** (1999) 28–35.

[98]   H. Yuan, Z. Yang, Y. Li, X. Zhang, J.D. De Bruijn, K. De Groot, Osteoinduction by calcium

phosphate biomaterials., J. Mater. Sci. Mater. Med. **9** (1998) 723–6.

[99] B.H. Fellah, O. Gauthier, P. Weiss, D. Chappard, P. Layrolle, Osteogenicity of biphasic calcium phosphate ceramics and bone autograft in a goat model, Biomaterials. **29** (2008) 1177–1188.

[100] S. Sánchez-Salcedo, D. Arcos, M. Vallet-Regí, Upgrading Calcium Phosphate Scaffolds for Tissue Engineering Applications, in: Key Eng. Mater., **2008**: pp. 19–42.

[101] A.M.C. Barradas, H. Yuan, C.A. Van Blitterswijk, P. Habibovic, T. Medicine, Osteoinductive Biomaterials: Current knowledge of properties, Eur. Cells Mater. **21** (2011) 407–429.

[102] E. Boanini, M. Gazzano, A. Bigi, Ionic substitutions in calcium phosphates synthesized at low temperature., Acta Biomater. **6** (2010) 1882–94.

[103] Z. Sheikh, M.-N. Abdallah, A. Hanafi, S. Misbahuddin, H. Rashid, M. Glogauer, Mechanisms of in Vivo Degradation and Resorption of Calcium Phosphate Based Biomaterials, Materials (Basel). **8** (2015) 7913–7925.

[104] Z. Sheikh, Y.L. Zhang, L. Grover, G.E. Merle, F. Tamimi, J. Barralet, In vitro degradation and in vivo resorption of dicalcium phosphate cement based grafts, Acta Biomater. **26** (2015) 338–346.

[105] F. Tamimi, Z. Sheikh, J. Barralet, Dicalcium phosphate cements: Brushite and monetite, Acta Biomater. **8** (2012) 474–487.

[106] H. Yuan, M. Van Den Doel, S. Li, C. a Van Blitterswijk, K. De Groot, J.D. De Bruijn, A comparison of the osteoinductive potential of two calcium phosphate ceramics implanted intramuscularly in goats., J. Mater. Sci. Mater. Med. **13** (2002) 1271–5.

[107] A. Gisep, R. Wieling, M. Bohner, S. Matter, E. Schneider, B. Rahn, Resorption patterns of calcium-phosphate cements in bone., J. Biomed. Mater. Res. A. **66** (2003) 532–40.

[108] E. Landi, G. Celotti, G. Logroscino, A. Tampieri, Carbonated hydroxyapatite as bone substitute, Ceram. Met. Interfaces. **23** (2003) 2931–2937. doi:10.1016/S0955-2219(03)00304-2.

[109] G. Spence, N. Patel, R. Brooks, W. Bonfield, N. Rushton, Osteoclastogenesis on hydroxyapatite ceramics: the effect of carbonate substitution., J. Biomed. Mater. Res. A. **92** (2010) 1292–300.

[110] L.J. Cardenas, A. Takeuchi, K. Tsuru, S. Matsuya, K. Ishikawa, The Third International Conference on the Development of Biomedical Engineering in Vietnam, Springer Berlin Heidelberg, Berlin, Heidelberg, **2010**.

[111] C. Capuccini, P. Torricelli, E. Boanini, M. Gazzano, R. Giardino, A. Bigi, Interaction of Sr-doped hydroxyapatite nanocrystals with osteoclast and osteoblast-like cells., J. Biomed. Mater. Res. A. **89** (2009) 594–600.

[112] E. Landi, G. Logroscino, L. Proietti, A. Tampieri, M. Sandri, S. Sprio, Biomimetic Mg-substituted hydroxyapatite: from synthesis to in vivo behaviour., J. Mater. Sci. Mater. Med. **19** (2008) 239–47.

[113] T.J. Webster, E.A. Massa-Schlueter, J.L. Smith, E.B. Slamovich, Osteoblast response to hydroxyapatite doped with divalent and trivalent cations, Biomaterials. **25** (2004) 2111–2121.

[114] A.S. Prasad, Zinc: The Biology and Therapeutics of an Ion, Ann. Intern. Med. **125** (1996) 142.

[115] S. Nakamura, T. Kobayashi, M. Nakamura, S. Itoh, K. Yamashita, Electrostatic surface charge acceleration of bone ingrowth of porous hydroxyapatite/beta-tricalcium phosphate ceramics., J. Biomed. Mater. Res. A. **92** (2010) 267–75.

[116] K. Yamashita, N. Oikawa, T. Umegaki, Acceleration and Deceleration of Bone-Like Crystal Growth on Ceramic Hydroxyapatite by Electric Poling, Chem. Mater. **8** (1996) 2697–2700.

[117] J.E. McBane, L. a. Matheson, S. Sharifpoor, J.P. Santerre, R.S. Labow, Effect of polyurethane chemistry and protein coating on monocyte differentiation towards a wound healing phenotype macrophage, Biomaterials. **30** (2009) 5497–5504.

[118] R. Sridharan, A.R. Cameron, D.J. Kelly, C.J. Kearney, F.J. O'Brien, F.J. O'Brien, Biomaterial based modulation of macrophage polarization: A review and suggested design principles, Mater. Today. **18** (2015) 313–325.

[119] W.G. Brodbeck, J. Patel, G. Voskerician, E. Christenson, M.S. Shive, Y. Nakayama, T. Matsuda, N.P. Ziats, J.M. Anderson, Biomaterial adherent macrophage apoptosis is increased by hydrophilic and anionic substrates in vivo., Proc. Natl. Acad. Sci. U. S. A. **99** (2002)

10287–92.

[120] T.N. Vo, F.K. Kasper, A.G. Mikos, Strategies for controlled delivery of growth factors and cells for bone regeneration, Adv. Drug Deliv. Rev. **64** (2012) 1292–1309.

[121] L. Zhang, E.M. Furst, K.L. Kiick, Manipulation of hydrogel assembly and growth factor delivery via the use of peptide-polysaccharide interactions., J. Control. Release. **114** (2006) 130–42.

[122] U. Edlund, S. Dånmark, A.-C. Albertsson, A strategy for the covalent functionalization of resorbable polymers with heparin and osteoinductive growth factor., Biomacromolecules. **9** (2008) 901–5.

[123] O.G. Cisneros-Pineda, W. Herrera Kao, M.I. Loría-Bastarrachea, Y. Veranes-Pantoja, J. V. Cauich-Rodríguez, J.M. Cervantes-Uc, Towards optimization of the silanization process of hydroxyapatite for its use in bone cement formulations, Mater. Sci. Eng. C. **40** (2014) 157–163.

[124] G.E. Friedlaender, C.R. Perry, J.D. Cole, S.D. Cook, G. Cierny, G.F. Muschler, G.A. Zych, J.H. Calhoun, A.J. LaForte, S. Yin, Osteogenic protein-1 (bone morphogenetic protein-7) in the treatment of tibial nonunions., J. Bone Joint Surg. Am. **83-A** Suppl (2001) S151–8.

[125] Y. Takahashi, M. Yamamoto, Y. Tabata, Enhanced osteoinduction by controlled release of bone morphogenetic protein-2 from biodegradable sponge composed of gelatin and beta-tricalcium phosphate., Biomaterials. **26** (2005) 4856–65.

[126] L. Russo, F. Taraballi, C. Lupo, A. Poveda, J. Jiménez-barbero, A. Tampieri, F. Nicotra, L. Cipolla, M. Sandri, Carbonate hydroxyapatite functionalization : a comparative study towards (bio) molecules fixation, Interface Focus. **4** (2014).

[127] S. Wang, S. Wen, M. Shen, R. Guo, X. Cao, J. Wang, X. Shi, Aminopropyltriethoxysilane-mediated surface functionalization of hydroxyapatite nanoparticles: synthesis, characterization, and in vitro toxicity assay., Int. J. Nanomedicine. **6** (2011) 3449–59.

[128] S. Gittens, K. Bagnall, J.R. Matyas, R. Löbenberg, H. Uludag, Imparting bone mineral affinity to osteogenic proteins through heparin-bisphosphonate conjugates., J. Control. Release. **98** (2004) 255–68.

[129] Y.-I. Chung, G. Tae, S. Hong Yuk, A facile method to prepare heparin-functionalized nanoparticles for controlled release of growth factors., Biomaterials. **27** (2006) 2621–6.

[130] A.N. Vasiliev, E. Zlotnikov, J.G. Khinast, R.E. Riman, Chemisorption of silane compounds on hydroxyapatites of various morphologies, Scr. Mater. **58** (2008) 1039–1042.

[131] J.D. Esko, R.J. Linhardt, Proteins that Bind Sulfated Glycosaminoglycans, Cold Spring Harbor Laboratory Press, **2009**.

[132] G. David, M. Bernfield, The Emerging Roles of Cell Surface Heparan Sutfate Proteoglycans, Matrix Biol. **17** (1998) 461–463.

[133] T.R. Rudd, M. a Skidmore, M. Guerrini, M. Hricovini, a K. Powell, G. Siligardi, E. a Yates, The conformation and structure of GAGs: recent progress and perspectives., Curr. Opin. Struct. Biol. **20** (2010) 567–74.

[134] J. Salbach, T.D. Rachner, M. Rauner, U. Hempel, U. Anderegg, S. Franz, J.-C. Simon, L.C. Hofbauer, Regenerative potential of glycosaminoglycans for skin and bone., J. Mol. Med. (Berl). **90** (2012) 625–35.

[135] A. Irie, M. Takami, H. Kubo, N. Sekino-Suzuki, K. Kasahara, Y. Sanai, Heparin enhances osteoclastic bone resorption by inhibiting osteoprotegerin activity., Bone. 41 (2007) 165–74. doi:10.1016/j.bone.2007.04.190.

[136] M. Baud'huin, C. Ruiz-Velasco, G. Jego, C. Charrier, N. Gasiunas, J. Gallagher, M. Maillasson, A. Naggi, M. Padrines, F. Redini, L. Duplomb, D. Heymann, Glycosaminoglycans inhibit the adherence and the spreading of osteoclasts and their precursors: role in osteoclastogenesis and bone resorption., Eur. J. Cell Biol. **90** (2011) 49–57.

[137] U. Hempel, C. Preissler, S. Vogel, S. Möller, V. Hintze, J. Becher, M. Schnabelrauch, M. Rauner, L.C. Hofbauer, P. Dieter, Artificial extracellular matrices with oversulfated glycosaminoglycan derivatives promote the differentiation of osteoblast-precursor cells and premature osteoblasts., Biomed Res. Int. **2014** (2014) 938368.

[138] V. Hintze, A. Miron, S. Moeller, M. Schnabelrauch, H.-P. Wiesmann, H. Worch, D. Scharnweber, Sulfated hyaluronan and chondroitin sulfate derivatives interact differently with human transforming growth factor-β1 (TGF-β1)., Acta Biomater. **8** (2012) 2144–52.

[139] V. Hintze, S.A. Samsonov, M. Anselmi, S. Moeller, J. Becher, M. Schnabelrauch, D. Scharnweber, M.T. Pisabarro, Sulfated glycosaminoglycans exploit the conformational plasticity of bone morphogenetic protein-2 (BMP-2) and alter the interaction profile with its receptor., Biomacromolecules. 15 (2014) 3083–92.

[140] J. Salbach-Hirsch, Sulfated glycosaminoglycans support osteoblast functions and concurrently suppress osteoclasts., J. Cell. Biochem. 115 (2014) 1101–11.

[141] J. Salbach, S. Kliemt, M. Rauner, T.D. Rachner, C. Goettsch, S. Kalkhof, M. von Bergen, S. Möller, M. Schnabelrauch, V. Hintze, D. Scharnweber, L.C. Hofbauer, The effect of the degree of sulfation of glycosaminoglycans on osteoclast function and signaling pathways., Biomaterials. 33 (2012) 8418–29.

[142] R. Lever, A. Smailbegovic, C. Page, Role of glycosaminoglycans in inflammation, Inflammopharmacology. 9 (2001) 165–169.

[143] L. Ramsden, C.C. Rider, Selective and differential binding of interleukin (IL)-1α, IL-1β, IL-2 and IL-6 to glycosaminoglycans, Eur. J. Immunol. 22 (1992) 3027–3031.

[144] J.G. Cripps, F.A. Crespo, P. Romanovskis, A.F. Spatola, R. Fernández-Botrán, Modulation of acute inflammation by targeting glycosaminoglycan–cytokine interactions, Int. Immunopharmacol. 5 (2005) 1622–1632.

[145] J. Salbach-Hirsch, J. Kraemer, M. Rauner, S.A. Samsonov, M.T. Pisabarro, S. Moeller, M. Schnabelrauch, D. Scharnweber, L.C. Hofbauer, V. Hintze, The promotion of osteoclastogenesis by sulfated hyaluronan through interference with osteoprotegerin and receptor activator of NF-κB ligand/osteoprotegerin complex formation., Biomaterials. 34 (2013) 7653–61.

[146] S. Mathews, S.A. Mathew, P.K. Gupta, R. Bhonde, S. Totey, Glycosaminoglycans enhance osteoblast differentiation of bone marrow derived human mesenchymal stem cells., J. Tissue Eng. Regen. Med. 8 (2014) 143–52.

[147] U. Hempel, V. Hintze, S. Möller, M. Schnabelrauch, D. Scharnweber, P. Dieter, Artificial extracellular matrices composed of collagen I and sulfated hyaluronan with adsorbed transforming growth factor β1 promote collagen synthesis of human mesenchymal stromal cells., Acta Biomater. 8 (2012) 659–66.

[148] V. Hintze, S. Moeller, M. Schnabelrauch, S. Bierbaum, M. Viola, H. Worch, D. Scharnweber, Modifications of hyaluronan influence the interaction with human bone morphogenetic protein-4 (hBMP-4)., Biomacromolecules. 10 (2009) 3290–7.

[149] J. Salbach-Hirsch, S.A. Samsonov, V. Hintze, C. Hofbauer, A.-K. Picke, M. Rauner, J.-P. Gehrcke, S. Moeller, M. Schnabelrauch, D. Scharnweber, M.T. Pisabarro, L.C. Hofbauer, Structural and functional insights into sclerostin-glycosaminoglycan interactions in bone., Biomaterials. 67 (2015) 335–45.

[150] A. Lode, A. Reinstorf, A. Bernhardt, C. Wolf-Brandstetter, U. König, M. Gelinsky, Heparin modification of calcium phosphate bone cements for VEGF functionalization., J. Biomed. Mater. Res. A. 86 (2008) 749–59.

[151] C.S. Goonasekera, K.S. Jack, G. Bhakta, B. Rai, E. Luong-Van, V. Nurcombe, S.M. Cool, J.J. Cooper-White, L. Grøndahl, Mode of heparin attachment to nanocrystalline hydroxyapatite affects its interaction with bone morphogenetic protein-2, Biointerphases. 10 (2015) 04A308.

[152] R. Vasita, I.K. Shanmugam, D.S. Katt, D. Katti, R. Vasita, K. Shanmugam, Improved biomaterials for tissue engineering applications: surface modification of polymers, Curr Top Med Chem. 8 (2008) 341–353.

Chapter 2

In vitro degradation of calcium phosphates: effect of multiscale porosity, textural properties and composition

Scope

The resorption of biomaterials can be achieved actively or passively by means of cellular activity (so-called bioresorption) and/or by the inherent physicochemical properties of materials, respectively. The following chapter aims to describe the physicochemical properties of a wide variety of CaPs and the extent to which each parameter can modulate degradation. Multiscale porosity, SSA and composition characterization during acidic degradation can shed light on the most effective properties to modulate biomaterial degradation and resorption, which is crucial and mandatory for the regenerative potential of bone grafts. An accelerated degradation method using an acidic media resembling osteoclast resorption environment (pH<4) has been used to unravel the extent to which each property affect CaPs degradation.
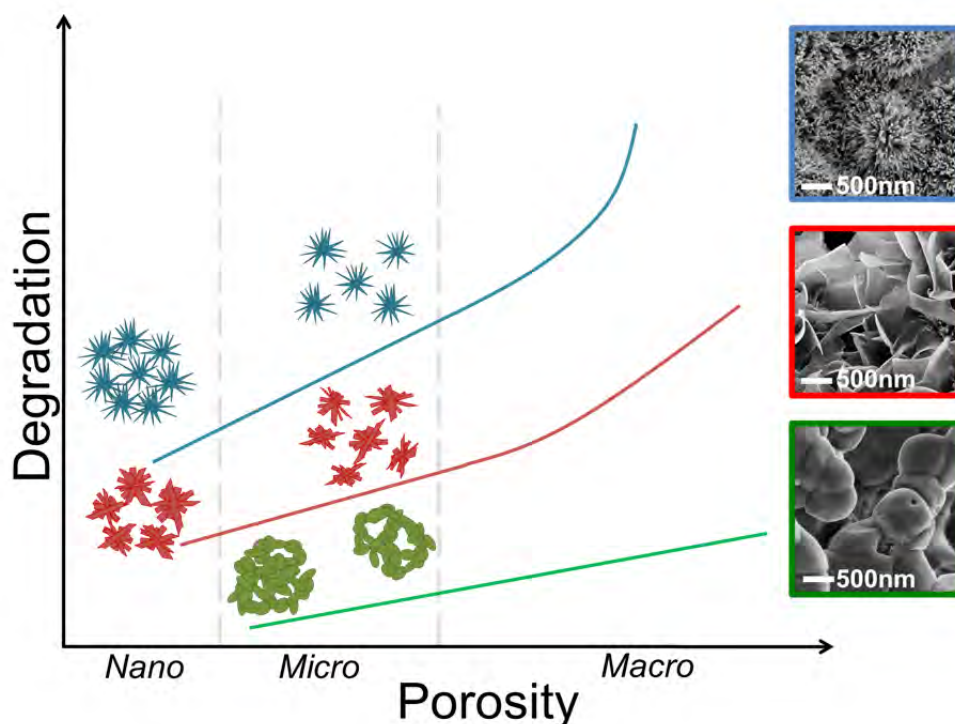
2.1. Introduction

Bone has a remarkable capacity for self-repair. However, this self-healing capacity is not sufficient to bridge critical sized bone defects and moreover it can be impaired in some pathological situations. In these cases, the use of bone grafts, either natural (autografts, allografts or xenografts) or synthetic, is crucial to restore bone function.[1] An ideal bone graft should provide initial strength at the implantation site while actively supporting bone remodeling. Therefore, it is important to have a tight synchronization between graft resorption and new bone deposition to allow a gradual replacement of the bone graft by newly formed bone.[2] Although bone autografts remain the gold standard for such applications, site morbidity and volume availability are major concerns that limit their use.[3] The need for synthetic bone grafts is clear, but their choice and design remain still complex due to many considerations such as material composition, architecture, mechanical stability, degradation products, etc. that can potentially affect the remodeling process.[4]

Among synthetic bone grafts,[5-7] calcium phosphates (CaP) are very interesting for remodeling purposes as they possess a close resemblance to the mineral phase of natural bone consisting of ~70 wt% of nanocrystalline hydroxyapatite (HA).[8] Owing to the close compositional resemblance of CaP to bone mineral, they can induce a biological response similar to that taking place during bone remodeling. Indeed, CaP can potentially be resorbed by osteoclastic cells and can also support bone formation under the action of osteoblastic cells.[9] However, despite the potential of CaP, there is presently no material matching the remodeling rates of natural bone. The bottleneck for most CaP formulations, including hydroxyapatite-based formulations, is their poor resorption rate, especially for sintered HA, which is one of the most commonly used materials.[10] *In vivo* studies have proved that even after 9 months of implantation sintered HA remained at the site with hardly any sign of resorption.[11,12] To circumvent this problem, HA has been combined with more soluble phases such as β-tricalcium phosphate (β-TCP).[13–16] Alternatively, more inherently soluble phases such as brushite/monetite have also demonstrated higher resorbability.[17,18] In addition, doping the crystal structure of HA with e.g. carbonate ions was found to enhance its resorption and to promote osteoclastic activity *in vitro*.[19–24]

However, not only composition plays a role in degradation rates. The modification of crystallinity, grain size, specific surface area,[25,26] or the porosity content[27–29] are relevant physicochemical features which have been shown to help tailor resorption rates, hence improving the *in vivo* performance of such implants.[30] Despite the various works proving increased degradation in materials with lower crystallinity, high SSA, decreased grain density, and a higher degree

of porosity, the extent to which each parameter influences resorption remains unclear. The complexity of isolating the contribution of each of these parameters lies in the close interrelation between these factors, as changing one can potentially affect the other/s.

One key aspect in the evaluation of the *in vitro* degradation of biomaterials is the selection of the degrading medium. Although degradation of CaP has been assessed in different solutions,[31–35] the simulation of the resorption process by osteoclasts requires working in solutions at acidic pH. This is because resorption by mature osteoclast proceeds through the development of a tight ring-like zone of adhesion (i.e. the sealing zone) that delimits the resorbing area onto which osteoclasts generate an acid milieu that can reach values below pH 3, resulting in the dissolution of the underlying mineral.[36] In this regards, studies performed at low pH can be used as predictors of osteoclastic degradation.[37–40]

The aim of this chapter was to provide quantitative information on the relative importance of CaP composition, specific surface area, and porosity in an *in vitro* model of CaP degradation. We took advantage of the possibility offered by the fabrication of hydroxyapatite scaffolds using biomimetic routes, i.e., by low temperature dissolution–precipitation reactions, to systematically introduce controlled levels of porosity at the nano, micro, and macroscale, as well as to modify the specific surface area.[41–43] Thus, the porosity at the nano-microscale and the specific surface area were modified by varying the L/P ratio and the particle size of the starting powder, respectively.[41,42] In turn, macroporosity was introduced through a foaming process.[43] Moreover, the effect of doping with carbonate ions on the degradation behavior was analyzed. Finally, the degradation behavior of the biomimetic scaffolds was compared to that of sintered materials, namely β-TCP and sintered HA, obtained after thermal treatment of the biomimetic scaffolds, which, in addition to the change in composition, exhibited different textural parameters. To facilitate comparison between materials and to discard any effect due to the use of different reagents (e.g. purity, presence of ionic traces of foreign ions, etc.), all materials were prepared from the same Ca and P sources.

2.2. Materials and Methods

2.2.1. Preparation of biomimetic calcium deficient hydroxyapatite

α-TCP was used for the preparation of biomimetic calcium deficient hydroxyapatite (CDHA) through a cementitious reaction. Briefly, α-TCP was obtained by heating calcium hydrogen phosphate ($CaHPO_4$, Sigma-Aldrich, St.

Louis, USA) and calcium carbonate ($CaCO_3$, Sigma-Aldrich, St. Louis, USA) at a 2:1 molar ratio at 1400°C for 15h and then quenching in air. Subsequently, the particles obtained were milled as described elsewhere[41] to obtain two different α-TCP powder sizes, coarse (C: 5.2µm median size) and fine (F: 2.8µm median size). α-TCP, with 2wt% of precipitated hydroxyapatite (PHA, Merck KGaA, Darmstadt, Germany), was mixed with a liquid phase consisting of an aqueous solution of 2.5wt% disodium hydrogen phosphate (Na_2HPO_4, Merck, Darmstadt, Germany) which acted as a reaction accelerant. Both phases were mixed in a mortar for 1min and the resulting paste was transferred into 15x2mm^2 PTFE disc moulds where the discs were left to set in water at 37°C for 7 days. CDHA samples with different liquid to powder ratios (L/P) were prepared, ranging from 0.35 to 0.65mL/g.

2.2.2. Preparation of biomimetic carbonate-doped hydroxyapatite

Carbonated calcium deficient hydroxyapatite (C-CDHA) was obtained by performing the setting of the cement in a saturated sodium bicarbonate solution ($NaHCO_3$, Sigma-Aldrich, St. Louis, USA) instead of water, for 17 days at 37°C. Samples were immersed in the carbonated setting medium once cohesion was achieved, i.e., approximately after 5h of preparation. In these specimens, water was used as the liquid phase of the cements instead of a disodium hydrogen phosphate solution.

2.2.3. Preparation of biomimetic foams

To prepare the macroporous scaffolds, the powder phase consisting of 98wt% α-TCP and 2wt% of precipitated hydroxyapatite (PHA) was mixed with an aqueous solution of 1wt% Polysorbate 80 (Sigma-Aldrich, St. Louis, USA) as foaming agent.[43] Both phases were foamed with a domestic food mixer for 30s at 7000rpm and then transferred to 6x12mm^2 PTFE cylindrical moulds where they were left to set in water at 37°C for 10 days. The L/P ratios for the foams were adjusted to 0.55 and 0.65mL/g for coarse and fine α-TCP powders respectively, as these proportions produced scaffolds with similar macroporosities for the two powders.

2.2.4. Preparation of sintered hydroxyapatite and beta-tricalcium phosphate

Sintering of CDHA and C-CDHA at 1100°C for 9h resulted in β-TCP and sintered HA (SHA). This protocol was applied both to non-foamed and foamed cements. The non-foamed specimens corresponding to β-TCP and SHA were

obtained from coarse particles since no differences were observed regarding their physicochemical features after sintering. Figure 2-1 summarizes the various synthesis procedures and the nomenclature assigned to the different materials.
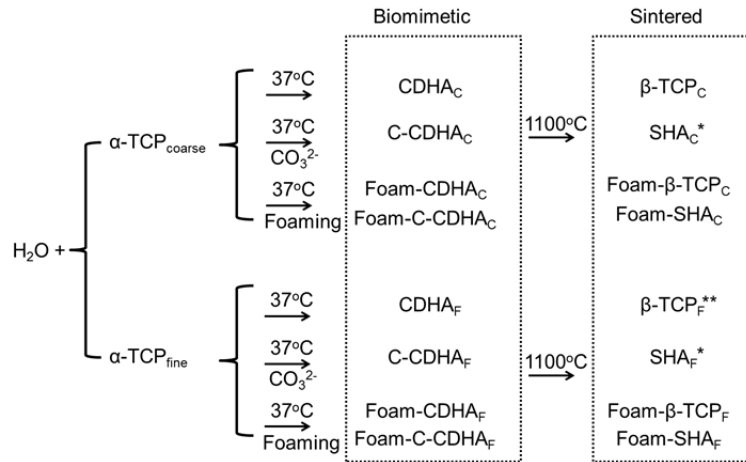
Figure 2-1. Sketch summarizing the various CaP synthesis procedures and sample nomenclature. C = carbonated; F = foam; CDHA = calcium deficient hydroxyapatite; SHA = sintered hydroxyapatite; β-TCP = beta tricalcium phosphate. C and F subscripts denote the size of starting α-TCP. * In this work, the degradation of sintered hydroxyapatite (SHA$_C$ and SHA$_F$) was only analyzed in foamed samples. ** The effect of microporosity on the degradation of non-foamed β-TCP was assessed using the coarse samples (β-TCP$_C$).

2.2.5.   Physicochemical Characterization

2.2.5.1. X-ray Diffraction (XRD)

Phase characterization of the samples was performed by XRD using a D8 Advance diffractometer (Bruker) equipped with a Cu Kα anode (monochromated, λ=1.5406Å), operated at 40kV, and 40mA. Data were collected in 0.02° steps over the 2θ range of 10°-80° with a counting time of 2s per step. Prior to analysis, the samples were finely ground into powders. The experimental patterns were compared to those of hydroxyapatite (JCPDS 09-0432), α-TCP (JCPDS 09-0348) and β-TCP (JCPDS 09-0169). Phase quantification was performed using analysis software (DIFFRAC.EVA software, Bruker). The analyses were based on reference intensity ratio values. Phase intensities of experimental diffractograms were adjusted to those of reference patterns. The algorithm calculations are performed taking into account the intensity ratio of the experimental phase with respect to a standard pattern (corundum, I/I_{cor}).

2.2.5.2. FTIR spectroscopy

Samples were analyzed by ATR-FTIR using a Nicolet 6700FTIR equipped with a He/Ne beam, CsI beam splitter and DTGS-CsI detector. 64 scans were acquired

with a resolution of 4cm^{-1} in the range of 4000 to 575cm^{-1} with a Germanium crystal.

2.2.5.3. Carbonate quantification

Elemental quantification of total carbon content was performed by bulk combustion using a Thermal combustion element analyzer, Thermo EA 1108(TC/EA), working in standard conditions (Helium flow at 120mL/min, combustion furnace at 1000°C, chromatographic column oven at 60°C, oxygen loop 10mL at 100kPa). The amount of carbonate was calculated according to the following equation:

$$\text{Percentage of Carbonate} = \frac{MW_{CO_3^{2-}}}{MW_C} \cdot \%_C$$

where, $MW_{CO_3^{2-}}$ is the molecular weight of carbonate ion, MW_C is the molecular weight of carbon, and $\%_C$ is the percentage of carbon given by the measurement. Prior to analysis, samples were crushed using an agate mortar, and the powders were dried at 120°C overnight.

2.2.5.4. Morphological analysis

Scanning electron microscopy (Zeiss Neon40dual beam FIB/SEM) was used to study the microstructure of the samples. All micrographs were taken from the cross-section of samples. Prior to imaging, samples were coated with carbon to enhance conductivity.

2.2.5.5. Specific Surface Area

The SSA area was determined by nitrogen adsorption using the BET method (ASAP 2020, Micromeritics). Prior to measurement, samples were outgassed in vacuum conditions (10µmHg) at a holding temperature of 100°C for 2 hours.

2.2.5.6. Porosity

The open porosity and pore entrance size distributions were obtained by MIP (Autopore IV Micromeritics). Mercury contact angle used was 130 degrees and a surface tension of 485 dynes/cm for the measurement analysis. All samples were dried at 100°C for 2 hours prior to measurement. Mercury intrusion-extrusion curves were recorded from 30 to 30000psia.

2.2.5.7. Skeletal density and compression tests

The skeletal density of samples was measured by helium picnometry (AccuPyc 133, Micromeritics) for the different compositions CDHA$_C$, CDHA$_F$, C-CDHA$_C$, β-TCP and HA. The compressive strength of the different compositions and L/P

ratios for non-foamed formulations were measured using a Universal Testing Machine (Instron 8511) at a cross-head speed of 1mm/min until fracture. Twelve cylindrical samples (6mm diameter by 12mm high) were analyzed for each composition and L/P. Foam specimens for the different compositions were analyzed for compression strength using a Bionix (MTS, Universal testing machine) and 20 cylindrical samples were tested.

2.2.6.   Accelerated degradation study

An accelerated degradation study was performed by immersing the samples in an acidic solution consisting of 0.01M hydrochloric acid (HCl, PanreacAppliChem) and 0.14M sodium chloride (NaCl, PanreacAppliChem) at 37°C, based on previous studies.[36,44] Prior to degradation, samples were dried at 120°C overnight until a constant weight was achieved. Since the solution was not buffered, to prevent any change in the solution pH that would alter the degradation behavior, the samples were immersed in a large volume of acidic medium (15mL) to keep the pH constant. The solutions were placed in sterile polypropylene tubes (50mL) over 8h under static conditions. Every hour, samples were transferred to new vials with fresh medium. After degradation, samples were rinsed thrice with distilled water and dried overnight at 120°C until constant weight. The weight loss percentage ($n=3$) was obtained by calculating the difference in weight according to the equation:

$$\text{Percentage of weight loss} = \frac{m_0 - m_f}{m_0} \cdot 100 \ [\%] \qquad \text{(Eq.2)}$$

where, m_0 is the initial sample mass and m_f is the final mass after drying. Supernatants at each time point were collected and pH values were measured using a pHmeter (MultiMeter MM 41).

2.2.7.   Statistical analyses

The degradation experiments were conducted with three samples. The results are presented as the average and standard deviation. Statistical significance with a level of $p<0.05$ was evaluated for dense and foamed samples. One-way ANOVA was used for dense samples since they presented a normal distribution. The analyses of foamed versus non-foamed specimens were carried out using the non-parametric Mann Whitney test since no normal distribution was found. Compressive strength is presented as mean and standard deviation. All statistics were performed using SPSS software (IBM).

2.3. Results

2.3.1. Physicochemical Characterization

Figure 2-2A shows the X-ray diffraction results for the different samples. The XRD profile of the biomimetic samples differed significantly from the sintered ones in terms of peak sharpness as a consequence of the low crystallinity of biomimetic CDHA. Lower crystallinity was more pronounced in $CDHA_F$ than in $CDHA_C$. The three CDHA samples contained traces of unreacted α-TCP (3wt%). It is noteworthy that the addition of carbonate altered the CDHA conversion kinetics, and 17 days were required for conversion of C-CDHA samples into similar levels as those of CDHA coarse and fine. Similarly, the absence of accelerant in the liquid phase, as is the case of foamed specimens required 10 days of setting. This was confirmed by the similar unreacted α-TCP levels. Upon sintering CDHA at 1100°C, pure β-TCP was obtained, whilst sintering of C-CDHA resulted into stoichiometric HA.

The ATR-FTIR spectra of the different materials studied are shown in Figure 2-2B. Similar to what was observed by XRD, sintered samples showed better resolved bands than biomimetic materials. This was particularly evident when comparing CDHA with SHA. Typical phosphate (PO_4^{3-}) bands in HA appear at 570, 600, 960, 1030 and 1090cm^{-1}, corresponding to vibrational modes v_4, v_1, v_3 respectively.[45]-[47] The stoichiometric high temperature SHA showed well defined and sharper bands than CDHA for the phosphate groups. The hydroxyl band, at 630 cm^{-1} appeared also sharper in SHA ($Ca_{10}(PO_4)_6(OH)_2$) than in CDHA, consistent with the non-stoichiometric nature of the apatites obtained by hydrolysis of α-TCP (i.e., $Ca_9(PO_4)_5(HPO_4)(OH)$).[47] The presence of HPO_4^{2-} in CDHA was proved by an additional band appearing at 870 cm^{-1}. Typical carbonate bands (CO_3^{2-}) at 1414 and 1471cm^{-1}, and at 871cm^{-1} were visible in C-CDHA, which are representative of v_2 vibrational mode accounting for a B-type carbonated apatite (i.e. phosphate substitution).[48,49] The β-TCP spectrum showed typical phosphate bands at 551, 604, 945, 970, 1024, 1042, 1080 and 1118cm^{-1}.[46,50]
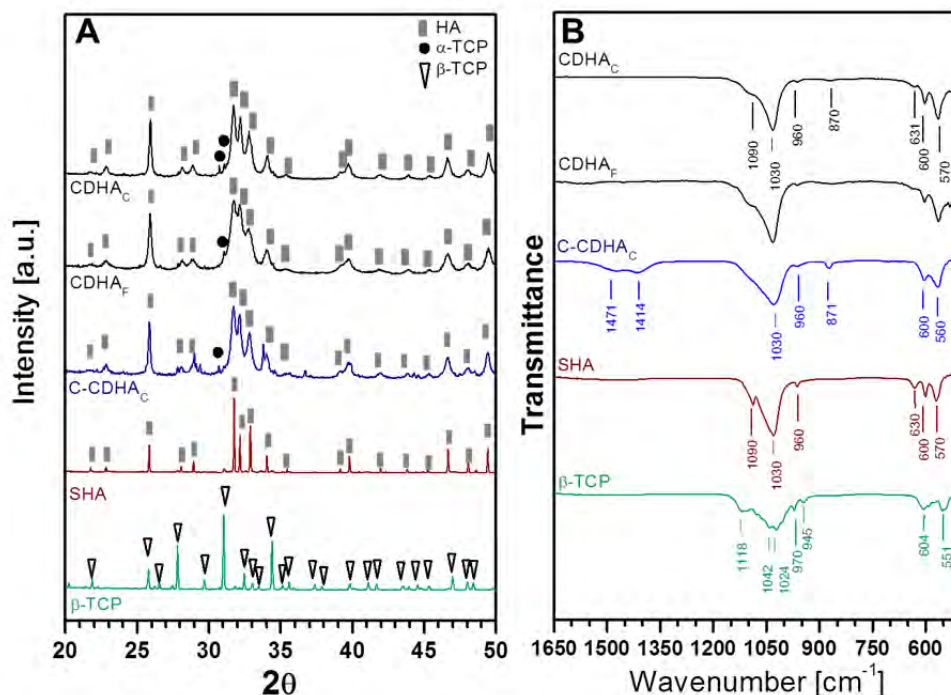
Figure 2-2. XRD patterns (A) and ATR-FTIR spectra (B) of all materials studied, prepared with a L/P ratio of 0.55mL/g

The skeletal density of the biomimetic compositions slightly differed. $CDHA_C$ and $CDHA_F$ resulted in $2.70\pm0.02g/cm^3$ and $2.67\pm0.02g/cm^3$ respectively, while the value for $C\text{-}CDHA_C$ decreased to $2.54\pm0.03g/cm^3$ consistent with the incorporation of carbonate in the crystal structure. As expected, sintered β-TCP and HA compositions, showed the highest values of density with 3.08 ± 0.02 and $3.18\pm0.04g/cm^3$ respectively. TC/EA analyses of carbonate-containing samples are summarized in Table 2-1. The carbonate levels were similar for all samples regardless of their porosity, ranging from 11 to 13%wt. Control samples of $CDHA_C$ and $CDHA_F$ were included and proved no carbonation occurring from ambient carbon dioxide or from precursor chemicals.

Table 2-1.Carbonate content of the different carbonated CDHA samples

	L/P ratio [mL/g]	Carbonate level [%wt]
$C\text{-}CDHA_C$	0.35	12.25 ± 0.78
	0.45	13.30 ± 1.27
	0.55	12.33 ± 0.25
	0.65	13.23 ± 0.04
$Foam\text{-}C\text{-}CDHA_C$	0.55	11.33 ± 0.39
$Foam\text{-}C\text{-}CDHA_F$	0.65	12.58 ± 0.32
$CDHA_{C/F}$	0.55	0.05 ± 0.07

Scanning electron micrographs of the different compositions are shown in Figure 2-3. The different biomimetic substrates showed microstructures consisting of aggregates of nano-micrometric crystals. For CDHA$_C$, the aggregates consisted of plate-like crystals. CDHA$_F$ instead consisted of needle-like crystals due to the smaller particle size of α-TCP used for its synthesis. The introduction of carbonate resulted in a plate-like morphology of the crystals, both for the C-CDHA$_C$ and C-CDHA$_F$ samples, which showed a very similar microstructure. The high temperature CaPs, β-TCP and SHA, showed the typical polyhedral grain structure of sintered samples.
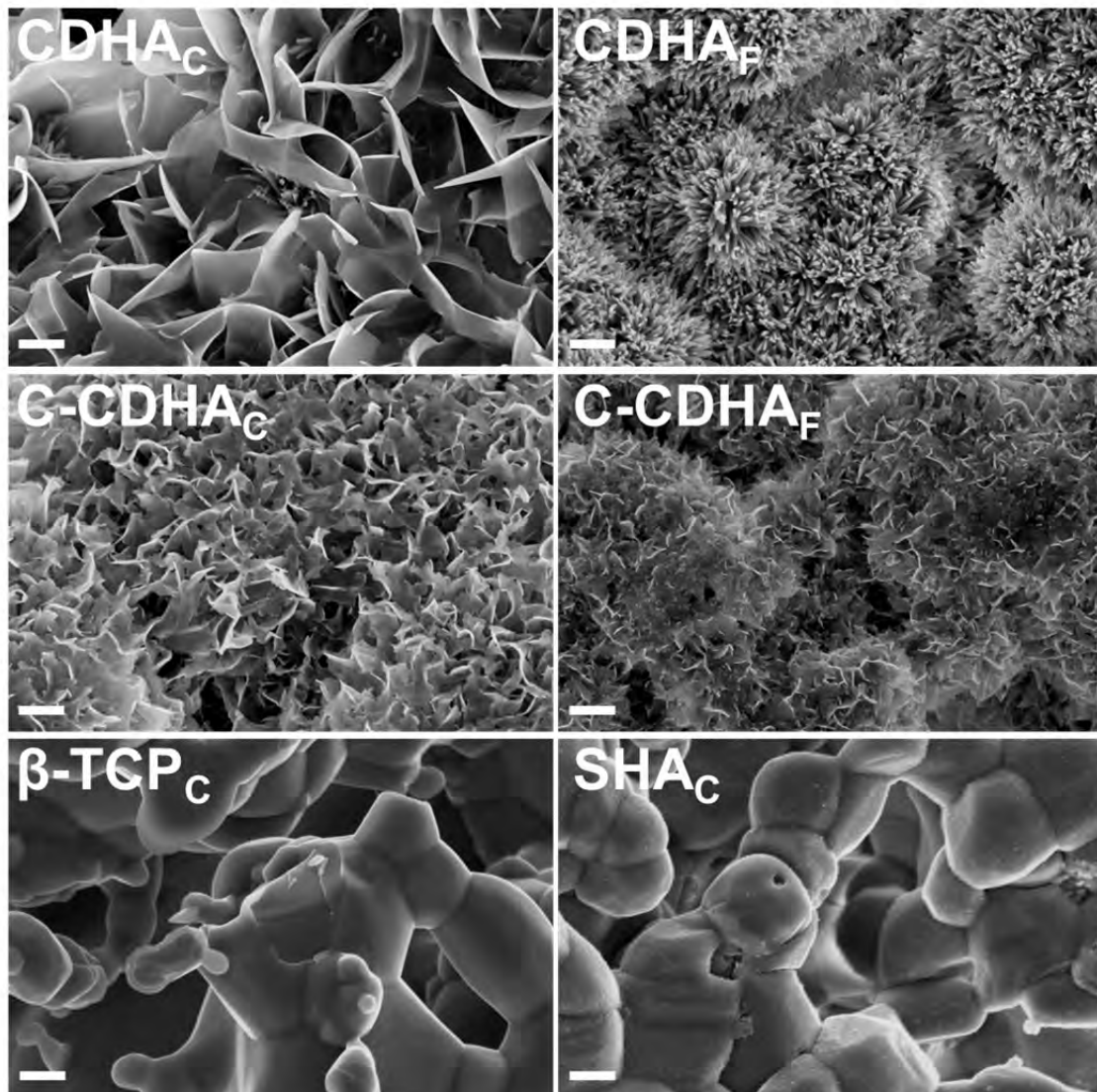
Figure 2-3. Scanning electron micrographs showing the microstructures of the different samples prepared with L/P ratio of 0.55mL/g (scale bar: 500nm).

Micrographs taken at a lower magnification of the CDHA and β-TCP non-foamed samples obtained at different L/P ratios and micrographs of the foamed samples revealed significant differences according to the processing methods of the materials (Figure 2-4). The increase in the L/P ratio led to more open

structures, consistent with an increase in the separation between the starting α-TCP particles, due to the higher amount of liquid. Foaming resulted in the formation of larger macropores, with pore interconnections, i.e., openings between adjacent macropores.
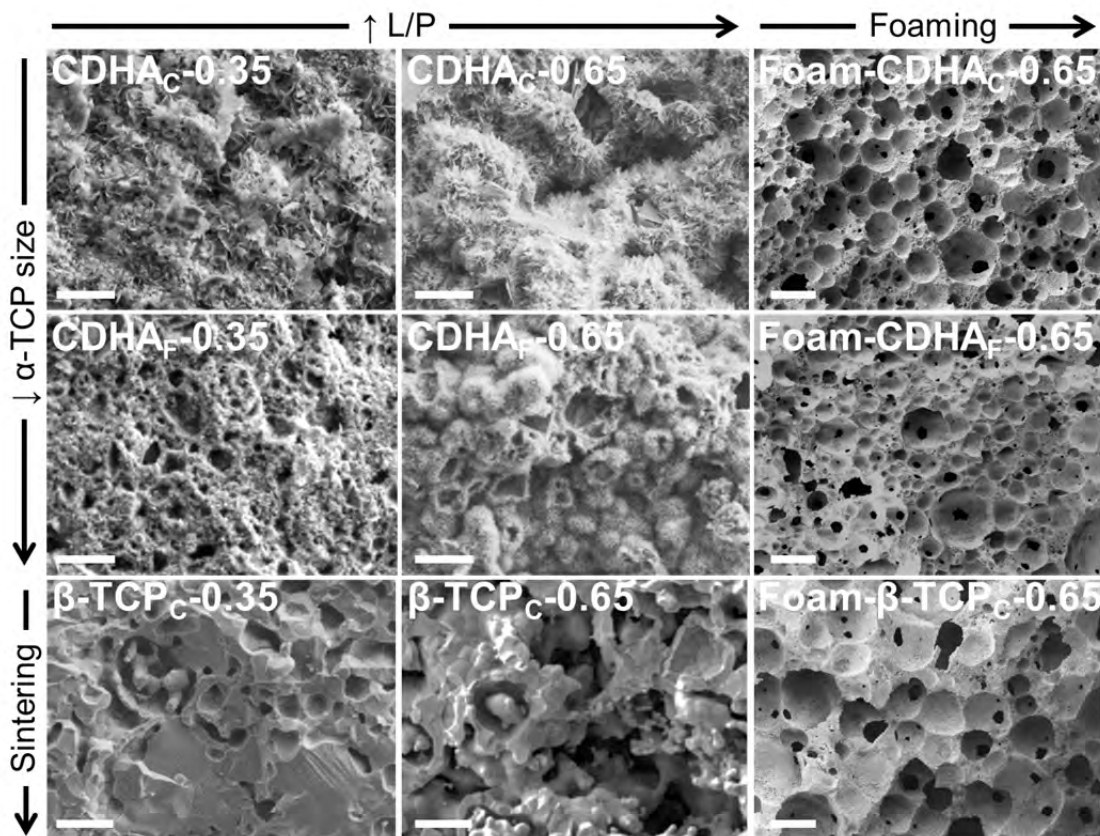
Figure 2-4. Scanning electron micrographs at low magnification of the non-foamed CDHA$_C$ and CDHA$_F$ and β-TCP$_C$ samples obtained with different L/P ratios (0.35 and 0.65mL/g), as well as of the foamed counterparts. The scale bar in the two first columns corresponds to 5μm, and in the third column (foams) to 100μm.

The specific surface area and total open porosity values for all materials are shown in Figure 2-5. Figure 2-5A displays the values for non-foamed materials and Figure 2-5B, for foamed analogues. Materials synthesized at high temperature showed low SSA values ($<1m^2$/g) whilst low temperature biomimetic substrates showed higher SSA values. Specifically, CDHA$_F$ with needle-like structure possessed the higher SSA values ($40m^2$/g) whereas CDHA$_C$, consisting of bigger plate-like crystals, showed lower values ($15m^2$/g). Carbonated samples (C-CDHA$_C$) showed values between those of CDHA$_C$ and CDHA$_F$ ($27m^2$/g). Carbonated CDHA fine (C-CDHA$_F$) was not analyzed since porosity, microstructure and SSA was equal to the coarse counterpart.

The L/P ratio did not have a significant effect on SSA values. Oppositely, L/P ratio had a great influence on porosity values. The increase in L/P ratio resulted

in higher percentages of open porosity, significantly evident after the foaming process, as assessed by MIP. The opening structure correlated to the increase in L/P ratio was also demonstrated by the decrease in mechanical properties. Compression strength showed a linear decrease upon L/P increase, independently from composition. Sintered β-TCP exhibited the highest compression strength, whilst biomimetic substrates showed similar resistance.
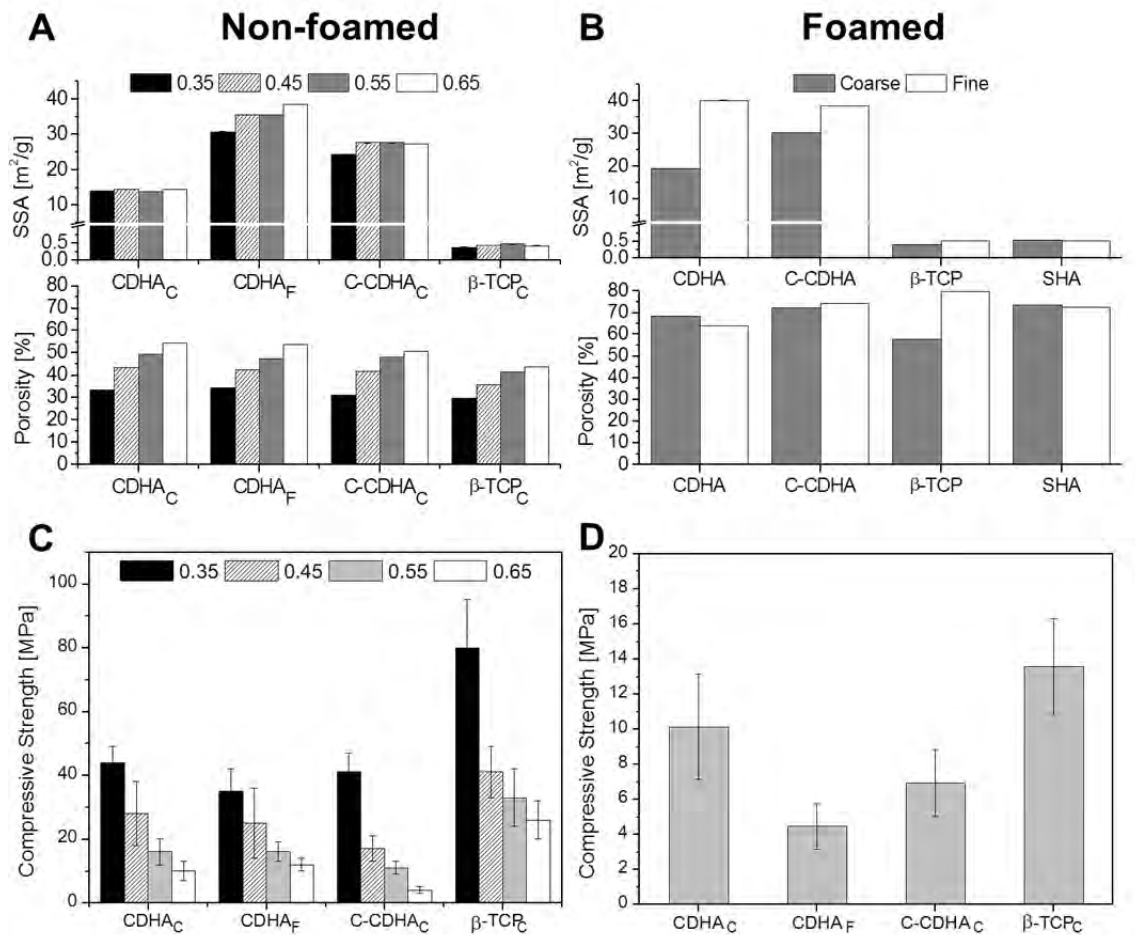
Figure 2-5. Specific surface area (SSA) and percentage of open porosity values for biomimetic and sintered non-foamed compositions (A) and for the corresponding foamed formulations (B). Note that for the foams two L/P were studied, 0.55 and 0.65mL/g, corresponding to coarse and fine formulations, respectively. Compression strength of the non-foamed samples for each L/P and for each different composition (C). Values corresponding to CDHA$_C$ and CDHA$_F$ were taken from reference [41]. Compression strength for the different foamed formulations (D).

Interestingly, in the non-foamed compositions, the increase of L/P ratio not only resulted in an increase in the total porosity, but also shifted the pore size distributions to larger sizes, as illustrated in Figure 2-6. All biomimetic samples (CDHA$_C$, CDHA$_F$ and C-CDHA$_C$) showed bimodal pore populations. Larger pores account for the pores in between aggregates (micrometric range), and the smaller pores relate to the distance between crystals (nanometric range). In contrast, sintered β-TCP samples exhibited a large peak centered around 1μm,

and an almost total disappearance of the nanoporosity, as a consequence of nanocrystal coalescence during the sintering process.

The effect of the foaming process on the pore size distribution is illustrated for biomimetic and sintered foams in Figure 2-6E and F, respectively. Biomimetic foams (Figure 2-6E) maintained the trend regarding nano-microporosities, with a superimposed macroporosity up to 100µm. Upon sintering, the macroporosity as well as the microporosity around 1µm were maintained, whereas no nanoporosity was observed as a result of the aforementioned coalescence of the nanocrystals (Figure 2-6F).
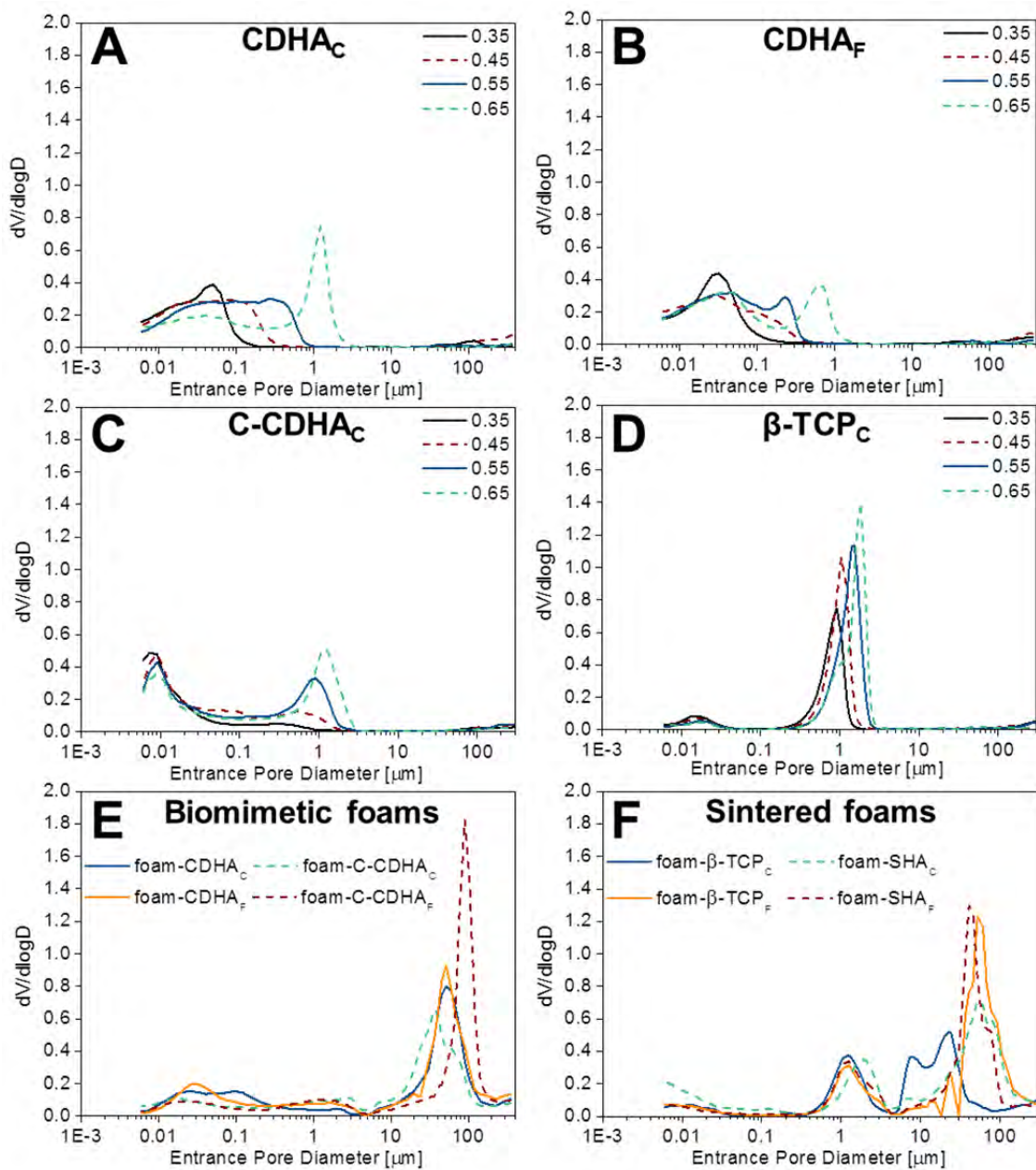
Figure 2-6. Pore entrance size distributions of the different samples, as determined by MIP.

2.3.2. Accelerated degradation study

The results of the accelerated degradation study are illustrated in Figure 2-7. Figure 2-7A depicts the degradation of the different non-foamed materials depending on their L/P ratio while Figure 2-7B shows the degradation of the foamed samples (non-foamed counterparts are included as control samples). Overall, when the liquid to powder ratio increased, the degradation increased for all samples but to varying degrees depending on their composition, microstructure, and textural properties. For a given L/P, $CDHA_F$ experienced a larger weight loss than the similar $CDHA_C$, and the degradation was more sensitive to the increase in L/P than the coarse counterpart. Surprisingly, the carbonated apatite (C-CDHA) exhibited the lowest degradation values of all samples, whereas β-TCP, despite being the most soluble phase, showed degradation values between CDHA and C-CDHA.
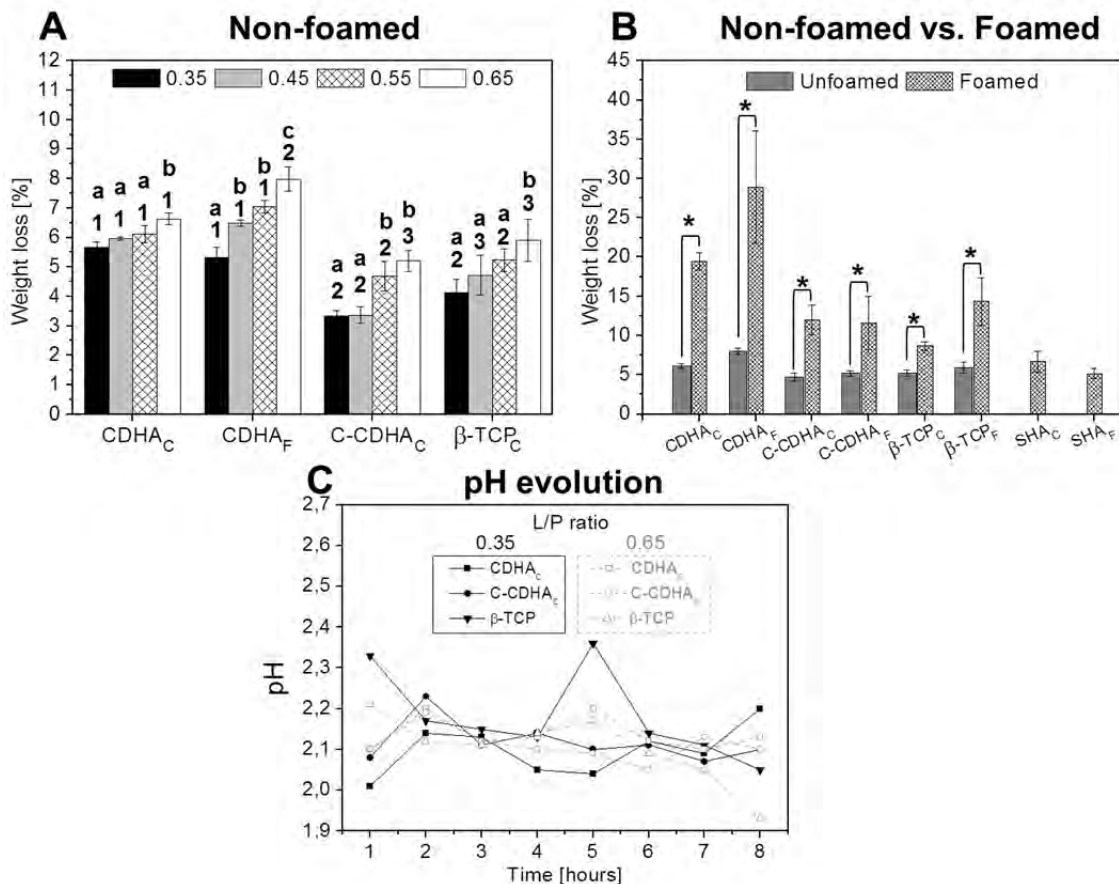
Figure 2-7. Accelerated *in vitro* degradation for biomimetic and sintered samples (n=3). A) Non-foamed samples groups identified by the same superscripts are not statistically different (P > 0.05). Letters indicate differences between different L/P within the same formulation; numbers identify differences between compositions for the same L/P (p<0.05); B) Degradation for foamed samples and non-foamed counterparts. According to subscripts, coarse samples have L/P of 0.55mL/g and fine analogues 0.65mL/g. * denotes statistically significant differences (p<0.05) between samples, dense and foamed, respectively, C) pH values for L/P ratio 0.35 and 0.65mL/g.

The incorporation of macroporosity in the foamed samples resulted in remarkable increases in degradation, compared to their non-foamed analogues (see Figure 2-7B). However, the extent of the increase was strongly dependent on the substrate. Thus, biomimetic CDHA showed the highest increase (three- and four-fold weight loss for the foamed $CDHA_C$ and $CDHA_F$ compared to their non-foamed counterparts). In the carbonated samples, C-CDHA, the impact of the macroporosity was smaller resulting in a three-fold weight loss increase irrespective of the α-TCP particle size. In the sintered β-TCP, the impact of foaming in the degradation was again dependent on the size of the starting α-TCP, being two or three-fold for β-TCP_C and β-TCP_F respectively. SHA foams showed the lowest degradation among all foamed materials, yielding similar resorption as non-foamed materials. Figure 2-7C shows the pH values measured during the degradation experiment. Steady values in pH were observed for all samples throughout the experiment, irrespective of sample composition and porosity.

Figure 2-8 combines the degradation results obtained for each material as a function of porosity. Despite that non-foamed formulations exhibited a linear increase with L/P (differences in slope were observed depending on sample type), the introduction of interconnected macropores in the foamed formulations led to marked changes in the degradation behavior. Degradation increased exponentially (exponential growth function) on the biomimetic samples with correlation coefficients (R^2) of 0.986, 0.799, and 0.855 for coarse, fine, and carbonated CDHA respectively, but remained linear for the sintered β-TCP (R^2= 0.938).

The samples were analyzed after degradation, to investigate possible changes in composition and morphology. The results for representative samples of each composition at a fixed L/P (0.55mL/g) are shown in Figure 2-9. XRD (Figure 2-9A) proved that no additional phases were re-precipitated. SEM images (Figure 2-9B) taken of the surface of the materials clearly demonstrated the degradation of the pristine plate and needle like crystals in the biomimetic CDHA samples, whilst images of β-TCP exhibited a less-obvious degradation only visible at the grain boundaries. The microstructure of the non-foamed samples cross-sections remained intact indicating that the acid was not penetrating the sample bulk.

47
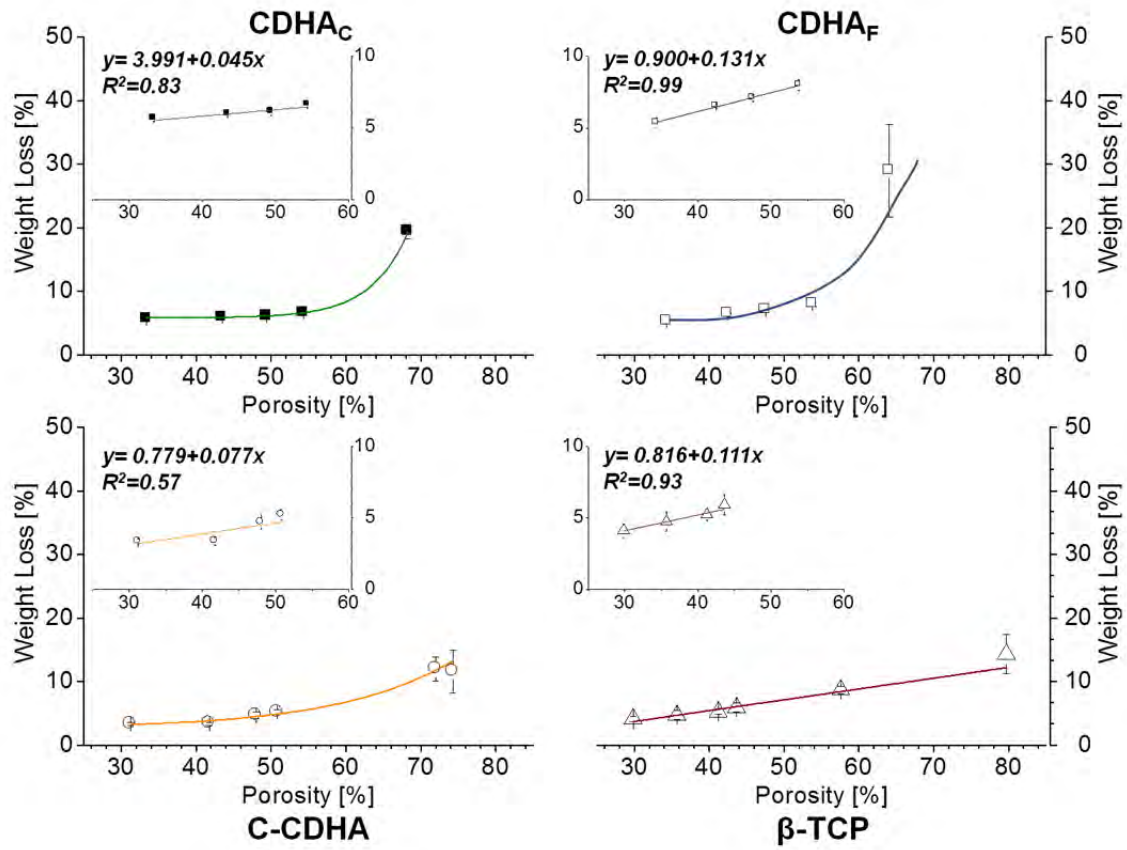
Figure 2-8. Degradation of the different samples as a function of the open porosity depicted in Figure 2-5. Insets for each type of material corresponds to dense formulations (including 4 different L/P ratios), while full graphs combine dense with the foamed specimens. C-CDHA$_C$ and β-TCP include the foamed coarse and fine specimens.
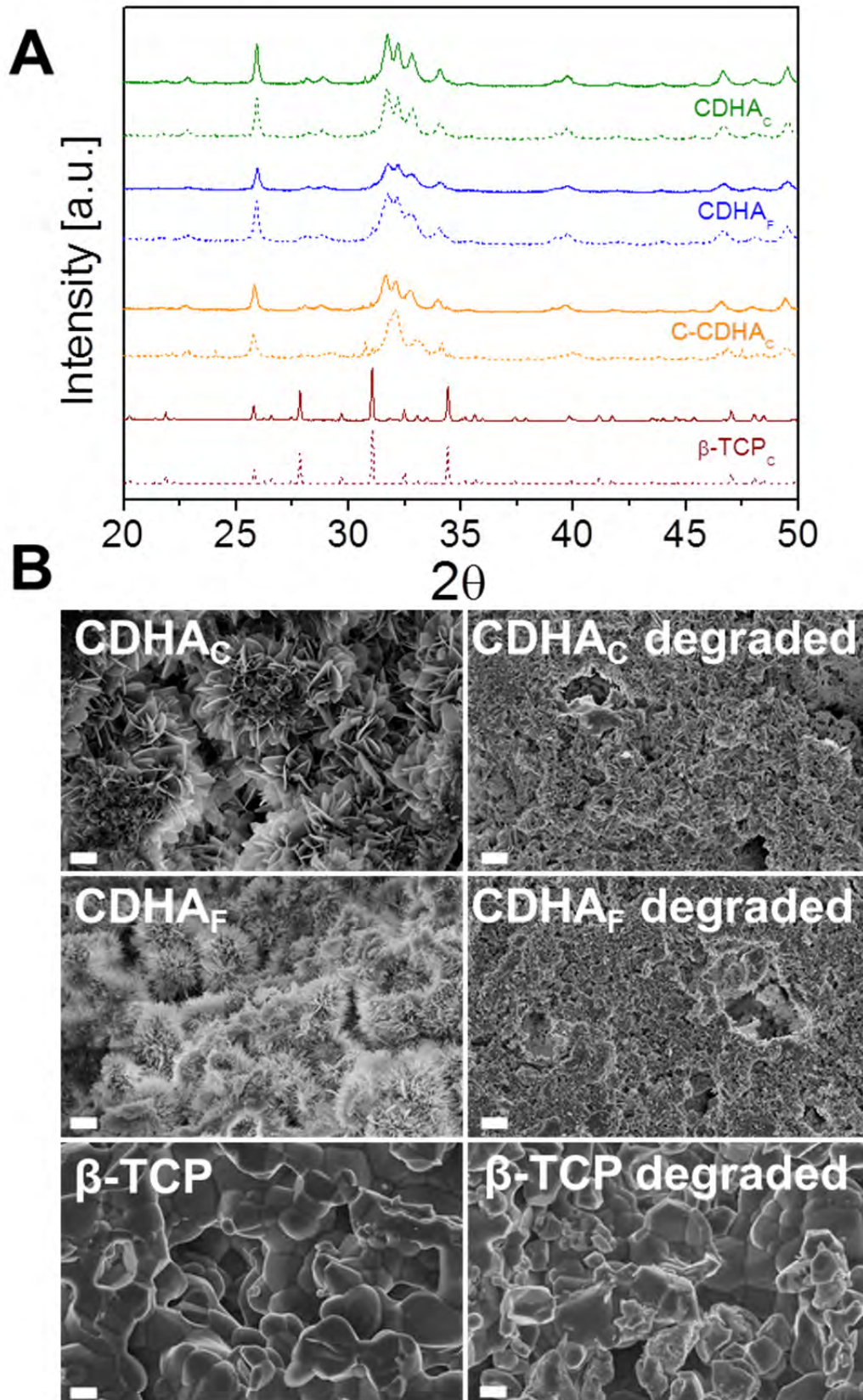
Figure 2-9. XRD (A) and SEM (B) images for different compositions with L/P of 0.55mL/g before (solid line) and after degradation (dashed line). SEM images of the surface of the specimens for the biomimetic CDHA (coarse and fine) and β-TCP, before and after degradation (scale bar: 1μm).

2.4. Discussion

The present study analyses the degradation behavior of different calcium phosphate biomaterials. The simple *in vitro* model used here does not capture all the complex mechanisms occurring during the degradation process of a biomaterial once implanted in the body. Therefore, the results obtained cannot directly be translated to material performance *in vivo*. However, this model facilitates comparison of the sensitivity to acidic degradation of different synthetic calcium phosphate ceramics, and, most importantly, it makes easier analyzing the relevance of some textural properties, i.e. specific surface area and porosity, during the acidic degradation of synthetic calcium phosphates.

The use of cementitious reactions in the formulation of biomimetic samples was vital to control the level of nano- and microporosity of the samples.[40] Indeed, the hydrolysis of α-TCP at body temperature results in the precipitation of an entangled network of crystal aggregates responsible for the presence of nanoporosity in the samples (Figure 2-4 and Figure 2-6). Increasing the L/P ratio during sample preparation gradually introduced an additional level of porosity within the micron range, due to an increase in the distance between crystal aggregates(Figure 2-4 and Figure 2-6).[40] Furthermore, the foaming process allowed introducing an interconnected network of macropores in the material (Figure 2-4 and Figure 2-6). This provided a platform to systematically assess the role of the multiscale level of porosity in the degradation behavior of calcium phosphates. On the other hand, the change in the starting α-TCP powder size from fine (F) to coarse (C) led to a change in the morphology of the nanocrystals from needles to plates -regardless of the L/P ratio- with a consequent change in SSA. The SSA was controlled by the surface area of the crystals which was readily available due to porous nature of cements (crystals precipitate forming an open entangled network) and was not affected by the L/P ratio. Modification of the cements composition was achieved either by incorporation of carbonate ions during precipitation or by a sintering process.

The degradation behavior of the different materials can be analyzed in two separate blocs: the degradation of the non-foamed samples, i.e. micro/nanoporous samples, versus the degradation of the foamed formulations, i.e., macroporous samples. Although all samples were inherently porous, non-foamed specimens possessed a maximum pore size below 3µm, whilst foamed formulations presented a superimposed macroporosity, typically above 10µm.

Regarding the non-foamed CDHA materials, despite the similar porosity values of biomimetic coarse and fine samples at a fixed L/P ratio, fine samples yielded higher resorption (Figure 2-7A), thus revealing the effect of SSA (the only

exception was for L/P 0.35). Thus, for a given porosity, $CDHA_F$ degraded more than $CDHA_C$. However, the difference in weight loss was small, and depended on the porosity and pore size of the specimens. Changing the L/P from 0.35 to 0.65mL/g led to a linear increase in the degradation of biomimetic C and F samples. This was due not only to the increase in total porosity with L/P, but also to the displacement of pore sizes to larger values, due to the increase in interaggregate spaces.[40,41] This led to the appearance of an interconnected pore network around 1-2μm (Figure 2-6A and B) through which the acidic media could improve penetration even if this was limited to the nearby surface. As shown in Figure 2-8, the increase of degradation with microporosity was more pronounced for the $CDHA_F$ than for $CDHA_C$ (from 5wt% to 6.5wt% and 8wt% respectively), leading to a three times larger slope (0.13 vs. 0.04). This can be associated to the higher SSA and is in agreement with the trend observed by Kuo *et al.* using calcium sulphate based materials.[51]

However, for the less porous formulations: $CHDA_C$ and $CDHA_F$ at L/P of 0.35, a similar degradation of around 5wt% was observed even if $CDHA_F$ doubled the SSA of $CHDA_C$. The lower packing efficiency of coarse samples results in interaggregate spaces slightly larger than those observed for fine samples (pores centered at 50nm and 30nm in Figure 2-6A and B, respectively) allowing more liquid penetration and the subsequent degradation of the exposed volume.

It is worth mentioning that in calcium phosphate cements the L/P ratio and the particle size of the starting powder, which determine the SSA and micro-nanoporosity (Figure 2-5 and Figure 2-6), are usually adjusted in order to optimize the mechanical and rheological properties, but their effect on the degradation rate is often overlooked. The results obtained show that they also influence the sensitivity to acidic degradation, and therefore, this should be taken into account in the design of the cement formulation.

The setting of the α-TCP cement in a carbonate solution produced a carbonate-doped calcium deficient apatite. Interestingly, despite the comparable values in SSA between carbonated doped HA ($C-CDHA_C$) and the non-carbonated substrates ($CDHA_C$, $CDHA_F$), the degradation behavior was significantly lower for the carbonated samples ($p<0.05$). This was unexpected, since the incorporation of carbonate ions in the hydroxyapatite lattice is known to markedly disturb the crystal lattice[52] increasing its solubility.[53–55] Quantitatively, $C-CDHA_C$ resorption was reduced by a 30-50% compared to $CDHA_F$, regardless of the L/P ratio. Figure 2-7C and Figure 2-9 showed that the carbonate ions released during degradation did not increase the pH of the degrading media, which could have altered the degradation behavior. Additionally, the ions released did not cause re-precipitation of secondary phases

either. Moreover, although in the present work high percentages of carbonate were obtained; those values were comparable to other reported works.[56] Most importantly, the position of the carbonate bands in the FTIR indicated the incorporation of carbonate ions in the phosphate positions as shown in Figure 2-2B. Typical bands of CO_3^{2-} at 1414 and 1471cm^{-1} [21,48,49] gave evidence of a preferred B-type substitution. However, due to the broad bands in carbonate region υ_2 region (871cm^{-1}) further analysis are necessary to discard some adsorbed or interstitial carbonate.

The reason for the unexpected decrease in degradation can be linked to the fact that in the present study, the degradation behavior of the carbonated samples was compared to calcium deficient hydroxyapatite instead of stoichiometric hydroxyapatite, as most authors do. The former, i.e. $Ca_9(PO_4)_5(HPO_4)(OH)$, is inherently more soluble than stoichiometric HA, i.e.$Ca_{10}(PO_4)_6(OH)_2$,[57] with solubility products of 85.1 (-log K_{PS}) and 116.8 (-log K_{PS}) respectively,[11] due to its distorted lattice and consequently lower crystallinity. The results obtained suggest that the incorporation of carbonate ions in this kind of pre-distorted lattice does not have the same effect than in stoichiometric HA; rather than increasing the solubility the opposite happens.

Figure 2-7A also displays the results for the degradation behavior of β-TCP samples at the different L/P. It is interesting to note that, in spite of having a much higher solubility, with a solubility product of 28.9 (-log K_{PS})[11,58] and larger pore sizes (Figure 2-6), its degradation was lower than that of CDHA, which can be explained by the much smaller SSA. Similar to what was already observed for the biomimetic samples, the increase in L/P led to a gradual increase of the degradation of sintered β-TCP samples from 4% to 6% for L/P 0.35 to 0.65, respectively, with a slope similar to that of CDHA$_F$.

The second part of the study aimed to discern the effect of macroporosity on the degradation rates of biomimetic and sintered samples. Since not all L/P could be foamed, only one L/P per material was selected to assess the effect of macroporosity on degradation, that being the one that allowed obtaining similar values of macroporosity in the different materials (Figure 2-6B). For biomimetic CDHA samples, foaming resulted in an increase of the extent of degradation to levels between a 20-30wt% (Figure 2-7B). The carbonated samples showed a smaller increase, in agreement with the decreased degradation observed in the non-foamed specimens. For the sintered samples, foaming led to a maximum of 15% of mass loss. The degradation values for β-TCP obtained upon sintering CDHA$_C$ were rather low if compared to β-TCP obtained from CDHA$_F$. This can be explained by the low porosity of the former formulation (Figure 2-5B).For comparison purposes, Figure 2-7B also included the degradation of a

stoichiometric HA foam. As expected, SHA presented the lowest degradation among all foams comparable to the non-foamed materials (5-7wt%) due to its low solubility and low SSA.

The benefits of having an open porous structure in the degradation of CaP was also observed by Schaefer *et al.* using 2D dense disks and 3D porous scaffolds consisting of sintered HA and β-TCP.[14] Figure 2-8 combines the degradation behavior obtained for the non-foamed and foamed materials as a function of porosity. The graph for each composition shows that for the biomimetic substrates, foaming results in an exponential increase in degradation, which can be explained by the large available area that becomes exposed to the acidic medium, and therefore is susceptible to degradation. The relevance of the SSA, in this respect, was highlighted by the observation that the introduction of similar levels of macroporosity resulted in a significantly higher increase in degradation for the fine than for the coarse CDHA foams (29% vs 19% weight loss), corresponding to a SSA of 30 and 14m^2/g respectively. Thus, similar levels of added macroporosity represented a 3-fold increase in degradation for the coarse CDHA, whereas for the fine CDHA the increase was 4-fold.

Interestingly, for the sintered β-TCP, the impact of the macroporosity introduced by foaming on the degradation was much lower, as it only resulted in a linear increase in degradation. On one hand, this can be explained by its low SSA, and on the other, by the larger size of the micropores already present in the substrate which may help to improve penetration of the acidic solution within the material, even in absence of macropores, therefore reducing the impact of the macroporosity. In spite of having a high SSA, an intermediate behavior was found for the carbonated hydroxyapatite samples that did not experience such a large increase in degradation upon foaming as did the CDHA samples, probably due to the low solubility already found in the non-foamed samples.

One important aspect to check was whether the degradation of the calcium phosphates generated any by-products due to the acidic environment during the experiment. Indeed, in previous works, where degradable polymers like polylactic acid or derivatives were incorporated[59,60] to increase the degradation of CaP, the precipitation of brushite was reported due to the acidic environment caused by the degradation of these polymeric phases.[61] As demonstrated by the XRD patterns (see Figure 2-9A), the composition of all samples remained unaltered after degradation, while SEM images evidenced the microstructural changes post-degradation (Figure 2-9B). However, whereas the microstructure of the CDHA surface appeared clearly degraded due to the acidic environment, the dissolution on sintered β-TCP was noticeable mainly at the grain boundaries, which induces the formation of cracks and irregularities on the grain surfaces and

was also highlighted by Koerten *et al.*[38] Despite the visible effects of degradation, the penetration degree of the acidic medium was limited to a few micrometers from the surface (e.g. up to 10µm for a L/P=0.55) for the non-foamed samples. In the case of the foamed samples, the presence of interconnected macropores allowed the penetration of the acidic medium throughout all material.

Overall, this study demonstrates the importance of textural properties, which can modulate or even outweigh the effect of other intrinsic properties such as the solubility of the compounds. The tuning of porosity and SSA at a multiscale level (nano, micro and macroporosity) is a powerful tool to control the degradation of CaPs, which can even exceed the effect of the intrinsic solubility of the material.

2.5.   Conclusions

The *in vitro* degradation behavior of different CaPs was compared in terms of composition, SSA, and multiscale porosity (nano, micro, and macroporosity) using an isotonic acidic solution of pH 2 to emulate the acidic osteoclastic environment during bone remodeling. The SSA played an important role in the degradation as shown by the comparison between biomimetic samples with different SSA and a range of porosities at different length scales. In this respect, it is important to stress the advantage offered by the biomimetic processing of CaP, which allows tuning the SSA in a much higher range than the high temperature sintering methods. However, the effect of SSA on degradation was dependent on the porosity and pore size, which conditioned the extent of acid penetration within the samples. The combination of SSA and porosity (nano-, micro- and macro) resulted in an exponential increase in the degradation for high SSA materials but to a linear increase in sintered materials with low SSA. Varying these parameters allowed tuning degradation from 3wt% up to 30wt%. Without the foaming step, degradation could not go beyond the 8wt%. In contrast to what happens with stoichiometric hydroxyapatite, doping with carbonate did not result in an increase of the chemical degradation of biomimetic CDHA, indicating that carbonate did not have the same effect, probably due to the lower crystallinity and the already distorted network of CDHA compared to stoichiometric hydroxyapatite.

2.6. References

[1]   J.P. Schmitz, J.O. Hollinger, The critical size defect as an experimental model for craniomandibulofacial nonunions., Clin. Orthop. Relat. Res. (**1986**) 299–308.
[2]   M. Bohner, Resorbable biomaterials as bone graft substitutes, Mater. Today. **13** (2010) 24–30.
[3]   R.A. Bhatt, T.D. Rozental, Bone graft substitutes., Hand Clin. **28** (2012) 457–468.
[4]   D.W. Hutmacher, J.T. Schantz, C.X.F. Lam, K.C. Tan, T.C. Lim, State of the art and future directions of scaffold-based bone engineering from a biomaterials perspective, J. Tissue Eng. Regen. Med. 1 (**2007**) 245–260.
[5]   J.R. Dimar, S.D. Glassman, The art of bone grafting, Curr. Opin. Orthop. **18** (2007) 226–233.
[6]   R. Dimitriou, E. Jones, D. McGonagle, P. V Giannoudis, Bone regeneration: current concepts and future directions, BMC Med. **9** (2011) 66.
[7]   D.W. Hutmacher, Scaffolds in tissue engineering bone and cartilage, Biomaterials. **21** (2000) 2529–2543.
[8]   M. Vallet-Regi, Calcium phosphates as substitution of bone tissues, Prog. Solid State Chem. **32** (2004) 1–31.
[9]   F. Barrère, C.A. Van Blitterswijk, Bone regeneration : molecular and cellular interactions with calcium phosphate ceramics, **1** (2006) 317–332.
[10]   S. V Dorozhkin, Bioceramics of calcium orthophosphates, Biomaterials. **31** (2010) 1465–1485.
[11]   C.P.A.T. Klein, A.A. Driessen, K. de Groot, A. van den Hooff, Biodegradation behavior of various calcium phosphate materials in bone tissue, J. Biomed. Mater. Res. **17** (1983) 769–784.
[12]   T. Okuda, K. Ioku, I. Yonezawa, H. Minagi, Y. Gonda, G. Kawachi, M. Kamitakahara, Y. Shibata, H. Murayama, H. Kurosawa, T. Ikeda, The slow resorption with replacement by bone of a hydrothermally synthesized pure calcium-deficient hydroxyapatite, Biomaterials. **29** (2008) 2719–2728.
[13]   S. Schaefer, R. Detsch, F. Uhl, U. Deisinger, G. Ziegler, How Degradation of Calcium Phosphate Bone Substitute Materials is influenced by Phase Composition and Porosity, Adv. Eng. Mater. **13** (2011) 342–350.
[14]   A. Ogose, T. Hotta, H. Kawashima, N. Kondo, W. Gu, T. Kamura, N. Endo, Comparison of hydroxyapatite and beta tricalcium phosphate as bone substitutes after excision of bone tumors, J. Biomed. Mater. Res. **72B** (2005) 94–101.
[15]   S. Gallinetti, C. Canal, M.-P. Ginebra, J. Ferreira, Development and Characterization of Biphasic Hydroxyapatite/β-TCP Cements., J. Am. Ceram. Soc. **97** (2014) 1065–1073.
[16]   S. Yamada, Osteoclastic resorption of calcium phosphate ceramics with different hydroxyapatite/β-tricalcium phosphate ratios, Biomaterials. **18** (1997) 1037–1041.
[17]   Z. Sheikh, Y.L. Zhang, L. Grover, G.E. Merle, F. Tamimi, J. Barralet, In vitro degradation and in vivo resorption of dicalcium phosphate cement based grafts, Acta Biomater. **26** (2015) 338–346.
[18]   F. Tamimi, Z. Sheikh, J. Barralet, Dicalcium phosphate cements: Brushite and monetite, Acta Biomater. **8** (2012) 474–487.
[19]   J.H. Shepherd, D. V Shepherd, S.M. Best, Substituted hydroxyapatites for bone repair., J. Mater. Sci. Mater. Med. **23** (2012) 2335–2347.
[20]   E. Boanini, M. Gazzano, A. Bigi, Ionic substitutions in calcium phosphates synthesized at low temperature., Acta Biomater. **6** (2010) 1882–1894.
[21]   R.Z. LeGeros, R. Kijkowska, C. Bautista, J.P. LeGeros, Synergistic effects of magnesium and carbonate on properties of biological and synthetic apatites., Connect. Tissue Res. **33** (1995) 203–209.
[22]   R.Z. LeGeros, Effect of Carbonate on the Lattice Parameters of Apatite, Nature. **206** (1965) 403–404.
[23]   J. Barralet, J.C. Knowles, S. Best, W. Bonfield, Thermal decomposition of synthesised carbonate hydroxyapatite, J. Mater. Sci. Mater. Med. **13** (2002) 529–533.
[24]   I.R. Gibson, W. Bonfield, Preparation and characterization of magnesium/carbonate co-substituted hydroxyapatites., J. Mater. Sci. Mater. Med. **13** (2002) 685–693.
[25]   H. Lapczyna, L. Galea, S. Wüst, M. Bohner, S. Jerban, A. Sweedy, N. Doebelin, N. van Garderen, S. Hofmann, G. Baroud, R. Müller, B. von Rechenberg, Effect of grain size and

microporosity on the in vivo behaviour of β-tricalcium phosphate scaffolds., Eur. Cell. Mater. **28** (2014) 299–319.

[26]   R. Murugan, S. Ramakrishna, Aqueous mediated synthesis of bioresorbable nanocrystalline hydroxyapatite, J. Cryst. Growth. **274** (2005) 209–213.

[27]   N. Specchia, A. Pagnotta, M. Cappella, A. Tampieri, F. Greco, Effect of hydroxyapatite porosity on growth and differentiation of human osteoblast-like cells, J. Mater. Sci. **37** (2002) 577–584.

[28]   D. Tadic, F. Beckmann, K. Schwarz, M. Epple, A novel method to produce hydroxyapatite objects with interconnecting porosity that avoids sintering, Biomaterials. **25** (2004) 3335–3340.

[29]   A. Tampieri, Porosity-graded hydroxyapatite ceramics to replace natural bone, Biomaterials. **22** (2001) 1365–1370.

[30]   R.J. Miron, Y.F. Zhang, Osteoinduction: a review of old concepts with new standards., J. Dent. Res. **91** (2012) 736–744.

[31]   F. He, J. Zhang, F. Yang, J. Zhu, X. Tian, X. Chen, In vitro degradation and cell response of calcium carbonate composite ceramic in comparison with other synthetic bone substitute materials, Mater. Sci. Eng. C. **50** (2015) 257–265.

[32]   H. Guo, J. Su, J. Wei, H. Kong, C. Liu, Biocompatibility and osteogenicity of degradable Ca-deficient hydroxyapatite scaffolds from calcium phosphate cement for bone tissue engineering, Acta Biomater. **5** (2009) 268–278.

[33]   M.T. Fulmer, I.C. Ison, C.R. Hankermayer, B.R. Constantz, J. Ross, Measurements of the solubilities and dissolution rates of several hydroxyapatites, Biomaterials. **23** (2002) 751–755.

[34]   P. Ducheyne, S. Radin, L. King, The effect of calcium phosphate ceramic composition and structure onin vitro behavior. I. Dissolution, J. Biomed. Mater. Res. **27** (1993) 25–34.

[35]   Z. Xue, H. Zhang, A. Jin, J. Ye, L. Ren, J. Ao, W. Feng, X. Lan, Correlation between degradation and compressive strength of an injectable macroporous calcium phosphate cement, J. Alloys Compd. **520** (2012) 220–225.

[36]   I.A. Silver, R.J. Murrills, D.J. Etherington, Microelectrode studies on the acid microenvironment beneath adherent macrophages and osteoclasts., Exp. Cell Res. **175** (1988) 266–276.

[37]   C.R. Hankermeyer, K.L. Ohashi, D.C. Delaney, J. Ross, B.R. Constantz, Dissolution rates of carbonated hydroxyapatite in hydrochloric acid, Biomaterials. **23** (2002) 743–750.

[38]   H.K. Koerten, J. van der Meulen, Degradation of calcium phosphate ceramics, J. Biomed. Mater. Res. **44** (1999) 78–86.

[39]   F. Despang, A. Bernhardt, A. Lode, R. Dittrich, T. Hanke, S.J. Shenoy, S. Mani, A. John, M. Gelinsky, Synthesis and physicochemical, in vitro and in vivo evaluation of an anisotropic, nanocrystalline hydroxyapatite bisque scaffold with parallel-aligned pores mimicking the microstructure of cortical bone, J. Tissue Eng. Regen. Med. **9** (2015) E152–E166.

[40]   M. Nakamura, R. Hiratai, T. Hentunen, J. Salonen, K. Yamashita, Hydroxyapatite with High Carbonate Substitutions Promotes Osteoclast Resorption through Osteocyte-like Cells, ACS Biomater. Sci. Eng. **2** (2016) 259–267.

[41]   M. Espanol, R.A. Perez, E.B. Montufar, C. Marichal, A. Sacco, M.P. Ginebra, Intrinsic porosity of calcium phosphate cements and its significance for drug delivery and tissue engineering applications, Acta Biomater. **5** (2009) 2752–2762.

[42]   D. Pastorino, C. Canal, M.-P. Ginebra, Multiple characterization study on porosity and pore structure of calcium phosphate cements, Acta Biomater. **28** (2015) 205–214.

[43]   E.B. Montufar, T. Traykova, C. Gil, I. Harr, A. Almirall, A. Aguirre, E. Engel, J.A. Planell, M.P. Ginebra, Foamed surfactant solution as a template for self-setting injectable hydroxyapatite scaffolds for bone regeneration, Acta Biomater. **6** (2010) 876–885.

[44]   K. Sariibrahimoglu, S.C.G. Leeuwenburgh, J.G.C. Wolke, L. Yubao, J.A. Jansen, Effect of calcium carbonate on hardening, physicochemical properties, and in vitro degradation of injectable calcium phosphate cements., J. Biomed. Mater. Res. A. **100** (2012) 712–719.

[45]   M.M. Figueiredo, J.A.F. Gamelas, A.G. Martins,Characterization of Bone and Bone-Based Graft Materials Using FTIR Spectroscopy, T. Theophanides (Ed.), Infrared Spectroscopy - Life and Biomedical Sciences, InTech., **2012**, pp. 315-339.

[46]   L. Berzina-Cimdina, N. Borodajenko, Research of Calcium Phosphates Using Fourier Transform Infrared Spectroscopy, in: Infrared Spectrosc. – Mater. Sci. Eng. Technol., **2012**: pp. 123–148.

[47]   R.M. Wilson, J.C. Elliott, S.E.P. Dowker, L.M. Rodriguez-Lorenzo, Rietveld refinements and spectroscopic studies of the structure of Ca-deficient apatite., Biomaterials. **26** (2005) 1317–1327.

[48]   C. Rey, B. Collins, T. Goehl, I.R. Dickson, M.J. Glimcher, The carbonate environment in bone mineral: A resolution-enhanced fourier transform infrared spectroscopy study, Calcif. Tissue Int. **45** (1989) 157–164.

[49]   M.E. Fleet, The carbonate ion in hydroxyapatite: recent X-ray and infrared results., Front. Biosci. (Elite Ed). **5** (2013) 643–652.

[50]   B. Kundu, D. Basu, J.M.F. Ferreira, Development of porous HAp and b -TCP scaffolds by strach consolidation with foaming methos and drug chitosan bilayered scaffold based drug delivery system, J. Mater. Sci. Mater. Med. **21** (2010) 2955–2969.

[51]   S.-T. Kuo, H.-W. Wu, W.-H. Tuan, Y.-Y. Tsai, S.-F. Wang, Y. Sakka, Porous calcium sulfate ceramics with tunable degradation rate, J. Mater. Sci. Mater. Med. **23** (2012) 2437–2443.

[52]   D.G.A. Nelson, J.D.B. Featherstone, J.F. Duncan, T.W. Cutress, Paracrystalline Disorder of Biological and Synthetic Carbonate-substituted Apatites, J. Dent. Res. **61** (1982) 1274–1281.

[53]   E. Landi, G. Celotti, G. Logroscino, A. Tampieri, Carbonated hydroxyapatite as bone substitute, Ceram. Met. Interfaces **23** (2003) 2931–2937.

[54]   R.Z. LeGeros, M.S. Tung, Chemical Stability of Carbonate- and Fluoride-Containing Apatites, Caries Res. **17** (1983) 419–429.

[55]   R.Z. LeGeros, Calcium phosphates in oral biology and medicine., Monogr. Oral Sci. **15** (1991) 1–201.

[56]   M.E. Fleet, Infrared spectra of carbonate apatites: v2-Region bands., Biomaterials **30** (2009) 1473–1481.

[57]   M.T. Fulmer, I.C. Ison, C.R. Hankermayer, B.R. Constantz, J. Ross, Measurements of the solubilities and dissolution rates of several hydroxyapatites., Biomaterials **23** (2002) 751–755.

[58]   S. V. Dorozhkin, Calcium Orthophosphates in Nature, Biology and Medicine, Materials **2** (2009) 399–498.

[59]   R.P. Félix Lanao, K. Sariibrahimoglu, H. Wang, J.G.C. Wolke, J.A. Jansen, S.C.G. Leeuwenburgh, Accelerated calcium phosphate cement degradation due to incorporation of glucono-delta-lactone microparticles., Tissue Eng. Part A. **20** (2014) 378–388.

[60]   K. Sariibrahimoglu, J. An, B.A.J.A. van Oirschot, A.W.G. Nijhuis, R.M. Eman, J. Alblas, J.G.C. Wolke, J.J.J.P. van den Beucken, S.C.G. Leeuwenburgh, J.A. Jansen, Tuning the degradation rate of calcium phosphate cements by incorporating mixtures of polylactic-co-glycolic acid microspheres and glucono-delta-lactone microparticles., Tissue Eng. Part A. **20** (2014) 2870–2882.

[61]   J. An, S.C.G. Leeuwenburgh, J.G.C. Wolke, J.A. Jansen, Effects of Stirring and Fluid Perfusion on the In Vitro Degradation of Calcium Phosphate Cement/PLGA Composites., Tissue Eng. Part C. Methods. **21** (2015) 1171–1177.

Chapter 3

Carbonation of low temperature macroporous calcium phosphates

Scope

Carbonate is the major substituting ion found in biological apatites. It has been attempted to be incorporated into synthetic bone grafts, as a strategy to further enhance their biological performance. Mimicking biological apatites composition can render several advantages towards the recognition and integration of bone grafts. The present chapter investigates different routes to dope low temperature CDHA with carbonate as a tool to enhance their biological performance. The carbonation routes have been applied to macroporous CDHA, preserving their macrostructure and controlling micro and nanostructure, separately from the carbonation content.

.
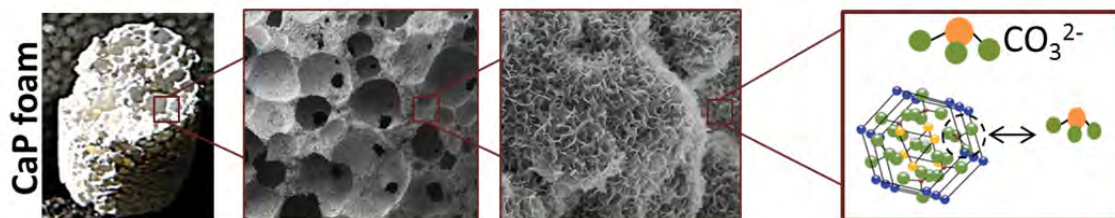
3.1.   Introduction

The development of biomimetic macroporous scaffolds, with a chemical composition and nanostructure close to the mineral phase of bone remains a major challenge. Biomaterials for bone regeneration need to adapt to the bone turn-over to help preserving the biological and mechanical characteristics of the bony site. This can be accomplished using macroporous scaffolds made of materials that closely mimic bone. It is widely accepted that biological apatites have a greater solubility than traditionally sintered calcium phosphate ceramics due to the nano-metric size of the crystals, their poor crystallinity and the presence of foreign ions where carbonate accounts for the major substitution (4-8%wt.).[1] Carbonate inclusion has indeed a major role in bone remodeling where bone resorbing cells, i.e. osteoclasts, have been closely associated to the selective resorption of regions of high carbonate inclusion[2] or by stimulating osteoblast activity.[3] This explains why biomimetic precipitation routes which provide nanosized crystals similar to those found in bone have been extensively investigated.[4–7] Unfortunately, in these studies the consolidation of nanoparticles into bulk samples require a sintering step negating any benefit of the nanoparticles.[8–10] Calcium phosphate (CaPs) cements are bulk bodies formed through biomimetic routes. One typical formulation is that of α-TCP that hydrolyses into a CDHA under physiological conditions, according to equation (1).

$$3Ca_3(PO_4)_2 + H_2O \rightarrow Ca_9(HPO_4)(PO_4)_5(OH) \quad\quad (Eq.\ 1)$$
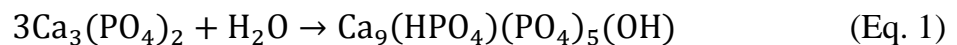
The setting reaction results in an entangled network of nano/submicron crystals with an intrinsic nano and microporosity and large SSA.[11] Additionally, CaP cements can be further modulated by the addition of macroporosity.[12,13] Variations in the local ionic environment during CDHA precipitation offer a suitable platform to incorporate foreign ions into the hospitable crystal structure of CDHA.[14]

Attempts to develop carbonated CPCs have been made by introducing sources of carbonate such as vaterite or calcite accomplishing high carbonation ratios.[15–20] The major side-effect of performing carbonation during the setting reaction was observed in the change of the rheological properties of the cement paste and the concomitant delay of the setting reaction. Unfortunately this requires re-adjusting the cement formulation to have setting times adequate for implantation. Del Real *et al.* added sodium bicarbonate in a CPC formulation as a method to create macropores due to the decomposition of CO_3^{2-} to CO_2.[21] However, while those formulations cannot be made injectable because of the risk of embolism, they have the added drawback that both carbonate and macropore content are coupled and cannot be adjusted separately.

The goal of the present chapter is to decouple carbonation from macropore formation by exploring different strategies for the carbonation of macroporous scaffolds based on

the hydrolysis of α-TCP. Carbonation was carried out either by introducing the carbonate during the setting reaction, i.e., simultaneously to the precipitation of CDHA, or by a post-treatment of the pre-set scaffolds. In both cases the macroporous structure of the scaffold was preserved. The extent of carbonate incorporation was investigated for the different methods varying the amount of carbonate and studying its textural and chemical implications.

3.2.   Materials and Methods

3.2.1.   Carbonation methods

Calcium phosphate foams (CPF) were prepared by mixing a powder phase consisting of α-TCP and 2wt% of precipitated HA with an aqueous solution containing 1wt% of polysorbate (Tween 80®, Sigma Aldrich, St.Louis, USA) that acted as surfactant.[22] Both phases were foamed at 7000rpm for 30s using a domestic food mixer, and the paste was transferred into 6x12mm^2 moulds. Three different carbonation routes were explored (Figure 3-1): i) carbonation during setting: the α-TCP foams were immersed in a NaHCO$_3$ solution (Sigma-Aldrich, St. Louis, USA) as setting medium, and either kept at 37 ºC for 17 days (coded as BC-S, standing for carbonation during biomimetic setting) or ii) subjected to an hydrothermal treatment by autoclaving at 121ºC and 1 bar for 30 minutes (HC-S, hydrothermal carbonation during setting). Prior to immersion in the carbonate solution the samples were left for 8h in a humid atmosphere at 37ºC to gain initial cohesion; and iii) post-setting carbonation: the hydrothermal treatment described above was applied to previously set CDHA foams, immersed in a NaHCO$_3$ solution (PS-HC, post-setting hydrothermal carbonation). Three different NaHCO$_3$ concentrations were used (2.5, 5 and 10wt% NaHCO$_3$). A control sample was prepared following method, using water as setting medium. Controls for BC-S and PS-HC were left 10 days for setting prior to carbonation treatment, whereas HC-S controls were autoclaved in water after 8h in humid atmosphere. After the treatment all samples were thoroughly rinsed with double distilled water to remove all dissolved salts. The schematic representation of the different carbonation methods is shown in Figure 3-1.
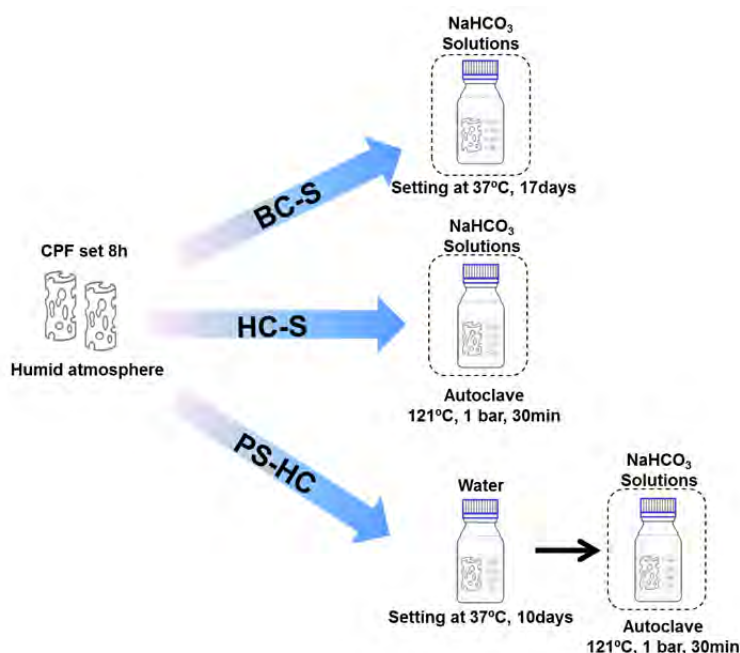
Figure 3-1. Schematic description of the different carbonation methods: i) BC-S, ii) HC-S and iii) PS-HC.

3.2.2. Characterization

The presence of carbonate was analyzed by ATR-FTIR (Nicolet 6700). Data was acquired in 64 scans with a resolution of 4cm^{-1} from 4000 to 575cm^{-1} with a Germanium crystal. The content of carbonate for the scaffolds processed using the highest concentration of carbonate (10wt% $NaHCO_3$) was analyzed by bulk combustion using a Thermal combustion element analyzer (Thermo EA 1108). The amount of carbonate was calculated according to the following equation (2).

$$\text{Percentage of Carbonate} = \frac{MW_{CO_3^{2-}}}{MW_C} \cdot \%_C \qquad \text{(Eq.2)}$$

where, $MW_{CO_3^{2-}}$ and MW_C are the molecular weight of carbonate and carbon, respectively, and $\%_C$ is the percentage of carbon given by the measurement. Samples were grinded and dried at 120°C overnight prior to analysis.

Phase composition was identified by XRD (D8 Advance diffractometer, Bruker) with a Cu Kα anode (monochromated, λ=1.5406Å), operated at 40kV, and 40mA. Data were acquired in 0.02° steps over the 2θ range of 10°-70° with 2s per step. For multiple phase quantification EVA software was used (Bruker). The textural properties of the foams were analyzed by scanning electron microscopy (SEM, Zeiss Neon40). Samples were coated with carbon to gain conductivity prior to imaging. The specific surface area of the scaffolds was determined by nitrogen adsorption using the BET (Brunauer-Emmett-Teller) method (ASAP Micromeritics).

3.3. Results and Discussion

3.3.1. Carbonation level and textural properties of the foams

The presence of carbonate as observed by FTIR (Figure 3-2) was highly dependent on the carbonation method. Carbonate bands specific for carbonate incorporation into CDHA were visible at 1471 and 1419cm^{-1}, corresponding to a B-type substituted apatite. The band at 874cm^{-1} can be assigned to both, HPO_4^{2-} or to a B-type carbonate substituted apatite.[4,23,24] The remaining bands were all attributed to typical vibrational modes of phosphate in apatite (stretching at 1030cm^{-1}, 964 and 1093cm^{-1} and the O-P-O bending modes at 604 and 563cm^{-1}).[25]

The PS-HC resulted in lower levels of carbonate compared to the other methods, as observed from the lower intensity of the carbonate bands. This result was expected, as carbonate ions needed to diffuse into the CDHA crystal structure. Increasing the carbonate content in the solution resulted in better defined bands by ATR-FTIR as observed with the increase in intensity of the v_3 CO_3^{2-} vibration mode (Figure 3-2). However, the maximum content of carbonate achieved by this method was 2.5wt%, obtained after immersion in 10wt% $NaHCO_3$ solution (Table 3-1). On the contrary, carbonation during setting, i.e. during precipitation of CDHA, either at 37°C (BC-S) or by the hydrothermal treatment (HC-S), increased the yield of carbonation (Figure 3-2). Moreover, increasing the content of carbonate in the setting medium increased the intensity of the carbonate bands in the precipitated apatite. The maximum levels of carbonate, obtained with the 10wt% $NaHCO_3$ solution, were 12.3% for BC-S method and 13.0% for HC-S method, similar to previous works.[26,27] The following table summarizes the maximum carbonate contents (using 10%wt. $NaHCO_3$) for each method, together with their SSA compared to control samples.

Table 3-1. SSA and maximum carbonate content for the different synthesis methods using 10%wt. NaHCO₃.

Method	CO_3^{2-} [%wt.]	SSA [m²/g] Control	SSA [m²/g] Carbonated
BC-S	12.3	20	30
HC-S	13	17	32
PS-HC	2.5	20	17
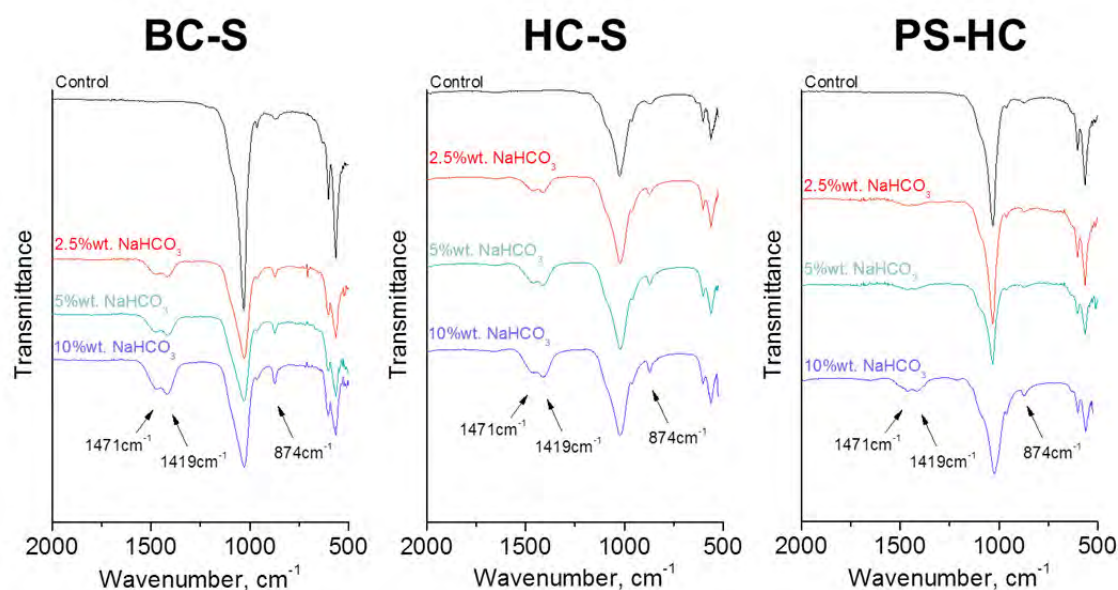
Figure 3-2. ATR-FTIR spectra for the samples obtained by the different carbonation methods, using carbonate solutions with different concentrations.

One fundamental aspect shared by all carbonation methods was their ability to preserve the structural integrity of the foams as shown in the low magnification SEM images of the foams cross-sections (Figure 3-3). BC-S method had a great impact on the microstructure of the precipitated crystals. When the dissolution of α-TCP and precipitation of CDHA took place in a carbonate-containing medium, a significant decrease in the crystal size was observed. The micrometric plate-like crystals found in the foams set in water (Figure 3-3A and inset) turned into smaller plates (Figure 3-3B and inset) in presence of carbonate, thus increasing the SSA from $20m^2/g$ to $30m^2/g$ respectively (Table 3-1). Similarly, HC-S method in water resulted in needle-like structures, whereas fine plate-like crystals were formed when the same treatment was done in presence of carbonate (Figure 3-3C inset and Figure 3-3D inset, respectively), the SSA increasing from 17 and $32m^2/g$, respectively. Finally, no changes in the microstructure were observed for PS-HC method, i.e. in CDHA foams (Figure 3-3E inset and Figure 3-3F inset), as in this case carbonate had to diffuse in pre-existing crystals. The SSA also showed no modification, with values of 20 and $17m^2/g$ for control and carbonated samples, respectively.
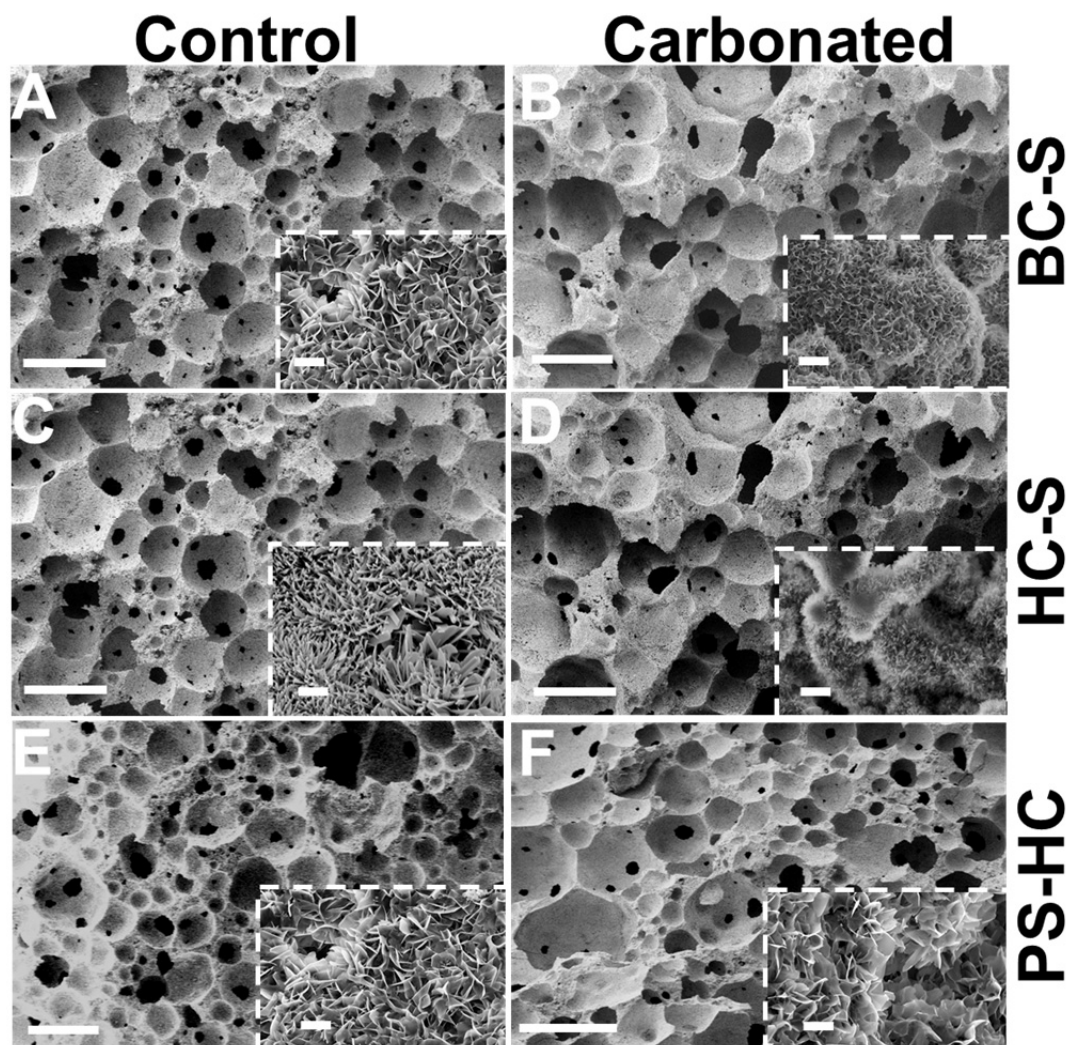
Figure 3-3. Representative SEM images of the pristine and carbonated foams at low magnification showing the interconnected macroporous geometry (scale bar: 500μm), and insetsat higher magnification (scale bar: 2μm) showing the representative micro-nanostructure of the crystals. The immersion solutions for the control and carbonated samples were water and 10%wt. NaHCO₃ respectively.

3.3.2. Composition of foams after carbonation

The presence of carbonate ions during setting can affect the setting kinetics, hence the importance of assessing total conversion to carbonated CDHA for each carbonation method. BC-S method required 17 days of setting to achieve the same degree conversion than the control samples after 10 days (Figure 3-4, grey solid line). Slight variations were found according to the amount of carbonate in solution. Unreacted α-TCP in control samples was slightly lower than in carbonated samples. According to the carbonate amount different contents of unreacted α-TCP were found (3 and 6% for the lowest and highest bicarbonate concentrations, respectively). Broader peaks were found as the carbonate content increased, owing to the crystal distortion provoked by carbonate incorporation into the CDHA and to the smaller size of the resulting

crystals. Importantly, no additional phases were found due to the incorporation of carbonate.

HC-S method considerably reduced the time required for the synthesis of carbonated apatite from days to hours. However, when the setting of control α-TCP foams, i.e. autoclaved in water, was performed in the autoclave, it resulted in a biphasic calcium phosphate consisting of 92% CDHA and 8% β-TCP (black dashed line), due to partial transformation of α-TCP into its allotropic phase. This transformation is in accordance with previously reported hydrothermal synthesis of α-TCP, where β-TCP appeared as an intermediate during the conversion to CDHA.[28,29] In contrast, hydrothermal setting in the presence of carbonate stabilized α-TCP instead of β-TCP. For the highest carbonate content solution (10wt% $NaHCO_3$) the resulting phase composition was 1% β-TCP, 9% α-TCP and 90% CDHA. Similar observations in terms of peak broadening were observed, in agreement with the lattice distortion caused by the incorporation of carbonate and the smaller size of the precipitated crystals. An additional non-identified phase appeared overlapped with the main peaks of hydroxyapatite (31.2º, 2θ) which was not possible to identify.

Interestingly, PS-HC method did not induce any alteration in XRD results in terms of peak broadening, as it would have been expected from the introduction of carbonate within the crystal lattice. This suggests that carbonate could be mostly concentrated in the hydrated layer rather than entering the crystal structure.[24] The lower carbonate content in PS-HC method is also consistent with the prominent shoulder at 630cm^{-1}, similar to control samples. Such behavior was also observed in the work by Combes *et al.* during carbonation of brushitic cements.[16] Slightly higher α-TCP was found as the bicarbonate concentration increased, possibly due to the α-TCP stabilizing effect of carbonate.
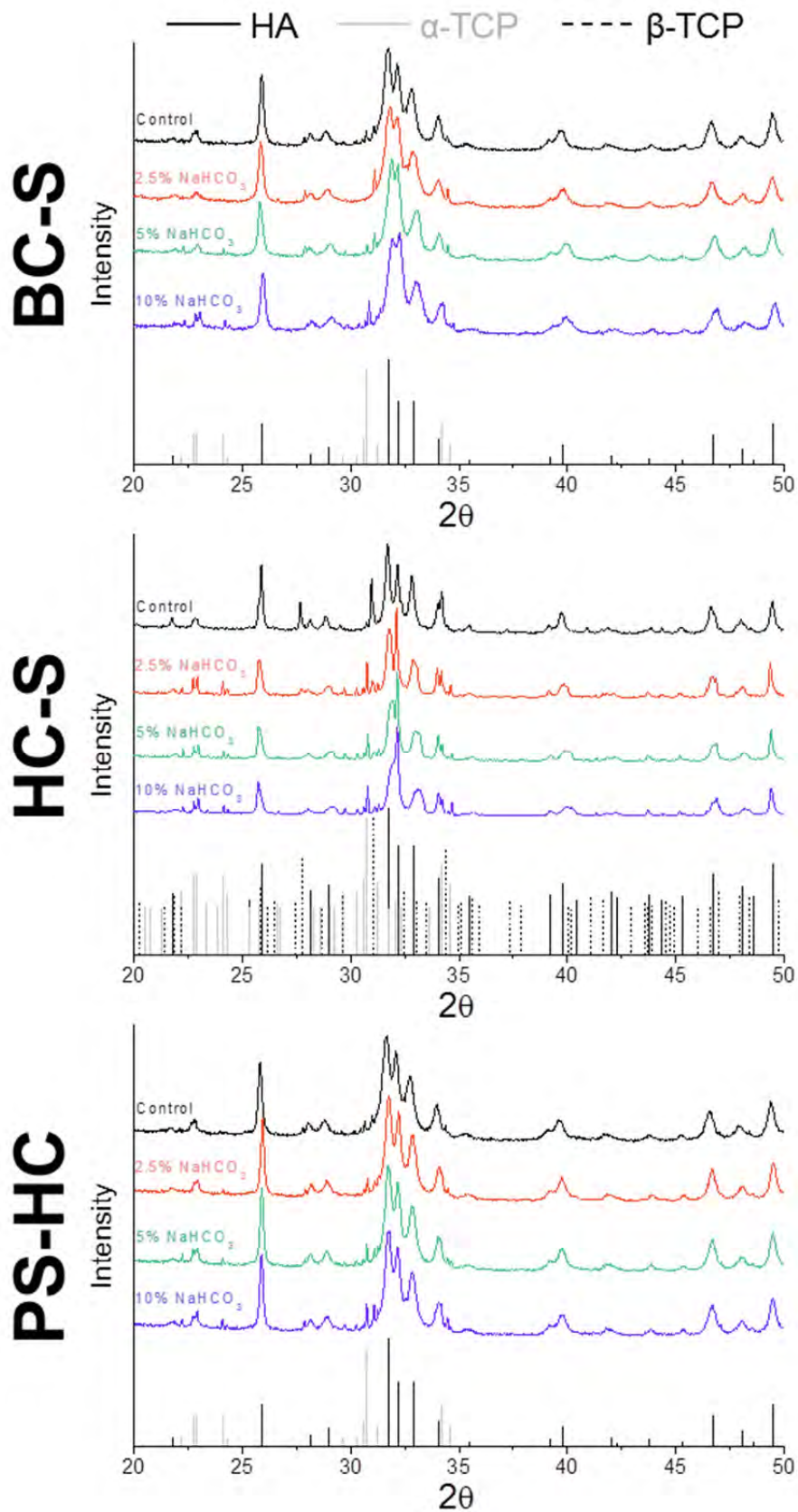
Figure 3-4. XRD patterns of the pristine and carbonated foams obtained using the different carbonation methods investigated. Patterns are shown at the bottom of each graph corresponding to HA (JCPDS 09-0432), α-TCP (JCPDS 09-0348) and β-TCP (JCPDS 09-0169).

3.4. Conclusions

The present chapter proves that is feasible to carbonate macroporous cements without compromising their three-dimensional integrity by decoupling carbonation from macropore structure formation. Three different strategies were explored which not only allowed controlling the carbonation degree but also the microstructure, phase composition and setting reaction. Controlling the carbonation degree of porous scaffolds without compromising the 3D network is fundamental for several biological events as it allows cell colonization, vascular tissue ingrowth and facilitates scaffold remodeling. The fact that the carbonate content can be tuned enables exploring how the degree of carbonation intervenes in the various biological events.

3.5. Appendix. Controlled biphasic calcium phosphate mixtures

Traditionally, BCP are obtained by sintering at high temperatures different calcium phosphate compounds with a specific Ca/P ratio. The composition of the biphasic formulations, which has great influence on the *in vivo* performance of CaPs implants,[30] can be adjusted through the Ca/P ratio.[31] The incorporation of controlled amounts of carbonate substituting phosphate groups in any of the carbonation processes earlier described (section 3.2.1), causes an alteration in the Ca/P ratio which could be used to prepare BCPs. The combination of macroporosity to allow angiogenesis, together with a source of calcium and phosphates prone to reprecipitated in the implant surrounding, has demonstrated to foster osteoinduction. Yuan *et al.* defined microporosity also as a requisite in bone formation.[32]

To prove the potential of obtaining BCP from carbonated samples, HC-S foams with different carbonate contents were prepared and sintered. For this purpose sodium hydrogen carbonate was first dissolved in water using different carbonate solution concentrations (0.1, 0.5, 1, 1.25, 1.5, 2.5, and 5%wt.) where CDHA foams were immersed and autoclaved (Figure 3-5). After hydrothermal setting, samples were sintered at 1100ºC for 9h and the phase composition was studied by XRD (D8 Advance diffractometer, Bruker). Phase quantification was performed using EVA software (Bruker), as previously described.

Depending on the amount of carbonate, the sintering process led to different compositions (Figure 3-6). Sintering of CDHA turns into pure β-TCP. The addition of 0.1wt% of sodium hydrogen carbonate already leads to a BCP composition consisting mainly of β-TCP (85%). The increase in carbonate further increases the content of HA phase, evidencing the carbonate substitution for phosphates. The decreasing in the phosphate content increases the Ca/P ratio, achieving a closer stoichiometric composition. Finally, 2.5wt% of carbonate addition transforms into pure HA. The

excess of carbonate might be detrimental since calcium oxide (Figure 3-6, red arrow) appears for carbonate contents above 2.5wt%, as is the case of 5wt% bicarbonate addition.
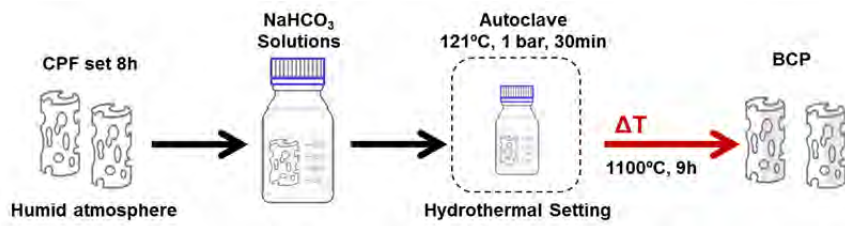
Figure 3-5. Hydrothermal carbonation setting of CPF and sintering process to obtain BCP.
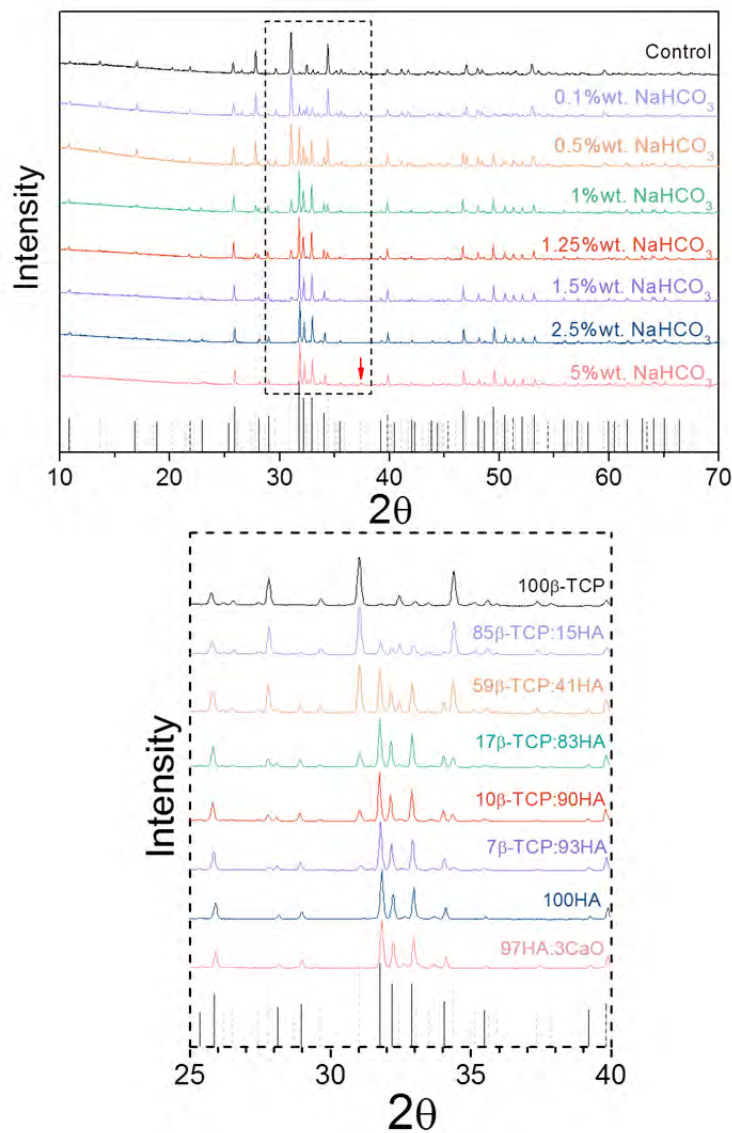
Figure 3-6. XRD data for foams autoclaved with different carbonate contents and sintered afterwards showing the phase composition of the BCP.

3.6.   References

[1]   M. Vallet-Regi, Calcium phosphates as substitution of bone tissues, Prog. Solid State Chem. **32** (2004) 1–31.

[2]   K. Pernelle, L. Imbert, C. Bosser, J.C. Auregan, M. Cruel, A. Ogier, P. Jurdic, T. Hoc, Microscale mechanical and mineral heterogeneity of human cortical bone governs osteoclast activity, Bone. **94** (2017) 42–49.

[3]   H. Nagai, M. Kobayashi-Fujioka, K. Fujisawa, G. Ohe, N. Takamaru, K. Hara, D. Uchida, T. Tamatani, K. Ishikawa, Y. Miyamoto, Effects of low crystalline carbonate apatite on proliferation and osteoblastic differentiation of human bone marrow cells, J. Mater. Sci. Mater. Med. **26** (2015) 99.

[4]   R. Murugan, S. Ramakrishna, Production of ultra-fine bioresorbable carbonated hydroxyapatite., Acta Biomater. **2** (2006) 201–6.

[5]   M. Vallet-Regi, D.A.A. Navarrete, Biomimetic Nanoceramics in Clinical Use, in: Royal Society of Chemistry, Cambridge, **2008**: pp. 25–60.

[6]   F.C.. Driessens, M.. Boltong, E.A.. de Maeyer, R. Wenz, B. Nies, J.. Planell, The Ca/P range of nanoapatitic calcium phosphate cements, Biomaterials. **23** (2002) 4011–4017.

[7]   Z. Zhao, M. Espanol, J. Guillem-Marti, D. Kempf, A. Diez-Escudero, M.-P. Ginebra, Ion-doping as a strategy to modulate hydroxyapatite nanoparticle internalization, Nanoscale. **8** (2016) 1595–1607.

[8]   E. Landi, G. Celotti, G. Logroscino, A. Tampieri, Carbonated hydroxyapatite as bone substitute, Ceram. Met. Interfaces. **23** (2003) 2931–2937.

[9]   I. Hofmann, L. Müller, P. Greil, F.A. Müller, Precipitation of Carbonated Calcium Phosphate Powders from a Highly Supersaturated Simulated Body Fluid Solution, J. Am. Ceram. Soc. **90** (2007) 821–824.

[10]   D. Tadic, F. Peters, M. Epple, Continuous synthesis of amorphous carbonated apatites, Biomaterials. **23** (2002) 2553–2559.

[11]   M.P. Ginebra, F.C.M. Driessens, J.A. Planell, Effect of the particle size on the micro and nanostructural features of a calcium phosphate cement: a kinetic analysis., Biomaterials. **25** (2004) 3453–62.

[12]   M.-P. Ginebra, J.-A. Delgado, I. Harr, A. Almirall, S. Del Valle, J.A. Planell, Factors affecting the structure and properties of an injectable self-setting calcium phosphate foam, J. Biomed. Mater. Res. Part A. **80A** (2007) 351–361.

[13]   M.P. Ginebra, M. Espanol, E.B. Montufar, R.A. Perez, G. Mestres, New processing approaches in calcium phosphate cements and their applications in regenerative medicine, Acta Biomater. **6** (2010) 2863–2873.

[14]   E. Boanini, M. Gazzano, A. Bigi, Ionic substitutions in calcium phosphates synthesized at low temperature., Acta Biomater. **6** (2010) 1882–94.

[15]   A. Cahyanto, M. Maruta, K. Tsuru, S. Matsuya, K. Ishikawa, Fabrication of bone cement that fully transforms to carbonate apatite, Dent. Mater. J. **34** (2015) 394–401.

[16]   C. Combes, R. Bareille, C. Rey, Calcium carbonate-calcium phosphate mixed cement compositions for bone reconstruction., J. Biomed. Mater. Res. A. **79** (2006) 318–28.

[17]   I. Khairoun, M.G. Boltong, F.C.M. Driessens, J.A. Planell, Effect of calcium carbonate on the compliance of an apatitic calcium phosphate bone cements, Biomaterials. **18** (1997) 1535–1539.

[18]   S. Nomura, K. Tsuru, M. Maruta, S. Matsuya, I. Takahashi, K. Ishikawa, Fabrication of carbonate apatite blocks from set gypsum based on dissolutionprecipitation reaction in phosphate-carbonate mixed solution., Dent. Mater. J. **33** (2014) 166–172.

[19]   K. Sariibrahimoglu, S.C.G. Leeuwenburgh, J.G.C. Wolke, L. Yubao, J. a Jansen, Effect of calcium carbonate on hardening, physicochemical properties, and in vitro degradation of injectable calcium phosphate cements., J. Biomed. Mater. Res. A. **100** (2012) 712–9.

[20]   K. Tsuru, A. Yoshimoto, M. Kanazawa, Y. Sugiura, Y. Nakashima, K. Ishikawa, Fabrication of carbonate apatite block through a dissolution-precipitation reaction using calcium hydrogen phosphate dihydrate block as a precursor, Materials (Basel). **10** (2017) 374.

[21]   R.P. del Real, J.G.C. Wolke, M. Vallet-Regí, J.A. Jansen, A new method to produce macropores in calcium phosphate cements., Biomaterials. **23** (2002) 3673–80.

[22]   E.B. Montufar, T. Traykova, C. Gil, I. Harr, A. Almirall, A. Aguirre, E. Engel, J.A. Planell, M.P. Ginebra, Foamed surfactant solution as a template for self-setting injectable hydroxyapatite scaffolds for bone regeneration, Acta Biomater. **6** (2010) 876–885.

[23]   M.E. Fleet, Infrared spectra of carbonate apatites: v2-Region bands., Biomaterials. **30** (2009) 1473–81.

[24]   I.R. Gibson, W. Bonfield, Novel synthesis and characterization of an AB-type carbonate-substituted hydroxyapatite., J. Biomed. Mater. Res. **59** (2002) 697–708.

[25]   S. Padilla, I. Izquierdo-Barba, M. Vallet-Regí, High Specific Surface Area in Nanometric Carbonated Hydroxyapatite, Chem. Mater. **20** (2008) 5942–5944.

[26]   V. Jokanović, D. Izvonar, M.D. Dramićanin, B. Jokanović, V. Zivojinović, D. Marković, B. Dacić, Hydrothermal synthesis and nanostructure of carbonated calcium hydroxyapatite., J. Mater. Sci. Mater. Med. **17** (2006) 539–46.

[27]   D. Marković, V. Jokanović, B. Petrović, T. Perić, B. Vukomanović, The efficacy of hydrothermally obtained carbonated hydroxyapatite in healing alveolar bone defects in rats with or without corticosteroid treatment, Vojnosanit. Pregl. **71** (n.d.) 462–466.

[28]   L. Galea, D. Alexeev, M. Bohner, N. Doebelin, A.R. Studart, C.G. Aneziris, T. Graule, Textured and hierarchically structured calcium phosphate ceramic blocks through hydrothermal treatment, Biomaterials. **67** (2015) 93–103.

[29]   T. Toyama, K. Nakashima, T. Yasue, Hydrothermal Synthesis of β-Tricalcium Phosphate from Amorphous Calcium Phosphate, J. Ceram. Soc. Japan. **110** (2002) 716–721.

[30]   A.M.C. Barradas, H. Yuan, C.A. Van Blitterswijk, P. Habibovic, T. Medicine, Osteoinductive Biomaterials: Current knowledge of properties, Eur. Cells Mater. **21** (2011) 407–429.

[31]   R.Z. LeGeros, Calcium phosphate-based osteoinductive materials., Chem. Rev. **108** (2008) 4742–53.

[32]   H. Yuan, Z. Yang, Y. Li, X. Zhang, J.D. De Bruijn, K. De Groot, Osteoinduction by calcium phosphate biomaterials., J. Mater. Sci. Mater. Med. **9** (1998) 723–6.

Chapter 4
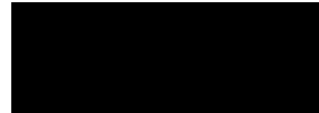
Heparinization of Beta Tricalcium Phosphate: Immunomodulatory effects and osteogenic potential

Scope

Surface functionalization has become a powerful tool to modulate the biological interactions of biomaterials. Ideally, surfaces mimicking the cellular microenvironment can help to enhance or stimulate specific cell responses of paramount importance during bone healing. Heparin is the most sulfated member of GAGs family. They are present in stem cells niche as part of the ECM and interact with several GF involved in inflammation, osteogenesis and osteoclastogenesis. The following chapter is devoted to the study of the functionalization of CaP substrates with heparin as a tool to modulate the response of inflammatory cells and mesenchymal stem cells.
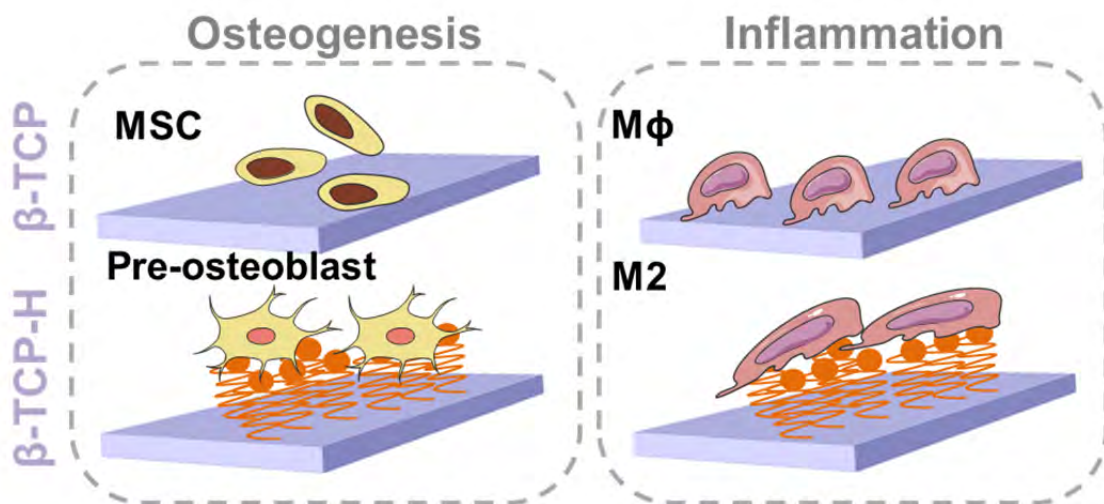
4.1. Introduction

The implantation of synthetic bone grafts in a host triggers a complex cascade of events, which ideally should lead, either to the graft's osseointegration or to its progressive resorption and replacement by new bone. The interaction of the biomaterial with different cells involved in these events is of paramount importance. However, the attention that has been paid to the different stages of this process has been uneven. Whereas most engineering approaches focus on the osteogenic potential of the material, other crucial events such as their immune response are often overlooked. The vital role of immune cells in regulating bone dynamics has been emphasized in recent years by the emerging field of osteoimmunology, which has identified the relevant role of immune cells during osteogenesis.[1,2]

After implantation, biomaterials cause a foreign body reaction that can critically determine the success or failure of the material. Briefly, the immune cascade starts with the formation of a transient protein layer on the surface of the biomaterial, followed by extravasation of cells such as neutrophils, monocytes or mast cells that try to phagocytize the biomaterial. At this stage, neutrophils and monocytes release proteolytic enzymes and reactive ROS to degrade the implant. Within a few days, neutrophils undergo apoptosis while monocytes, which have adhered to the substrate, turn into macrophages. These macrophages may develop distinct dynamic phenotypes, known as M1 or M2, with pro-inflammatory or anti-inflammatory functions respectively.[3–6] M1 releases chemokines and cytokines that enhance inflammation while M2 secrete anti-inflammatory cytokines, and promote bone remodeling and repair, by regulating osteogenesis and osteoclastogenesis.[7] The polarization of macrophages can be influenced by materials properties. Thus, features such as topography,[8–11] surface chemistry,[12–17] mechanical stimuli,[18,19] or porosity[20,21] are known to determine immune cells fate.

GAGs are interesting as modulating molecules for both immune and skeletal systems. GAGs are ubiquitous in tissues (e.g., as part of stem cells niche and the extracellular matrix) and are known for their potential to interact with growth factors.[22–24] GAGs assembled into proteins (PG) are highly present within injured sites. After injury, GAGs are released from their PG back-bone, become soluble and initiate the healing cascade.[25,26] GAGs can bind chemo- and cytokines that alter leukocyte migration, endothelial extravasation or cytokine expression.[25,27–30] Decades ago, the anti-inflammatory effect of the most sulfonated GAG, heparin, was demonstrated by Dandona *et al*., showing an inhibitory effect on ROS release by leucocytes.[31] In more recent studies, Zhou *et al.* also found the down-regulation of inflammatory cytokines such as IL-1β in presence of GAG multilayers.[32]

Due to their ubiquitous nature, GAGs not only interact with the immune system, but also with bone cells.[33] Their ability to bind proteins such as GF has been used by several authors to regulate cell behavior. The degree and position of sulfate groups on GAGs has been shown to influence the affinity for BMPs,[34,35] and to foster osteoblast differentiation[36] by blocking sclerostin which is an inhibitor of Wnt signaling for osteoblast differentiation.[37] In a similar manner, GAGs can foster osteoclastogenesis by blocking OPG, which competes with RANKL, necessary for osteoclast maturation. [38–40]

Overall, the studies performed using GAGs have mostly focused on their supplementation in cell cultures but little has been done using them as substrates or as surface platforms in combination with biocompatible substrates, besides their application as artificial ECM in combination with collagen or other organic molecules.[23,24,41–45] We hypothesize that the combination of bioactive, osteoconductive and inductive substrates such as calcium phosphate (CaP) materials with the regenerative potential of GAGs can result in an enhancement of their biological performance.

β-TCP as a member of CaP family is similar to natural bone's mineral phase and has been used successfully in the clinic for decades. Nevertheless, the main focus of many investigations has been their osteogenic potential, while their interaction with the immune system has often been overlooked. Chen *et al.* have recently made a step forward towards unraveling the tight link between osteogenesis and immunology on ceramic substrates,[16,46,47] mainly β-TCP or porous alumina. However, the studies performed were limited to the evaluation of the effect of β-TCP extracts on cells rather than involving direct cell seeding on the material. The importance of osteoimmunology in the design of bone grafts, and the involvement of GAGs both in inflammatory and osteogenic processes has encouraged the present work. Some studies have previously explored the functionalization of CaP with heparin, as a strategy for the controlled delivery of growth factors.[48–50] The focus of this study is different, as it aims at investigating the functionalization of β-TCP with heparin as a method to modulate the response of inflammatory cells (i.e. human neutrophils, monocytes and macrophages), and mesenchymal stem cells.

4.2.   Materials and Methods

4.2.1.   Preparation of calcium phosphates

β-TCP was obtained by sintering CDHA. CDHA discs were obtained by hydrolysis of α-TCP through a self-setting reaction. α-TCP was prepared by solid state reaction of calcium hydrogen phosphate ($CaHPO_4$, Sigma-Aldrich, St. Louis, USA) and calcium carbonate ($CaCO_3$, Sigma-Aldrich, St. Louis, USA) mixed at a 2:1 molar ratio and

heated for 15h at 1400°C followed by quenching in air. Subsequently, the particles obtained were milled to a final median size of 5.2µm[51] and mixed with 2wt% of precipitated hydroxyapatite (PHA, Merck KGaA, Darmstadt, Germany). This powder was then mixed for 1min in a mortar with distilled water at a liquid to powder ratio (L/P) of 0.35mL/g, resulting in a paste that was transferred into two different size moulds: 15x2 and 5x1mm^2 (diameter x thickness) PTFE moulds. The discs were immersed in water at 37°C for 10 days, to allow for complete hydrolysis to CDHA. The discs were subsequently subjected to a sintering process at 1100°C for 9h to obtain the final β-TCP.

4.2.2. Heparinization

Heparin immobilization on the surface of β-TCP was performed using two different routes, either physical adsorption or chemisorption, i.e. chemical covalent binding (Figure 4-1A and B, respectively). Freshly prepared heparin (BioIberica S.A.U. Barcelona, Spain) solutions in PBS (phosphate buffer saline, Thermo Fisher Scientific) were used. Physical adsorption was carried out by immersing the samples in the heparin solution for 2 hours under gentle agitation (100 rpm). Heparin covalent binding was accomplished via a 2-step functionalisation method: i) First, silanization with aminopropyltrietoxysilane (APTES, Sigma-Aldrich, St. Louis, USA) was performed using a modified procedure from previous work.[52] Discs were immersed in a solution of APTES (2% vol., i.e. 80mM) in absolute Ethanol (Panreac,AppliedChem) in the presence of distilled water (3% vol.) and left for different times (1 hour or overnight) under agitation. Afterwards, the discs were removed and sonicated in an ultrasonic bath (Ultrasons-HD, J.P. Selecta, Barcelona) in absolute ethanol solution for 5min, followed by three ethanol rinses to remove any unbound APTES; ii) The second functionalization step consisted in the covalent immobilization of heparin onto the aminated surfaces of the materials. Carbodiimide (1-(3-dimethylaminoporpyl)-3-ethylcarbodiimide, EDC, Sigma-Aldrich, St. Louis, USA) and *N*-hydrosuccinimide (NHS, Sigma-Aldrich, St. Louis, USA) were used to couple heparin via its carboxyl groups to the amino groups of the silane. Freshly prepared solutions of heparin in PBS at different concentrations were firstly activated for 15min at pH ~6.5 in presence of EDC/NHS (100 and 150mM, respectively). Upon activation, pH was raised to 7.5 and the silanized discs were immersed in the activated heparin solution (1mL) for 2h under agitation (100rpm).
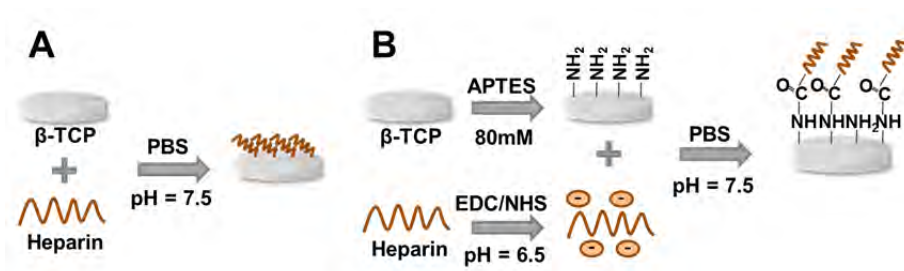
Figure 4-1. Diagram of the two heparin immobilization methods. A) physisorption and B) chemisorption.

The heparin saturation curves were determined on the overnight silanized surfaces by immersing the samples in activated heparin solutions with different concentrations (10, 25, 50, 75, 100, 150, and 200µg/mL) for 2h. Supernatants were collected, and the amount of heparin was determined using a colorimetric assay modified from the literature.[53] Briefly, a solution of 0.005wt% Toluidine blue (Sigma-Aldrich, St. Louis, USA) was prepared in 0.01M hydrochloric acid (HCl, Panreac AppliChem) and 0.2wt% sodium chloride (NaCl, Sigma-Aldrich, St. Louis, USA). Heparin supernatants were mixed with the Toluidine solution at a 1:1 ratio using vortex and centrifuged for 5min at 15000 relative centrifugal force (rcf). Afterwards, 200µL of the sample solutions were placed in a 96-wellplate and the absorbance was read at 631nm (Infinite 200 PRO Microplate reader, TECAN). A standard calibration curve was made, measuring solutions with known heparin concentrations up to 25µg/mL.

4.2.3.   Materials characterization

SSA of the discs was measured by nitrogen adsorption using the BET method (ASAP 2020 Micromeritics). The porosity and pore size distribution were obtained by MIP (Autopore IV Micromeritics). Phase composition was assessed by XRD (D8 Advance, Bruker) using a Cu Kα anode (monochromated, $\lambda=1.5406$Å) operated at 40kV and 40mA. Data were collected in 0.02° steps over the 2θ range of 10°-80° with a counting time of 2 per step. Phase identification was accomplished comparing the resulting patterns to that of β-tricalcium phosphate (JCPDS 09-0169).

SEM (FIB Zeiss Neon40) was used to study the microstructure of the samples. Prior to imaging, samples were coated with carbon to enhance conductivity. The microstructure of the samples was studied before and after functionalization to investigate possible morphological changes. X-ray photoelectron spectroscopy (XPS) was used to analyze surface composition of the pristine (control) and functionalized samples. Spectra were acquired in ultra-high vacuum (5 10^{-9}mbar) with an XR50 Mg anode source operating at 150W and a Phoibos 150 MCD-9 detector (D8 advance, SPECS Surface Nano Analysis GmbH, Germany). Spectra were recorded at pass energy of 25eV with a step size of 0.1eV for C1s, N1s, O1s, Si2p, Ca2p, P2p, and S2p. C1s peak was used as a reference. CasaXPS software (Casa Software Ldt, UK) was

used for the determination of atomic elemental composition applying the manufacturer set of relative sensitivity factors.

4.2.4. Cell isolation

The inflammatory response was evaluated using primary human cells isolated from blood obtained from anonymous volunteer donors at the Uppsala University Hospital. Monocytes and neutrophils were isolated from buffy coats by two different separation procedures. Firstly, monocytes were isolated from blood (15mL) which were then diluted in 1xPBS at a 1:1 ratio and mixed gently by inversion. Afterwards, diluted blood (30mL) were gently poured onto Ficoll-Paque Plus (15mL) (GE Healthcare, Chicago USA) followed by centrifugation at 400rcf for 30min. The upper human plasma layer was collected and kept at 4°C for later use. The monocytes layer was pelleted and resuspended in 1xPBS (10mL) and centrifuged at 100rcf for 15min for a total of 3 washes. Next, the monocytes pellet was resuspended in PBS (2 mL) and the cells were counted by Trypan blue exclusion method (1:5) in a cytometer. Finally, cells were diluted in cell culture medium (4PBS/1RPMI-1640/100mM glucose) containing 10% of human plasma.

Secondly, to extract the PMNC, the blood pellet layer obtained after centrifugation and removal of plasma and the mononuclear layer was resuspended in 20mL of 3% Dextran (Sigma) in 0.9% saline solution and incubated for 25min. The supernatant was collected and centrifuged at 250rcf for 10min. Afterwards, the supernatant was treated with 20mL of 0.2% saline for 20s, followed by 20mL more of 1.6% saline in order to lyse erythrocytes. The cell suspension was then centrifuged at 250rcf for 10min. The PMNC pellet was resuspended in PBS and cells were counted using acetic acid (6%) in a cytometer. Finally, cells were diluted in cell culture medium (4PBS/1RPMI-1640/100mM glucose) with 10% of human plasma.

4.2.5. Chemiluminescence study

A luminol amplified chemiluminescence assay was used to quantify the reactive oxygen species (ROS) generated by both monocytes and neutrophils under phorbol-12-myristate-13-acetate (PMA, Sigma Aldrich) activation[54,55]. Prior to the analyses, the 5x1mm^2 discs were sterilized in 70% ethanol for 3h, followed by three PBS rinses of 15min each. 200µL of cells were seeded on the pristine and heparinized β-TCP discs at a cellular density of 10^6cells/mL, followed by the addition of 100µL of luminol solution (500µM). Previously, a luminol solution was prepared by adding 1% of luminol stock solution and 0.2% horseradish peroxidase (1mg/mL, Jackson Immuno Research) as signal amplifier. The luminol stock solution was obtained by dissolving luminol (Fisher Scientific) to 50mM in 0.2M NaOH. Both cell types and positive controls (TCPS+) were activated with 1µM PMA, which was added into the cell

suspension solution. A negative control consisting of non-activated cells seeded on tissue culture polystyrene was added (TCPS). Luminescence was monitored in a microplate reader (Infinite M200, Tekan, Männedorf, Switzerland) at 37ºC every 2 min up to 2h. Measurements were conducted using triplicates for each material type (n=3). The experiment was then repeated with two independent blood donors.

4.2.6. Macrophage cell culture

Macrophage cell culture assays were performed using 15x2mm^2 discs. Upon isolation, monocytes were resuspended in complete RPMI cell culture medium supplemented with 10% fetal bovine serum (FBS, Thermo Scientific Hyclone), 2% HEPES (Sigma-Aldrich, St. Louis, US) and 1% Penicillin/streptomycin (Thermo Scientific). Prior to seeding, pristine and heparinized β-TCP discs were sterilized as previously described and immersed overnight in 1ml of complete medium. Seeding was performed by adding 1ml of cells in complete medium at a cell density of $2 \cdot 10^5$cells/mL. All substrates were supplemented with 1ng/mL of lypopolysaccharide (LPS, Sigma-Aldrich, St. Louis, US) including a positive control (TCPS+). The negative controls (TCPS) consisted in cells without LPS supplementation. Cells were cultured for 3 days. Supernatants of macrophage cultures were collected at 6, 24, 48, and 72h and analyzed with ELISA kits to detect Tumor Necrosis Factor (human TNF-α, KHC3012, Invitrogen), Interleukin 1 (human IL-1β, KHC0012, Invitrogen) and Interleukin 10 (human IL-10, KHC0103, Invitrogen). Duplicates were used for each single experiment and three biological replicas were conducted with three independent blood buffy coats.

Cell viability at each time point was quantified by lactate dehydrogenase release (LDH KitMAK066, Sigma Aldrich, St. Louis, US). 400μL of 1% Triton-X100 (Sigma Aldrich, St. Louis, US) solution in PBS was used to lyse cells followed by three freezing and thawing steps. Cytokines values were normalized to the obtained cell number at each time point and to the values of TCPS+ at 6h.

Cell morphology was assessed by scanning electron microscopy (SEM, Zeiss 1530, Germany) at 6, 24, 48, and 72 h. Cells were fixed using a 2.5% glutaraldehyde solution in PBS at 4°C for 2 h, followed by 3 rinses in PBS of 15 min each. Afterwards, a series of ethanol dehydration steps were carried out for 15 min each (10-30-50-70-90-99%). Finally, samples were vacuum dried and coated with Au/Pd to enhance conductivity. Image analyses of macrophage morphology were processed by FIJI (ImageJ software) to investigate the elongation ratio (n=30 except for β-TCP at 6h and TCPS at 72h where n=10).

4.2.7. Mesenchymal stem cell culture

Rat mesenchymal stem cells (rMSCs) extracted from young Lewis rats and used at passage 3 were used to investigate the osteogenic potential of the heparinized surfaces. All samples were sterilized as previously described. Afterwards, 15x2mm² discs were left overnight in supplemented cell culture medium as preconditioning prior to seeding. rMSCs were cultured on the pristine and heparinized β-TCP discs ($8 \cdot 10^4$cells/mL, 1mL) with Advanced DMEM (AdvDMEM) supplemented with 10% FBS, 2% HEPES and 1% of penicillin/streptomycin and L-glutamine (Invitrogen). Tissue culture polystyrene (TCPS) was used as control. Cells were cultured over 6h, 3, 7 and 14 days refreshing medium every day. At day four, osteogenic medium consisting of supplemented advDMEM with 50µg/mL ascorbic acid, 10mM β-glycerophosphate and 100nM dexamethasone was used as cell culture medium for all substrates. At each time point, samples were rinsed thrice with PBS and lysed with M-PER® (Mammalian Protein Extraction Reagent, Thermo Scientific, Waltham, MA, USA; 300µL). Cytotoxicity Detection Kit LDH (Roche Applied Science, Penzberg, Germany) was used to quantify cell proliferation. The results were expressed as a relative fold change compared to the cell number obtained on TCPS after 6h and to the area of the discs. The alkaline phosphatase (ALP) activity was quantified as a marker of osteogenic differentiation (SensoLyte®pNPP Alkaline Phosphatase Assay Kit, AnaSpec).

4.2.8. Statistics

Data are presented as mean values and standard deviation for ROS experiments including triplicates for each material and two different donors. Cytokines and elongation ratio are expressed as mean values and standard errors out of duplicates for each material type and three independent donors. One way ANOVA was used to analyze statistical differences ($p<0.05$) followed by Tukey post-hoc analysis for all experiments using SPSS statistics software (IBM). T-test for independent samples was applied to evaluate statistical differences between neutrophils and monocytes for the ROS integrated values.

4.3. Results

4.3.1. Material characterization

XRD analysis revealed that the ceramic substrate consisted of phase-pure β-TCP, with all peaks matching those in the JCPDS 09-0169 card (Figure 4-2A). The samples were porous, as evidenced by MIP, with interconnected pores below 1µm (Figure 4-2B). The specific surface area of β-TCP discs was low and typical of high temperature sintered ceramics (Figure 4-2C). The microstructure observed by SEM showed the

porous nature of the discs and was consistent with the low SSA values from the polyhedral grain microstructure after the sintering process (Figure 4-2D).
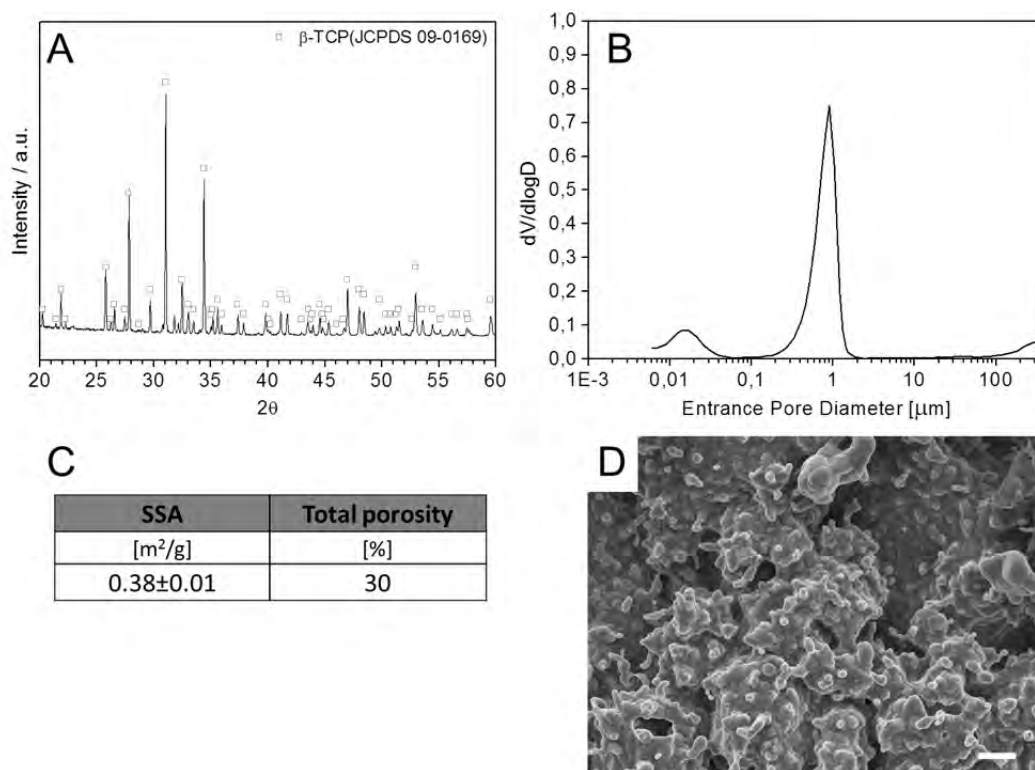
Figure 4-2. Physico chemical properties of the β-TCP discs. A) X-ray diffraction pattern; B)Pore entrance size distribution measured by MIP; C) Specific surface area measured by nitrogen adsorption, and total open porosity according to MIP; and D) SEM image of the surface of the material (scale bar: 2μm).

4.3.2. Heparin immobilization

The effect of the immobilization method on the amount of heparin retained on the surface is depicted in Figure 4-3A. The percentage of immobilized heparin (100μg/mL, 1mL) after 2h increased drastically when the surface was previously silanized, compared to physical adsorption. Moreover, the silanization time allowed tuning the final amount of immobilized heparin. One hour of silanization followed by two hours of immersion in a heparin solution resulted in approximately 10% of the heparin in solution becoming immobilized on the surface. Overnight silanization boosted this percentage up to 30%. Heparin surface saturation studies were performed to investigate the maximum amount of heparin bound to the substrate in two hours, after overnight silanization (Figure 4-3B). As the concentration of heparin in solution increased, the surface reached a saturation value of ~25μg of adsorbed heparin for concentrations of 50μg/mL and above. From XPS results, the composition of the substrates displayed mainly calcium, phosphorous and oxygen which is in agreement with the chemical composition of pristine β-TCP (Figure 4-3C). The detected carbon was attributed to ambient hydrocarbon contamination. The presence of silicon and

nitrogen, together with decreased Ca and P in the overnight silanized sample (β-TCP-Sil) proved the success of this step. The increase in carbon content on the silanized substrate was associated with the ethoxy groups present in APTES. The presence of heparin on the heparinized samples (β-TCP-H) was evidenced by the presence of sulfur. The decrease in the ratio of silicon and calcium was associated with the covering of both the substrate and the silane layer by heparin. The SEM micrograph displayed in Figure 4-3D shows that surface functionalization did not induce any morphological change in the substrate.
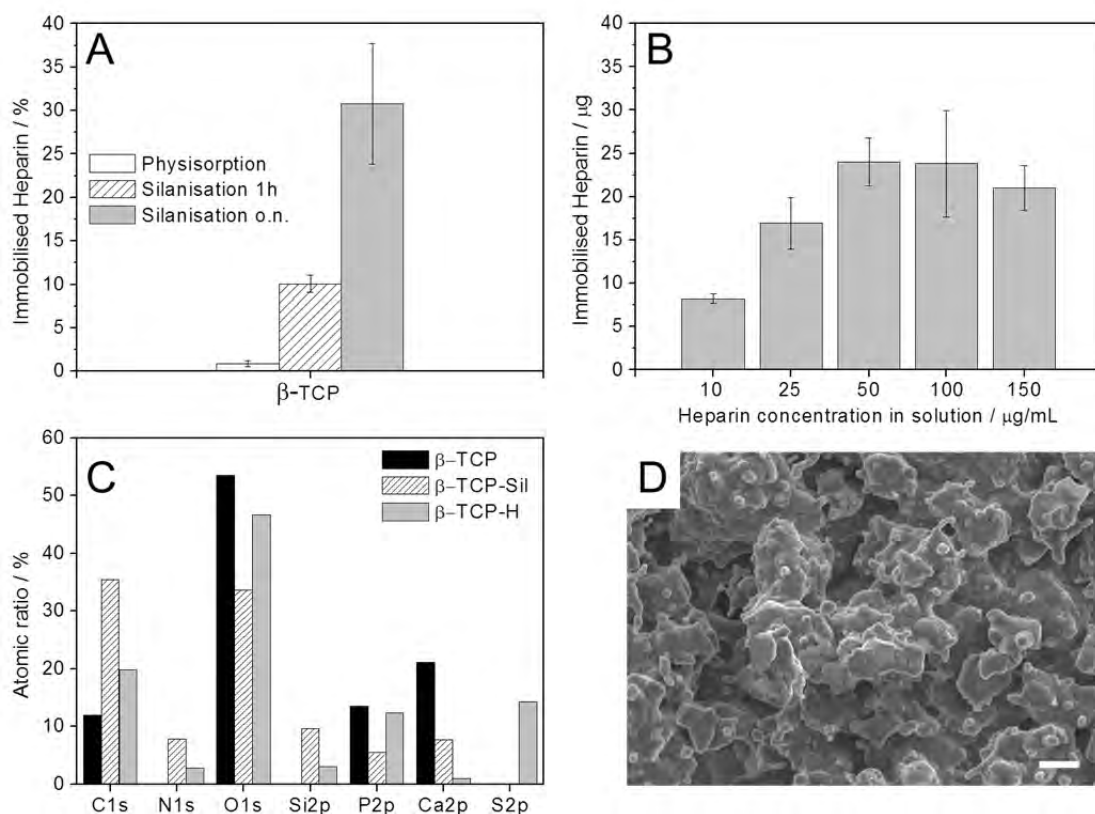
Figure 4-3. Characterization of the heparin-functionalized surfaces. A) Effect of the immobilization method on the amount of heparin immobilized on the surface after 2 h immersion in a 100μg/mL heparin solution. Pristine samples, where heparin was adsorbed by physisorption, are compared to silanized samples, with two different silanization times, 1h or overnight (o.n.); B)Saturation of heparin onto the β-TCP surface. The silanized discs (overnight silanization) were immersed for 2h in solutions with different concentrations of heparin; C) XPS spectra of the pristine material (β-TCP), overnight silanized β-TCP (β-TCP-Sil) and heparinized β-TCP (β-TCP-H), this last prepared by 2h immersion of o.n. silanized samples in a 150μg/mL heparin solution; D) SEM morphology of the surface of β-TCP-H, after heparin functionalization.

Taking into account the results described above, the heparinization protocol selected for the cell culture studies consisted of overnight silanization followed by 2h immersion in a 150μg/mL heparin solution.

4.3.3. Cell culture studies

4.3.3.1. Reactive oxygen species generated by monocytes and neutrophils in vitro

The results of ROS (specifically hydrogen peroxide) release kinetics and total ROS released by monocytess and PMNCs obtained from blood from two donors, following cell activation with PMA are depicted in Figure 4-4. The data for two cell types was normalized to the maximum value reached by the positive control (TCPS+) and expressed as percentage. PMNC showed a delayed release compared to monocytes. β-TCP-H down-regulated inflammation 15% for monocytes and 20% for neutrophils compared to positive control. Moreover, the total amount of ROS released by both types of cells when cultured on the heparinized surface, measured as the area below the curve and expressed as unit fraction, was lower than when cultured on bare β-TCP or on TCPS+ (Figure 4-4B).
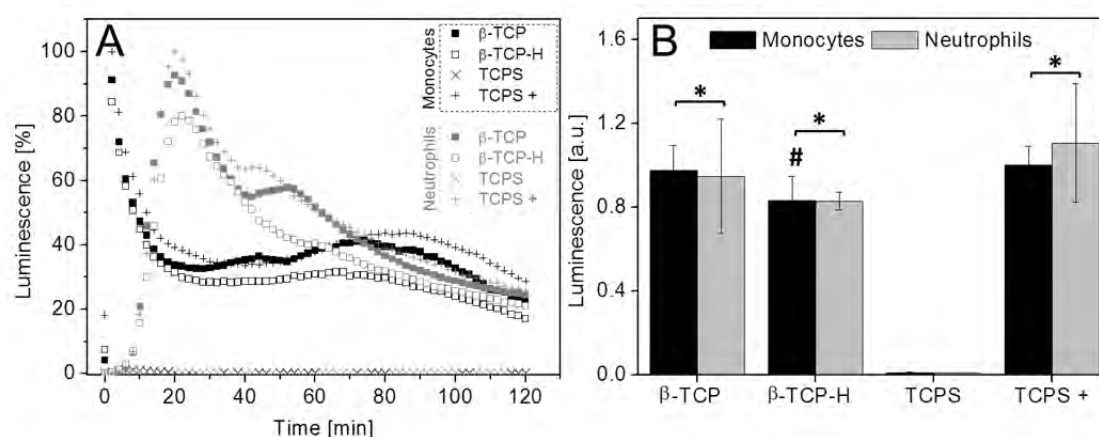
Figure 4-4. ROS release study on PMA-activated cells. Non-activated cells were used as negative control (TCPS). A) H$_2$O$_2$ release evolution profiles over time; B) Integration of the total area under the curves (N=6 from two independent buffy coats, from two donors). * indicates statistically significant differences compared to the negative control TCPS (p<0.05) and # indicates statistically significant differences with respect to β-TCP (p<0.05).

4.3.3.2. Macrophage cell culture assays

MNCs were seeded on the different substrates, where they adhered turning into macrophages. The release of pro-inflammatory cytokines by macrophages, specifically TNF-α, IL-1β and IL-10, normalized to cell number at each time point, and expressed as fold change with respect to TCPS+/6h (relative fold change) is represented in Figure 4-5, in three graphs corresponding to independent buffy coats. The results were compared with controls with/without LPS stimulation (TCPS+ and TCPS, respectively). In general, for TNF-α and IL-1β, the cytokine release pattern from macrophages confirmed a lower inflammatory response of β-TCP and heparinized β-

TCP-H compared to the positive control TCPS+. β-TCP-H led to lower TNF-α level compared to pristine β-TCP, irrespective of the donor. Interestingly, in donors 2 and 3, the amount of TNF-α released by macrophages cultured on β-TCP-H was lower than that of the negative control (TCPS). Similar results were observed for IL-1β secretion, which was lowered upon contact with heparinized surfaces for all buffy coats, which showed slightly lower values than those of control without stimulation (TCPS). IL-10 was not detectable for any of the groups. Due to the variability in native and acquired immune systems between donors, data are presented individually for each donor.
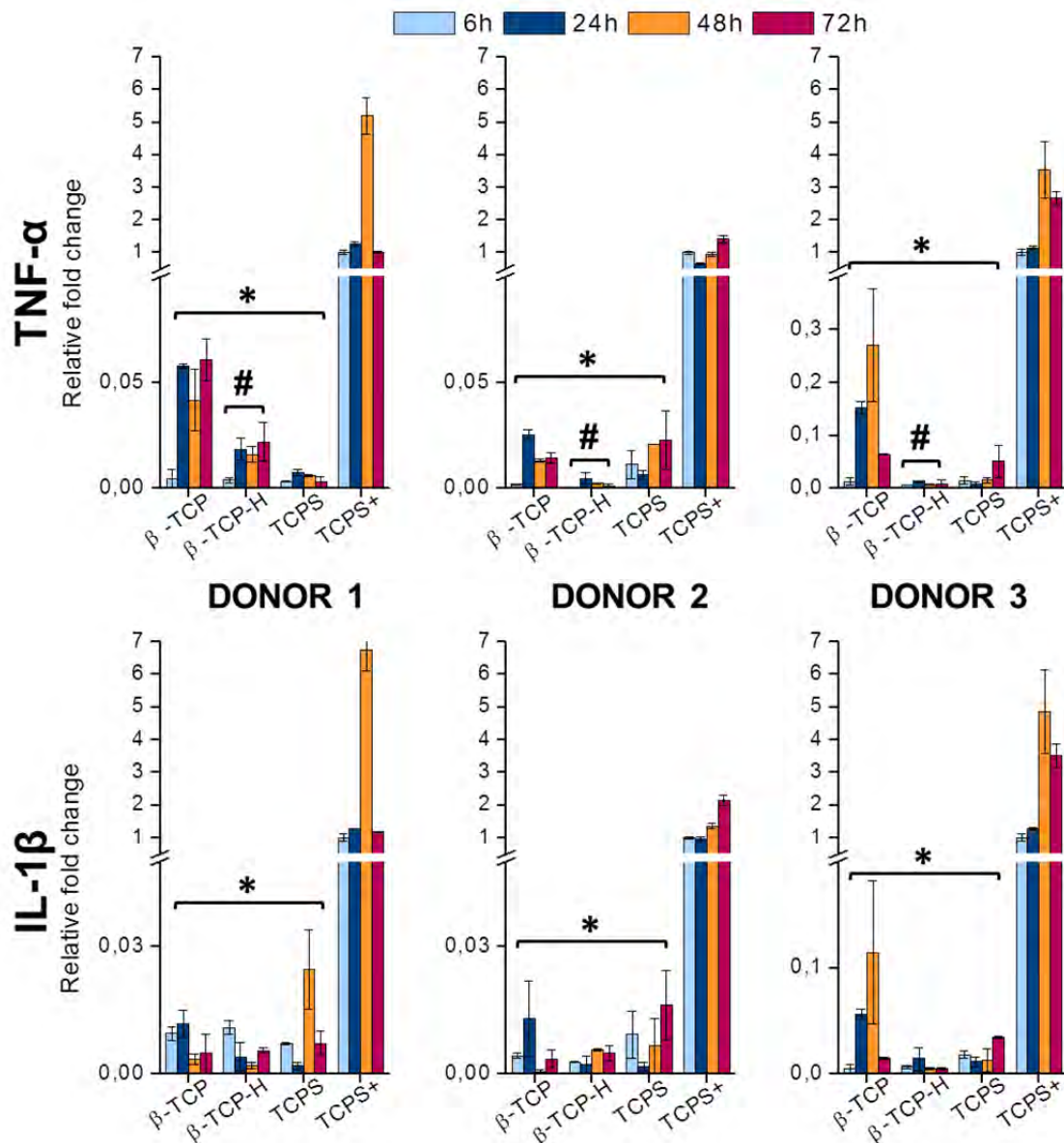
Figure 4-5. Cytokine release by macrophages cultured on substrates for 6, 24, 48 and 72h. The three graphs correspond to buffy coats from three different donors. Tumor necrosis factor alpha(first row) and Interleukin 1 beta (second row). TCPS+ and TCPS correspond to the positive and negative controls, with/without LPS stimulation respectively.* indicates statistical difference compared to positive control TCPS+ and # to β-TCP (p<0.05).

Macrophage morphology on the different substrates was evaluated by SEM at each time point (Figure 4-6). All substrates promoted macrophage adhesion over time. Some of the cells retained the original round shape whereas others had a more elongated shape. This is relevant since macrophage morphology can be used to assess phenotype polarization.[56] Cell elongation was observed on both β-TCP and β-TCP-H substrates, whereas TCPS and TCPS+ were prone to form cell clusters. TCPS at 72h (Figure 4-6G) showed flattened cells with no filopodia (Figure 4-6G inset) which suggests apoptosis, whilst TCPS+ exhibited cell clusters (Figure 4-6H) with connecting filopodia (Figure 4-6H inset). Higher cell elongation was found on β-TCP-H compared to bare β-TCP substrate, which at 72h showed still rounded cells (Figure 4-6E and F, red colored). Image analyses of macrophage morphology showed a higher elongation ratio for the cells adhered on β-TCP-H (Figure 4-6I), especially at 72h, with a 25% higher elongation rate compared to TCPS.
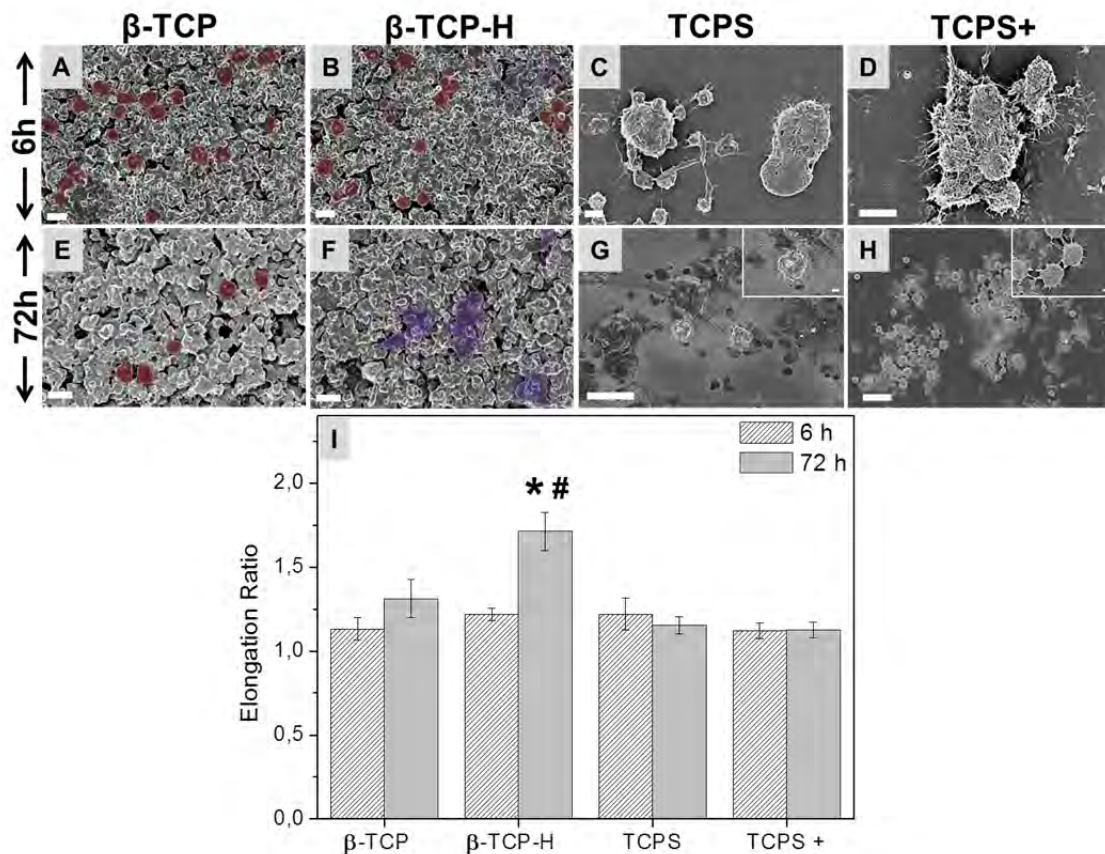
Figure 4-6. Representative SEM images of macrophages on β-TCP at 6h (A) and 72h (E); β-TCP-H at 6h (B) and 72h (F); TCPS at 6h (C) and 72h (G); TCPS+ corresponding to LPS stimulated cells at 6h (D) and 72h (H). Scale bar in images A, B, E, F: 10μm; C, D: 2μm; G, H: 20 μm, inset scale bar: 2μm. Red colored cells represent round macrophages and purple ones represent elongated ones. I) elongation ratio of cells at 6 and 72h (* denotes statistically significant differences from TCPS and TCPS+ at 72h, and # statistically significant differences between time-points).

4.3.3.3. Mesenchymal stem cell proliferation and differentiation

Cell culture with rMSCs showed a slow but sustained proliferation on all β-TCP substrates over 14days measured by lactate dehydrogenase (LDH), (Figure 4-7A). Cell proliferation studies exhibited no statistically significant differences between β-TCP and β-TCP-H. Lower adhesion on heparinized substrates was found at 6h as well as significantly lower proliferation at 7 days comparing both calcium phosphate substrates. Nevertheless, no differences were found at 14 days, where cell proliferation rates were similar, irrespective of functionalization. Both substrates promoted lower proliferation than TCPS, which increased over 7 days until a plateau was reached. The measurement of ALP activity demonstrated earlier differentiation on the heparinized substrate β-TCP-H (Figure 4-7B). In the absence of exogenous supplementation, β-TCP-H induced higher differentiation than TCPS at 6 hours and 3 days. After the addition of osteogenic medium (day 4), TCPS exhibit higher differentiation rate (7 days) compared to calcium phosphate substrates, which decreased at 14 days.
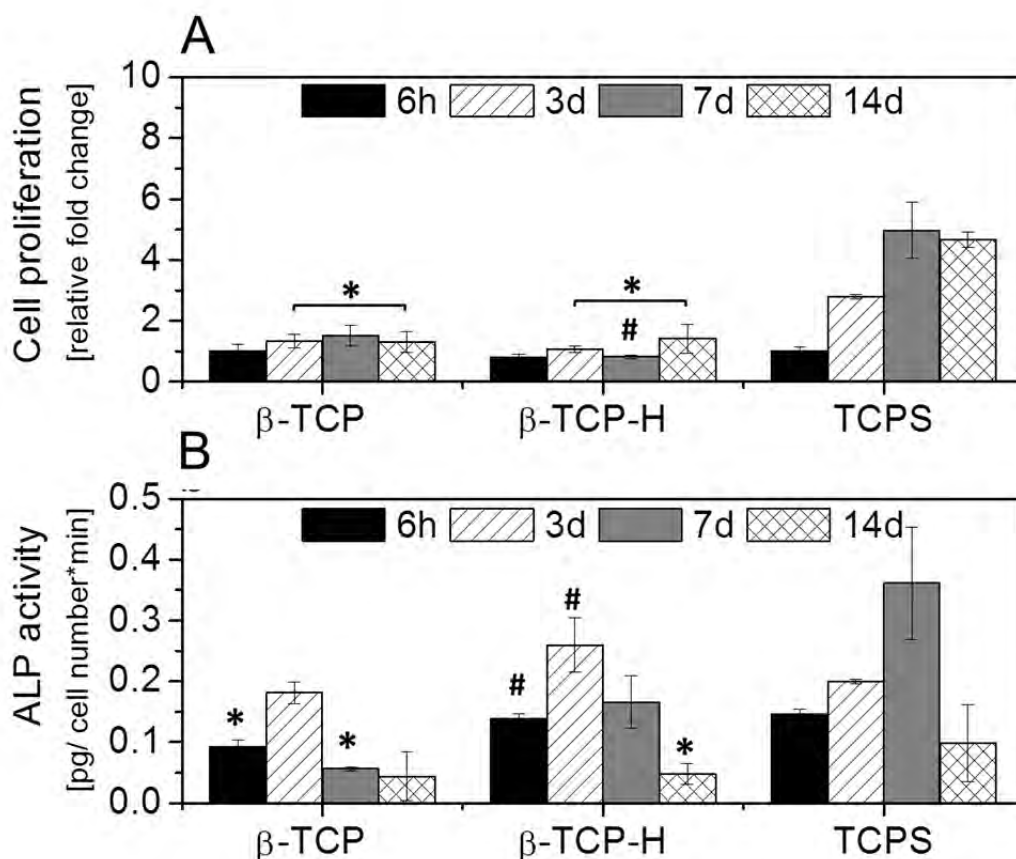
Figure 4-7. Cell proliferation and early differentiation of rMSCs cultured on β-TCP, β-TCP-H and TCPS as control. A) cell proliferation over time (14d) measured by LDH; data has been normalized to area and to cell number of TCPS at 6h and expressed as relative fold change. B) ALP activity over culture time. On day 4, the cell culture medium was replaced by osteogenic medium. * indicates statistically significant differences compared to control TCPS for the same time point (p<0.05) and # indicates statistically significant differences with respect to β-TCP for the same time point (p<0.05).

4.4. Discussion

Calcium phosphates are widely used in clinical procedures. However, although their close resemblance to the composition of bone and other advantages such as bioactivity, osteoconduction and osteoinduction make them good candidates for bone grafting, they are not able to outperform autologous grafts in highly demanding situations. The design of new strategies to foster the interaction with the host tissue during the whole process of bone remodeling may lead to the development of materials with superior performance.

The bone healing cascade is orchestrated by the cells of both the skeletal and the immune system through different shared mediators such as cytokines, receptors, signaling molecules and transcription factors. Recent studies have demonstrated that some ubiquitous biomolecules that are involved in the cross-talk between the immune and skeletal system, can be used to tune osteogenesis and osteoclastogenesis to achieve proper bone regeneration rates.[1,2,16,57]

In this context, the present work explores the immune and osteomodulatory effect of heparin immobilized on β-TCP substrates. Previous works have proved the potential of heparin applied on model glass surfaces as an anti-inflammatory molecule.[32] Moreover, heparin is known have great affinity to growth factors, and this has been exploited with collagen, polyacrylamide, chitosan and other organic substrates as a way to stimulate bone regeneration.[24,42,44,54] The high affinity of heparin for growth factors is highly relevant in the case of β-TCP because, even though numerous proteins have high binding affinity to calcium phosphates via amino acids with phosphate- or carboxylate-terminated side chains, most growth factors lack a specific mineral-binding domain.[43] The functionalization with heparin can help to circumvent this limitation. However, studies pertaining to the heparinization of calcium phosphates are scarce, and limited to its use as an anchoring molecule for the immobilization of growth factors on the surface of the biomaterial, for its subsequent delivery.[43,49]

Heparin can bind to CaP by physical adsorption or by covalent attachment, as demonstrated in other works with HA.[49] Physical adsorption of heparin takes place through electrostatic interaction between the charged sulfate/carboxylate groups in heparin with exposed Ca ions on the crystal surface of the CaP. Covalent binding is typically accomplished through a silanization step to covalently graft amine groups that can react with the carboxylate groups from heparin through amide bond formation.[49,66] Heparin binding through covalent bonds is more stable than physically adsorbed heparin. It has been reported that in complex environments like body fluids, the presence of other charged molecules can compete for binding, thus displacing electrostatically bound heparin from the surface of the CaP.[58] The results obtained in

the present work for β-TCP show that a covalent binding yielded higher amounts of heparin than mere physical adsorption. Figure 4-3A shows increased heparin grafting densities following covalent immobilization than physical adsorption, and this was further improved with increased silanization time. The maximum amount of heparin that was adsorbed on the surface of β-TCP was around 25μg, but this dose could be tuned depending on the concentration of heparin used during binding (Figure 4-3B).

To assess the osteogenic and immunomodulation ability of heparin on β-TCP, covalent attachment was preferred for stability reasons as well as to test heparin's ability to recruit endogenous GF which can help modulate cell function.[59,60] During the early inflammation process, immune cells can signal the following biological cascades. Neutrophils and monocytes interacting with materials release H_2O_2, which act as anti-inflammatory signaling molecule. H_2O_2 can cause cell dysfunction and tissue injury depending on the concentration.[61] High concentrations of H_2O_2 and other ROS are deleterious to cells; optimal concentration is required to properly modulate the inflammation cascade by stimulating the balance between pro and anti-inflammatory cytokines. In the present work, primary human cells were used to assess the inflammatory response of the materials as they reflect better the *in vivo* scenario upon biomaterial implantation. Lower hydrogen peroxide levels were detected after contact with heparinized β-TCP surfaces compared to the non-heparinized ones (Figure 4-4). The release kinetics were different for the two cell types; whereas neutrophils exhibited a clear monomodal pattern, monocytes showed an acute release within the first 5min followed by a second raise after 80min. Nevertheless, β-TCP-H (Figure 4-4, blank squares) still displayed the lowest percentage of release. The role of GAGs on inflammation has been previously studied by local administration.[25,30,62] Campo *et al.* found a down-regulation of ROS and inflammatory cytokines in LPS-induced mouse chondrocytes by several GAGs.[30] The highest inhibitory effect was exerted by chondroitin sulfate and heparan sulfate supplementation. Nevertheless, the effect of GAGs has been mainly studied as a supplement in cell culture. Although in the present work the reduction of ROS is low, probably due to low heparin concentration, the trend observed for the heparinized β-TCP surfaces confirm the anti-oxidative activity of heparin.

Activated macrophages secrete cytokines, which also modulate the inflammatory response depending on the interaction with the biomaterial and the implant environment.[63] Mantovani *et al.* extensively described the cytokine system derived from macrophage polarization[3,4] and highlighted the dynamism of this polarization. Even though for decades M1 pro-inflammatory macrophages were seen as mediators of fibrous encapsulation, nowadays it is widely accepted that both M1 and M2 subtypes promote degradation of implants and healing.[64] In the present work, pro-inflammatory (TNF-α, IL-1β), pro-wound healing (IL-1β) and anti-inflammatory

cytokines (IL-10) were investigated using primary human cells, which although entailing a certain degree of variability between donors, mimic more closely the *in vivo* scenario. The cytokine release profiles (Figure 4-5) showed similar trends to those of ROS release. TCPS+ exhibited the highest levels of cytokine release upon LPS stimulation. Neither β-TCP nor β-TCP-H caused cells to secrete more cytokines than LPS-activated TCPS (TCPS+). Similarly to previous works with β-TCP particles,[65,66] β-TCP substrates induced higher release of TNF-α and IL-1β than TCPS. Functionalization with heparin of these substrates resulted in a reduction of TNF-α and IL-1β release, which was below the levels of TCPS in all three donors for IL-1β, and in two donors for TNF-α. IL-10, an anti-inflammatory cytokine, was not detected by ELISA in any of the substrates. Overall, the reduction in the inflammatory response caused by heparin on the surface of the β-TCP substrate was in agreement with previous results obtained in GAG multilayer substrates by Zhou *et al.*[32]

Besides the cytokines release profile, cell shape can provide information on macrophage phenotype which can also be supported by immunostaining techniques for specific markers on macrophages. Sridharan *et al.* concluded that macrophage elongation can be associated to a pro-healing phenotype (M2), whereas pro-inflammatory macrophages (M1) present more rounded shapes.[63] Similarly, McWorther *et al.* found elongated shapes being compatible with an expression of M2 phenotype on patterned TCPS.[56] SEM images showed early elongation on β-TCP substrates at 6h (Figure 4-6A and B), which continued up to 72h, more pronounced on heparinized β-TCP-H (Figure 4-6E and F). Image analyses of cell morphology revealed significantly higher elongation ratio for β-TCP-H at 72h (Figure 4-6I), which can be related to M2 polarization, in agreement to the lower cytokine release (Figure 4-5).

Osteogenic cell proliferation and differentiation are required to continue the healing process. Some studies have determined that the binding affinity between GAGs and osteogenic markers such as osteocalcin, osteonectin or osterix, is necessary for osteoblast maturation.[67,68] However, these studies took a direct stimulation approach by supplementing GAGs into the cell media or by attaching them on TCPS. The use of osteoconductive substrates such as CaPs in combination with GAGs can further enhance their biological response. β-TCP and TCPS showed similar rMSCs adhesion, while a slightly lower cell adhesion was found for heparinized β-TCP-H, even no significant differences were depicted from statistics analyses (Figure 4-7A). Noteworthy, early differentiation was stimulated by the presence of heparin as there was increased ALP activity compared to pristine β-TCP (Figure 4-7B). Although after osteogenic stimulation (7 and 14 days) ALP expression was higher on TCPS, this might be influenced by cell confluence, as denoted by the plateau reached in cell proliferation for TCPS (Figure 4-7B). Additionally, ALP expression occurred at

shorter times on CaPs substrates, but at lower levels even the osteogenic stimulation. Hence the platform proposed here presents a novel step forward in the design of osteoimmunomodulatory biomaterials taking advantage of the intrinsic properties of CaPs together with immobilized GAGs on their surface.

4.5. Conclusions

Heparin was covalently attached on β-TCP substrates by a silanization process and achieved significantly higher grafting densities compared to physisorption. The presence of heparin clearly influenced the response of both immune and osteogenic cells. Heparinization decreased the levels of hydrogen peroxide and inflammatory cytokines released from human immune cells in contact with the material. Cells elongation ratio was found higher on heparinized β-TCP-H, which denote a M2 or pro-healing phenotype correlated to the down-regulation of pro-inflammatory cytokines. In addition, heparinized substrates resulted in higher ALP expression in rat mesenchymal stem cells after 3 days of culture in the absence of osteogenic medium, compared to non-heparinized substrates. This may indicate that heparinized surfaces enhance osteogenic differentiation, but this would need to be validated in further studies.

4.6.　　References

[1]　　H. Takayanagi, Osteoimmunology: shared mechanisms and crosstalk between the immune and bone systems, Nat. Rev. Immunol. **7** (2007) 292–304.

[2]　　J.R. Arron, Y. Choi, Osteoimmunology: Bone versus immune system, Nature. **408** (2000) 535–536.

[3]　　A. Mantovani, S.K. Biswas, M.R. Galdiero, A. Sica, M. Locati, Macrophage plasticity and polarization in tissue repair and remodelling, J. Pathol. **229** (2013) 176–185.

[4]　　A. Mantovani, A. Sica, S. Sozzani, P. Allavena, A. Vecchi, M. Locati, The chemokine system in diverse forms of macrophage activation and polarization., Trends Immunol. **25** (2004) 677–86.

[5]　　D.M. Mosser, J.P. Edwards, Exploring the full spectrum of macrophage activation., Nat. Rev. Immunol. **8** (2008) 958–69.

[6]　　R.D. Stout, J. Suttles, Functional plasticity of macrophages: reversible adaptation to changing microenvironments., J. Leukoc. Biol. **76** (2004) 509–13.

[7]　　Z. Chen, T. Klein, R.Z. Murray, R. Crawford, J. Chang, C. Wu, Y. Xiao, Osteoimmunomodulation for the development of advanced bone biomaterials, Mater. Today. **19** (2016) 304–321.

[8]　　S. Chen, J.A. Jones, Y. Xu, H.-Y. Low, J.M. Anderson, K.W. Leong, Characterization of topographical effects on macrophage behavior in a foreign body response model, Biomaterials. **31** (2010) 3479–3491.

[9]　　M.L. Godek, J.A. Sampson, N.L. Duchsherer, Q. McElwee, D.W. Grainger, Rho GTPase protein expression and activation in murine monocytes/macrophages are not modulated by model biomaterial surfaces in serum-containing in vitro cultures, J. Biomater. Sci. Polym. Ed. **17** (2006) 1141–1158.

[10]　　P.C.S. Bota, A.M.B. Collie, P. Puolakkainen, R.B. Vernon, E.H. Sage, B.D. Ratner, P.S. Stayton, Biomaterial topography alters healing in vivo and monocyte/macrophage activation in vitro, J. Biomed. Mater. Res. Part A. **95A** (2010) 649–657.

[11]　　B. Wójciak-Stothard, A. Curtis, W. Monaghan, K. Macdonald, C. Wilkinson, Guidance and Activation of Murine Macrophages by Nanometric Scale Topography, Exp. Cell Res. **223** (1996) 426–435..

[12]　　Y. Arima, H. Iwata, Effect of wettability and surface functional groups on protein adsorption and cell adhesion using well-defined mixed self-assembled monolayers, Biomaterials. **28** (2007) 3074–3082.

[13]　　N. Faucheux, R. Schweiss, K. Lützow, C. Werner, T. Groth, Self-assembled monolayers with different terminating groups as model substrates for cell adhesion studies, Biomaterials. **25** (2004) 2721–2730.

[14]　　S. Pujari-Palmer, M. Pujari-Palmer, M. Karlsson Ott, Reduced oxidative stress in primary human cells by antioxidant released from nanoporous alumina, J. Biomed. Mater. Res. Part B Appl. Biomater. **104** (2016) 568–575.

[15]　　R.J. Schutte, A. Parisi-Amon, W.M. Reichert, Cytokine profiling using monocytes/macrophages cultured on common biomaterials with a range of surface chemistries, J. Biomed. Mater. Res. Part A. **88A** (2009) 128–139.

[16]　　Z. Chen, J. Yuen, R. Crawford, J. Chang, C. Wu, Y. Xiao, The effect of osteoimmunomodulation on the osteogenic effects of cobalt incorporated β-tricalcium phosphate, Biomaterials. **61** (2015) 126–138.

[17]　　J.E. McBane, L.A. Matheson, S. Sharifpoor, J.P. Santerre, R.S. Labow, Effect of polyurethane chemistry and protein coating on monocyte differentiation towards a wound healing phenotype macrophage, Biomaterials. **30** (2009) 5497–5504.

[18]　　V. Ballotta, A. Driessen-Mol, C.V.C. Bouten, F.P.T. Baaijens, Strain-dependent modulation of macrophage polarization within scaffolds, Biomaterials. **35** (2014) 4919–4928.

[19]　　A. Mevoy, M. Jeyam, G. Ferrier, C.. Evans, J.. Andrew, Synergistic effect of particles and cyclic pressure on cytokine production in human monocyte/macrophages: proposed role in periprosthetic osteolysis, Bone. **30** (2002) 171–177.

[20]   E.M. Sussman, M.C. Halpin, J. Muster, R.T. Moon, B.D. Ratner, Porous Implants Modulate Healing and Induce Shifts in Local Macrophage Polarization in the Foreign Body Reaction, Ann. Biomed. Eng. **42** (2014) 1508–1516

[21]   D. Bezuidenhout, N. Davies, P. Zilla, Effect of well defined dodecahedral porosity on inflammation and angiogenesis., ASAIO J. **48** (1992) 465–71.

[22]   T. Takada, T. Katagiri, M. Ifuku, N. Morimura, M. Kobayashi, K. Hasegawa, A. Ogamo, R. Kamijo, Sulfated polysaccharides enhance the biological activities of bone morphogenetic proteins., J. Biol. Chem. **278** (2003) 43229–35.

[23]   S. Teixeira, L. Yang, P.J. Dijkstra, M.P. Ferraz, F.J. Monteiro, Heparinized hydroxyapatite/collagen three-dimensional scaffolds for tissue engineering., J. Mater. Sci. Mater. Med. **21** (2010) 2385–92.

[24]   B.E. Uygun, S.E. Stojsih, H.W.T. Matthew, Effects of immobilized glycosaminoglycans on the proliferation and differentiation of mesenchymal stem cells., Tissue Eng. Part A. **15** (2009) 3499–512.

[25]   J.G. Cripps, F.A. Crespo, P. Romanovskis, A.F. Spatola, R. Fernández-Botrán, Modulation of acute inflammation by targeting glycosaminoglycan–cytokine interactions, Int. Immunopharmacol. **5** (2005) 1622–1632.

[26]   K.R. Taylor, R.L. Gallo, Glycosaminoglycans and their proteoglycans: host-associated molecular patterns for initiation and modulation of inflammation, FASEB J. **20** (2006) 9–22.

[27]   L. Ramsden, C.C. Rider, Selective and differential binding of interleukin (IL)-1α, IL-1β, IL-2 and IL-6 to glycosaminoglycans, Eur. J. Immunol. **22** (1992) 3027–3031.

[28]   M.S. Douglas, D.A. Rix, J.H. Dark, D. Talbot, J.A. Kirby, Examination of the mechanism by which heparin antagonizes activation of a model endothelium by interferon-gamma (IFN-gamma)., Clin. Exp. Immunol. **107** (1997) 578–84.

[29]   S.J. Fritchley, J.A. Kirby, S. Ali, The antagonism of interferon-gamma (IFN-gamma) by heparin: examination of the blockade of class II MHC antigen and heat shock protein-70 expression., Clin. Exp. Immunol. **120** (2000) 247–52.

[30]   G.M. Campo, A. Avenoso, S. Campo, A. D 'ascola, P. Traina, D. Samà, A. Calatroni, Glycosaminoglycans Modulate Inflammation and Apoptosis in LPS-Treated Chondrocytes, J. Cell. Biochem. **106** (2009) 83–92.

[31]   P. Dandona, T. Qutob, W. Hamouda, F. Bakri, A. Aljada, Y. Kumbkarni, W.. Shin, J.. Liao, G.. Gensini, G.. N. Serneri, Heparin inhibits reactive oxygen species generation by polymorphonuclear and mononuclear leucocytes., Thromb. Res. **96** (1999) 437–43.

[32]   G. Zhou, M.S. Niepel, S. Saretia, T. Groth, Reducing the inflammatory responses of biomaterials by surface modification with glycosaminoglycan multilayers, J. Biomed. Mater. Res. Part A. **104**(2015)493-502.

[33]   J. Salbach, T.D. Rachner, M. Rauner, U. Hempel, U. Anderegg, S. Franz, J.-C. Simon, L.C. Hofbauer, Regenerative potential of glycosaminoglycans for skin and bone., J. Mol. Med. (Berl). **90** (2012) 625–35.

[34]   V. Hintze, S.A. Samsonov, M. Anselmi, S. Moeller, J. Becher, M. Schnabelrauch, D. Scharnweber, M.T. Pisabarro, Sulfated glycosaminoglycans exploit the conformational plasticity of bone morphogenetic protein-2 (BMP-2) and alter the interaction profile with its receptor., Biomacromolecules. **15** (2014) 3083–92.

[35]   V. Hintze, S. Moeller, M. Schnabelrauch, S. Bierbaum, M. Viola, H. Worch, D. Scharnweber, Modifications of hyaluronan influence the interaction with human bone morphogenetic protein-4 (hBMP-4)., Biomacromolecules. **10** (2009) 3290–7.

[36]   U. Hempel, C. Preissler, S. Vogel, S. Möller, V. Hintze, J. Becher, M. Schnabelrauch, M. Rauner, L.C. Hofbauer, P. Dieter, Artificial extracellular matrices with oversulfated glycosaminoglycan derivatives promote the differentiation of osteoblast-precursor cells and premature osteoblasts., Biomed Res. Int. **2014** (2014) 938368.

[37]   J. Salbach-Hirsch, S.A. Samsonov, V. Hintze, C. Hofbauer, A.-K. Picke, M. Rauner, J.-P. Gehrcke, S. Moeller, M. Schnabelrauch, D. Scharnweber, M.T. Pisabarro, L.C. Hofbauer, Structural and functional insights into sclerostin-glycosaminoglycan interactions in bone., Biomaterials. **67** (2015) 335–45.

[38]   A. Irie, M. Takami, H. Kubo, N. Sekino-Suzuki, K. Kasahara, Y. Sanai, Heparin enhances osteoclastic bone resorption by inhibiting osteoprotegerin activity., Bone. **41** (2007) 165–74.

[39]   J. Salbach, S. Kliemt, M. Rauner, T.D. Rachner, C. Goettsch, S. Kalkhof, M. von Bergen, S. Möller, M. Schnabelrauch, V. Hintze, D. Scharnweber, L.C. Hofbauer, The effect of the degree of sulfation of glycosaminoglycans on osteoclast function and signaling pathways., Biomaterials. **33** (2012) 8418–29.

[40]   J. Salbach-Hirsch, J. Kraemer, M. Rauner, S.A. Samsonov, M.T. Pisabarro, S. Moeller, M. Schnabelrauch, D. Scharnweber, L.C. Hofbauer, V. Hintze, The promotion of osteoclastogenesis by sulfated hyaluronan through interference with osteoprotegerin and receptor activator of NF-κB ligand/osteoprotegerin complex formation., Biomaterials. **34** (2013) 7653–61.

[41]   M. Tichá, B. Železná, V. Jonáková, K. Filka, Immobilization of heparin on polyacrylamide derivatives, J. Chromatogr. B Biomed. Sci. Appl. **656** (1994) 423–426.

[42]   U. König, A. Lode, P.B. Welzel, Y. Ueda, S. Knaack, A. Henß, A. Hauswald, M. Gelinsky, Heparinization of a biomimetic bone matrix: integration of heparin during matrix synthesis versus adsorptive post surface modification., J. Mater. Sci. Mater. Med. **25** (2014) 607–21.

[43]   S. Gittens, K. Bagnall, J.R. Matyas, R. Löbenberg, H. Uludag, Imparting bone mineral affinity to osteogenic proteins through heparin-bisphosphonate conjugates., J. Control. Release. **98** (2004) 255–68.

[44]   U. Edlund, S. Dånmark, A.-C. Albertsson, A strategy for the covalent functionalization of resorbable polymers with heparin and osteoinductive growth factor., Biomacromolecules. **9** (2008) 901–5.

[45]   D.S. Bramono, S. Murali, B. Rai, L. Ling, W.T. Poh, Z.X. Lim, G.S. Stein, V. Nurcombe, A.J. van Wijnen, S.M. Cool, Bone marrow-derived heparan sulfate potentiates the osteogenic activity of bone morphogenetic protein-2 (BMP-2)., Bone. **50** (2012) 954–64.

[46]   Z. Chen, C. Wu, W. Gu, T. Klein, R. Crawford, Y. Xiao, Osteogenic differentiation of bone marrow MSCs by β-tricalcium phosphate stimulating macrophages via BMP2 signalling pathway, Biomaterials. **35** (2014) 1507–1518.

[47]   Z. Chen, A. Bachhuka, S. Han, F. Wei, S. Lu, R.M. Visalakshan, K. Vasilev, Y. Xiao, Tuning Chemistry and Topography of Nanoengineered Surfaces to Manipulate Immune Response for Bone Regeneration Applications, ACS Nano. **11**(2017) 4494-4506.

[48]   W. Pompe, M. Gelinsky, A. Lode, A. Reinstorf, A. Bernhardt, U. Ko, Calcium phosphate bone cements , functionalized with VEGF : release kinetics and biological activity, Biomed. Mater. Res. A. **81** (2007) 474–483.

[49]   C.S. Goonasekera, K.S. Jack, G. Bhakta, B. Rai, E. Luong-Van, V. Nurcombe, S.M. Cool, J.J. Cooper-White, L. Grøndahl, Mode of heparin attachment to nanocrystalline hydroxyapatite affects its interaction with bone morphogenetic protein-2, Biointerphases. **10** (2015) 04A308.

[50]   A. Lode, A. Reinstorf, A. Bernhardt, C. Wolf-Brandstetter, U. König, M. Gelinsky, Heparin modification of calcium phosphate bone cements for VEGF functionalization., J. Biomed. Mater. Res. A. **86** (2008) 749–59.

[51]   M. Espanol, R.A. Perez, E.B. Montufar, C. Marichal, A. Sacco, M.P. Ginebra, Intrinsic porosity of calcium phosphate cements and its significance for drug delivery and tissue engineering applications, Acta Biomater. **5** (2009) 2752–2762.

[52]   R.L. Williams, Development of multifunctional calcium phosphate particles for drug delivery and formation of cross-linked materials, University of Birmingham, **2014.**

[53]   M.S. Ahola, E.S. Säilynoja, M.H. Raitavuo, M.M. Vaahtio, J.I. Salonen, A.U.O. Yli-Urpo, In vitro release of heparin from silica xerogels, Biomaterials. **22** (2001) 2163–2170.

[54]   C. Dahlgren, A. Karlsson, Respiratory burst in human neutrophils, J. Immunol. Methods. **232** (1999) 3–14.

[55]   G. Mestres, M. Espanol, W. Xia, C. Persson, M.-P. Ginebra, M.K. Ott, Inflammatory response to nano- and microstructured hydroxyapatite., PLoS One. **10** (2015) e0120381.

[56]   F.Y. McWhorter, T. Wang, P. Nguyen, T. Chung, W.F. Liu, Modulation of macrophage phenotype by cell shape., Proc. Natl. Acad. Sci. U. S. A. **110** (2013) 17253–8.

[57]   C.J. Ferrante, S.J. Leibovich, Regulation of Macrophage Polarization and Wound Healing., Adv. Wound Care. **1** (2012) 10–16.

[58]   D.T. Hughes Wassell, G. Embery, Adsorption of chondroitin-4-sulphate and heparin onto hydroxyapatite--effect of bovine serum albumin., Biomaterials. **18** (1997) 1001–1007.

[59]   G. a. Hudalla, J.T. Koepsel, W.L. Murphy, Surfaces that sequester serum-borne heparin amplify growth factor activity, Adv. Mater. **23** (2011) 5415–5418.

[60]   D.G. Belair, N.N. Le, W.L. Murphy, Design of growth factor sequestering biomaterials, Chem. Commun. **50** (2014) 15651–15668.

[61]   M. Mittal, M.R. Siddiqui, K. Tran, S.P. Reddy, A.B. Malik, Reactive Oxygen Species in Inflammation and Tissue Injury, Antioxid. Redox Signal. **20** (2014) 1126–1167.

[62]   R. Lever, A. Smailbegovic, C. Page, Role of glycosaminoglycans in inflammation, Inflammopharmacology. **9** (2001) 165–169.

[63]   R. Sridharan, A.R. Cameron, D.J. Kelly, C.J. Kearney, F.J. O'Brien, Biomaterial based modulation of macrophage polarization: a review and suggested design principles, Mater. Today. **18** (2015) 313–325.

[64]   R. Klopfleisch, Macrophage reaction against biomaterials in the mouse model – Phenotypes, functions and markers, Acta Biomater. **43** (2016) 3–13.

[65]   T. Lange, A.F. Schilling, F. Peters, F. Haag, M.M. Morlock, J.M. Rueger, M. Amling, Proinflammatory and osteoclastogenic effects of beta-tricalciumphosphate and hydroxyapatite particles on human mononuclear cells in vitro., Biomaterials. **30** (2009) 5312–8.

[66]   T. Lange, A.F. Schilling, F. Peters, J. Mujas, D. Wicklein, M. Amling, Size dependent induction of proinflammatory cytokines and cytotoxicity of particulate beta-tricalciumphosphate in vitro., Biomaterials. **32** (2011) 4067–75.

[67]   C. Dombrowski, S.J. Song, P. Chuan, X. Lim, E. Susanto, A.A. Sawyer, M.A. Woodruff, D.W. Hutmacher, V. Nurcombe, S.M. Cool, Heparan Sulfate Mediates the Proliferation and Differentiation of Rat Mesenchymal Stem Cells, Stem Cells Dev. **18** (2009) 661–670.

[68]   S. Mathews, S.A. Mathew, P.K. Gupta, R. Bhonde, S. Totey, Glycosaminoglycans enhance osteoblast differentiation of bone marrow derived human mesenchymal stem cells., J. Tissue Eng. Regen. Med. **8** (2014) 143–52.

Chapter 5

Effect of heparinization on the inflammatory response and osteoclastogenesis of biomimetic CDHA

Scope

In the previous chapter it was demonstrated that the use of ECM molecule, like heparin, on conventional synthetic bone grafts was a promising strategy to enhance the materials' biological interactions. The purpose of this chapter is to explore the functionalization of more complex samples, i.e. biomimetic calcium phosphates, and to focus the biological screening to the early stages of healing where immune cells and osteoclasts (OC) modulate the inflammation and resorption potential of the biomaterial, respectively.

Chapter 5
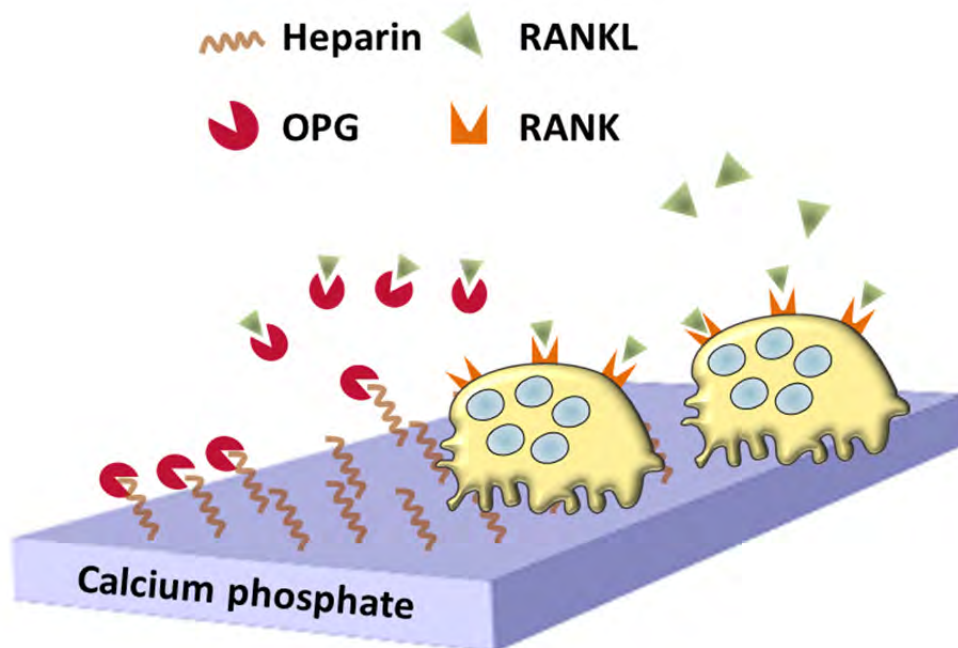
5.1.   Introduction

The success of synthetic bone grafts upon implantation is usually related to their ability to favorably modulate the host response. The biological cascade triggering the success or failure of a biomaterial depends on its interactions with the host tissue. These interactions mainly involve the immune and the skeletal systems in what nowadays is known as osteoimmunology.[1,2] The immune system plays a role in the inflammatory response upon implantation/injury while the skeletal system will orchestrate the osteogenic/osteoclastogenic response to interact with the biomaterial[3,4] The resolution of this first inflammatory response is related to homeostasis, inflammation and the consequent tissue repair and regeneration.[5] The main actors during inflammation are blood cells arriving to the injured site by extravasation. Neutrophils (polymorphonuclear cells, PMNC), monocytes and monocyte-derived cells, such as macrophages, are the first interacting cells, which will trigger the biological cascade by releasing reactive species, such as ROS and NOS, respectively, chemokines and cytokines.[6–8] Hence, the modulation of this early response has recently drawn the attention in the effort to enhance the tissue regeneration potential of biomaterials.

Reducing or switching-off inflammation upon implantation is one desired mechanism which can foster the success of an implanted material.[9] One interesting approach is the use of GAG as anti-inflammatory molecules. Hyaluronic acid, chondroitin sulphate and heparin have shown good anti-inflammatory properties by binding to chemo- and cytokines.[10] As an example of how GAGs interact with the pro-inflammatory chemokine, interleukin–8 (CXCL8)/neutrophil-mediated inflammation has been recently described.[11] In addition, GAGs are part of the extracellular matrix (ECM),and they are known to interact with several signaling proteins involved not only in the immune system but also in the skeletal pathways.[12,13] Recent works have highlighted the affinity of GAGs for osteogenic proteins such as bone morphogenetic proteins (BMPs),[14–17] thanks to the presence of heparin binding domains in BMPs.[13] Hempel *et al.* pointed to the degree of sulfonation of GAGs as a key to control such interactions.[18,19] Likewise, Hintze *et al.* reported a higher binding affinity of oversulfated GAGs with human BMP-4 compared to the absence of sulfonation.[20] Even though the osteogenic potential of GAGs, and specifically heparin has been reported, it is still controversial whether GAGs enhance or inhibit osteoclast maturation.[21–23]

In this chapter, we propose to exploit the capacity of GAGs to interact with the bone remodeling cascade at different stages, by combining them with a calcium phosphate substrate. CaPs are ideal candidates to support bone regeneration. Moreover, they possess a close resemblance to mineral bone phase, i.e. HA.

Some authors have investigated engineered routes to enhance their biological interactions. Lode *et al.* improved the angiogenic response of endothelial cells *in vitro* by functionalization of CaPs with heparin.[24] Likewise, König *et al.* investigated the effect of heparinized collagen-HA matrices on fibroblast, endothelial cells and mesenchymal stem cells resulting in improved biological interactions compared to non-heparinized matrices. [25] However, one of the main drawbacks of synthetic HA is its poor resorption rate. Hence, promoting their resorption is also a good strategy to develop successful bone grafts, able to be transformed in new bone.

In fact, the control of the materials' resorption is a key aspect during the bone remodeling process. Promoting osteoclastogenesis and the bi-directional crosstalk between osteoclasts (OC) and osteoblasts (OB) is crucial for bone tissue regeneration, and GAGs have been shown to be a good tool to foster these interactions. Thus, Salbach *et al.* studied the effect of sulfonation of GAGs to promote OB and OC activity. They found that GAGs were preferentially binding OPG, a decoy receptor of RANKL which blocks the interactions RANKL-RANK, crucial pathway to OC maturation.[26] Similarly, Irie *et al.* investigated the effects of heparin on osteoclasts formation, highlighting as well the heparin interaction with OPG.[17]In their study, osteoclast formation was promoted due to the dual exposure to RANKL and OPG. Heparin bound to OPG thus increasing the RANKL available for OC maturation. Ling *et al.* also described the interfering ability of GAGs to modulate RANKL-induced osteoclastogenesis by solubilizing GAGs on cell culture media using RAW murine cells.[27]

The aim of the present chapter was to use heparin as a tool to tune the inflammatory response and osteoclastogenesis of a CaP which are crucial events at early stages of bone remodeling. The effect of heparin functionalization ona CDHA substrate was analyzed using primary human cells. A widely known synthetic bone graft, β-TCP was used as control, together with tissue culture polystyrene (TCPS).

5.2.   Materials and Methods

5.2.1.   Preparation and characterization of calcium phosphates

CDHA was obtained by hydrolysis of α-TCP. α-TCP was produced by solid state reaction at 1400°C of calcium hydrogen phosphate ($CaHPO_4$, Sigma-Aldrich, St. Louis, USA) and calcium carbonate ($CaCO_3$, Sigma-Aldrich, St. Louis, USA) at a 2:1 molar ratio for 15h and then quenched in air. The α-TCP was milled to a final median size of 5.2μm.[28] α-TCP containing 2wt% of precipitated HA (PHA,

Merck KGaA, Darmstadt, Germany) was mixed with a liquid phase consisting of distilled water at a liquid to powder (L/P) ratio of 0.35mL/g, resulting in a paste that was transferred into PTFE moulds to fabricate discs of either 15 mm diameter x2 mm thickness or 5mm diameter x1mm thickness. The discs were left to set at 37°C for 10 days in water to allow for complete hydrolysis to CDHA. β-TCP discs were obtained by sintering the previously obtained CDHA discs at 1100ºC for 9h and cooling down in air.

Phase identification was performed by XRD (Bruker, Cu Kα, λ=1.5406Å, 40kV, 40mA). Data were collected in 0.02° steps over the 2θ range of 10°-80° with a counting time of 2s per step. The experimental patterns were compared to those of hydroxyapatite (JCPDS 09-0432), α-TCP (JCPDS 09-0348) and β-TCP (JCPDS 09-0169). Pore size distribution was investigated by MIP (Autopore IV Micromeritics) recording intrusion-extrusion curves from 30 to 30000 psia. The SSA was assessed by nitrogen adsorption using the BET method (ASAP 2020, Micromeritics). Finally, the microstructure of the substrates was investigated by SEM (FIB Zeiss Neon40).

5.2.2.   Surface functionalization with heparin

Heparin immobilization was performed through an amidation reaction using a first step of silanization with aminopropyltrietoxysilane (APTES, Sigma-Aldrich, St. Louis, USA) followed by (1-(3-dimethylaminoporpyl)-3-ethylcarbodiimide, EDC, Sigma-Aldrich, St. Louis, USA) and N-hydrosuccinimide (NHS, Sigma-Aldrich, St. Louis, USA) adapted from literature[29] to couple heparin by its carboxyl groups. CDHA discs were immersed in absolute ethanol solution with 2%v/v APTES and 3%v/v distilled water and left for overnight agitation at 100 rpm in order to obtain aminated surfaces. Afterwards, the discs were rinsed in absolute ethanol and sonicated for 5 minutes. Subsequently, different concentrations of heparin were activated to study the saturation onto discs surface. Heparin solutions in phosphate buffer saline (PBS, Gibco) were prepared and activated by dropping pH to 6.5 for 15 minutes in presence of EDC/NHS. Immediately after, pH was raised to 7.5 and 1mL of activated heparin solution was poured onto the aminated discs and left under agitation for 2 hours for coupling. Supernatants were collected for heparin quantification through an indirect colorimetric method based on toluidine blue, adapted from literature.[30] Finally, the heparinized discs (CDHA-H) were rinsed in PBS and sonicated for 5 minutes in order to remove non-covalently attached heparin.

5.2.3. Inflammatory response

Monocytes and PMN were isolated in two steps from human buffy coats from volunteer donors at Uppsala University Hospital similar to previously reported. [31] Briefly, for monocytes isolation, 15mL of human blood diluted in PBS (1:1) were layered onto Ficoll-Paque Plus (GE Healthcare) and monocytes were isolated by density gradient centrifugation. The upper plasma layer was collected and kept at 4ºC for later use. Mononuclear ring was collected and washed 3 times with PBS. Cells were resuspended in PBS and counted by exclusion method using Trypan blue (1:5) in a cytometer. PMN underwent a second separation step using 20mL of 3% Dextran in 0.9% saline solution. After 25 minutes of incubation, supernatant was centrifuged and treated with 0.2% saline solution over 20 seconds and 1.6% saline solution to remove erythrocytes. Cell suspension was further centrifuged and resuspended in PBS. A solution containing 6%wt. acetic acid was used to count cells in a cytometer.

Luminol amplified chemiluminescence was used to study the inflammatory response of cells in contact with $5x1mm^2$ discs by monitoring the release of reactive oxygen species over a time of 2 hours. Cells were activated with 1µM phorbol-12-myristate-13-acetate (PMA, Sigma Aldrich) in a luminol solution as signal amplifier. A negative control consisting of TCPS was used without PMA stimulation. Luminol solution was prepared from stock (50mM of luminol in 0.2 M NaOH) with 1% luminol stock and 0.2% horseradish peroxidase (1mg/mL) and activated with 1µM phorbol-12-myristate-13-acetate (PMA, Sigma Aldrich). Prior to luminol kinetic study, $5x1mm^2$ discs were placed in opaque white 96 well-plates (Perkin Elmer) and sterilized with 70% ethanol for 3 hours, followed by thrice rinsing with PBS for 15 minutes each prior to cell seeding. Both cell types were diluted in cell culture media (4PBS/1RPMI-1640/100Mm glucose) at a density of $1 \cdot 10^6$cells/mL. For the plasma containing studies, 10% of human plasma was added to the cell medium. 200µL of cells were added to opaque 96 well-plates (Perkin Elmer) followed by the addition of 100µL of Luminol solution (500µM). Luminescence was monitored at 37ºC every 2 min over 2h of total kinetic study as previously described.[32] Triplicates for each material were used (n=3) and the experiment was repeated twice with independent donor buffy coats.

5.2.4. Osteoclast cell cultures

Peripheral blood MNC (PBMC), containing the precursors of human osteoclasts, were isolated from buffy coats of healthy voluntary blood donors to the National Blood Transfusion Service. Donation was anonymous, and institutional review board (IRB) approval was not required. Density centrifugation with Ficoll-

Histopaque gradient (Sigma–Aldrich) was used to isolate the mononuclear cells as described in previous work.[33] Cells were resuspended in Dulbecco's Modified Eagle's Medium–High Glucose (DMEM, Euroclone, Milan, Italy) supplemented with 10% fetal bovine serum (FBS, Euroclone) and 1% Penicillin/Streptomycin (complete DMEM). CDHA, CDHA-H, β-TCP and TCPS were sterilized using 70% ethanol for 3h, followed by three rinses with PBS for 15min each. Complete medium was added after the sterilization and kept overnight prior to cell seeding to minimize ionic exchange as preconditioning treatment.

Mononuclear cells were resuspended in complete DMEM and seeded on discs and TCPS at a density of $6 \cdot 10^6$ cells/cm^2 and $3 \cdot 10^6$ cells/cm^2, respectively. After 2h of incubation, non-adherent cells were gently removed and complete DMEM supplemented with 25% RANKL-containing human osteoblast supernatant (differentiation medium) was added to induce the differentiation of osteoclast precursors (OCP).[34,35] Cell cultures were performed up to 28 days and differentiation medium was refreshed every 3 days.

5.2.4.1. Osteoclast morphology

Osteoclast morphology at 14, 21 and 28 days of culture was investigated using Scanning Electron Microscopy (SEM, FIB Zeiss Neon40). At each time point, cells were rinsed with PBS and fixed using 2%paraformaldehyde/2% glutaraldehyde in 0.1M cacodylate buffer overnight at 4ºC. Afterwards, samples were dehydrated in ethanol series and dried. A thin carbon layer was sputtered prior to imaging to impart conductivity.

Tartrate-resistant acid phosphatase and Hoechst staining (TRAP-Hoechst) at 14, 21 and 28 days was used to study OC morphology and differentiation. At each time point, cells were fixed using 3% paraformaldehyde-2% sucrose for 30 min. Afterwards, cell membrane was permeabilized with Triton 0.5% in HEPES for 5 min at room temperature, and finally stained using naphthol AS-BI phosphoric acid and tartrate solution (Acid Phosphatase kit, Sigma–Aldrich) for 60 min at 37ºC for the cytoplasm and with 2.25µg/mL of Hoechst 33258 (Sigma–Aldrich) for 10 min in the dark to for the cell nuclei. TRAP-Hoechst stained samples were analyzed by optical fluorescence microscopy at 360nm excitation and 470nm emission. ImageJ software was used to perform a semi-quantitative analysis of the multinucleated cells found by optical microscopy. Duplicates of 5x1mm^2 material discs were used for the staining study and duplicates of plastic chamber slide were used as controls.

5.2.4.2. Osteoclast activity

In order to assess OC differentiation, tartrate-resistant acid phosphatase (TRAP) activity was quantified both in cells and culture supernatants at the end of the experiment (28 days). Briefly, cells grown on material substrates were rinsed in PBS and lysed with 0.1% Triton X-100/1M NaCl (Sigma-Aldrich). 50μl of the cell lysate were transferred to a new plate and 50μl 4-nitrophenyl phosphate (4.61 mg/ml)/40mM Na-tartrate/50mM Na-acetate (pH 4.8) were added. After 1 hour incubation at 37 ℃, the reaction was stopped with 50μl of sodium hydroxide (NaOH, 0.2M), and the absorbance was measured at 405nm in a spectrophotometer (Infinite F200 Pro Microplate Reader; TECAN, Mannedorf, Switzerland).

Bicinchoninic acid colorimetric assay (BCA, Pierce BCA Protein Assay Kit, Rockford, USA) was used to quantify the total protein in lysates according to manufacturer's instructions. Material substrates without cells (blank) were measured and subtracted from cell-seeded materials. TRAP activity was then normalized by the total protein content after blank subtraction.

Tartrate-resistant acid phosphatase isoform 5b (TRAP5b) activity was investigated after 28 days of culture. Cell supernatants were collected, centrifuged at 400g for 5 min and assayed using the BoneTRAP® Assay kit (Pantecs.r.l., Torino, Italy), according to the manufacturer's instructions. The concentration of TRAP5b protein in the supernatants was determined by reading the absorbance at 405nm in a spectrophotometer. Data are expressed as mean concentration (units/L) after subtraction of the corresponding cell-free readout (blank).

Calcium release and pH were monitored over the experimental time at 0, 3, 7, 14, 21 and 28 days. At each time point supernatants were collected, centrifuged at 2800rpm for 5 minutes and kept at 4℃ until measurement. Calcium release was measured using a colorimetric method based on ortho-cresolphthalein complexone (OCPC, Sigma-Aldrich) adapted from previous works[36,37] and the absorbance was measured at 570nm using a UV-vis spectrophotometer (Infinite M200 Pro Microplate Reader; TECAN, Manndorf, Switzerland). The values of pH were measured using a pH-meter (MultiMeter MM 41). Triplicates of 15x2mm^2 material discs were used for all experiments.

5.2.5. Statistics

Data were obtained using triplicates for each experiment. Data are represented as mean value ± standard error of the mean. Data groups for TRAP measurements and multinucleated cells counting were normally distributed (homogeneous

variance, Levene>0.05) and were analyzed using one way ANOVA and post-hoc Tukey test was used to assess significant differences. The differences in the number of nuclei were not normally distributed and non-parametric Kruskal-Wallis was used to assess significant differences. Values of $p<0.05$ were considered as significant. All statistics were performed using IBM® SPSS® Statistics 24 software.

5.3.   Results

5.3.1.   Physicochemical properties of CaP substrates

Phase composition as measured by XRD (Figure 5-1A) showed that CDHA consisted of a poorly crystalline hydroxyapatite phase (JCPDS 09-0432), as indicated by the broad peaks. A small amount of unreacted α-TCP was detected (JCPDS 09-0348), amounting a 2wt%, as quantified by EVA Software. β-TCP samples were phase-pure and showed the sharp peaks typical of crystalline sintered materials (JCPDS 09-0169). According to MIP analysis (Fig. 1B), CDHA exhibited a broad pore size distribution ranging from 10 to 100nm. In contrast, β-TCP specimens presented larger pores, centered around 1µm, although they exhibited also some nanoporosity. The total porosity was similar for both substrates (Figure 5-1C). The microstructure of the two ceramic substrates was clearly different. Whereas CDHA consisted of an entangled network of plate-like crystals, β-TCP presented a smooth polyhedral grain microstructure (Figure 5-1C,a and b), which resulted in very different values of SSA, i.e. 24m^2/g for CDHA and 0.4 m^2/g for β-TCP. Finally, the results of the heparin adsorption isotherms are displayed in Figure 5-1D. The maximum covalent attachment yield was achieved with 500µg/mL, which allowed for the immobilization of approximately 200µg of heparin on the material surface.
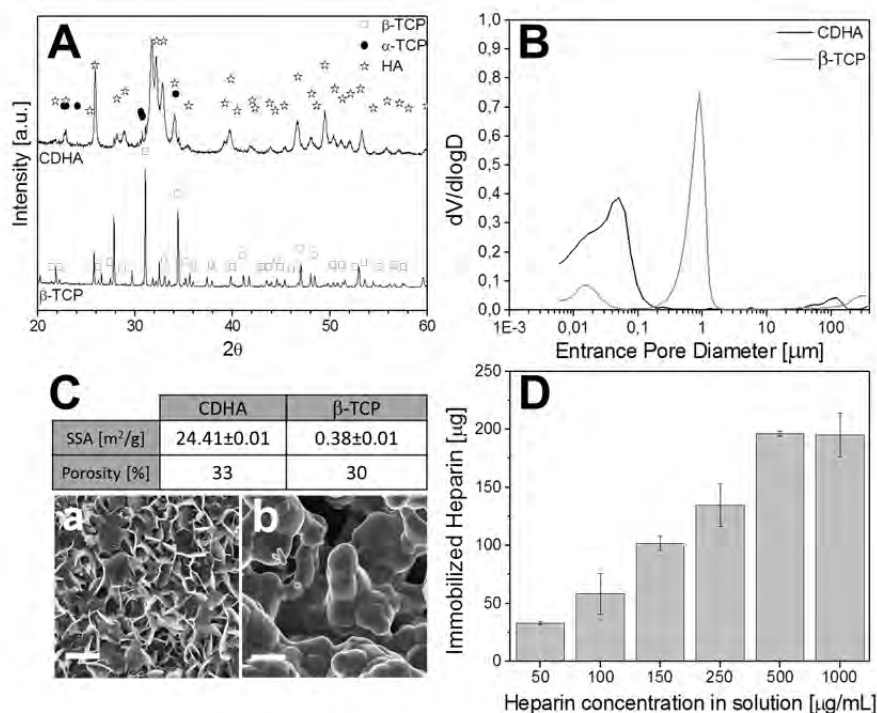
Figure 5-1. Physicochemical properties of CaP substrates. A: XRD patterns of CDHA and β-TCP; B: pore entrance size distribution; C: Specific surface area (SSA) and porosity values with representative SEM microstructures for CDHA and β-TCP (a and b, respectively, scale bar: 2μm); D: heparin adsorption isotherms on CDHA after 2h incubation in heparin solutions.

5.3.2.   Inflammatory response

The release of ROS by PMN and monocytes upon contact with the surface of the different materials activated with PMA is depicted in Figure 5-2 and Figure 5-3. The inflammatory response of PMN with and without plasma is shown in Figure 5-2A and B, respectively. CDHA exhibited the lowest ROS release among all substrates either with or without plasma (black and grey curves, respectively), followed by CDHA-H and β-TCP. All PMA-stimulated substrates showed a peak within the first 5 minutes, shorter times than those presented on Chapter 4 (Figure 4-4A), which could be related to the handling of PMA activation and measurement. Plasma containing studies showed a slight increase in ROS signal compared to the absence of plasma. No release of ROS was observed in the negative control (TCPS) without PMA activation.

Figure 5-2. Kinetics of ROS release by neutrophils in contact with substrates over 2h. A: ROS release in presence of 10% human plasma, and B: ROS release without plasma.

ROS kinetic release upon contact with monocytes in absence of plasma showed higher values than PMN Figure 5-3A, however ROS peaks were shifted to longer time (20min). TCPS activated (TCPS+) showed a bimodal kinetic, with two ROS peaks at 20 and 50min.Biomimetic substrates CDHA and CDHA-H exhibited the lowest ROS signals, approximately 60% and 30%, in the presence and absence of plasma respectively, showing a mean peak at 20min in all substrates (Figure 5-3A and B). The presence of plasma increased the signal of ROS for both CDHA and CDHA-H, which was though diminished after 1h to half of its value (Figure 5-3A). No effect of plasma was found for β-TCP which yielded approximately 70-80% of ROS for both absence and presence of plasma.
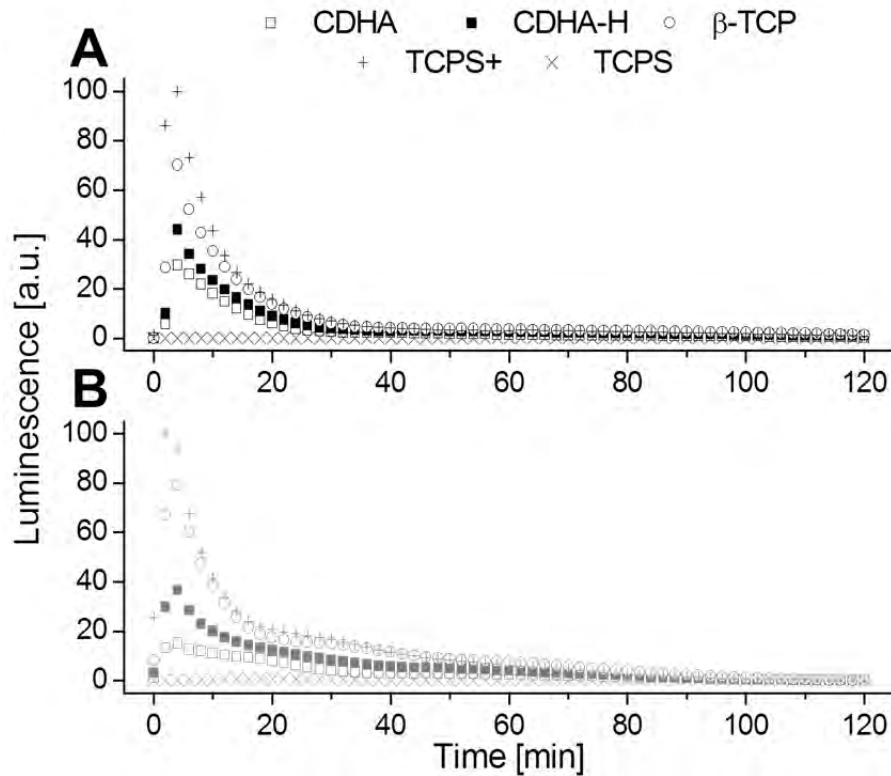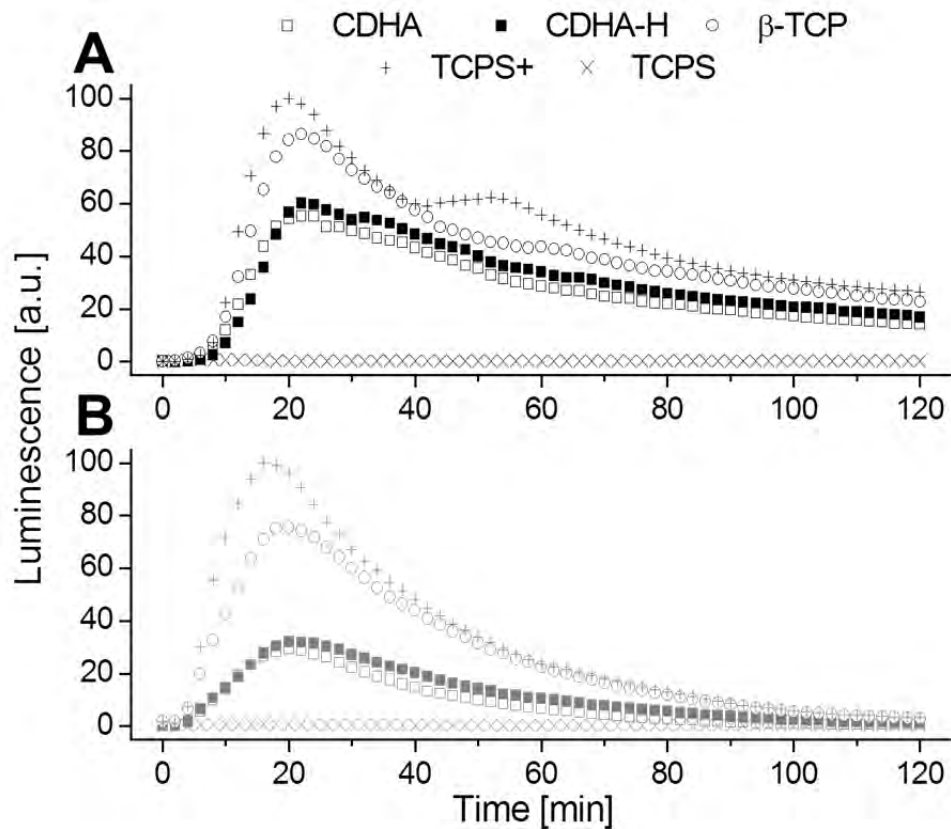
Figure 5-3. ROS release kinetic of monocytes in contact with substrates over 2h. A: ROS release in presence of 10% human plasma, and B: ROS release without plasma.

5.3.3. Osteoclast morphology

The evolution of osteoclast morphology was qualitatively evaluated by SEM. Figure 5-4 shows the OC morphology on substrates at 14, 21 and 28 days. On TCPS, round cells were found at 14 days, which became bigger and more spread after 21 and 28 days. At 28 days, protuberances surrounded by a flat halo were visible for all cells, compatible with mature OC morphology. β-TCP substrate showed a high number of round cells at 14 days which spread and showed several connecting filopodia at 21 days and 28 days. Biomimetic substrates, CDHA and CDHA-H, also supported OC adhesion as shown in the results at 14 days. After 21 days, cells appeared more elongated on CDHA-H than on CDHA at 28 days the presence of cell clusters were observed in some regions of the sample particularly for CDHA-H
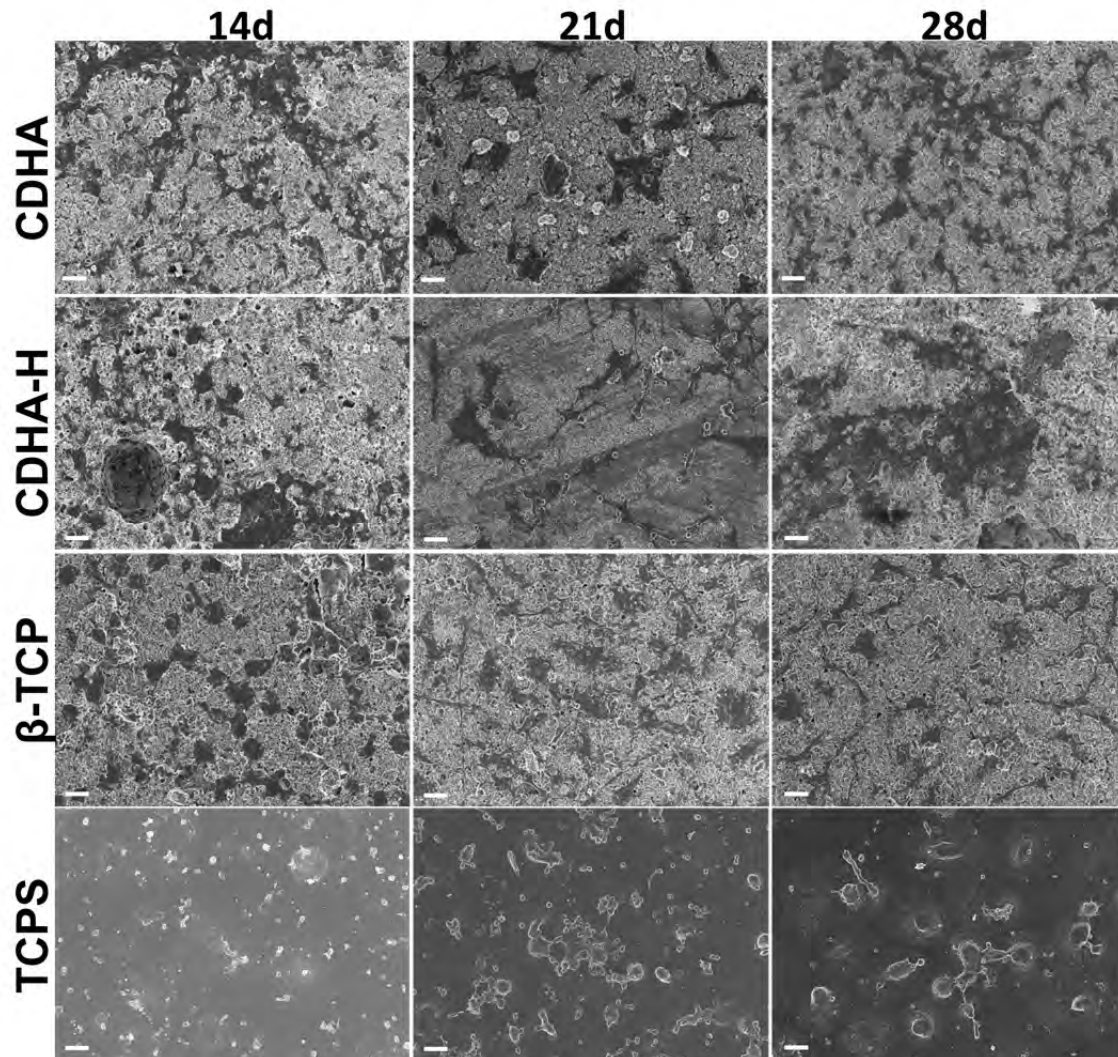
Figure 5-4. SEM images of osteoclasts cultured on substrates at different time points (14 days, first column; 21 days, second column, and 28 days, third column) Scale bar: 20µm.

Higher magnification images of CDHA-H at 28 days showed regions with degraded crystals compared to pristine plate-like microstructure of the material. This was compatible with OC resorption and was especially evident close to the cells (Figure 5-5). Figure 5-5B shows that the plate-like crystals typical from CDHA appeared degraded at the adjacent zones of OC.

The differentiation of OC was monitored using TRAP-Hoechst staining at each time points (14, 21 and 28 days). Few adherent cells were observed on the biomimetic substrates compared to sintered β-TCP. At 14 days, multinucleated cells were evident only on TCPS and CDHA-H (Figure 5-6D and J, black arrows). This aspect was maintained over 21 and 28 days for both substrates (Figure 5-6E and F for CDHA-H, and Figure 5-6K and L for TCPS). Only at 28 days few multinucleated cells were found on CDHA and β-TCP, even if some cell clusters were visible already at 21 days for CDHA (Figure 5-6B).
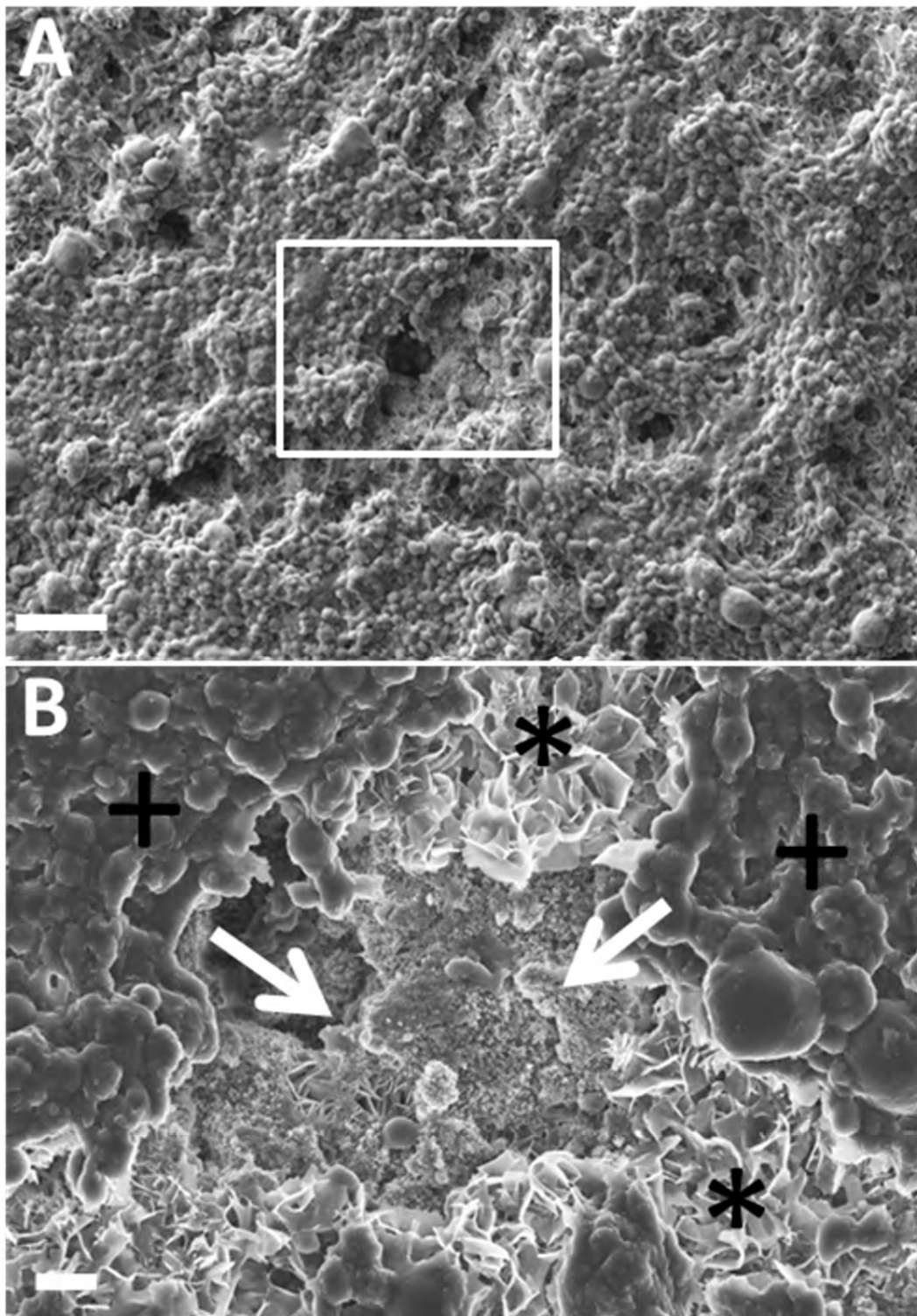
Figure 5-5. SEM images of CDHA-H at 28 days showing distorted crystals from OC activity. A: low magnification image showing a covered surface by OC (scale bar:10μm), and B: higher magnification image showing degraded plate crystals (white arrows) compared to the pristine crystal morphology (*) at the adjacent zone to cells (+), (scale bar:2μm).
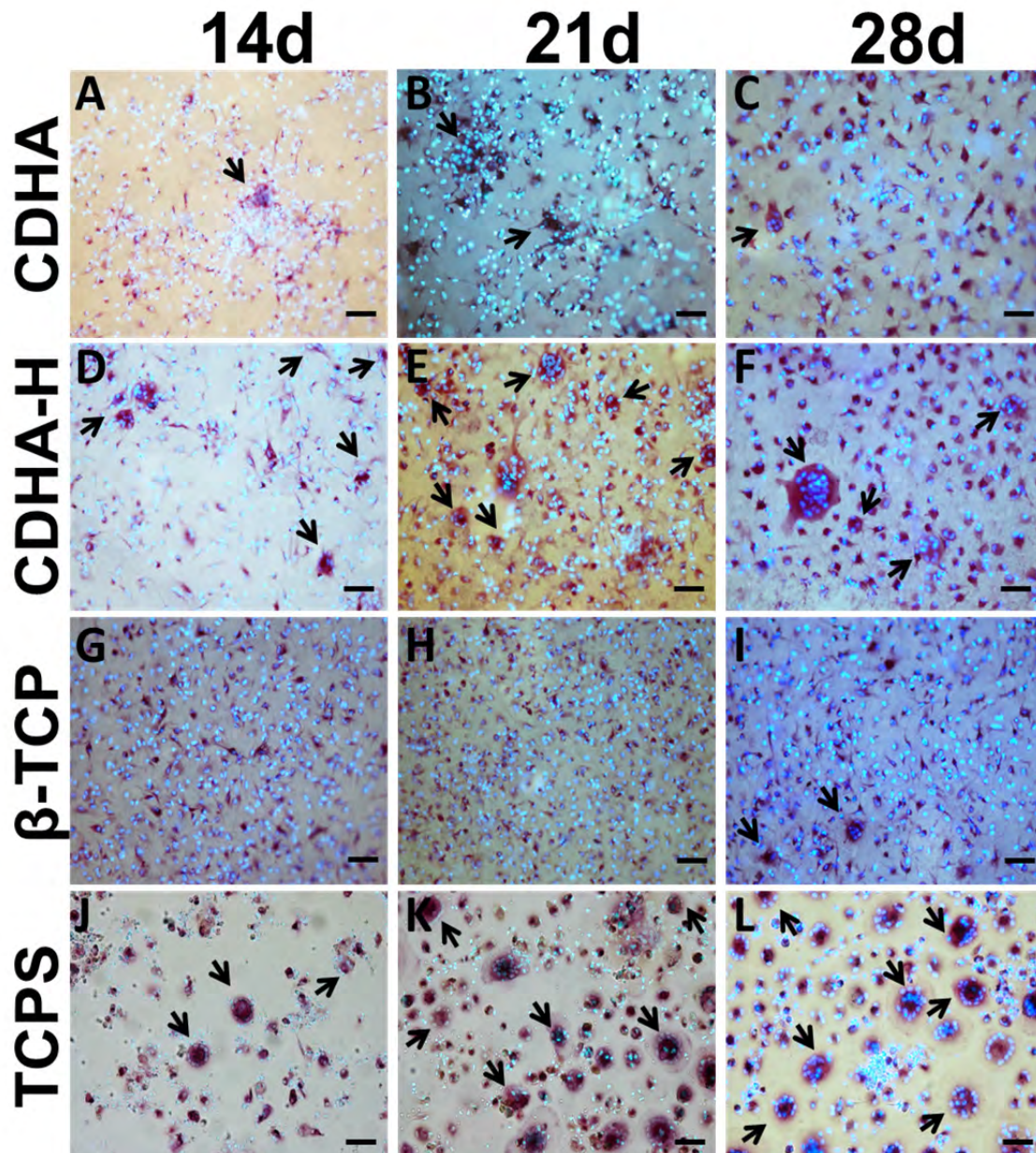
Figure 5-6. TRAP-Hoechst staining showing OC differentiation over time on CDHA (A, B and C), on CDHA-H (D, E and F), on β-TCP (G, H and I) and on TCPS (I, K and L).). Scale bar:25µm. Black arrows indicate multinucleated cells (OC).

Image analyses based on TRAP-Hoechst optical images disclosed different cell behaviors (Figure 5-7A). A higher number of multinucleated cells was found on TCPS since 14 days, which was increasing with time (21 and 28 days). CaPs substrates displayed lower number of multinucleated cells compared to TCPS. For CDHA, the presence of heparin (CDHA-H) produced higher number of multinucleated cells at all-time points, whereas β-TCP and bare CDHA showed similar number of multinucleated cells but with less nuclei. A more in-depth study on the morphology of the nucleated cells revealed different fusion patterns over time. Figure 5-7B illustrates the comparison of the number of nuclei in the

multinucleated cells counted in Figure 5-6A. The substrates yielding higher number of multinucleated cells, i.e. CDHA-H and TCPS, showed also a higher number of cells with 3 to 5 or 6 to 10 nuclei regardless of time.
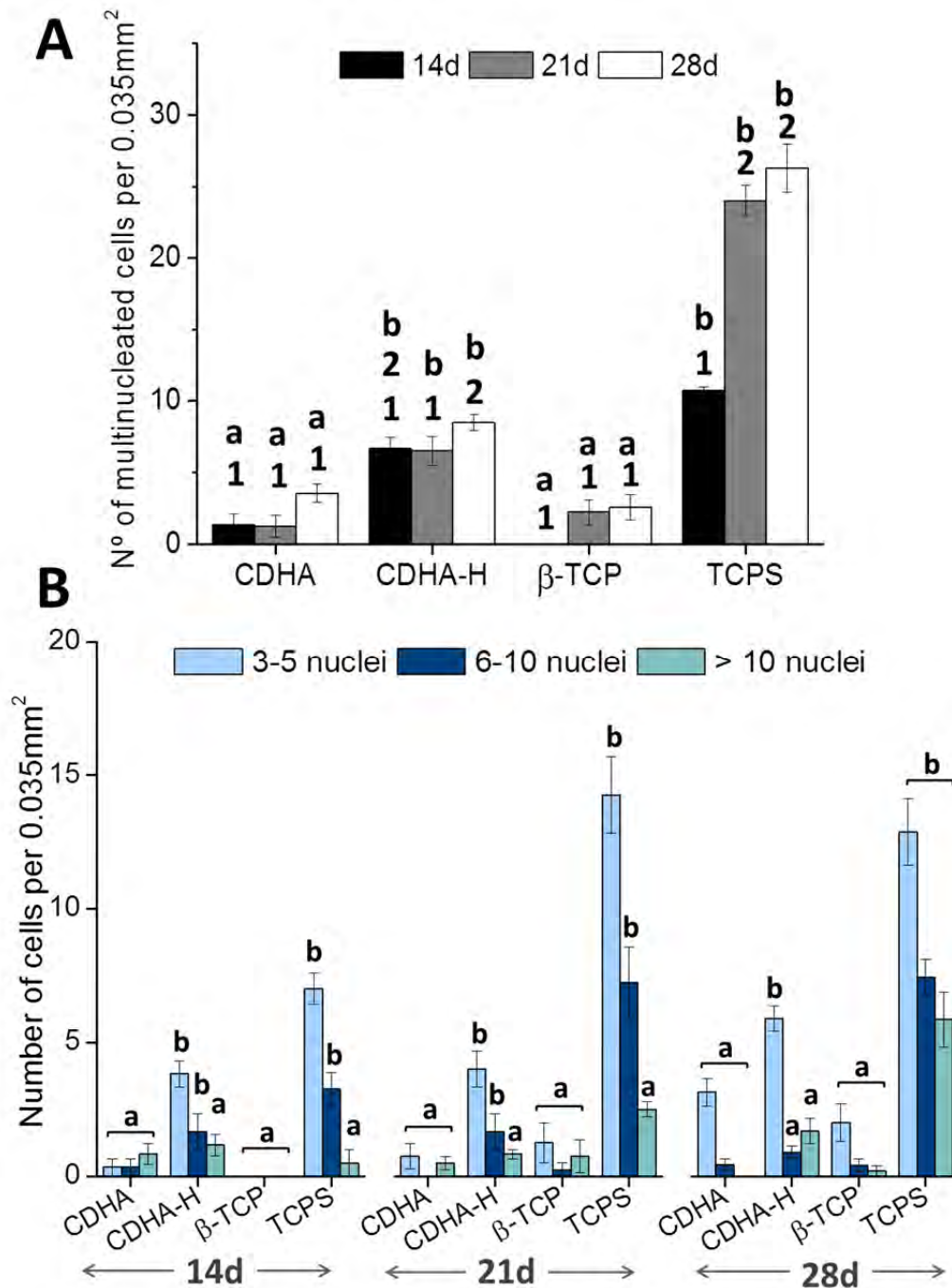
Figure 5-7. A) Number of multinucleated cells on the different substrates at different time points. Groups identify by the same superscripts are not statistically different (p>0.05). Numbers indicate differences between the time points within the same sample. Letters identify differences between different substrates at each time point. B) Distribution of multinucleated cells according to the number of nuclei at the different time points. Letters indicate differences between the number of nuclei for each type of sample. All calculations correspond to sample triplicates cultured using one single donor osteoclasts precursor cells.

5.3.4.   Osteoclast activity

The number of OC and their activity on the different substrates was investigated by TRAP5b isoform and TRAP activity respectively after 28 days of culture, and normalized by the total protein content. Figure 8A shows the total protein in the lysates at 28 days. Heparinized CDHA-H showed the highest protein content, followed by CDHA and β-TCP, TCPS showing the lowest protein content. The TRAP activity normalized by the protein content led to similar levels for the different CaP substrates (Figure 5-8B). The presence of heparin resulted in a decrease of TRAP activity, although the difference with the pristine CDHA was not statistically significant. The concentration of the TRAP5b isoform released by the cells cultured on the CaP substrates was smaller than in the control TCPS, and similar for all the materials (Figure 5-8C).
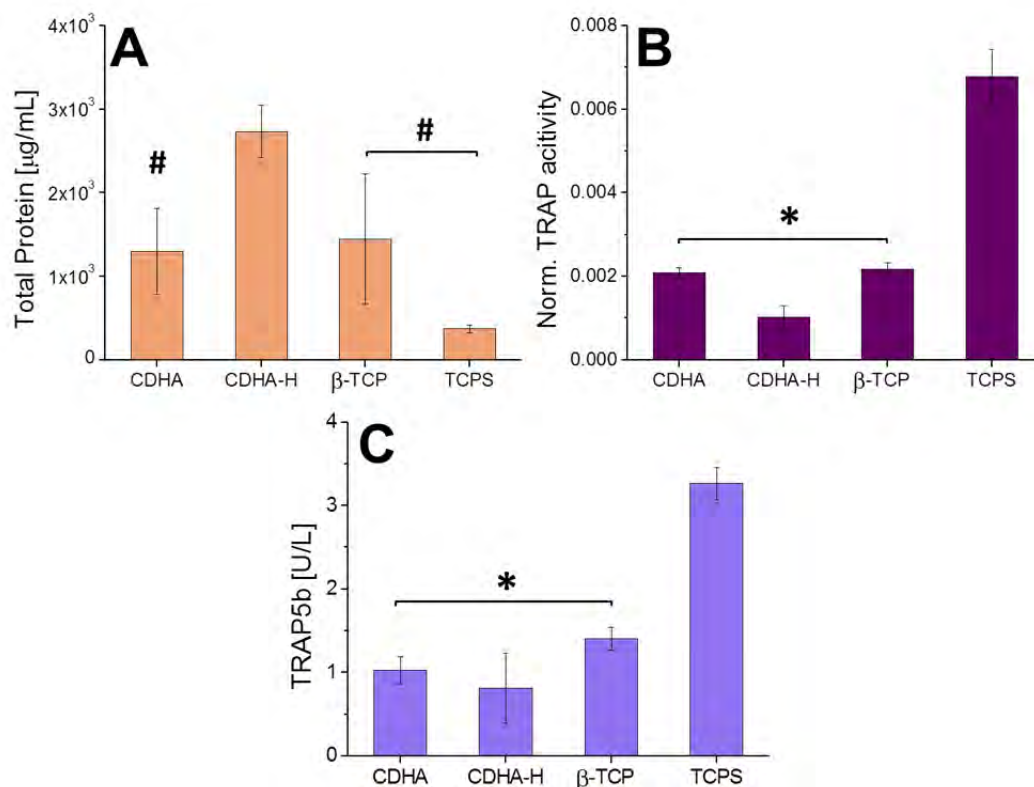
Figure 5-8. OC activity and number on substrates at 28 days in terms of TRAP activity. A: Total protein in the cell lysates measured by BCA. (#) indicates statistically significant differences compared to CDHA-H; B: TRAP activity normalized by total protein in the cell lysates (*) indicates statistically significant differences compared to control TCPS; C: TRAP5b isoform measured by ELISA (*) indicates no statistically significant differences compared to TCPS. Statistical significance of p<0.05.

Osteoclast activity can also be analyzed in terms of calcium release and pH change due to the resorptive activity of OC, although caution needs to be taken when studying CaP substrates, as dissolution-precipitation events can affect these data. For this reason, experiments were performed using substrates with and

without cells. Figure 5-9A represents the mean values of Ca^{2+} release at each time point. The highest Ca^{2+} concentration was registered when OC precursors were cultured on β-TCP. Both biomimetic substrates showed an uptake of calcium from the medium, showing similar Ca^{2+} values irrespective of heparin functionalization (Figure 5-9B). Yet, in presence of cells, the concentration of Ca^{2+} in the culture medium increased. The values for TCPS, both with and without cells, exhibited a decrease up to 28 days. In contrast, the cell culture medium showed a slight acidification in presence of cells for all substrates, which was more pronounced on the CaP substrates, especially at early time points (Figure 5-9C). Due to the presence of carbon dioxide in incubator which can be diffuse into cell culture medium, all samples showed slightly higher pH than physiological conditions. The variation of pH comparing the presence and absence of cells showed higher acidification for CDHA-H and β-TCP maintained over time (Figure 5-9D).

Figure 5-9. Evolution of the extracellular calcium concentration (A) and pH values (C) in the cell culture medium in presence (full symbols) or absence of cells (hollow symbols) from 0 to 28 days. Each time point values represent the average of three samples. The variations of calcium and pH in the culture medium with cells compared to that without cells are represented in B and D, respectively.

5.4.   Discussion

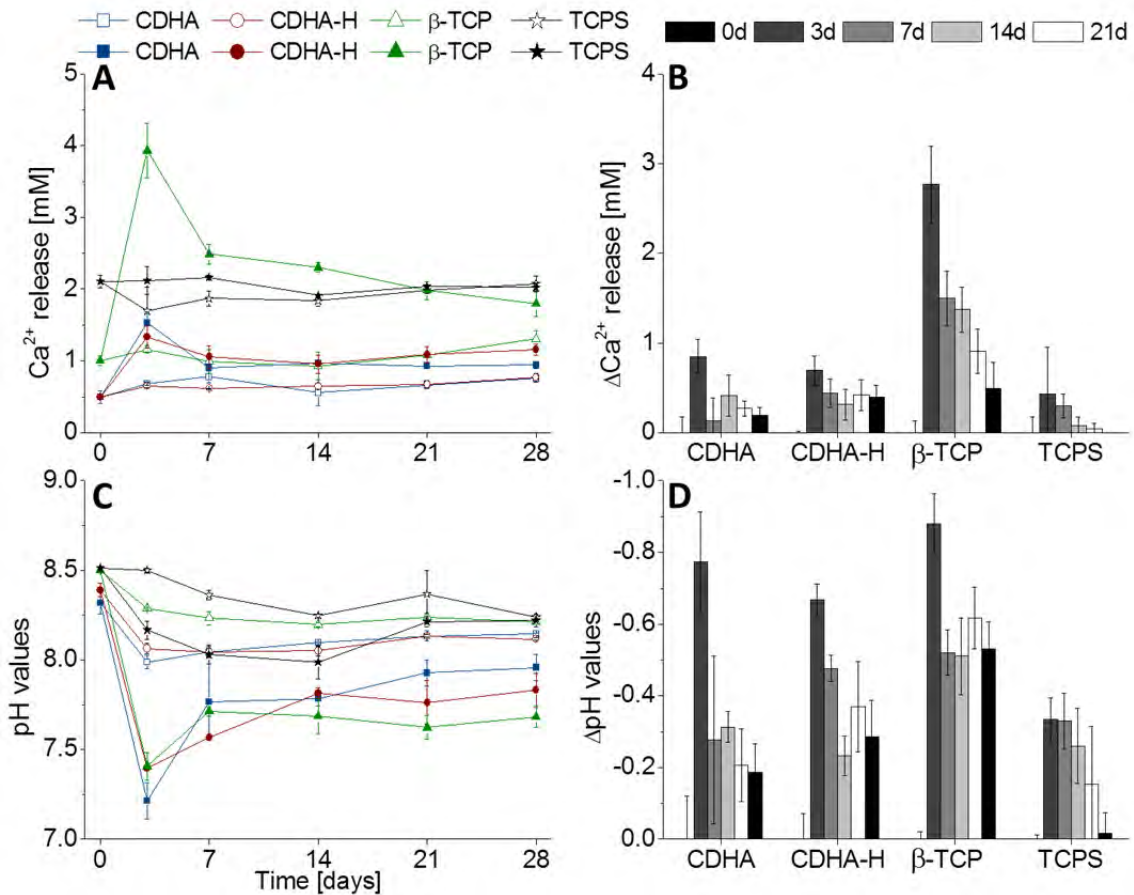The engraftment of any material in the human body is bound to cause tissue damage, thus evoking an inflammatory response. The study of human neutrophils (PMN) and monocytes, with their oxidative and hydrolytic activities, as well as of macrophage functions is crucial during injury, as a predictor of the inflammatory cascade evolution. Typical inflammation occurs by early recruitment of monocytes and neutrophils to the injured site, which will drive the host response. This in turn, will lead to either healing or chronic inflammation by sustained immune response, with over expression of inflammatory molecules and fibrous tissue encapsulation of the material.[3,4,38] Recently, it has been shown that the immune system plays a central role in tissue repair and regeneration, also when biomaterials/scaffolds are introduced.[39–41]

The initial cellular responses are firstly modulated by the ROS release activating signal transduction pathways.[6] ROS are known to be signaling molecules regulating a number of physiological functions, such as gene activation, cellular growth, and modulation of chemical reactions in the cell.[42,43] Too high concentrations of ROS can lead to cell death by apoptosis/necrosis.[44] On the contrary, low ROS levels can stimulate cell signaling to, for instance, enhance phagocytosis.[45] Moreover, it has been recently shown that, regardless of the sources of ROS, osteogenic and adipogenic differentiation of mesenchymal stromal cells (MSC) are partly ROS dependent, so establishing a pivotal role for ROS in MSC differentiation.[8]

CaP ceramics, such HA and β-TCP, are widely used as bone substitutes or prosthesis coatings because of their osteoconductive properties, and are known to evoke a consistent inflammatory cell response when tested as particles[46] or following the resorption of calcium-containing biomaterials.[47]

In this chapter, we investigated whether the functionalization of CDHA with heparin had an effect on the inflammatory response of neutrophils and monocytes. The grafting density of heparin onto high SSA CDHA yielded 10-fold higher heparin compared to smooth sintered β-TCP (Section 4.3.2 Heparin immobilization, p. 85)

PMNs functions must be appropriately regulated in order to avoid excessive or unresolved inflammation with ROS-dependent tissue and material damage. Recently, some authors have explored the immune response to GAGs. The claimed anti-inflammatory effect of some GAGs[48–53] such as heparin in reducing the PMA-induced ROS release from neutrophils was not confirmed in the present study, where, in fact, lower ROS levels were observed on pristine

CDHA than on CDHA-H. In addition, the anti-oxidant effect of human plasma, attributed to the scavenging role of proteins was not observed.[52] Although the neutrophil response was not particularly affected by the presence of plasma, monocytes presented the opposite trend, with lower percentages of ROS in the absence of plasma. Among the different CaP substrates, biomimetic CDHA and CDHA-H induced the lower ROS release under PMA activation, irrespective of the presence or not of heparin (Figure 5-2 and Figure 5-3), which confirms that no specific response was activated upon monocytes or PMN in contact with heparin. Sintered β-TCP yielded the higher oxidative stress among all CaP substrates, in agreement with previous results reported by other authors.[54]

Macrophages and osteoclasts are known to be tightly related, as in fact OC are derived from specifically stimulated macrophages. Three main molecules play pivotal roles in the OC maturation from OCP or macrophages, which are RANKL, OPG and M-CSF.[55] These molecules are secreted by stromal cells and osteoblasts, which have been pointed as necessary for osteoclast precursors maturation, as investigated by Udagawa et al.[56] RANKL and OPG are tightly linked since OPG is a decoy receptor which competes with RANK for RANKL. The balance between these two molecules usually dictates osteoclastogenesis.[57] Inhibition of osteoclastogenesis has been found to occur when OPG binds to RANK receptor; on the contrary, stromal cells and osteoblasts can secrete higher doses of RANKL to enhance bone resorption.[58] With regards to OPG-RANKL balance, some authors have pointed to GAGs to interact with OPG.[59] Irie et al. found that the addition of heparin in the culture medium of mouse bone marrow cell–osteoblast co-cultures promoted osteoclastic activity.[21] This was due to the interaction of heparin with OPG, leading to higher RANKL rates to bind to RANK receptors in osteoclasts.

One of the limiting factors of apatitic CaPs is their poor resorption rates. Hence, our hypothesis was that heparin functionalization could be used to enhance osteoclast formation and resorption onto CaP substrates by interactions in the RANKL and OPG balance. This was tested by culturing osteoclast precursor cells on the surface of a biomimetic CDHA covalently functionalized with heparin (CDHA-H), and comparing the cell response with that on pristine CDHA (CDHA).

The effect of heparin was clearly demonstrated by the TRAP-Hoechst staining (Figure 5-6). Even macrophage fusion and OC formation on CaPs was lower in number than on control TCPS, the presence of heparin (CDHA-H) highly increased the number of multinucleated cells compared to pristine CDHA (Figure 5-7A). An important aspect that has to be further investigated is whether the substrates could lead to the formation of foreign body giant cells (FBGC), which

are related to OC and are also multinucleated cells. FBGC are usually TRAP-positive, but nevertheless they possess higher number of nuclei (>10).[60] The formation of multinucleated cells with less than 10 nuclei was evident on all substrates, except for β-TCP at 14 days (Figure 5-7B). Multinucleated cells (>3 nuclei) were found on CDHA-H at 14 days (Figure 5-6D), while on the pristine substrates similar OC were found only after 21or 28 days (Figure 5-6B and C), and in smaller amounts. Sintered β-TCP and CDHA had similar number of OC formed at 28 days (Figure 5-6I and C, respectively).

Overall, the presence of heparin on CDHA-H demonstrated an enhancement in osteoclastogenesis, similar to TCPS but in lower cell number, probably due to the CDHA roughness which might hamper higher cell adhesion. Webster *et al.* found OC maturation after 10 to 13 days; conversely, they emphasized that this maturation was achieved preferably on nanostructured alumina and HA over microstructured surfaces using rat bone marrow cells.[61] However, some other authors have pointed to an opposite behavior. Costa *et al.* found that OC attach and mature preferably on smooth surfaces since rough surfaces might hamper the formation of sealing zones necessary for OC resorptive activity.[62] Likewise, Costa-Rodrigues *et al.* disclosed that an increase in the surface area, microporosity and wettability, resulted in less OC differentiation and function, compared to microsized grain topography.[63]

Recently, in a previous work, we showed that rough surfaces, such as biomimetic CDHA with different nanotopographies were permissive for OC formation after 21 days.[33] Even if no resorption pits were clearly evident, it has been reported that using focus ion beam (FIB) to transversally section cells and observing both, the cells and the underlying substrate, it was possible to detect early stages of OC activity.[64] In the present study, no clear resorption pits were observed in the SEM images of OC on the CaP substrates, irrespective of their roughness (Figure 5-4). Only on the CDHA-H substrate, regions with damaged nanostructure were found (Figure 5-5) compatible with a resorptive OC activity, as observed by Leeuwenburgh *et al.* on biomimetic coatings[65] and by Schilling *et al.* on CaP cements.[66] Both authors found similar morphological changes in the microstructure of their substrates upon contact with OC.

To assess OC number and their functionality, TRAP5b isoform and TRAP activity were investigated. No significant differences were found among CaP substrates at 28 days neither in TRAP activity (Figure 5-8B) nor in TRAP5b (Figure 5-8C). Therefore, no conclusive information can be drawn from these analyses. Since OC were already formed after 14 days for CDHA-H or 21 days for the other CaP substrates, one possible explanation could be that OC at 28 days had already exceeded the peak of TRAP5b expression. Remarkable

differences in TRAP and TRAP5b were noticed only when CaP substrates were compared to TCPS.

An indirect information on OC activity can be inferred from the extracellular calcium and pH measurements, being both parameters indicative of OC activity.[66] Osteoclastic resorption of the substrate should lead to an increase in Ca^{2+} concentration in the culture medium. However, this can be masked by the variations in calcium merely caused by cell culture medium in contact with the CaP substrates, even in absence of cells compared to TCPS. The three CaPs analyzed in this study were prone to uptake calcium from cell culture medium, although this uptake was more pronounced for biomimetic CDHA, as recently reported.[67] In presence of OC, calcium concentration increased for all substrates, which can be associated to OC activity. This increase was more marked for β-TCP (Figure 5-9B), probably due to its inherent higher solubility compared to CDHA.[68] Also for CDHA, the presence of cells led to an increase in calcium concentration in solution, which was more sustained for heparinized CDHA-H samples. Additionally, acidification, which is related to OC activity, was demonstrated for all CaP substrates in the presence of cells compared to TCPS (Figure 5-9D). β-TCP showed the highest pH variations, followed by CDHA-H, which were maintained over the time points of the experiment.

Overall, we can conclude that heparin plays an important role as osteoclastogenesis modulator due to the high number of multinucleated cells. Additionally, SEM images supported the OC activity by degraded microstructures adjacent to cells in accordance as well with calcium and pH variations. Similarly to recent literature, we hypothesize the heparin effect on OC maturation is due to the interactions in the OPG/RANKL pathway, even these conclusions cannot be extended to all bone PGs.[69]

This behavior, together with heparin participation in other stages of wound healing and tissue regeneration,[70,71] support the development of heparin-mimicking materials in tissue engineering and treatment of various diseases.[72]

5.5. Conclusions

Biomimetic CDHA substrates showed a lower inflammatory response in terms of ROS release when compared to sintered β-TCP substrates; however, no further reduction of the inflammatory reaction was observed when the surface of CDHA was functionalized with heparin. On the contrary, OC were highly stimulated by the presence of heparin. Heparin immobilized on CDHA-H induced an earlier OC precursors fusion and maturation at 14 days, similar to that found on control TCPS, whereas the number of multinucleated cells on the pristine CaPs was

significantly lower at 14 days, and remained smaller also at longer times. Even if TRAP activity and TRAP5b at 28 days did not demonstrate clear differences in the OC activity, morphological assays (SEM and TRAP-Hoechst) showed well spread and mature OC on the surfaces of CDHA-H. Material degradation was found on CDHA-H due to OC activity as depicted from microstructural changes of the typical plate-like crystals. Overall, we can conclude that heparin binding to CDHA plays a important role as osteoclastogenesis modulator due to the high number of multinucleated cells. This could have an impact in the control of the resorption of bone grafts, and could represent a useful tool to integrate the biomaterial in the bone remodeling cycle.

5.6.   Appendix. Osteogenic response to heparinized CDHA

In vitro cell studies with MSC on CDHA and heparinized CDHA were performed to further investigate the osteogenic potential of the substrates. CDHA discs were cultured in presence of rat MSC ($2.85 \cdot 10^4$cells/mL) up to 3 days. Gene expression in terms of ALP, BMP-2, COLL and osteonectin (ON) was investigated at 6h, 1 and 3 days. TCPS was included as control. After the first time point (6h), osteogenic media (om) consisting of 50µg/mL ascorbic acid, 10mM β-glycerophosphate and 100mM dexamethasone, was supplemented to all substrates, except to TCPS control.

RNA was extracted at each time and quantified by spectrophotometer (NanoDrop ND-1000,Thermo Fisher Scientific Inc., Waltham, USA). QuantiTect Reverse Transcription Kit (Qiagen GmbH, Hilden, Germany) was used for the synthesis of 150µg of complementary DNA. DNA templates were amplified using the primers shown in Table 5-1 using QuantiTect SYBR Green RT-qPCR Kit (Qiagen GmbH, Hilden, Germany) in an RT-qPCR StepOnePlus (Applied Biosystems, Thermo Fisher Scientific Inc., Waltham, USA). RT-qPCR runs for specificity of primers was determined by melt curves analyses. Data was normalized by the expression of housekeeping gene (β-actin) and relative fold changes were calculated related to TCPS control at 6h, according to the following equation:

$$E_{target}^{\Delta Cq \text{ target (TCPS 6h – sample)}} / E_{housekeeping}^{\Delta Cq \text{ housekeeping (TCPS 6 h – sample)}} \quad \text{(Eq. 1)}$$

where C_q represents the median value of the quantification cycle of the triplicate of each sample and E corresponds to the efficiency of amplification and is determined from the slope of the log-linear portion of the calibration curve, as $E=10^{(-1/slope)}$.

Table 5-1. Sequences of the primers used for quantification of gene expression (fw: forward; and rv: reverse).

Gene	Gene symbol	Primer' sequences (5' to 3')
β-actin	ACTB	fw:CCCGCGAGTACAACCTTCT rv:CGTCATCCATGGCGA ACT
Bone morphogenetic protein-2	BMP-2	fw:CCCCTATATGCTCGACCTGT rv:AAAGTTCCTCGATGGCTTCTT
Alkalinephosphatase	ALP	fw:GCACAACATCAAGGACATCG rv:TCAGTTCTGTTCTTGGGGTACAT
Collagen	COLL	fw:GCAGCTGACTTCAGGGATGT rv:CATGTTCAGCTTTGTGGACCT
Osteonectin	ON	fw:GTTTGAAGAAGGTGCAGAGGA rv:GGTTCTGGCAGGGGTTTT

The presence of heparin on CDHA (CDHA-H) demonstrated to increase the ALP, COLL and ON at earlier time points (6h) compared to pristine CDHA and TCPS, maintaining their expression after 1d and finally decreasing at 3d (Figure 5-10). Surprisingly, BMP-2 was not enhanced on CDHA-H, since pristine CDHA registered higher expression levels. However, whilst BMP-2 expression for CDHA and TCPS followed a peak expression with a subsequent decay, in CDHA-H, the expression of BMP-2 was maintained throughout the experimental time. Overall, these results provide some preliminary data that suggest the presence of heparin surfaces on CDHA may produce a stimulatory osteogenic effect, but this require further study.
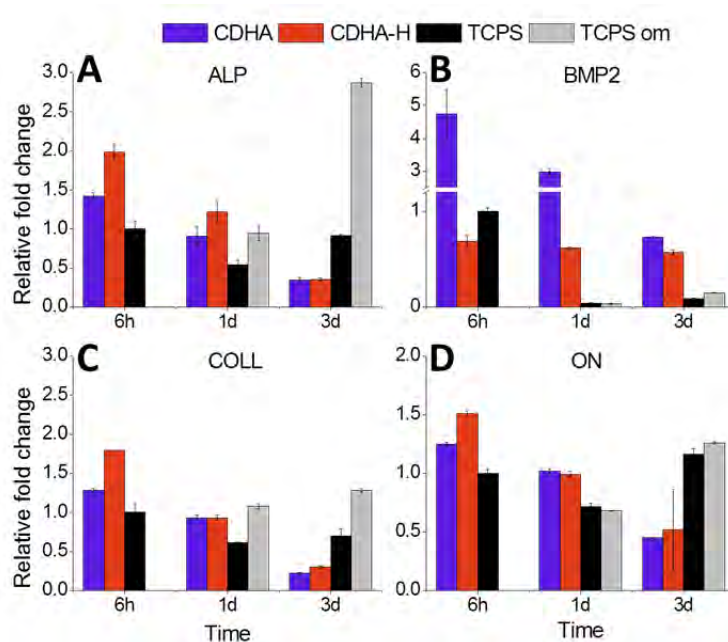

Figure 5-10. Gene expression of CDHA and heparinized CDHA-H, together with controls TCPS and osteogenic medium-stimulated TCPS, cultured with rMSC for 3 days.

5.7. References

[1]   J.R. Arron, Y. Choi, Osteoimmunology: Bone versus immune system, Nature. **408** (2000) 535–536.

[2]   S. Franz, S. Rammelt, D. Scharnweber, J.C. Simon, Immune responses to implants – A review of the implications for the design of immunomodulatory biomaterials, Biomaterials. **32** (2011) 6692–6709.

[3]   J.M. Anderson, A. Rodriguez, D.T. Chang, Foreign body reaction to biomaterials., Semin. Immunol. **20** (2008) 86–100.

[4]   J.M. Anderson, Biological responses to biomaterials, Annu. Rev. Mater. Res. **31** (2001) 81–110.

[5]   S.A. Eming, M. Hammerschmidt, T. Krieg, A. Roers, Interrelation of immunity and tissue repair or regeneration, Semin. Cell Dev. Biol. **20** (2009) 517–527.

[6]   H. Jay Forman, M. Torres, Redox signaling in macrophages, Mol. Aspects Med. **22** (2001) 189–216.

[7]   Y. Zhang, S. Choksi, K. Chen, Y. Pobezinskaya, I. Linnoila, Z.-G. Liu, ROS play a critical role in the differentiation of alternatively activated macrophages and the occurrence of tumor-associated macrophages, Cell Res. **23** (2013) 898–914.

[8]   F. Atashi, A. Modarressi, M.S. Pepper, The Role of Reactive Oxygen Species in Mesenchymal Stem Cell Adipogenic and Osteogenic Differentiation: A Review, Stem Cells Dev. **24** (2015) 1150–1163.

[9]   F. Loi, L.A. Córdova, J. Pajarinen, T. Lin, Z. Yao, S.B. Goodman, Inflammation, fracture and bone repair, Bone. **86** (2016) 119–130.

[10]   I.C. Severin, A. Soares, J. Hantson, M. Teixeira, D. Sachs, D. Valognes, A. Scheer, M.K. Schwarz, T.N.C. Wells, A.E.I. Proudfoot, J. Shaw, Glycosaminoglycan analogs as a novel anti-inflammatory strategy., Front. Immunol. **3** (2012) 293. d

[11]   M. Gschwandtner, E. Strutzmann, M.M. Teixeira, H.J. Anders, M. Diedrichs-Möhring, T. Gerlza, G. Wildner, R.C. Russo, T. Adage, A.J. Kungl, Glycosaminoglycans are important mediators of neutrophilic inflammation in vivo, Cytokine. **91** (2017) 65–73.

[12]   A.D. Theocharis, S.S. Skandalis, C. Gialeli, N.K. Karamanos, Extracellular matrix structure, Adv. Drug Deliv. Rev. **97** (2016) 4–27.

[13]   I. Capila, R.J. Linhardt, Heparin-protein interactions., Angew. Chem. Int. Ed. Engl. **41** (2002) 391–412.

[14]   R. Ruppert, E. Hoffmann, W. Sebald, Human Bone Morphogenetic Protein 2 Contains a Heparin-Binding Site which Modifies Its Biological Activity, Eur. J. Biochem. **237** (1996) 295–302.

[15]   T. Takada, T. Katagiri, M. Ifuku, N. Morimura, M. Kobayashi, K. Hasegawa, A. Ogamo, R. Kamijo, Sulfated polysaccharides enhance the biological activities of bone morphogenetic proteins., J. Biol. Chem. **278** (2003) 43229–35.

[16]   S. Teixeira, L. Yang, P.J. Dijkstra, M.P. Ferraz, F.J. Monteiro, Heparinized hydroxyapatite/collagen three-dimensional scaffolds for tissue engineering., J. Mater. Sci. Mater. Med. **21** (2010) 2385–92.

[17]   D.S. Bramono, S. Murali, B. Rai, L. Ling, W.T. Poh, Z.X. Lim, G.S. Stein, V. Nurcombe, A.J. van Wijnen, S.M. Cool, Bone marrow-derived heparan sulfate potentiates the osteogenic activity of bone morphogenetic protein-2 (BMP-2)., Bone. **50** (2012) 954–64.

[18]   U. Hempel, C. Preissler, S. Vogel, S. Möller, V. Hintze, J. Becher, M. Schnabelrauch, M. Rauner, L.C. Hofbauer, P. Dieter, Artificial extracellular matrices with oversulfated glycosaminoglycan derivatives promote the differentiation of osteoblast-precursor cells and premature osteoblasts., Biomed Res. Int. **2014** (2014) 938368.

[19]   U. Hempel, V. Hintze, S. Möller, M. Schnabelrauch, D. Scharnweber, P. Dieter, Artificial extracellular matrices composed of collagen I and sulfated hyaluronan with adsorbed transforming growth factor β1 promote collagen synthesis of human mesenchymal stromal cells., Acta Biomater. **8** (2012) 659–66.

[20]   V. Hintze, S. Moeller, M. Schnabelrauch, S. Bierbaum, M. Viola, H. Worch, D. Scharnweber, Modifications of hyaluronan influence the interaction with human bone morphogenetic protein-4 (hBMP-4)., Biomacromolecules. **10** (2009) 3290–7.

[21]   A. Irie, M. Takami, H. Kubo, N. Sekino-Suzuki, K. Kasahara, Y. Sanai, Heparin enhances osteoclastic bone resorption by inhibiting osteoprotegerin activity., Bone. **41** (2007) 165–74.

[22]   J. Salbach, S. Kliemt, M. Rauner, T.D. Rachner, C. Goettsch, S. Kalkhof, M. von Bergen, S. Möller, M. Schnabelrauch, V. Hintze, D. Scharnweber, L.C. Hofbauer, The effect of the degree of sulfation of glycosaminoglycans on osteoclast function and signaling pathways., Biomaterials. **33** (2012) 8418–29.

[23]   J. Salbach-Hirsch, Sulfated glycosaminoglycans support osteoblast functions and concurrently suppress osteoclasts., J. Cell. Biochem. **115** (2014) 1101–11.

[24]   A. Lode, A. Reinstorf, A. Bernhardt, C. Wolf-Brandstetter, U. König, M. Gelinsky, Heparin modification of calcium phosphate bone cements for VEGF functionalization., J. Biomed. Mater. Res. A. **86** (2008) 749–59.

[25]   U. König, A. Lode, P.B. Welzel, Y. Ueda, S. Knaack, A. Henß, A. Hauswald, M. Gelinsky, Heparinization of a biomimetic bone matrix: integration of heparin during matrix synthesis versus adsorptive post surface modification., J. Mater. Sci. Mater. Med. 25 (2014) 607–21.

[26]   H.K. Väänänen, H. Zhao, M. Mulari, J.M. Halleen, The cell biology of osteoclast function., J. Cell Sci. **113** (Pt 3 (2000) 377–81.

[27]   L. Ling, S. Murali, G.S. Stein, A.J. van Wijnen, S.M. Cool, Glycosaminoglycans modulate RANKL-induced osteoclastogenesis., J. Cell. Biochem. **109** (2010) 1222–31.

[28]   M. Espanol, R.A. Perez, E.B. Montufar, C. Marichal, A. Sacco, M.P. Ginebra, Intrinsic porosity of calcium phosphate cements and its significance for drug delivery and tissue engineering applications, Acta Biomater. **5** (2009) 2752–2762.

[29]   R.L. Williams, Development of multifunctional calcium phosphate particles for drug delivery and formation of cross-linked materials, University of Birmingham, 2014.

[30]   M.S. Ahola, E.S. Säilynoja, M.H. Raitavuo, M.M. Vaahtio, J.I. Salonen, A.U.O. Yli-Urpo, In vitro release of heparin from silica xerogels, Biomaterials. **22** (2001) 2163–2170.

[31]   S. Pujari-Palmer, M. Pujari-Palmer, M. Karlsson Ott, Reduced oxidative stress in primary human cells by antioxidant released from nanoporous alumina, J. Biomed. Mater. Res. Part B Appl. Biomater. **104** (2016) 568–575.

[32]   G. Mestres, M. Espanol, W. Xia, C. Persson, M.P. Ginebra, M.K. Ott, Inflammatory response to nano- And microstructured hydroxyapatite, PLoS One. **10** (2015) 1–20.

[33]   G. Ciapetti, G. Di Pompo, S. Avnet, D. Martini, A. Diez-Escudero, E.B. Montufar, M.-P. Ginebra, N. Baldini, Osteoclast differentiation from human blood precursors on biomimetic calcium-phosphate substrates, Acta Biomater. **50** (2017) 102–113.

[34]   D. Granchi, I. Amato, L. Battistelli, G. Ciapetti, S. Pagani, S. Avnet, N. Baldini, A. Giunti, Molecular basis of osteoclastogenesis induced by osteoblasts exposed to wear particles, Biomaterials. **26**(2005) 2371–2379.

[35]   S. Avnet, R. Pallotta, F. Perut, N. Baldini, M.G. Pittis, A. Saponari, E. Lucarelli, B. Dozza, T. Greggi, N.M. Maraldi, C. Capanni, E. Mattioli, M. Columbaro, G. Lattanzi, Osteoblasts from a mandibuloacral dysplasia patient induce human blood precursors to differentiate into active osteoclasts, Biochim. Biophys. Acta - Mol. Basis Dis. **1812** (2011) 711–718.

[36]   S. Schaefer, R. Detsch, F. Uhl, U. Deisinger, G. Ziegler, How Degradation of Calcium Phosphate Bone Substitute Materials is influenced by Phase Composition and Porosity, Adv. Eng. Mater. **13** (2011) 342–350.

[37]   S. Gallinetti, C. Canal, M.P. Ginebra, Development and characterization of biphasic hydroxyapatite/beta-TCP cements, J. Am. Ceram. Soc. **97** (2014) 1065–1073.

[38]   C.J. Ferrante, S.J. Leibovich, Regulation of Macrophage Polarization and Wound Healing., Adv. Wound Care. **1** (2012) 10–16.

[39]   Z. Julier, A.J. Park, P.S. Briquez, M.M. Martino, Promoting tissue regeneration by modulating the immune system, Acta Biomater. **53** (2017) 13–28..

[40]   Z. Chen, T. Klein, R.Z. Murray, R. Crawford, J. Chang, C. Wu, Y. Xiao, Osteoimmunomodulation for the development of advanced bone biomaterials, Mater. Today. **19** (2016) 304–321.

[41]   Z. Chen, C. Wu, W. Gu, T. Klein, R. Crawford, Y. Xiao, Osteogenic differentiation of bone marrow MSCs by β-tricalcium phosphate stimulating macrophages via BMP2 signalling pathway, Biomaterials. **35** (2014) 1507–1518.

[42]   S. Di Meo, T.T. Reed, P. Venditti, V.M. Victor, Role of ROS and RNS Sources in Physiological and Pathological Conditions, Oxid. Med. Cell. Longev. **2016** (2016) 1–44.

[43]   G.S. Selders, A.E. Fetz, M.Z. Radic, G.L. Bowlin, An overview of the role of neutrophils in innate immunity, inflammation and host-biomaterial integration, Regen. Biomater. **4** (2017) 55–68.

[44]   F.R. Livingston, E.M.K. Lui, G.A. Loeb, H.J. Forman, Sublethal oxidant stress induces a reversible increase in intracellular calcium dependent on NAD(P)H oxidation in rat alveolar macrophages, Arch. Biochem. Biophys. **299** (1992) 83–91.

[45]   I.A. Gamaley, K. Ksenia M., I. V. Klyubin, Activation of murine macrophages by hydrogen peroxide, Cell. Signal. **6** (1994) 949–957.

[46]   F. Velard, J. Braux, J. Amedee, P. Laquerriere, Inflammatory cell response to calcium phosphate biomaterial particles: an overview., Acta Biomater. **9** (2013) 4956–63.

[47]   F.C. Edwards, A. Taheri, S.C. Dann, J.F. Dye, Characterization of cytolytic neutrophil activation in vitro by amorphous hydrated calcium phosphate as a model of biomaterial inflammation, J. Biomed. Mater. Res. Part A. **96A** (2011) 552–565.

[48]   R. Lever, A. Smailbegovic, C. Page, Role of glycosaminoglycans in inflammation, Inflammopharmacology. **9** (2001) 165–169.

[49]   K.R. Taylor, R.L. Gallo, Glycosaminoglycans and their proteoglycans: host-associated molecular patterns for initiation and modulation of inflammation, FASEB J. **20** (2006) 9–22.

[50]   G. Zhou, M.S. Niepel, S. Saretia, T. Groth, Reducing the inflammatory responses of biomaterials by surface modification with glycosaminoglycan multilayers, J. Biomed. Mater. Res. Part A.**104** (2016) 493-502.

[51]   G.M. Campo, A. Avenoso, S. Campo, A. D 'ascola, P. Traina, D. Samà, A. Calatroni, Glycosaminoglycans Modulate Inflammation and Apoptosis in LPS-Treated Chondrocytes, J. Cell. Biochem. **106** (2009) 83–92.

[52]   S. Das, J.S. Maras, M.S. Hussain, S. Sharma, P. David, S. Sukriti, S.M. Shasthry, R. Maiwall, N. Trehanpati, T.P. Singh, S.K. Sarin, Hyperoxidized albumin modulates neutrophils to induce oxidative stress and inflammation in severe alcoholic hepatitis, Hepatology. **65** (2017) 631–646.

[53]   S.R.S. Ting, J.M. Whitelock, R. Tomic, C. Gunawan, W.Y. Teoh, R. Amal, M.S. Lord, Cellular uptake and activity of heparin functionalised cerium oxide nanoparticles in monocytes, Biomaterials. **34** (2013) 4377–4386.

[54]   M. Yamada, H. Minamikawa, T. Ueno, K. Sakurai, T. Ogawa, N-acetyl cysteine improves affinity of beta-tricalcium phosphate granules for cultured osteoblast-like cells, J. Biomater. Appl. **27** (2012) 27–36.

[55]   S.L. Teitelbaum, Bone Resorption by Osteoclasts, Science (80-.). 289 (2000).

[56]   N. Udagawa, N. Takahashi, T. Akatsu, H. Tanaka, T. Sasaki, T. Nishiharat, T. Kogat, T.J. Martins, T. Suda, Origin of osteoclasts: Mature monocytes and macrophages are capable of differentiating into osteoclasts under a suitable microenvironment prepared by bone marrow-derived stromal cells, Cell Biol. **87** (1990) 7260–7264.

[57]   D.. Lacey, E. Timms, H.-L. Tan, M.. Kelley, C.. Dunstan, T. Burgess, R. Elliott, A. Colombero, G. Elliott, S. Scully, H. Hsu, J. Sullivan, N. Hawkins, E. Davy, C. Capparelli, A. Eli, Y.-X. Qian, S. Kaufman, I. Sarosi, V. Shalhoub, G. Senaldi, J. Guo, J. Delaney, W.. Boyle, Osteoprotegerin Ligand Is a Cytokine that Regulates Osteoclast Differentiation and Activation, Cell. **93** (1998) 165–176.

[58]   S.-K. Lee, J.A. Lorenzo, Parathyroid Hormone Stimulates TRANCE and Inhibits Osteoprotegerin Messenger Ribonucleic Acid Expression in Murine Bone Marrow Cultures: Correlation with Osteoclast-Like Cell Formation 1, Endocrinology. **140** (1999) 3552–3561.

[59]   F. Lamoureux, M. Baud'huin, L. Duplomb, D. Heymann, F. Rédini, Proteoglycans: key partners in bone cell biology, BioEssays. **29** (2007) 758–771.

[60]   B. ten Harkel, T. Schoenmaker, D.I. Picavet, N.L. Davison, T.J. de Vries, V. Everts, The Foreign Body Giant Cell Cannot Resorb Bone, But Dissolves Hydroxyapatite Like Osteoclasts., PLoS One. **10** (2015) e0139564.

[61]   T.J. Webster, C. Ergun, R.H. Doremus, R.W. Siegel, R. Bizios, Enhanced osteoclast-like cell functions on nanophase ceramics, Biomaterials. **22** (2001) 1327–1333.

[62]   D. Geblinger, B. Geiger, L. Addadi, Surface-Induced Regulation of Podosome Organization and Dynamics in Cultured Osteoclasts, ChemBioChem. **10** (2009) 158–165.

[63]   J. Costa-Rodrigues, S. Carmo, I.P. Perpétuo, F.J. Monteiro, M.H. Fernandes, Osteoclastogenic differentiation of human precursor cells over micro- and nanostructured hydroxyapatite topography., Biochim. Biophys. Acta. **1860** (2016) 825–835.

[64]   A. Diez-Escudero, M. Espanol, E.B. Montufar, G. Di Pompo, G. Ciapetti, N. Baldini, M.-P. Ginebra, Focus Ion Beam/Scanning Electron Microscopy Characterization of Osteoclastic Resorption of Calcium Phosphate Substrates, Tissue Eng. Part C Methods. **23** (2017) 118–124.

[65]   S. Leeuwenburgh, P. Layrolle, F. Barrère, J. de Bruijn, J. Schoonman, C.A. van Blitterswijk, K. de Groot, Osteoclastic resorption of biomimetic calcium phosphate coatings in vitro., J. Biomed. Mater. Res. **56** (2001) 208–15.

[66]   A.F. Schilling, W. Linhart, S. Filke, M. Gebauer, T. Schinke, J.M. Rueger, M. Amling, Resorbability of bone substitute biomaterials by human osteoclasts, Biomaterials. **25** (2004) 3963–3972.

[67]   J.M. Sadowska, J. Guillem-Marti, E.B. Montufar, M. Espanol, M.-P. Ginebra, Biomimetic versus Sintered Calcium Phosphates: The in vitro Behavior of Osteoblasts and Mesenchymal Stem Cells, Tissue Eng. Part A. (**2017**),(Epub ahead of print).

[68]   S. V Dorozhkin, Bioceramics of calcium orthophosphates., Biomaterials. **31** (2010) 1465–85.

[69]   F. Lamoureux, M. Baud'huin, L. Duplomb, D. Heymann, F. Rédini, Proteoglycans: key partners in bone cell biology, BioEssays. **29** (2007) 758–771. doi:10.1002/bies.20612.

[70]   P. Olczyk, Ł. Mencner, K. Komosinska-Vassev, K. Komosinska-Vassev, Diverse Roles of Heparan Sulfate and Heparin in Wound Repair, Biomed Res. Int. **2015** (2015) 1–7.

[71]   L. Ling, E.T. Camilleri, T. Helledie, R.M. Samsonraj, D.M. Titmarsh, R.J. Chua, O. Dreesen, C. Dombrowski, D.A. Rider, M. Galindo, I. Lee, W. Hong, J.H. Hui, V. Nurcombe, A.J. van Wijnen, S.M. Cool, Effect of heparin on the biological properties and molecular signature of human mesenchymal stem cells, Gene. **576** (2016) 292–303.

[72]   S.J. Paluck, T.H. Nguyen, H.D. Maynard, Heparin-Mimicking Polymers: Synthesis and Biological Applications, Biomacromolecules. **17** (2016) 3417–3440.

Chapter 6

Focus Ion Beam-Scanning Electron Microscopy Characterization of Osteoclastic Resorption of Calcium Phosphate Substrates

Scope

Osteoclastic activity is of paramount relevance to evaluate the capacity of bone grafts to be implemented in the bone remodeling process. Bone regeneration requires implants that are placed temporarily and slowly resorbed integrating them in the regenerative process. The active resorption by osteoclasts is crucial to allow new bone formation while implant is degraded. The study of OC activity in rough materials is often tricky due to the inherent irregularities in materials surface. The present chapter is devoted to the study of OC activity by focus ion beam (FIB). This novel technique allows cross-sectioning OC to investigate the cell underlying structure. CaP substrates, having similar compositions but different microstructures, have been cultured in presence of OC and their activity in terms of resorption pits formation and degradation of the subjacent microstructure have been investigated by FIB-SEM.
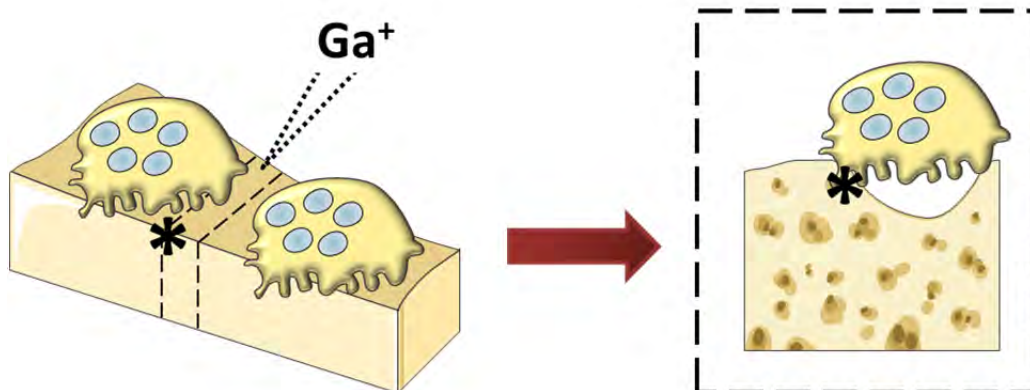
6.1.   Introduction

In recent years, Focus Ion Beam (FIB) systems have gained interest as a technique for the evaluation of biological samples. Although microscopic evaluation of biological matter is challenging, FIB equipped with scanning electron microscopy (SEM) or energy dispersive X-ray spectroscopy (EDX/EDS) provides an enhanced working environment for studying biomaterials. [1]

The regenerative potential of bone substitute materials is usually evaluated *in vitro* by assessing how cultures of relevant cells interact with them. Briefly, at the early stages of implantation, inflammation occurs and a cascade of chemical signals which drive the monocyte/macrophage phenotype are triggered.[2] In an ideal scenario, these cells will fuse to form osteoclasts (OC), that is, bone resorbing cells.[3,4] Recent research indicates that osteoclasts can establish a cross-talk with osteoblasts leading to subsequent bone remodeling.[5]

Several pre-clinical studies of bone substitutes have focused on these early interactive stages and, particularly, on the biomaterial-osteoclasts interactions in terms of OC adhesion, gene expression and evaluation of resorption pits.[6-8] Usually, these investigations require, on the one hand, the study of OC differentiation and activity, such as gene expression or marker identification, and on the other hand, the evaluation of morphological changes in the substrates, which implies staining or removal of cells in order to visualize the underlying structure. In this context, FIB-SEM technique offers the possibility of evaluating both cells and subjacent microstructural changes simultaneously. Various studies have used FIB for biological sample evaluation,[9-15] and the interest in the field has been increasing over recent years. Nevertheless, studies on osteoclast resorption on substrates of challenging topography are lacking. Thus, this chapter aims to assess the potential of FIB-SEM technique as a tool to evaluate cell morphology together with the microstructural changes caused by OC-mediated degradation beneath the cells. Three substrates with similar composition and different nano-microstructures are investigated to disclose to what extent FIB-SEM analysis may allow assessing the resorption activity of the cells on substrates with different topographies.

6.2.   Materials and Methods

Three types of calcium phosphate substrates were prepared. Low temperature biomimetic CDHA was obtained through the hydrolysis of α-TCP (α-$Ca_3(PO_4)_2$) powders at 37°C. Powders with two different particle sizes, coarse (C: 5.2 µm median size) and fine (F: 2.8 µm median size), were mixed with a 2.5wt% solution of sodium hydrogen phosphate (Na_2HPO_4, Merck) at a liquid to powder ratio of 0.35mL/g, to produce materials with microstructure consisting of an entangled network of plate-like

(CDHA-C) and needle-like (CDHA-F) CDHA crystals (both with a Ca/P ratio of 1.5) respectively.[16] High temperature stoichiometric sintered HA (sin-HA) was obtained by solid state reaction of a mixture of calcium hydrogen phosphate ($CaHPO_4$, Sigma–Aldrich C7263) and calcium carbonate ($CaCO_3$, Sigma–Aldrich C4830) with a calcium to phosphorous ratio of 1.67 at 1100°C for 11h. All materials were produced into discs of 14mm diameter and 0.25mm thickness.

Cell cultures were performed using human peripheral blood mononuclear cells (PBMC), from healthy 30-35 year old male voluntary blood donors. Donations were anonymous, so institutional review board (IRB) approval was not required. Mononuclear cells were isolated by centrifugation with Ficoll-Histopaque (Sigma-Aldrich) and seeded at a density of $6 \cdot 10^6$ cells/cm^2 on calcium phosphate discs. PBMC were differentiated into osteoclast precursors with RANKL-containing cell culture medium (DMEM) from human osteoblast supernatants. Cells were seeded on two discs for each substrate. The experiment was repeated twice using cells from two independent donors. OC precursors were cultured for 21 days. Afterwards, the cells were rinsed with PBS (Gibco, UK), fixed with paraformaldehyde/glutaraldehyde in 0.1M sodium cacodylate buffer, and post-fixed in 2% osmium tetroxide (OsO_4) at room temperature for 2 hours in order to achieve higher contrast. Then, samples were dehydrated in an ethanol series followed by hexamethyldisilazane (HMDS) drying to preserve osteoclasts morphology.[17,18] A thin gold-palladium film was sputtered before FIB-SEM examination to impart conductivity to samples.

SEM in combination with FIB (Zeiss Neon 40) was used to examine both the surface of cells/materials and the microstructural features underneath the cells. As a first step conventional SEM was used to evaluate both the microstructure of the substrates and the morphology of the cells. Two representative cells were then selected for FIB cross-sectioning using gallium ions (Ga+). Prior to cutting, a thin layer of protective platinum (Pt) was deposited on the surface by ion-beam assisted deposition in order to reduce the curtaining effect. This effect can result in image artefacts due to changes in the sputtering yield, as the beam passes over different composition regions, resulting in the appearance of parallel patterns in the ablated zones. The deposition of Pt helps obtaining smoother cross-sections, thus minimizing the curtaining effect.[13] Afterwards, a rough (coarse) milling was performed with a maximum current of 10nA to quickly remove most of the material up to a depth of approximately 20 µm nearby the region of interest. Finally, a polished cross-section was attained by subsequently reducing the Ga^+ beam current from 2nA down to 500pA when approaching the Pt layer. This procedure reduces the ion beam damage on the sample and any re-deposition effect, and allows the observation of smoother cross-sections of the cell and the underlying microstructure with minimal modifications.

6.3.   Results and Discussion

Sintered and biomimetic calcium phosphates have long been used in bone regeneration applications.[19,20] Despite biomimetic CaP substrates can better mimic the microstructure and composition of the mineral phase of bone than sintered CaP, *in vitro* assays on biomimetic materials are often more challenging.[21,22] The rough microstructure that results from the precipitation of nano/submicron crystals compared to the smoother textures of the high-temperature processed materials can have great impact on cell behavior. When challenged with osteoclasts the role of surface topography is particularly relevant, as osteoclastic resorption is dependent on the formation of an actin-rich sealing zone that precedes degradation.[23,24] *In vitro* studies had shown that too rough textures can hinder the formation of a proper sealing zone, impairing material degradation.[6,25]

The possibility offered by FIB, to closely look at the cell-substrate interface can help shedding new light on the evaluation of resorption events on challenging biomimetic substrates compared to traditional sintered substrates. But FIB is a complex technique that requires accurate setting of the processing parameters to minimize the generation of artifacts during sectioning. Only artifact-free sections will allow drawing accurate conclusions. FIB tomographic studies have successfully been performed to analyze at different depths the delicate nature of biomimetic CaP consisting of an interlocked network of thin plate-like crystals, proving that artifact-free sections can be obtained.[26]The situation is more complex, however, when FIB is used to section cells cultured on these substrates. Drobne *et al.,* as well as other authors*,* extensively described the potential of FIB milling to process biological samples and shed light on the optimal processing parameters in order to avoid shrinkage, melting effect, Ga^+ implantation or side-wall artifacts.[18, 27-30] These effects can be effectively reduced by a first Pt layer deposition which protects the sample surface against re-deposition of ablated atoms, provides mechanical stability and reduces curtain effects. In addition, damage can be minimized by working with low ion beam currents and low acceleration voltages, especially during the final steps of the cross-section polishing.[29] All these strategies have been applied in the present study to investigate a series of three apatitic substrates consisting of two biomimetic formulations and a sintered material.

Figure 1 shows the SEM images of the three different substrates in the absence (Figure 6-1A, C and E) and in the presence (Figure 6-1B, D, F, and G) of cells after 21 days of culture. Biomimetic substrates obtained at 37°C, i.e. CDHA-C and CDHA-F, consisted of an entangled network of plate-like crystals (Figure 6-1A) and needle-like crystals (Figure 6-1C), respectively, whereas sin-HA presented a smoother polyhedral grain surfaces (Figure 6-1E) typical of high temperature ceramics.
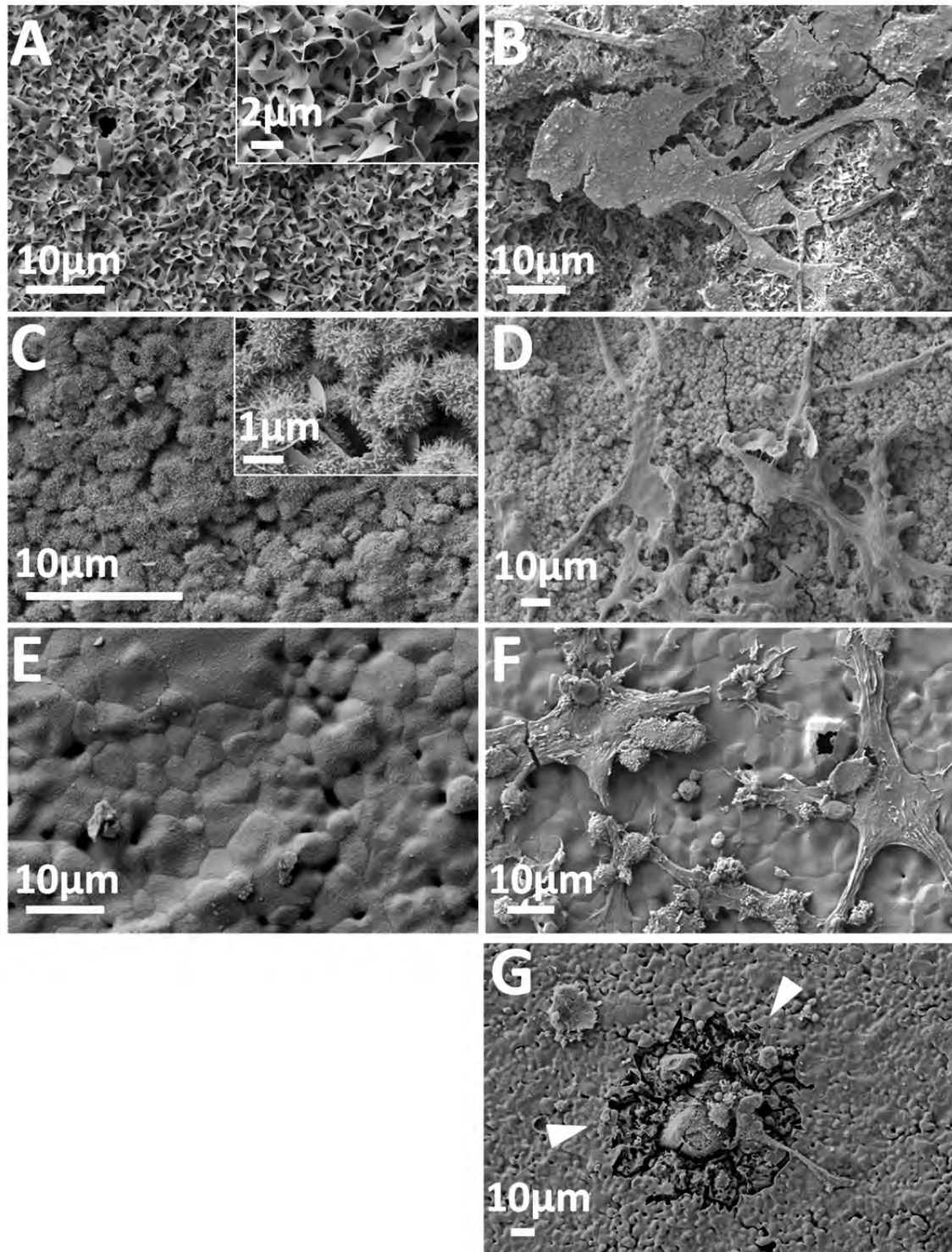
Figure 6-1. SEM images of the surface of pristine CaP substrates (A, C and E) and cells on the substrates (B, D, F and G): CDHA-C (A, B); CDHA-F (C, D) and sin-HA (E, F, G).White arrows indicate a resorption pit.

SEM evaluation of the seeded substrates showed similar cell morphologies consisting of flat and well spread cells ranging 20-30μm with various connecting filopodia (Figure 6-1B, D, and F). As illustrated in Figure 6-1G, resorption pits were easily visualized on some substrates (white arrows), namely sintered HA, where typical 30-

135

50µm sized resorption lacunae were observed. In contrast, no clear resorption pits were evident on the rough and tortuous surfaces of biomimetic CDHA samples. In this case, FIB cuts could provide useful information to assess if any potential osteoclastic degradation is taking place locally, at the surface underneath the cell.

The sequence to obtain the vertical section of a cell and the underlying substrate by FIB is shown in Figure 6-2, for biomimetic CDHA-F. No signs of resorption were observed in this case in the material under the cell (Figure 6-2D and d), as the needle-like crystals appeared intact, when compared with the microstructure of the pristine material (Figure 6-1C, insert). One possible explanation is that the high roughness of the substrate prevented the OC from sealing the substrate, thus hampering the degradation process, as described in previous works.[6,25] One aspect worth noticing is the fact that the microstructure of the pristine material was revealed intact beneath the cell, thus confirming that there was no damage associated to FIB-sectioning.
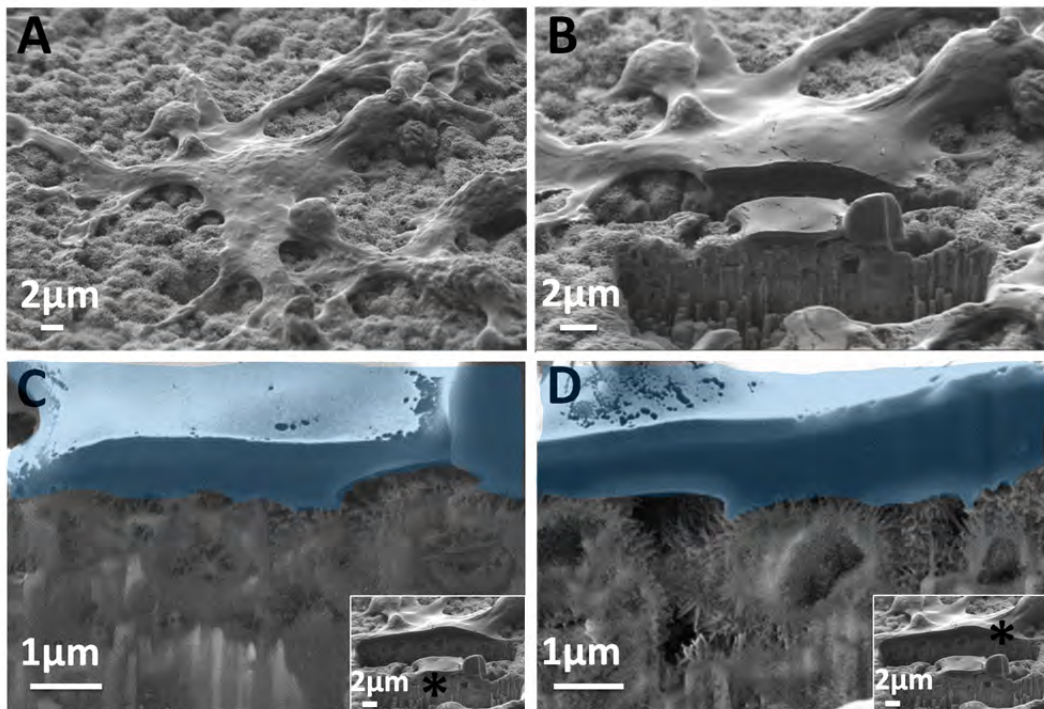

Figure 6-2. Sequence to obtain vertical sections of a cell (blue colored) on the CDHA-F substrate (A-B). No signs of degradation are visible in the material underlying the cell, where the needle-like crystal morphology can be clearly observed (C and D; the asterisk in the insert indicates the region that has been magnified in the image; cell has been colored in blue).

Interestingly, when on the same substrate a different cell of bigger size and with a more spread morphology, compatible with an osteoclastic or macrophage phenotype was analyzed, FIB/SEM images revealed that resorption was taking place in the underlying material (Figure 6-3). Thus, acid etching was evident in the subjacent microstructure where the needle-like crystals were no longer visible (Figure 6-3B* and C). Few needle-like crystals were only visible in the outer part of the cell (Figure

6-3D). The presence of both, resorptive and non-resorptive cells could evidence the multiple and reversible macrophage phenotype.[31]
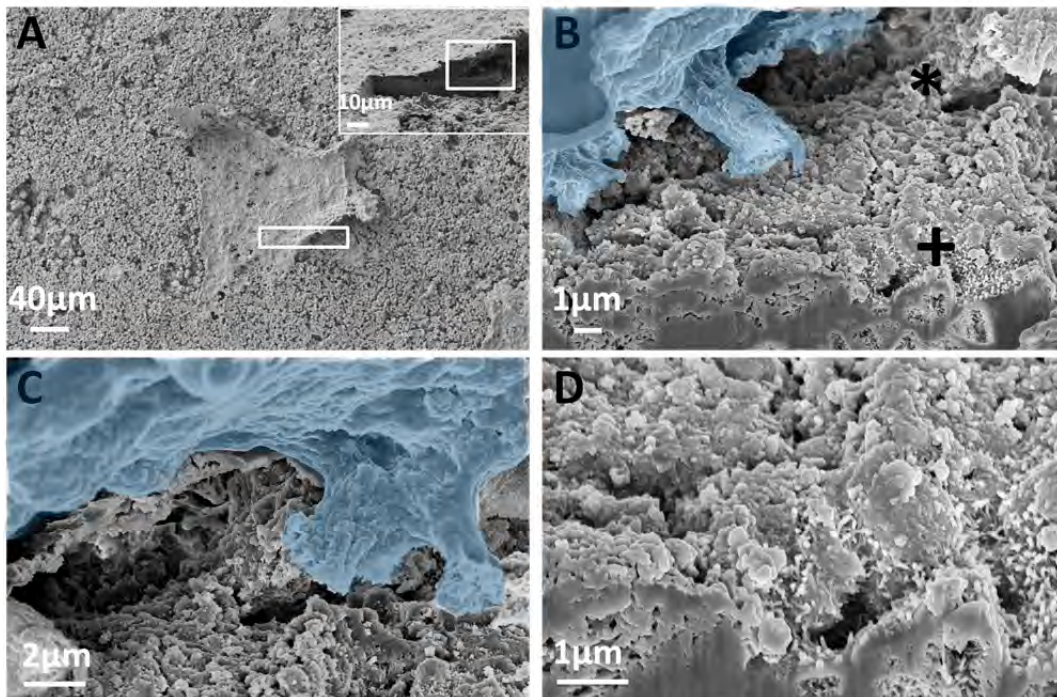

Figure 6-3. FIB-SEM images of a well spread cell (blue colored) on CDHA-F substrate with the insert showing the FIB cut performed (A). Higher magnification of the cell section and the subjacent area (B). A region with degraded crystals, marked with * in B is shown at a higher magnification (C), whereas non-degraded crystals in the periphery of the cell, marked with + in B are shown at a higher magnification (D).

FIB-SEM images for the CDHA-C substrate are shown in Figure 6-4. As for CDHA-F, no resorption pits were found on the surface, and no signs of degradation even underneath the cells were detected by FIB cuts (Figure 6-4C and D), as revealed by the presence of the original plate-like crystals in the areas subjacent to the cell (*). As observed by traditional SEM imaging, numerous resorption pits and several flat and spread cells were observed on the sin-HA substrate (Figure 1F and G). Previous works have shown the resorptive capacity of osteoclast-like cells derived from mice bone marrow on similar substrates.[32,33] However, the study of osteoclast activity using primary human cells is less common, despite providing a closer understanding of the physiology of human bone resorption. FIB-SEM images of a cell on sin-HA are shown in Figure 6-5. Figure 6-5A shows a few cavities on the substrate at low magnification, corresponding to osteoclastic resorption pits (white arrows) clearly different from the intrinsic porosity of the material (+). Intergranular dissolution of the ceramic was displayed just under the cell (Figure 6-5C), with excavated cavities penetrating several micrometers into the substrate. This preferential dissolution in the grain boundaries is a frequently observed phenomenon, due to the higher reactivity of these regions that have a high free energy. Moreover, the surface of the polyhedral grains under the cells

137

presented a rougher aspect compared to the smoother appearance of the pristine ceramic, consistent with an acidic etching process (Figure 6-5C and D).
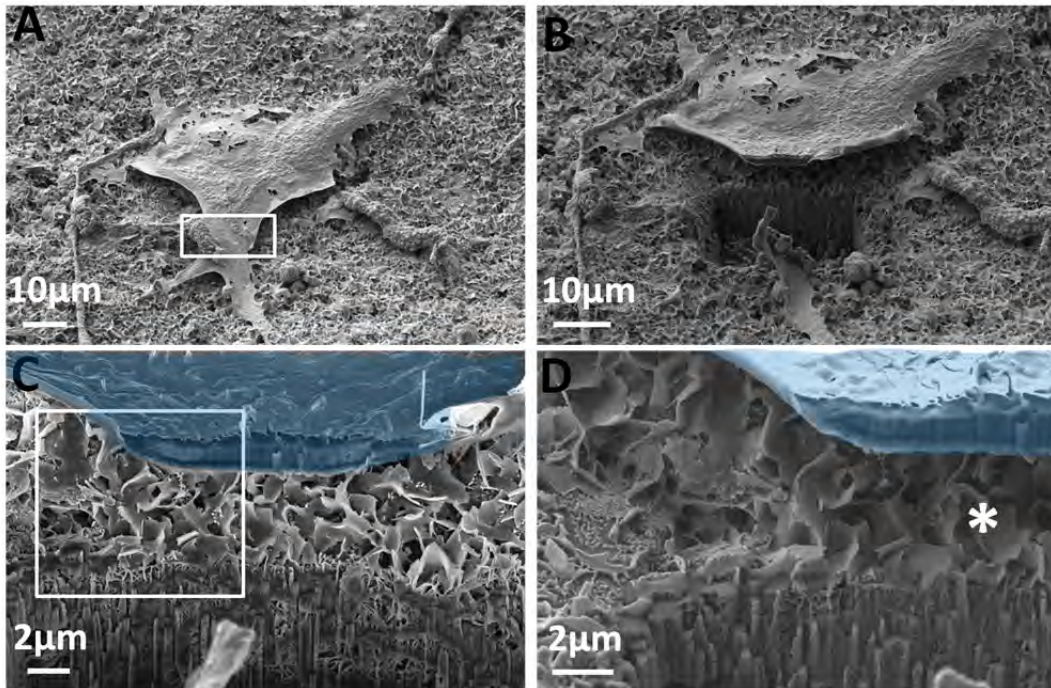
Figure 6-4. FIB-SEM images of a cell (blue colored) on CDHA-C. The FIB section (B-D) show that the pristine microstructure, consisting of plate-like crystals, was not degraded under the cell (C and D, marked with *).

Figure 6-5. SEM image showing various resorption pits (arrows) and intrinsic pores marked with + on sin-HA (A). FIB sections at higher magnification are shown (B-D), illustrating the underlying microstructure. Rougher grains are visible in (C) and (D) compared to the smooth original grains visible in (B), marked with *.

6.4.   Conclusions

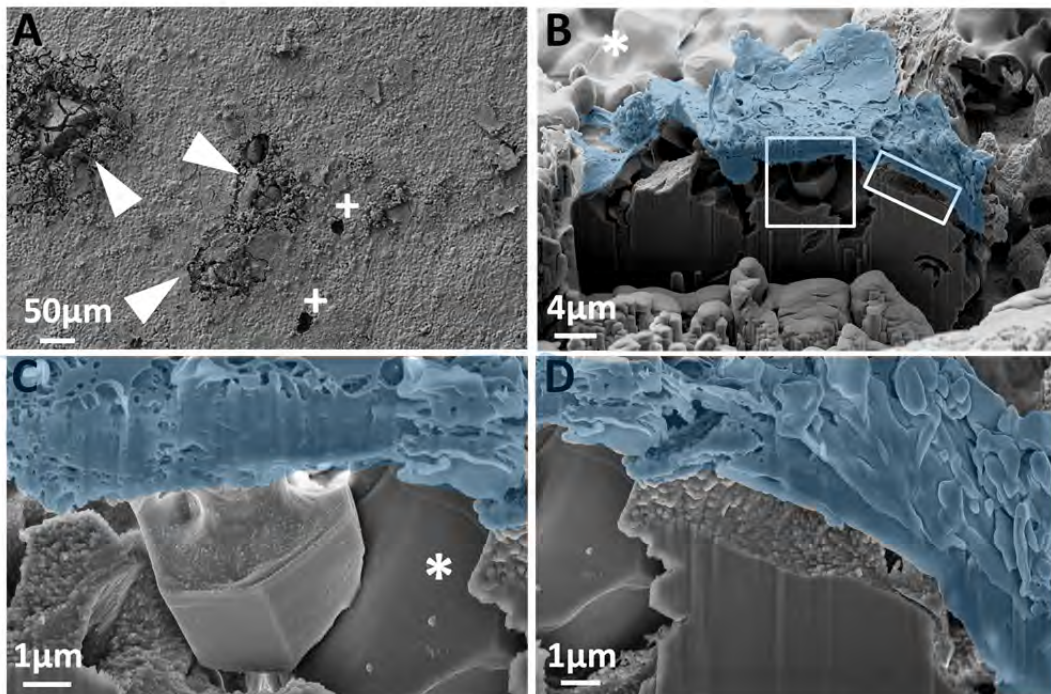The FIB-SEM technique has been shown to be a useful technique to assess the *in vitro* cell resorption activity, even at early stages of the process. The present study on different calcium phosphate substrates proved the potential of this technique to evaluate both the cell morphology and the microstructure of the substrate underneath. Indeed, this technique may disclose the initial activity of resorbing cells when not evident yet using other analytical methods, or may confirm and support morphological and biochemical evidences of osteoclast degradation capability *in vitro*. Sintered HA surfaces showed visible resorption pits and FIB cuts across the cell demonstrated the initial degradation of the ceramic as a consequence of acid etching promoted by the cells, which resulted in intergranular dissolution and roughening of the grain surface. In contrast, in low temperature biomimetic HA substrates, where no clear signs of degradation on the surface were visible by standard SEM imaging, possibly due to the higher roughness of these materials, different situations were found by FIB cuts. For some cells, no signs of degradation of the underlying material were observed, probably due to the lack of a sealing actin ring and a resorbing lacuna formation. However, at different sites where large flattened cells and more spread cells were observed, signs of degradation were clearly seen in the material underneath the cells, with the etching of the needle-like crystals. These findings underline the potential of the FIB-SEM technique to evaluate cell-mediated resorption in rough, irregular or coarse substrates. Indeed, FIB milling of resorbing cells allows exploring their underlying structure to unravel early degradation processes at stages when resorption pits have not yet occurred or are virtually impossible to detect.

6.5. References

[1]   Grandfield, K., and Engqvist, H. Focused Ion Beam in the Study of Biomaterials and Biological Matter. Adv Mater SciEng **2012**, 2012.

[2]   Mestres, G., Espanol, M., Xia, W., Persson, C., Ginebra, M.P., and Ott, M.K. Inflammatory response to nano- and microstructured hydroxyapatite. PLoS One **10** (3), e0120381, 2015.

[3]   Davison, N.L., ten Harkel, B., Schoenmaker, T., Luo, X., Yuan, H., Everts, V, Barrère-de Groot, F., de Bruijn, J. D. Osteoclast resorption of beta-tricalcium phosphate controlled by surface architecture. Biomaterials **35**, 7441, 2014.

[4]   Gordon, S., and Taylor, P.R. Monocyte and macrophage heterogeneity. Nat Rev Immunol., **5**, 953, 2005.

[5]   Sims, N.A., and Martin, T.J. Coupling signals between the osteoclast and osteoblast: How are messages transmitted between these temporary visitors to the bone surface? Front Endocrinol**6**, 41, 2015.

[6]   Costa, D.O., Prowse, P.D.H., Chrones, T., Sims, S.M., Hamilton, D.W., Rizkalla, A.S., et al. The differential regulation of osteoblast and osteoclast activity by surface topography of hydroxyapatite coatings.Biomaterials **34**, 7215, 2013.

[7]   Miyazaki, T., Miyauchi, S., Anada, T., Imaizumi, H., and Suzuki, O. Evaluation of osteoclastic resorption activity using calcium phosphate coating combined with labeled polyanion. Anal Biochem**410**, 7, 2011.

[8]   Morimoto, Y., Hoshino, H., Sakurai, T., Terakawa, S., and Nagano, A. Quantitative evaluation of bone resorption activity of osteoclast-like cells by measuring calcium phosphate resorbing area using incubator-facilitated and video-enhanced microscopy. Microsc Res Tech **72**, 317, 2009.

[9]   Narayan, K., Danielson, C.M., Lagarec, K., Lowekamp, B.C., Coffman, P., Laquerre, A., et al. Multi-resolution correlative focused ion beam scanning electron microscopy: Applications to cell biology. J StructBiol. **185**, 278, 2014.

[10]   Liu, B., Yu, H.H., Ng, T.W., Paterson, D.L., Velkov, T., Li, J., Fu, J. Nanoscale Focused Ion Beam Tomography of Single Bacterial Cells for Assessment of Antibiotic Effects. MicroscMicroanal **20**, 537, 2014.

[11]   Martinez, E., Engel, E., Lopez-Iglesias, C., Mills, C.A., Planell, J.A., and Samitier, J. Focused ion beam/scanning electron microscopy characterization of cell behavior on polymer micro-/nanopatterned substrates: A study of cell-substrate interactions. Micron **39**, 111, 2008.

[12]   Kim, D.-J., Kim, G.-S., Hyung, J.-H., Lee, W.-Y., Hong, C.-H., and Lee, S.-K. Direct observation of CD4 T cell morphologies and their cross-sectional traction force derivation on quartz nanopillar substrates using focused ion beam technique. Nanoscale Res Lett **8**, 332, 2013.

[13]   Friedmann, A., Hoess, A., Cismak, A., and Heilmann, A. Investigation of cell-substrate interactions by focused ion beam preparation and scanning electron microscopy. ActaBiomater.**7**, 2499, 2011.

[14]   Xia, Z., Grover, L. M., Huang, Y., Adamopoulos, I. E., Gbureck, U., Triffitt, J. T., Barralet, J. E. In vitro biodegradation of three brushite calcium phosphate cements by a macrophage cell-line. Biomaterials, **27**, 4557, 2006.

[15]   Drobne, D., Milani, M., Zrimec, A., Leser, V., BerdenZrimec M. Electron and ion imaging of gland cells using the FIB/SEM system. Journal of Microscopy **219**, 29, 2005.

[16]   Ginebra, M.P., Driessens, F.C.M., and Planell, J.A. Effect of the particle size on the micro and nanostructural features of a calcium phosphate cement: A kinetic analysis. Biomaterials **25**, 3453, 2004.

[17]   Ciapetti, G., Granchi, D., Devescovi, V., Baglio, S.R., Leonardi, E., Martini, D., et al. Enhancing osteoconduction of PLLA-based nanocomposite scaffolds for bone regeneration using different biomimetic signals to MSCs. Int J MolSci **13**, 2439, 2012.

[18]   Lešer, V., Drobne, D., Pipan, Z., Milani, M., Tatti, F. Comparison of different preparation methods of biological samples for FIB milling and SEM investigation. Journal of Microscopy **233**, 309, 2009.

[19]   Bohner, M. Calcium orthophosphates in medicine: from ceramics to calcium phosphate cements. Injury **31** Suppl 4, 37, 2000.

[20]   LeGeros, R.Z. Calcium phosphate-based osteoinductive materials. Chem Rev **108**, 4742, 2008.

[21]   Engel, E., Del Valle, S., Aparicio, C., Altankov, G., Asin, L., Planell, J.A, Ginebra, M. P. Discerning the role of topography and ion exchange in cell response of bioactive tissue engineering scaffolds. Tissue Eng Part A**14**(8), 1341, 2008.

[22]   Gustavsson, J., Ginebra, M.P., Planell, J., Engel, E. Osteoblast-like cellular response to dynamic changes in the ionic extracellular environment produced by calcium-deficient hydroxyapatite. J Mater Sci Mater Med**23**(10), 2509, 2012.

[23]   Teitelbaum, S. L. Bone Resorption by Osteoclasts. Science **289**, 1504, 2000.

[24]   Anderegg, F., Geblinger, D., Horvath, P., Charnley, M., Textor, M., et al. () Substrate adhesion regulates sealing zone architecture and dynamics in cultured osteoclasts. PLoS ONE **6**, e28583, 2011.

[25]   Costa-Rodrigues, J., Carmo, S., Perpetuo, I., Monteiro, F., Fernandes, M..Osteoclastogenic differentiation of human precursor cells over micro- and nano-structured hydroxyapatite topography. BiochimBiophysActa - Gen Subj**1860**, 825,2016.

[26]   Gallinetti, S., Canal, C., Ginebra, M.P. Development and Characterization of Biphasic Hydroxyapatite/β-TCP Cements. Journal of the American Ceramic Society, **97** (4), 1065, 2014.

[27]   Drobne, D., Milani, M., Lešer, V., Tatti, F. Surface damage induced by FIB milling and imaging of biological samples is controllable. Microscopy Research and Technique **70**, 895, 2013.

[28]   Drobne, D.3D Imaging of cells and tissues by Focused Ion Beam/ Scanning Electron Microscopy (FIB/SEM). Nanoimaging(Totowa NJ: Humana Press), 275-292, 2013.

[29]   Frey, L., Lehrer, C., Ryssel, H. Nanoscale effects in focused ion beam proocessing. Applied Physics A: Materials Science and Processing **76**, 1017, 2003.

[30]   Kizilyaprak, C., Bittermann, A. G., Daraspe, J., Humbel, B. M. FIB-SEM tomography in biology. Methods in Molecular Biology **1117**, 541, 2014.

[31]   Sridharan, R., Cameron, A.R., Kelly, D.J., Kearney, C.J., O'Brien, F.J. Biomaterial based modulation of macrophage polarization: a review and suggested design principles. Materials Today **18**, 313, 2015.

[32]   Gomi, K., Lowenberg, B., Shapiro, G., & Davies, J. E. Resorption of sintered synthetic hydroxyapatite by osteoclasts in vitro. Biomaterials **14**, 91, 1993.

[33]   Leeuwenburgh, S., Layrolle, P., Barrère, F., de Bruijn, J., Schoonman, J., van Blitterswijk, C. A., & de Groot, K. Osteoclastic resorption of biomimetic calcium phosphate coatingsinvitro.Journal of Biomedical Materials Research **56**, 208, 2001.

Chapter 7
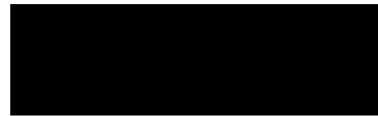
GENERAL CONCLUSIONS

This thesis was devoted to gaining insight into some strategies that can be implemented to enhance the performance of calcium phosphate bone grafts, focusing specifically on tuning some intrinsic physicochemical properties and on the surface functionalization with heparin. The effect on *in vitro* degradation and the response of relevant cell types was addressed, reaching the following conclusions:

Chapter 2. *In vitro* degradation of calcium phosphates: effect of multiscale porosity, textural properties and composition

- Microstructure, composition, specific surface area and porosity of CaPs modulated the materials' degradation in acidic medium to different extents. Biomimetic CDHA with high SSA and low crystallinity presented the highest degradation rates, exceeding even the more soluble β-TCP.

- The effect of SSA on degradation was dependent on the porosity and pore size, which conditioned the extent of acid penetration within the sample.

- The combination of SSA and porosity (nano-, micro-, and macro) resulted in an exponential increase in degradation for high SSA substrates, but to a linear increase in sintered materials with low SSA.

- Textural properties were shown to be crucial to modulate the degradation behavior, even outweighing the effect of other features such as the solubility of the compounds.

Chapter 3. Carbonation of low temperature macroporous calcium phosphates

- Carbonation of biomimetic CDHA foams can be achieved through different methods, either performing the setting reaction of α-TCP in a carbonate-containing solution in biomimetic conditions or applying an hydrothermal treatment. Alternatively, the hydrothermal treatment in presence of carbonate solution can also be applied in pre-set CDHA foams.

- The biomimetic setting in presence of carbonate solution prolonged the hydrolysis reaction of α-TCP and allowed high levels of mainly B-type carbonate substitution (12.3%wt.)

- Hydrothermal carbonation during the setting reaction of the foams was accomplished in 30min and it also resulted in high levels of carbonate incorporation (13%wt.). The product was however a mixture of CaPs (BCP).

- Hydrothermal carbonation after setting of the foam did not alter the material composition but was the least efficient, allowing a very limited incorporation of carbonate of 2.5%wt.

- The macrostructure of the foams was preserved in all carbonation methods but the nanostructure and SSA varied due to the different crystal morphologies formed during synthesis.

Chapter 4. Heparinization of beta-tricalcium phosphate: immunoregulatory effects and osteogenic potential

- Two different methods were successfully used for the incorporation of heparin onto CaP. Physisorption and chemisorption yielded different heparin grafting densities. Chemisorption performed through two step functionalization improved considerably the amount of heparin grafted. Especially, heparin density on β-TCP surface increased when longer silanization times were used, providing a higher degree of amines on surface to consequent attachment of heparin through carboxylates. Additionally, heparin immobilization did not alter the intrinsic textural properties of the substrate.

- Heparinized β-TCP demonstrated to down-regulate ROS release and pro-inflammatory cytokine release compared to pristine β-TCP. β-TCP-H yielded 10% lower ROS than β-TCP, together with the down-regulation of TNF-α and IL-1β.

- The pro-healing effect of heparin β-TCP was assessed also through the macrophage phenotype. Macrophage morphology was prone to evolve towards

elongated shapes in contact with heparinized surfaces which is consistent with a pro-healing macrophage phenotype.

- The osteogenic potential of heparinized β-TCP was demonstrated by its interaction with rat MSC. β-TCP-H promoted rat MSC proliferation and additionally, enhanced the differentiation towards osteogenic lineage at earlier times than pristine β-TCP and the TCPS control.

## Chapter 5. Effect of heparinization on the inflammatory response and osteoclastogenesis of biomimetic CDHA

- The amount of heparin immobilized on the surface was significantly increased on high specific surface area substrates such as biomimetic CDHA compared to sintered β-TCP substrates (Chapter 4). The amount of grafted heparin increased 10-fold on CDHA-H compared to β-TCP-H. As shown in the previous chapter 4, the heparinization preserved the nanostructural features of the substrates were preserved after heparinization.

- The anti-inflammatory effect on heparinized CDHA was similar to pristine CDHA. However, ROS levels showed a substantial reduction compared to β-TCP. CDHA-H showed a down-regulation of 70% of ROS compared to control TCPS.

- Biomimetic CDHA substrates supported adhesion and proliferation of OC precursors. Interestingly, heparinized CDHA clearly promoted OC fusion at earlier time-points than pristine CDHA, demonstrating an enhancement of osteoclastogenesis.

- Even if TRAP activity did not show clear differences amongst substrates, degraded zones due to OC activity were clearly observed by SEM on heparinized CDHA.

- The osteogenic potential of CDHA-H was assessed in a pilot study using rat MSC cultures through gene expression analysis. Higher expression of

147

osteogenic markers such as COLL, ALP and ON was found on CDHA-H at earlier times than CDHA and TCPS.

Chapter 6. Focus Ion Beam-Scanning Electron Microscopy Characterization of Osteoclastic Resorption of Calcium Phosphate Substrates

- The evaluation of resorption by FIB-SEM imaging allowed the observation of early resorptive stages which are usually overlooked by other techniques.

- Smooth surfaces such as those of sintered HA enhanced the resorption by OC, which was associated to the greater ease in creation of a sealing ring typical from these cells.

- The nanostructure demonstrated to influence as well OC resorption. Needle-like crystals were more effectively resorbed than plate-like crystals probably due to the high roughness of plates which hampered OC sealing zone creation.

Chapter 8
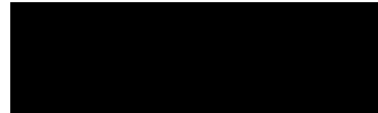
FUTURE PERSPECTIVES

The results obtained in the present thesis represent a promising platform for the field of tissue engineering and regenerative medicine. The novel platform to immobilize organic motifs onto CaPs offers a broad range of unknown interactions which need further characterization, and are likely to be enlightening. Understanding the interactions of this platform with different tissue involved in bone remodeling could be interesting to shed further light on the biological interactions occurring at bone-biomaterials interface.

The *in vivo* osteogenic properties of the macroporous biomimetic CDHA, and biphasic CaP materials developed in this thesis have been investigated to understand their inherent capacity to induce new bone formation in an animal study (*in vivo*) in collaboration with the Veterinary Faculty at Universitat Autònoma de Barcelona, Spain. The first results analyses have shown that nanostructured macroporous materials boosted the osteoinductive potential of these substrates.

Regarding the development of macroporous scaffold, the implementation of heparin functionalization on such scaffold could be a great benefit for bone grafting. Macroporous foams have shown to improve substantially the degradation; hence further fostering with heparin immobilization can enhance their biological response.

Stability measurements of heparin grafted are necessary to understand the potential of this functionalization. Heparin stability in solution has been previously studied due to their use as anticoagulant. Heparin can be stored in isotonic conditions over 24h, however, no stability studies upon grafting were performed. It could be interesting to know the extent of heparin activity over time.

Additionally, heparin effects could be measured by its interactions with specific proteins. The binding affinity of heparin and different proteins involved in bone remodeling process could explain the mechanisms of heparin activity.

According to the anti-inflammatory effects of heparin, more experiments should be performed in order to understand the modulatory effects of heparin. In the present work, three cytokines were analyzed, combining pro-inflammatory and anti-inflammatory ones. However, other important cytokines play crucial roles during inflammation and could be interesting to know the extent of modulation over a wider range of cytokines.

The osteogenic potential of GAGs has been investigated by several authors. Nevertheless, studies have focused on the mere interactions of GAGs and not of them in combination with CaP substrates. Further characterization by PCR is required to

understand the process by which mesenchymal cells are differentiated into osteoblasts by heparin.

Interestingly, the interactions of heparin with different cell lineages might be beneficial to gain knowledge on the complex interactions of different cells. For instance, heparin has shown to have a great influence on endothelial cells which allow extravasation of blood cells to injured site by signals mediated by GAGs. The biological evaluation of heparin modified CaPs using endothelial cells can help understanding the effects during angiogenesis. *In vitro* testing culturing endothelial cells on heparinized substrates could help to compose a larger picture of what is the biological response of such substrates.

Annex

Publications and conferences
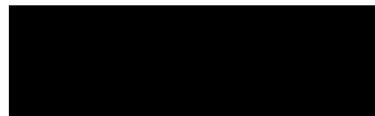
Publications

A.Diez-Escudero, M. Espanol, X. Lu, C. Persson, M.-P. Ginebra, *Heparinization of beta-tricalcium phosphate: osteoimmunoregulatory effect*, Adv. Healthcare Mat.,(under revision, July 2017).

A. Diez-Escudero, M. Espanol, S. Beats, M.-P. Ginebra, *In vitro degradation of calcium phosphates: Effect of multiscale porosity, textural properties and composition*, Acta Biomater. 60, 81–92 (2017)

A. Diez-Escudero, M. Espanol, E.B. Montufar, G. Di Pompo, G. Ciapetti, N. Baldini, and M.-P. Ginebra, *Focus Ion Beam/Scanning Electron Microscopy Characterization of Osteoclastic Resorption of Calcium Phosphate Substrates*, Tissue Eng. Part C Methods, 23, 118–124 (2017).

G. Ciapetti, G. Di Pompo, S. Avnet, D. Martini, A. Diez-Escudero, E.B. Montufar, M.-P. Ginebra, and N. Baldini, *Osteoclast differentiation from human blood precursors on biomimetic calcium-phosphate substrates,* Acta Biomater., 50 102–113 (2017).

Z. Zhao, M. Espanol, J. Guillem-Marti, D. Kempf, A. Diez-Escudero, and M.-P. Ginebra, *Ion-doping as a strategy to modulate hydroxyapatite nanoparticle internalization,* Nanoscale, 8, 1595–1607 (2016).

- **Under preparation:**

A. Diez-Escudero, M. Espanol, G. Di Pompo, E. Torreggiani, G. Ciapetti, N. Baldini and M.-P. Ginebra, *Heparinization of biomimetic CDHA enhances osteoclastogenesis.*

A. Diez-Escudero, M. Espanol, and M.-P. Ginebra, *Carbonation of macroporous biomimetic CDHA.*

Conference participation

A. Diez-Escudero, M. Espanol, G. Di Pompo, E. Torreggiani, G. Ciapetti, N. Baldini, MP. Ginebra. *Heparinised calcium phosphates enhance osteoclastic differentiation.* European Orthopedics Research Society-EORS, Bologna (Italy), September 2016. **Oral communication**

G. Di Pompo, **A. Diez-Escudero**, EB. Montufar, M. Espanol, G. Ciapetti, N. Baldini, MP. Ginebra. *Microstructural effects of bioceramics on osteoclast differentiation and activity.* European Orthopedics Research Society-EORS, Bologna (Italy), September 2016. **Oral communication**

A. Diez-Escudero, M. Espanol, X. Lu, C. Persson, MP. Ginebra. *Osteoinductive potential of heparinised calcium phosphates and their inflammatory response.* TERMIS-EU, Uppsala (Sweden), June-July 2016. **Poster**

A. Barba, K. Rappe, P. Fontecha, A. Diez-Escudero, Y. Maazouz, M. Espanol, C. Öhman, C. Persson, M.C. Manzanares, J. Franch, M.P. Ginebra. Biomimetic nanostructured calcium phosphate scaffolds: osteoinduction and osteogenesis. 2016 eCM XVII: Stem cells, Bone Fixation, Repair & Regeneration, Davos (Switzerland), June 2016. **Oral communication**

A. Barba, K. Rappe, P. Fontecha, A. Diez-Escudero, Y. Maazouz, E. Montufar, M. Espanol, M.C. Manzanares, J. Franch, M.P. Ginebra. *Intrinsic osteoinduction of biomimetic nanostructured calcium phosphate scaffolds.* 10th World Biomaterials Congress, Montreal (Canada), May 2016. **Oral communication**

A. Diez-Escudero, EB. Montufar, G. Di Pompo, M. Espanol, G. Ciapetti, N. Baldini, MP. Ginebra. *Evaluation of the osteoclastic resorption on ceramic substrates by Focus Ion Beam.* XXXVIII Conferencia de la Sociedad Ibérica de Biomecánica y Biomateriales, Barcelona (Spain), November 2015. **Oral communication**

A. Diez-Escudero, M. Espanol, MP. Ginebra. *Heparinisation of calcium phosphates: towards enhancing biological performance.* BioboneSymposium, Santiago de Compostela (Spain), October 2015. **Oral communication**

A. Diez-Escudero, M. Espanol, M.P. Ginebra. *Heparinization of Calcium Phosphates: towards enhancing biological performance.* 27th Annual Conference of the European Society for Biomaterials, Krakow (Poland), August-September 2015. **Poster**

A. Diez-Escudero, S. Beats, M. Espanol, M.P. Ginebra. *Tuning the degradation of calcium phosphates cements by controlled porosity incorporation.* 26th Symposium and Annual Meeting of the International Society for Ceramics in Medicine, Barcelona (Spain), November 2014. **Oral communication**

A. Diez-Escudero, M. Espanol, Y. Maazouz, M.P. Ginebra. *Controlled and reliable carbonation of low temperature calcium phosphates.* 26th Annual Conference of the European Society for Biomaterials, Liverpool (United Kingdom), August-September 2014. **Oral communication**

Bone is the most transplanted tissue after blood and can potentially rise as the fourth largest cause of disability within the next years. Despite the natural ability of bone to self-heal it cannot bridge large bone defects without the help of a material. Biomaterials are nowadays required not only to replace bone tissue but also to foster its regeneration. Even though autografts are the gold standard in most clinical procedures, they have several limitations that need to be overcome. Synthetic bone grafts are excellent candidates to accommodate the high demands of a global ageing population.

Synthetic calcium phosphates possess outstanding properties such as biocompatibility, bioactivity and osteoconduction which help them mimic the mineral phase of bone, hydroxyapatite. However, their integration in the bone remodeling cycle to help the process of bone regeneration is still unbalanced mainly due to their poor resorbability. The balancing of implant resorption with its progressive replacement by new bone can be achieved either by modulating the material's physicochemical properties, or by combining the substrate with biological molecules capable of adequately orchestrating the various cells involved in the bone healing process.

This thesis seeks to explore, on the one hand, the feasibility of modulating the physicochemical properties of calcium phosphates towards improving its degradation behavior, and, on the other hand, to investigate the potential calcium phosphates functionalization with heparin as a strategy to improve their biological performance at the various stages of bone healing: during the initial phase of inflammation, and during the stages of bone resorption and bone growth.